

Overview of S-type asteroid Itokawa, based on the studies on samples returned by Hayabusa.

T. Yada¹, M. Abe¹, T. Okada¹, M. Nishimura¹, R. Kanemaru¹, H. Soejima^{1,2}, K. Kumagai^{1,2}, K. Sakamoto¹, T. Usui¹, and M. Fujimoto¹

¹*Institute of Space and Astronautical Science, Japan Aerospace Exploration Agency, Sagami-hara, Kanagawa 252-5210, Japan,*

²*Marine Works Japan Inc., Yokosuka, Kanagawa 237-0063, Japan.*

Introduction: Hayabusa spacecraft, which was launched in May 2003, reached near-Earth S-type asteroid 25143 Itokawa in September 2005. It landed onto the surface of the smooth terrain called “MUSES-Sea” of Itokawa twice in November 2005, even though its touchdown sampling system had not fully functioned [1]. Hayabusa spacecraft had overcome a series of troubles happened after the 2nd sampling and during its returning cruise back to Earth, and return its reentry capsule including its sample container to the Woomera prohibited area in South Australia in June 2010. After a series of procedures in the curation facility in JAXA, sub-mm sized mineral grains were recovered from its sample canister [2, 3]. A series of preliminary examination analyses on those grains revealed that they originated from surface regolith of asteroid Itokawa and that were comparable to equilibrated LL chondrites [4-9].

Initial descriptions and distributions of Itokawa samples: The sample canister is separated into two rooms, room A and B, and those from the 1st touchdown should be recovered into the room A and those from the 2nd one should be in the room B, even though the gap of the division plate between the two rooms sizes around 0.5mm and those smaller than the size of gap might be mixed up between the two rooms. The sample container was introduced into the clean chamber and opened in static vacuum condition in order to recover gas sample in the container even though it did not contain detectable amount of sample gas. The sample canister was extracted from the container in purified nitrogen condition and samples grains inside the sample canister were recovered onto quartz glass or aluminum plates due to compulsive fall by tapping the canister in upside down orientation. Individual sample grains were handpicked and handled with an electrostatically controlled micro-manipulation system developed for Hayabusa returned samples and installed in the clean chamber of purified nitrogen condition [10]. They were transferred to the sample chamber of the field emission secondary electron microscope equipped with the energy dispersive X-ray spectrometer (FE-SEM/EDS) Hitachi S-4300SE/N or SU6600 without exposing to the air and examined for their backscattered electron images and qualitative chemical composition. After sent back to the clean chamber, they were placed onto gridded quartz glass slides, lately individual quartz glass containers, to be stored in its purified nitrogen condition and given individual identification numbers. So far, 1344 of individual Hayabusa grains have been described and given sample IDs. The sample IDs start from “RA” are from room A, which comprise 605 grains, “RB” from room B, 404 grains, “RC” from a rotation cylinder situated between the two rooms, 86 grains, and “RX” are from both rooms, 249 grains [11]. All the initial description information of Hayabusa sample grains are also published on the sample catalog website (<https://curation.isas.jaxa.jp/curation/hayabusa/index.html>). Among them, 20 of grains and one Teflon spatula containing fine Itokawa grains have been distributed to NASA, based on Memorandum of Understanding between JAXA and NASA for the Hayabusa mission. On the other hand, international announcement of opportunity of Hayabusa samples have been conducted since 2012, and 254 of individual Hayabusa grains have been distributed to 69 of research plans of AO so far, which result in various kind of scientific achievements mentioned below.

Equilibrated chondritic body Itokawa: Modal abundance, average fayalite content in olivine and ferrosilite content in low-Ca pyroxene, and oxygen isotopic compositions of Itokawa grains match those of LL chondrites [4, 5, 12, 13], and distribution of fayalite contents in olivine and petrologic observation indicated its petrologic type ranges from type 4 to type 6 [4]. Olivine-spinel geothermometer and plagioclase geothermometer have been applied for Itokawa mineral grains, indicating that peak temperature they experienced during thermal metamorphism in asteroid should have reached 800°C and it slowly cooled down to 600°C, which corresponds to petrologic type <5 [4, 14, 15]. The thermal metamorphism it experienced should have occurred in a body predate asteroid Itokawa. Assuming ²⁶Al as a heat source of such body, the size of the precursor body of asteroid Itokawa should have sized 20km in radius based on numerical simulation [16]. Concerning about its shock stage, detailed studies on olivine and plagioclase in Itokawa grains indicate they experienced shock stage 2, moderately shocked, which corresponds to 5-10 GPa in shock pressure. Thus, Itokawa is an LL chondritic breccia body of various petrologic type ranging from type 4 to 6. The U-Pb chronology obtained from phosphates found in Itokawa grains show a single isochron age of 4.64 ± 0.18 Ga, indicating the precursor body should have formed in the early solar system [17]. Also a lower intersection age of the U-Pb system is 1.51 ± 0.85 Ga, indicating catastrophic break-up event should have occurred for the precursor body of Itokawa at this age. This age is consistent with a result of complete degas age estimated from ⁴⁰Ar-³⁹Ar system as 1.3 ± 0.3 Ga [18], whereas it is inconsistent with the degas age by ⁴⁰Ar-³⁹Ar system as 2.3 ± 0.1 Ga [19]. It seems that further confirmation is

needed for the chronological study.

What happens on asteroid Itokawa: Because Itokawa samples are the only surface regolith sample of the S-type asteroid among all kinds of planetary samples, a series of studies for space weathering have been conducted for these samples. Surface of Itokawa grains shows thin (30-60 nm) amorphous layer, containing ~2nm of nano phase Fe particles [7]. The very surface of the amorphous layers are enriched in not only Fe but also S, redeposition of nano phase FeS after micrometeoroids impact should occur and this must redden reflectance spectrum of the asteroid effectively. Solar flare tracks are recognized in olivine in Itokawa grains just below the amorphous phase and its track densities indicate their short surface exposure time on the order of 10^3 to 10^4 years [20]. The fact that the exposure ages of Itokawa grains much shorter than that of Lunar regolith (>several tens million years) are consistent with the result of exposure age estimated from cosmogenic ^{21}Ne concentrations of Itokawa grains as 3 million years, which is much shorter than Lunar regolith as ~400 million years [9]. Short exposure time of Itokawa grains also pointed from little cosmogenic ^{10}B contribution in B isotopic composition observed in Itokawa grains [21]. The short exposure time of Itokawa regolith also indicates that large surface mass loss rate such as several tens of cm per million years, further implied the lifetime of Itokawa as 100 to 1000 million years [9]. Different from silicate minerals, space weathering on the surface of sulfides cause ~1 μm to several hundreds nm of iron whiskers on their surfaces caused by loss of sulfur from sulfide surfaces and deposition onto them due to long exposure to the energetic ions of the solar wind [22]. As mentioned before, surfaces of Itokawa grains also experienced micrometeoroids impact. Microimpact craters are reported on the surfaces of Itokawa grains [23], which results in melt splashes and adhering particles [24] and even secondary submicrometer craters distributed on their surfaces, assuming their exposure time as 10^2 to 10^4 years [25, 26].

New insights of S-type asteroid: Itokawa samples bring us new insights of S-type asteroid. For example, ~1 mole% enrichment of water and hydroxyl on the surface of olivine in Itokawa samples, which is caused by continuous exposure of solar wind to the asteroid surface, indicating ubiquitous presence of such water on airless bodies. They further assume a part of potential sources of Earth's ocean in the early solar system [27]. Concerning about water, euhedral NaCl crystals and KCl, which should have formed by water-rock interaction in Itokawa or its precursor body, were discovered on the surface and interior of Itokawa grains and nanoscale NaCl grains were discovered in an Itokawa grain, indicating S-type asteroid might have once contained certain amount of water and provided water to ancient Earth [28, 29, 30]. S-type asteroids are thought to be poor in organic matters as ordinary chondrites, but indigenous organic matters were discovered from carbon-rich Hayabusa grains [30, 31]. They discovered nanocrystalline graphite and disordered polyaromatic hydrocarbon in carbon-rich grains recovered from the Hayabusa sample canister, showing D- and ^{15}N -enrich isotopic compositions. In another report, they discovered non-protein amino acids, racemic β -aminoisobutyric acid and β -amino-n-butyric acid in carbon-rich grains, indicating their non-biological, non-terrestrial origins.

Concluding remarks: As mentioned above, Itokawa samples continue providing new and striking scientific results. Even though we have (will have) other new returned asteroid samples like Ryugu from C-type asteroid [32] and Bennu from B-type asteroid [33], Itokawa samples remain important because they are still the only S-type asteroid samples for human being.

References:

- [1] Kawaguchi J. et al. 2008. *Acta Astronautica* 62: 639.
- [2] Abe M. et al. 2011. Abstract #1638. 42nd LPSC.
- [3] Yada T. et al. 2014. *Meteoritics & Planetary Science* 49:135.
- [4] Nakamura T. et al. 2011. *Science* 333: 1113.
- [5] Yurimoto H. et al. (2011) *Science* 333: 1116.
- [6] Ebihara M. et al. (2011) *Science* 333: 1119.
- [7] Noguchi T. et al. (2011) 333: 1121.
- [8] Tsuchiyama et al. (2011) *Science* 333: 1125.
- [9] Nagao K. et al. (2011) *Science* 333: 1128.
- [10] Yada T. et al. (2022) JAXA Repository, JAXA-RR-21-009E.
- [11] Kanemaru R. et al. (2023) JAXA Repository, JAXA-SP-22-005E.
- [12] Nakashima D. et al. (2013) *Earth Planet. Sci. Lett.* 379: 127.
- [13] Tsuchiyama A. et al. (2014) *Meteoritics Planet. Sci.* 49: 172.
- [14] Tanaka M. et al. (2014) *Meteoritics Planet. Sci.* 49: 237.
- [15] Mikouchi T. et al. (2014) *Earth Planets Space* 66: 82.
- [16] Wakita S. et al. (2014) *Meteoritics Planet. Sci.* 49: 228.
- [17] Terada K. et al. (2018) *Scientific Reports* 8: 11806.
- [18] Park J. et al. (2015) *Meteoritics Planet. Sci.* 50: 2087.
- [19] Jourdan F. et al. (2017) *Geology* 45: 819.
- [20] Keller L. P. and Berger E. L. (2014) *Earth Planets Space* 66: 71.
- [21] Fujiya W. et al. (2016) *Meteoritics Planet. Sci.* 51: 1721.
- [22] Matsumoto T. et al. (2020) *Nat. Comm.* 11: 1117.
- [23] Nakamura E. et al. (2012) *Proc. Nation. Acadm. Sci.* 109: E624.
- [24] Dobrica E. and Oglione R. C. (2016) *Earth Planets Space* 68: 21.
- [25] Harries D. et al. (2016) *Earth Planet. Sci. Lett.* 450: 337.
- [26] Matsumoto T. et al. (2018) *Icarus* 303: 22.
- [27] Daly L. et al. (2021) *Nat. Astron.* <https://doi.org/10.1038/s41550-021-01487-w>.
- [28] Noguchi T. et al. (2014) *Meteoritics Planet. Sci.* doi: 10.1111/maps.12333.
- [29] Che S. and Zega T. J. (2023) *Nat. Astron.* <https://doi.org/10.1038/s41550-023-02012-x>.
- [30] Chan Q. H. S. et al. (2021) *Scientific Reports* 11: 5125.
- [31] Parker E. T. et al. (2022) *Meteoritics Planet. Sci.* 57: 776.
- [32] Yada T. et al. (2022) *Nat. Astron.* 6: 214.
- [33] Lauretta D. et al. (2022) *Science* 10.1126/science.abm1018.

Summary of Hayabusa2 and Status of JAXA curation

Tomohiro Usui¹

¹*Institute of Space and Astronautical Science, Japan Aerospace Exploration Agency, Japan*

Japan Aerospace Exploration Agency (JAXA) has a strategic small-body sample return program to understand the formation, evolution, and migration of planetary building blocks, water, and organics in the early solar system. The JAXA's sample return program started with Hayabusa for S-type asteroid Itokawa in 2010, followed by Hayabusa-2 for C-type asteroid Ryugu in 2020, and the future mission of Martian Moons eXploration (MMX) for Phobos in 2029. My presentation covers the recent achievement of Hayabusa 2 curation and sample analysis. I also present an overview of MMX, particularly how we leverage the Hayabusa 2 experience to develop the MMX curation and sample science.

Hayabusa 2 team has completed the initial curation and sample analysis of the Ryugu samples. The Hayabusa 2 curation/sample analysis is unique in having a role as a "bridge" between the remote sensing and the sample analysis communities. Along with the conventional curation tools (e.g., optical microscope and balance), JAXA installed remote sensing instruments (e.g., ONC: Optical Navigation Camera) in the curation facility for ground truthing. Moreover, a flight spare of MicrOmega (infrared hyperspectral microscope) detected important minor phases (clays, carbonates, organics) in the apparently black Ryugu samples in the early stage of the curation. Following the initial sample analysis/curation activity, Ryugu samples are now publicly available <<https://jaxa-ryugu-sample-ao.net/>>.

JAXA plans a Phobos sample return mission MMX in 2024-2029. The MMX spacecraft is scheduled to be launched in 2024, orbit Phobos and Deimos (multiple flybys), and retrieve and return >10 g of Phobos regolith to Earth in 2029. The Phobos regolith represents a mixture of endogenous Phobos building blocks and exogenous materials that contain solar system projectiles (e.g., interplanetary dust particles and coarser materials) and ejecta from Mars and Deimos. The MMX Sample Analysis Working team started designing the curation and sample analysis protocol to identify Phobos' fragments with different origins. Under the condition that remote sensing observations guarantee the representativeness of the sampling sites in the geologic context of Phobos, laboratory analysis of the returned sample will provide crucial information about the moon's origin: the capture of an asteroid or in-situ formation by a giant impact.

Future perspective of sampling and curation for extraterrestrial materials in JAXA's small body exploration

Ryota Fukai¹

¹ISAS/JAXA

Introduction

Japan Aerospace Exploration Agency (JAXA) successfully completed the sample return planetary exploration missions for the small bodies Itokawa (Hayabusa; 2003–2010) and Ryugu (Hayabusa2; 2014–2020). JAXA is preparing to receive the next return samples to Institute of Space and Astronautical Science (ISAS) and planning new missions for the next decade. I introduce the concept and tentative plan for the curation of the Bennu sample returned by Origins, Spectral Interpretation, Resource Identification, Security, Regolith Explorer (OSIRIS-REx; NASA), the Phobos sample collected by Martian Moon Exploration (MMX; JAXA), and the comet sample collected by Next-Generation Small Body Sample Return (NGSR; JAXA). The concept of curation in the future is threefold: ground truthing of remote-sensing and in-situ data, certification for the curation data, and in-house contamination control. Subsequently, I introduce the scientific scopes and the key techniques for sampling the comet materials in the NGSR mission.

Curation

Ground truthing of remote-sensing and in-situ data. Ground truthing for remote-sensing and in-situ analysis data obtained by the mission instruments should be done to complete the mission objectives in the sample return mission. The curation phase of the return samples is the chance for ground truthing without any sample biases. In the MMX curation, the initial description will be done with the ToF-type mass spectrometer, visible/infrared spectral imager, and Raman spectrometer, corresponding to the mission instruments in the MMX spacecraft [1]. In addition, the simulator of Optical Radiometer composed of CHromatic Imagers (OROCHI), an optical camera of the MMX spacecraft, will be installed in the Bennu clean chamber to help plan the MMX's curation strategy [2].

Certification for the curation data. Whereas the observation in the clean chamber is useful to characterize the bulk-scale return sample, the analytical method is limited to a totally non-destructive way. For instance, we estimated the bulk density of Ryugu grains with the information from the weight and optical image [3]. To confirm the accuracy of the curation data within the clean chamber, we will conduct the coordinated analysis for the return sample (e.g., Ryugu, Bennu) outside the clean chamber, such as X-ray Computed Tomography (XCT) and Scanning Electron Microscope- Energy Dispersive Spectroscopy (SEM-EDS). This dataset is available as additional information for outreach and allocation in the Announcement of Opportunity (AO).

In-house contamination control. Regular monitoring for the contamination of clean environments is essential to maintain cleanliness levels. We newly introduce the method for sampling the metal particles within clean rooms and chambers by Gas Exchange Device- Inductively Coupled Plasma- Mass Spectrometer (GED-ICP-MS). We can count the number of metal particles without any biases in the sample preparation. We can attain the cross-check for possible contamination in the return samples by mass spectrometric techniques developed with in-house contamination control.

Next-generation sample return mission

Scientific scopes. Following small-body explorations such as the Hayabusa and Hayabusa2 missions, we should explore more primitive targets in the Solar System. Our target for the next sample return is a comet, which potentially possesses the record of the early Solar System and "presolar" system in the Milky Way Galaxy, avoiding the secondary alteration within the parent body. Kurokawa et al. [4] will report the scientific concept of NGSR in detail.

Subsurface sampling. The surface of a comet should have non-primitive layers such as recondensed and/or consolidated surfaces up to ~1 m depth [5]. Therefore, subsurface sampling for the comet is critical to attain the scientific objectives in NGSR. We are developing the subsurface sampling system using a Small Carry-on Impactor (SCI) and bullet-system sampler.

References: [1] Fukai, R. et al. *in revision*. [2] Fukai, R. et al. (2023) *METSOC*. [3] Yada, T. et al. (2021) *Nature Astronomy*, **6**, 214–220. [4] Kurokawa, H. et al. (2023) *this symposium*. [5] El-Maarry, M. R. et al. (2019) *Space Science Review*, **215** (36).

Updates on OSIRIS-REx: Return journey to Earth and the sample from Benu

Shogo Tachibana¹, Harold C. Connolly, Jr.^{2,3,4}, Dante S. Lauretta⁴, and the OSIRIS-REx Sample Analysis Team

¹*UTOPS, University of Tokyo / ISAS, JAXA*

²*Department of Geology, School of Earth & Environment, Rowan University*

³*Department of Earth and Planetary Science, American Museum of Natural History*

⁴*Lunar and Planetary Laboratory, University of Arizona*

NASA's OSIRIS-REx (Origins, Spectral Interpretation, Resource Identification, Security and Regolith-Explorer) spacecraft explored B-type near-Earth asteroid (101955) Benu from December 2018 to May 2021. [1]. The spacecraft data indicated that Benu's surface material contains hydrous silicates, carbonates, magnetite, and organic matter [2-4], suggesting that it experienced aqueous alteration within a parent body. In October 2020, the spacecraft collected a sample of surface material from a site nicknamed Nightingale within the 20-m-diameter Hokioi crater. The in-flight inspection of the sample with the SamCam imager showed that millimeter- to centimeter-sized particles were successfully collected [5]. Analysis of various telemetry data from before and after sample collection yielded an estimated sample mass of 250 ± 101 g, well above the mission goal (60 g) [5]. The spacecraft will fly by Earth and drop the Sample Return Capsule (SRC) into the Utah desert in the western United States on September 24, 2023. As of writing (September 21, 2023), the spacecraft is on track targeting Earth. After retrieval, the SRC will be delivered to the NASA Johnson Space Center (JSC) to be curated in a new cleanroom dedicated to the Benu sample [6]. At the symposium, we will report updates on the SRC retrieval operation, curation processes at JSC, and the sample.

References

- [1] Lauretta D. S. et al. 2019. *Nature* 568: 55-60. [2] Hamilton V. E. et al. 2019. *Nat. Astron.* 3:332-340. [3] Kaplan H. H. et al. 2020. *Science* 370:eabc3557. [4] Simon A. A. et al. 2020. *Science* 370:eabc3522. [5] Lauretta D. S. et al. 2022. *Science* 377:285-291. [6] Righter K. et al. 2023. *Meteorit. Planet. Sci.* 58: 572-590.

Developing European Curation for MMX Samples

Aurore Hutzler¹, Aliz Zemeny², Jörn Helbert³, Jean Duprat⁴, Elliot Sefton-Nash¹, Enrica Bonato^{3,5} and Kamini Manick²

¹*ESTEC, European Space Agency, The Netherlands*

²*ECSAT, European Space Agency, United Kingdom*

³*Institute for Planetary Research, German Aerospace Center (DLR), Germany*

⁴*Institut de Minéralogie, de Physique des Matériaux et de Cosmochimie (IMPMC), France*

⁵*Museum für Naturkunde Berlin, Germany*

Curation of extraterrestrial samples is imperative for maximizing science return. Despite Europe's established meteorite and overall museal curation expertise, it currently lacks specialized infrastructure for samples directly returned from space. An opportunity to enhance capabilities in this area is provided by the Martian Moon eXploration (MMX) mission. MMX is led by the Japan Aerospace Exploration Agency (JAXA) and is planned to return >10g of core and regolith material from Phobos to Earth in July 2029 [1, 2].

Cooperative discussions between partnering space agencies and European institutions regard possible transfer of a portion of the anticipated MMX sample collection for long-term curation in European institutions, following the period of initial description at JAXA and the initial scientific analysis conducted by the MMX Science Sub-Teams (i.e., post-2030). Leading this initiative are the Centre National d'Études Spatiales (CNES) and the Museum National d'Histoire Naturelle (MNHM) in France and the German Aerospace Center (DLR) in Germany. Both are actively engaged in designing advanced curation facilities to receive, curate, and handle Phobos samples.

The Centre National de la Matière Extraterrestre (CNME, National Center for Extraterrestrial Materials) is a joint program supported locally by the National Museum of Natural History (MNHN), Sorbonne University and the Institut de physique du globe de Paris (IPGP) and, at the national level, by the French spatial and scientific research agencies (CNES and CNRS). The CNME will be built in the historical Geology and Mineralogy Gallery of MNHN in the center of Paris. The CNME will be designed to ensure long-term curation of unrestricted extra-terrestrial samples allocated to France from past and future space missions such as MMX, together with existing major collections of extra-terrestrial samples including: the national meteorite collection from MNHN, large polar micrometeorites collections and terrestrial analogues from the geology/mineralogy collections. The CNME will consist in a clean-room infrastructure, divided in separated modules with ISO7 to ISO5 environments, together with an adjacent laboratory for sample preparations and experiments not requiring a cleanroom environment. The CNME curation team will work under the supervision of CNES on the recently funded MARCUS project to build a dedicated apparatus for small sample (solid and gas) handling under restricted conditions (pure nitrogen glove boxes) and bio-contained environment. Instrumentation in the CNME will focus on acquisition of the basic properties on samples (from μm to cm scales), including optical 2D and 3D microscopy and imaging, weighting, magnetic susceptibilities, scanning electron microscopy, Raman and infrared (IR) microspectroscopy, XRD, with a dedicated suite of instruments to achieve initial characterization and cataloging of samples before allocation.

At the DLR Institute for Planetary Research in cooperation with the Museum für Naturkunde in Berlin, the Sample Analyses Laboratory (SAL) and its extension, the Sample Curation Facility are currently being setup [3]. The target date for completion is in the summer of 2024. It is mainly dedicated to the analyses of unrestricted extra-terrestrial materials from sample return missions. SAL will focus on spectroscopic, geochemical, mineralogical analyses at microscopic level. The instrumentation includes a Malvern Panalytical Empyrean X-ray diffraction (XRD), a JEOL iHP200F Field Emission - electron microprobe analyzer (FE-EMPA), a Field Emission - scanning electron microscope (FE-SEM), Keyence VHX-7000 3D microscope, and a vis-IR-microscope (Bruker Hyperion 2000), all housed in a clean room that is currently being built. Samples will be processed, handled and analyzed in pure nitrogen or vacuum conditions to minimize alteration and contamination.

Within the European Centre for Space Applications and Telecommunications (ECSAT) site of the European Space Agency (ESA), the recently established Vulcan Analogue Sample Facility (formerly SACF) is actively involved in the development of a robust European network dedicated to both existing and prospective extra-terrestrial analogue sample procurement, production, and supply chain management. The Vulcan Facility is further oriented towards advancing the scientific investigation of planetary analogues encompassing lunar, Martian, and other celestial bodies. This is accomplished through the provision of state-of-the-

art benchtop instrumentation for fundamental analyses encompassing geochemical, mineralogical, and crystal lattice properties (SEM-EDS, XRD, FTIR and Raman). Additionally, the Vulcan Facility offers geotechnical property characterization capabilities (ViseSize particle size analyser, pycnometer, and TGA). Concurrently, Vulcan lends support to the curation of extra-terrestrial materials and associated technology development initiatives (glovebox systems and a Double-Walled Isolator [DWI] with robotic arm equipped with a micromanipulator). The strategic focus of Vulcan on analogue samples is anticipated to play a pivotal role in addressing the curation and research challenges associated with upcoming and future extraterrestrial sample return missions.

Between partners of any joint sample return activity, a tightly-coordinated approach on curation protocols, and mutually high level of technical proficiency and training, is fundamental to achieving the main goal of long-term curation: preparing for techniques that have yet to be conceived, enabling testing theories that have not yet been developed, and catering for the ideas and needs of future scientists.

The implications of capability development in Europe for handling returned samples extend beyond the MMX mission. Establishing these curation facilities and developing a collaborative framework for distributed long-term curation will increase the readiness of European involvement in future sample return missions. In particular, developments in sample handling and curation infrastructure may be synergistic with that required by the long-term curation of Martian samples that are planned to be returned by the NASA/ESA Mars Sample Return (MSR) campaign.

References

1. Kuramoto K, Kawakatsu Y, Fujimoto M, et al (2022) Martian moons exploration MMX: sample return mission to Phobos elucidating formation processes of habitable planets. *Earth, Planets and Space* 74:.
<https://doi.org/10.1186/S40623-021-01545-7>
2. Usui T, Bajo K, Fujiya W, et al (2020) The Importance of Phobos Sample Return for Understanding the Mars-Moon System. *Space Sci Rev* 216:49. <https://doi.org/10.1007/s11214-020-00668-9>
3. Bonato E, Helbert J, Schwinger S, et al (2023) The Sample Analysis Laboratory at DLR and its Extension to Curation Facility for MMX. In: 86th Annual Meeting of the Meteoritical Society. pp 6035–6035
4. Aliz Zemeny and Kamini Manick (2023) Lunar Highland Simulant Selection of The Luna Analogue Facility Dust Chamber For Future Missions – Space Resources Week, Luxembourg

The DLR Sample Analysis Laboratory – the final countdown

Joern Helbert¹, Enrica Bonato¹, Ansgar Greshake², Alessandro Maturilli¹, Giulia Alemanno¹, Aurelie van den Neucker¹
and Lutz Hecht²

¹*DLR, Institute for Planetary Research, Berlin, Germany*

²*Museum für Naturkunde, Berlin, Germany*

Laboratory measurements of extra-terrestrial materials like meteorites and ultimately materials from sample return missions can significantly enhance the scientific return of the global remote sensing data. This motivates the ongoing addition of a dedicated Sample Analysis Laboratory (SAL) to complement the work of well-established facilities like the Planetary Spectroscopy Laboratory (PSL) and the Planetary Atmosphere Simulation LABORatory (PASLAB) within the Department of Planetary Laboratories at DLR, Berlin. SAL is being developed in preparation to receive samples from sample return missions such as JAXA Hayabusa 2 and MMX missions, the Chinese Chang-E 5 and 6 missions as well as the NASA Osiris-REX mission. SAL is focusing on spectroscopic, geochemical, mineralogical analyses at microscopic level with the ultimate aim to derive information on the formation and evolution of planetary bodies and surfaces, search for traces of organic materials or even traces of extinct or extant life and presence of water.

SAL is currently being set up at the Institute for Planetary Research at the DLR location in Berlin-Adlershof in Germany. The cleanroom environment is on the ground floor of the main DLR building in Berlin-Adlershof with a room for support infrastructure in the basement below.

Procurement of the instruments is almost complete and first instruments are already been delivered. SAL will be equipped with a vis-IR-microscope (Bruker Hyperion 2000), a Malvern Panalytical Empyrean X-ray diffraction (XRD) system with Bragg-Brentano geometry which can be switched to parallel beam geometry, equipped with a Cu K α source, 1Der detector and automated incident beam optics, a Field Emission – scanning electron microscope (FE-SEM), a JEOL iHP200F Field Emission – electron microprobe analyzer (FE-EMPA), petrographic and stereo microscopes, Keyence VHX-7000 3D microscope and a set of gloveboxes.

The Bruker Hyperion 2000 and the Keyence VHX-7000 3D microscope are already in operation at PSL and PASLAB and have been used recently to study Ryugu sample A0112. The JEOL iHP200F is currently setup at JEOL in Freising, Germany. Acceptance tests were successfully completed in March 2023. Commissioning, calibration, testing and initial training was completed in summer of 2023. The instrument has been used recently for work on meteorites and will be transferred to DLR in early 2024 with an additional delta commissioning planned after final installation. The X-ray diffraction system has been delivered in December 2022 and is currently in storage and will be setup as soon as the cleanrooms are ready. SEM procurement is currently under way with a delivery expected in summer of 2024.

In collaboration with the Natural History Museum (MfN) in Berlin, SAL will also have the expertise and facilities for carrying out curation of sample return material which will be made available for the whole European scientific community. DLR is already curating a 0.45 mg of Lunar regolith collected from the Luna 24 Soviet mission and the first analyses of the material are being planned.

Currently, the curatorial expertise is being developed on the existing expertise from the Meteorite Collection based at the MfN and in collaboration with the JAXA and NASA curation facilities. Current curators, together with the younger generation are being trained and working on skillset exchange

Curation of Extraterrestrial samples in France and the future center for extraterrestrial materials in Paris.

J. Duprat¹, J.-C. Viennet¹, M. Roskosz¹, B. Doisneau¹, S. Pont¹, M. Verdier-Paoletti¹, S. Bernard¹, M. Gounelle¹, J. Aléon¹, P. Sans-Jofre¹, B. Zanda¹, G. Avicé², F. Moynier², R. Brunetto³, C. Pilorget³, F. Poulet³, C. Engrand⁴, L. Delauche⁴, E. Dartois⁵, J. Gattacceca⁶, C. Maurel⁶, L. Piani⁷, Y. Marrocchi⁷, A. Barucci⁸, L. Bonal⁹, L. Lemelle¹⁰, A. Simionovici¹¹, G. Libourel¹²

¹IMPMC, CNRS-MNHN-Sorbonne Université, UMR 7590, 57 rue Cuvier, Paris, France ; ²Université Paris Cité, Institut de physique du globe de Paris (IPGP), CNRS, Paris, France ; ³IAS, Université Paris-Saclay, CNRS, UMR 8617, Orsay, France ; ⁴IJCLab, Université Paris-Saclay, CNRS/IN2P3, Orsay, France ; ⁵ISMO, Université Paris-Saclay, CNRS, Orsay, France, ⁶CEREGE, Aix-Marseille Université, CNRS, INRAE, IRD, Aix-en-Provence, France, ⁷CRPG—CNRS 15 rue Notre Dame des Pauvres, BP 2054501 Vandœuvre-les-Nancy, France, ⁸LESIA-Observatoire de Paris, Université PSL, CNRS, Sorbonne Université, Université de Paris Cité, 92195 Meudon Principal Cedex, France, ⁹IPAG, Université Grenoble Alpes; 38000 Grenoble, France, ¹⁰LGL-TPE, CNRS, UCBL, ENS de Lyon, ¹¹ISTERRE, CNRS, Université Grenoble Alpes, 38058 Grenoble, France, ¹²Université Côte d'Azur, Observatoire de la Côte d'Azur, CNRS, LAGRANGE, France.

The coming decade will witness important developments in curation facilities dedicated to pristine samples from space missions. The return of samples from asteroid Bennu by the OSIRIS-REx NASA-led mission [4] is imminent and, on a longer term, samples will be returned from the Martian moon Phobos by the MMX JAXA-led mission [5]. After 2030, samples from the Martian surface are expected to be returned to Earth by the NASA/ESA Mars Sample Return (MSR) mission [6]. Advanced curation studies are on-going [9, 10] in major curation facilities at JAXA and NASA [7-9] while others facilities are currently into construction, such as the SAL in Berlin [see e.g. 11 and this meeting]. Many laboratories in France have experience in handling samples from spatial missions or from existing collections of extra-terrestrial materials (meteorites, micrometeorites, IDPs...). These experiences cover a whole range of expertise from curation itself to dedicated samples handling (e.g. micromanipulation, fragmentation...), first-order characterization by non-invasive or non-destructive techniques and dedicated sample preparation (e.g. thin and ultra-thin sections, polished sections, ...) in clean-room environments.

The CNME project was launched in 2022 to build a national curation facility for extra-terrestrial materials at MNHN. This project is supported, at the national level, by the French spatial and scientific research agencies (CNES and CNRS) and will be supported locally by the National Museum of Natural History (MNHN), Sorbonne University and the Institut de physique du globe de Paris (IPGP). This project will benefit from the local experience in curation of existing collection of meteorites and micrometeorites and from expertise developed in other French laboratories. A key objective of CNME will be to ensure the long-term curation of a fraction of samples from the future MMX JAXA-led mission [5]. As a result of on-going agreements between JAXA and the French space agency CNES and ESA, a fraction of Phobos (MMX) samples are expected to be transferred to the CNME at MNHN and after the period of initial description at JAXA-ISAS sample receiving laboratory and after the first scientific analysis by the MMX Science Sub-Teams (i.e. after 2030). In the long-term, the CNME will be designed to allow the reception of un-restricted samples from MSR mission, i.e. once they will be out of the Sample Receiving Facility.

The design of CNME will be modular to allow flexible configuration of different environments for the curation of samples from different space missions. The CNME clean-room infrastructure will be divided in separated modules (ISO7 to ISO5 [24]) environments, together with a laboratory dedicated to sample preparations. It will contain secured cabinets and glove boxes under controlled atmospheres (dry and purified N₂, Ar, vacuum, ...). In the long-term perspective of MSR, the CNME team is involved in the MARCUS project to study, under the supervision of CNES, a dedicated apparatus for small sample (solid and gas) handling in clean and bio-contained (BSL4-like) environment. The CNME will include a dedicated space for rehearsal activities on the MARCUS apparatus (before operation in BSL4-like laboratories). Instrumentation in CNME will focus on acquisition of the basic properties on samples with sizes going from μm up to cm scales, including optical 2D and 3D microscopy and imaging, weighting, magnetic susceptibility measurements, scanning electron microscopy, XRD, Raman and infrared (IR)

micro-spectroscopy with a dedicated suite of instruments, to achieve initial characterization and cataloguing of samples. The control of terrestrial contamination within CNME cleanrooms will be achieved by real-time monitoring of inorganic, organic and biological contamination.

The CNME will include instruments and advanced storage facilities developed by several French laboratories. The magnetic environment of the samples and the magnetic properties of the handling tools will be monitored to ensure preservation of the original paleomagnetic record of the samples. The CNME will develop research programs to improve existing curation techniques and new technological solutions for the mid to long-term curation of volatile elements contained in samples collected by future space missions, e.g. ice and gas from cometary objects or planetary atmospheres (see G. Avice et al. this meeting). A specific setup will be developed at IAS in order to allow a multi-scale (from mm down to μm) IR reflectance micro-imaging characterization of samples. The analysis will be fully non-destructive and non-invasive with no need for specific sample preparation, it will be performed within a dedicated bench in a controlled atmosphere (e.g., N_2). Other setups for samples preparation and/or first-order characterization are currently in study in French laboratories with the aim to build a national network of experts in curation-related activities. At the international level, the CNME team will develop in-depth collaboration with other teams currently managing major curation centers in Europe and on a world-wide scale (see A. Hutzler et al this meeting).

The CNME will ensure the long-term curation of the MNHN historical meteorite collection that include a rich panel of Martian samples (Shergottites, Chassignites, Nakhilites) [17] and several emblematic primitive chondrites (e.g. Orgueil CI-chondrite). The MNHN meteorite collection is actively used for cosmochemistry research projects and is constantly growing with new additions every year, thanks to collections performed by a joint team from CEREGE and MNHN in Atacama Desert (see e.g. [14]). The CNME will also have the responsibility for the long-term curation of micrometeorite collections recovered from both Greenland and Antarctica [15] including the Concordia micrometeorites collection (currently in a dedicated curation cleanroom at IJCLab) that contains thousands of micrometeorites with minimal terrestrial weathering [16]. Beside these collections, CNME will also ensure the long-term curation of samples from the Chinese mission Chang'e5 recently donated to France.

In this presentation, I will summarize the general landscape of curation activities in France and present the current status of the CNME project.

Acknowledgement: The CNME is a joint project supported by MNHN, IPGP, Sorbonne University, University Paris Cité, CNES and CNRS. The curation-related instruments and apparatus currently under development benefit from funding by Région Ile de France (DIM-ACAV⁺ contract C³E), CNES, CNRS, MNHN and ANR contract (COMETOR 18-CE31-0011). The collection of micrometeorites benefited from the pluri-annual funding by IPEV and PNRA (Program #1020)

References: [1] Brownlee D. (2014) *Ann. Rev. Earth Planet. Sci.* **42**, 179-205. [2] Yano H., et al. (2006) *Science* **312**, 1350-1353. [3] Watanabe S., et al. (2019) *Science*, eaav8032. [4] Lauretta D.S., et al. (2017) *Space Sci. Rev.* **212**, 925-984. [5] Kuramoto K., et al. (2022) *Earth, Planets and Space* **74**, 12. [6] Beaty D.W., et al. (2019) *Meteorit. Planet. Sci.* **54**, S3-S152. [7] Yada T. et al. *Meteorit. Planet. Sci.* **49**, 135-153 [8] Evans C., et al. (2018) **42**, B4.2-49-18. [9] McCubbin F.M., et al. (2019) *Space Sci. Rev.* **215**, 48. [10] Hutzler A. et al. *EURO-CARES D7.1 Final technical Report*. [11] Helbert J., et al. (2020), EPSC2020-250. [12] ISO 14644-1 [13] Caillet Komorowski C.L.V. (2006) *Geol. Soc. London Spec. Pub.* **256**, 163-204. [14] Gattacceca et al. (2011) *MAPS* **46**, 1276-1287, Hutzler et al. (2016) *MAPS* **51**, 468-182 [15] Maurette M., et al. (1986) *Science* **233**, 869-872. Maurette M., et al. (1991) *Nature* **351**, 44-47. Duprat J., et al. (2007) *Adv. Space Res.* **39**, 605-611. Rojas J., et al. (2021) *Earth Planet. Sci. Lett.* **560**, 116794. [16] Duprat J., et al. (2010) *Science* **328**, 742-745.

Mars Sample Return: curation activities and planning.

Aurore Hutzler¹, Andrea D. Harrington², William E. Page³ and Alvin L. Smith².

¹*ESTEC, European Space Agency, The Netherlands*

²*NASA, Johnson Space Center, Houston, TX, USA*

³*Jet Propulsion Laboratory, USA*

Curation of extra-terrestrial samples is a multifaceted process that aims to balance the conservation of a collection with its efficient use. Therefore, a robust curation plan will maximize the science conducted in the first years after sample return while ensuring a representative collection remains available to enable science for decades.

The Mars Sample Return (MSR) campaign, initiated in 2020 with the launch of the Perseverance Rover, represents an international collaboration between the United States National Aeronautics and Space Administration (NASA) and the European Space Agency (ESA) for the purpose of bringing Martian geological samples back to Earth for scientific investigations. This ambitious undertaking marks the first instance of sample return from another planet and the first return classified as Restricted since Apollo 14. The Restricted classification requires rigorous backward planetary protection requirements (BPP), which impacts how samples can be curated and analysed.

NASA and ESA have agreed to jointly proceed on science and curation and are in the formulation phase of the joint NASA/ESA Sample Receiving Project (SRP). After the sample arrive on earth and are transported to the Sample Receiving Facility, initial characterization begins. The aim on initial characterization is to generate a robust catalogue, which is a mandatory element to the allocation process. Sample requests for scientific research accomplished in the first years after sample return will be openly competed and jointly selected by ESA and NASA; this includes allocations for objective science completed within the SRP (first planned AO nominally in 2026) as well as opportunity science outside of the SRP. Proposals from a consortium of institutions proposing a coordinated analysis plan will be encouraged, to ensure efficiency and accountability.

While the Martian samples are expected to be back as soon as 2033, preparatory activities for protocols, hardware and infrastructure are underway. NASA and ESA have selected several working groups from the scientific community to advise on: 1) measurements to be conducted on the samples, 2) appropriate contamination control parameters, and 3) necessary requirements for handling and analysing the collection. Several curation and engineering teams in the United States and in Europe, coordinated by the NASA/ESA Joint Curation Office (JCO), are in close interaction with the NASA/ESA Joint Science Office and are working on developing hardware and strategies for the Sample Receiving Facility. The JCO is developing a curation plan following guidelines from the NASA NPR 7100.5 [1] (pending validation by NASA and ESA upcoming agreements).

The JCO is also considering long-term curation of the collection, separate from the SRP as part of their planning. It is expected that long-term curation might not require high-containment, and that while only one Sample Receiving Facility is planned, there might be several MSR curation facilities.

Latest updates on curation, science, and R&D planning will be shared, with an emphasis on synergies between the MSR curation team and the science community.

References

[1] https://nodis3.gsfc.nasa.gov/displayDir.cfm?Internal_ID=N_PR_7100_0005_&page_name=main&search_term=7100.5

Mars Sample Return: Considerations for the Curation of Astromaterials from a Restricted Planet

Andrea D. Harrington¹, Aurore Hutzler², and Francis M. McCubbin¹

¹NASA, Johnson Space Center, Houston, TX, USA

²ESTEC, European Space Agency, The Netherlands

The joint NASA/ESA Mars Sample Return (MSR) campaign is underway. The Perseverance Rover has already collected a returnable sample suite currently cached at Three Forks and the pairs to these samples are stored on the Rover with more compelling samples planned to be collected. The MSR collection would represent the most geologically diverse astromaterial collection ever returned and should provide information on topics ranging from Martian geological and biological history to Martian environmental hazards and in situ resource utilization to support potential human exploration [1]. Although Jezero Crater and the surrounding area are not Mars special regions, the scientific opinion is that Mars as a whole is of significant interest to the process of chemical evolution and/or the origin of life. Therefore, due to possibility, however remote, that the samples could contain extraterrestrial life, MSR is classified as a Category V: Restricted Earth Return mission by the NASA Planetary Protection Office. As a result of this classification, a MSR Sample Receiving Facility (SRF) must not only provide a pristine environment to ensure samples are protected from terrestrial contamination for scientific investigations, but it must also provide high-containment to isolate the samples from Earth's biosphere until the samples are deemed safe for release and/or sterilized.

The SRF is first and foremost a curation facility, however it will be utilized for an array of tasks and scientific objectives, including:

- Receive the flight hardware containing the sample collection (e.g., Earth Entry System, Orbiting Sample)
- Deintegrate the sample tubes from the hardware and put in a stable state
- Characterize the sample tubes (Pre-Basic Characterization)
- Open the sample tubes (e.g., collect headspace gas, extract samples while maintain stratigraphy)
- Perform initial sample characterization and cataloging
- Conduct a sample safety assessment
- Execute preliminary examination of samples for science
- Enable select competed/early science
- Prepare, sterilize, and distribute samples for science outside of the SRF
- Sample isolation/storage

The SRF is not intended to be the long-term curation facility for Martian samples. The nominal utilization period for the SRF is anticipated to be 2-5 years. However, to account for possible delays in schedule or the identification of extant life, this anticipated period of time must be flexible to accommodate schedule extensions and contingency plans. Due to the high-containment requirements, a traditional receiving/curation facility cannot be utilized for MSR.

As a result of the complexity of designing, constructing, and operating a contamination-controlled high-containment facility, NASA initiated an assessment of current technologies. Personnel toured both contamination-controlled and high-containment facilities around the world, exploring the implementation of new technology and standard practices. The report, entitled: "Tours of High-Containment and Pristine Facilities in Support of Mars Sample Return (MSR) Sample Receiving Facility (SRF) Definition Studies" compiles the knowledge of experts in their fields and offers recommendations for the best path forward [2]. NASA and ESA have used this data, as well as outputs from numerous MSR science working groups, to perform the Mars SRF Assessment Study (MSAS) and the European Extraterrestrial Sample Infrastructure (EETSI) System Study.

While EETSI investigated the preliminary design, costs, and schedules for new, traditionally built fixed SRF and Sample Curation Facilities (SCF), MSAS was a scoping study, designed to assess the feasibility of utilizing traditional versus more novel infrastructure, specifically:

1. Lease and renovation of existing space
2. Construction of a new, traditional fixed facility
3. Construction of a modular facility (new or within an existing building)

4. Construction or renovation of a hybrid facility to address requirements with multiple modalities that may include a combination of modalities 1-3.

The assessment also considered the following aspects of the SRF for each modality:

- Ability to meet requirements
 - o Regulatory
 - o Planetary protection
 - o Contamination control
 - o Science and curation
- Ability to meet changing needs for equipment, timelines, and facility use
- Timelines for design, construction, commissioning, installation of equipment, testing, training, and operational readiness drills
- Cost for construction and operation, including those associated with hazard resilience
- Ease of access for international users
- Decommissioning, repurposing, sale, or lease following use of the facility
- Uncontained preparatory laboratory spaces
- Uncontained ancillary spaces
- Waste management

The outputs for MSAS and EETSI have been critical to understand the potential trades and identify priorities for the SRF. However, while options were able to be refined, a second phase (MSAS2) will develop high-concept designs at multiple locations in order to optimize the technical capabilities, cost, and schedule of the SRF. As part of the next steps in planning, the NASA/ESA Mars Sample Receiving Project (SRP) Joint Curation Office (JCO) is developing a curation plan following guidelines from the NASA NPR 7100.5 [3] and supporting the Measurement Definition Team (MDT). The MDT is chartered to evaluate the measurements and instrumentation needs for the SRF. Outputs from this team, as well as the Sample Safety Assessment Protocol (SSAP) Tiger Team, will be critical for SRF design. Upon completion of MSAS2, the SRF design concepts would be utilized to inform site-specific design but the location of the SRF will not be finalized until NASA's completion of the National Environmental Policy Act (NEPA) process.

Every sample return mission offers scientists and engineers unique challenges and opportunities, MSR is certainly not an exception. While differences in robotics and spacecraft are often apparent, differences in the approach for the curation of a given collection are usually more nuanced. NASA's Astromaterial Acquisition and Curation Office, and other international space agency partners, have developed strong foundations of best-practices and lessons learned. Although MSR represents the first Restricted Earth return in five decades, the knowledge gained from the development and operations of the Lunar Receiving Laboratory are informing the potential curation strategies for MSR. Whether the SRF is reutilized by NASA for another Restricted Earth return after the MSR samples are deemed safe or turned over to a partner for other types of high-containment work, the knowledge gained during technology development, SRF design, construction, and operations will lay the foundation for sample return missions for the next five decades.

References

- [1] Czaja A. D. et al. 2023. *Meteoritics & Planetary Science* 58: 885-896. [2] Mattingly R. L. et al. 2020. JPL/NASA Report. [3] https://nodis3.gsfc.nasa.gov/displayDir.cfm?Internal_ID=N_PR_7100_0005_&page_name=main&search_term=7100.5

Fostering future missions and curation: fine-particle simulant characterization for a lunar highland testbed (ESA, European Astronaut Centre - EAC)

Aliz Zemeny¹ and Kamini Manick¹

¹European Space Agency (ESA), Vulcan Analogue Sample Facility, European Centre for Space Applications and Telecommunication (ECSAT), Fermi Avenue, Harwell Campus, Oxfordshire, United Kingdom

In the framework of the European Centre for Space Applications and Telecommunications (ECSAT), the UK site of the European Space Agency (ESA), the Vulcan Analogue Sample Facility is actively engaged in the establishment of a robust European network devoted to the acquisition, production, and management of extraterrestrial analogue samples (or simulants), both existing and prospective. The Vulcan Facility is primarily oriented towards advancing scientific inquiries into planetary analogues, encompassing celestial bodies such as the Moon and Mars. This pursuit is facilitated through the deployment of benchtop instrumentation for fundamental property analyses, and support for the curation of extraterrestrial materials and the development of associated technologies. European simulant priorities were determined following a user survey and simulant supplier workshop in 2022 (Table 1).

As part of supporting the European simulants network, Vulcan's role encompasses choosing the optimal fine-particle highland feedstock option for the 'Dust Chamber' [1] of the Luna Analogue Sample Facility in Cologne, Germany (EAC, ESA). The selection process entails a comprehensive exploration of the European network of simulant providers and both commercial and academic laboratories, entailing an exhaustive evaluation of the availability and logistical aspects of materials accessible in the market. This consideration encompasses critical factors such as loading times and associated costs. Furthermore, a rigorous assessment of simulant properties is conducted, including but not limited to particle size distribution, shape, and abrasivity. These parameters hold significant importance in the context of primary geotechnical and geomechanical objectives within the 'Dust Chamber'.

Nonetheless, these deliberations serve to refine the pool of potential highland simulants obtainable in Europe. Ultimately, the most suitable simulant candidate will be meticulously chosen to facilitate comprehensive testing of geotechnical and engineering-related activities within the Dust Chamber. It comprises due diligence of the full simulant supply chain (including assessment of the source site, excavation and processing methods, and quality control). Consequently, discerning selection process aims to contribute substantively to the accumulation of essential knowledge, thus enhancing our readiness for the upcoming sample return and human lunar surface missions in this decade.

Table 1. Priority activities, among 36 simulant users surveyed in 2022 (35 European-based, 1 Japan-based), centring around exploration hardware and resource extraction studies. Red: 25-28%; Yellow: 11-16%; Green: 3-8%; Grey: No data.

	Lunar	Martian	Asteroids / Meteorites	Other
Spacecraft, instruments and/or software	Red	Yellow	Green	Yellow
ISRU (Resource extraction)	Red	Green	Grey	Green
ISRU (Additive manufacturing)	Yellow	Green	Grey	Green
ISRU (Unspecified)	Green	Green	Grey	Green
Planetary Science Research	Green	Yellow	Green	Green

References

[1] A. Zemeny and K. Manick (2023) Lunar highland simulant selection of the Luna Analogue Facility Dust Chamber for future missions – Space Resources Week, Luxembourg

Nanoscale infrared characterization (AFM-IR) of Ryugu samples returned by the Hayabusa-2 space mission

J. Mathurin¹, E. Dartois², A. Dazzi¹, A. Deniset-Besseau¹, L. Bejach³, C. Engrand³, J. Duprat⁴, Y. Kebukawa⁵, H. Yabuta⁶, H. Yurimoto⁷, T. Nakamura⁸, T. Noguchi⁹, R. Okazaki¹⁰, H. Naraoka¹⁰, K. Sakamoto¹¹, S. Tachibana^{11,12}, S. Watanabe¹³, Y. Tsuda¹¹, and the initial-analysis IOM and STONE teams

¹Institut Chimie Physique (ICP), Univ. Paris-Saclay/CNRS, 91405 Orsay, France

²ISMO, Univ. Paris-Saclay/CNRS, 91405 Orsay, France

³IJCLab, Univ. Paris-Saclay/CNRS, 91405 Orsay, France

⁴IMPMC/MNHN, SU, Paris, France

⁵Faculty of Engineering, Yokohama National University, Japan

⁶Hiroshima University, Higashi-Hiroshima 739-8526, Japan

⁷Hokkaido University, Sapporo 060-0810, Japan

⁸Tohoku University, Sendai 980-8578, Japan

⁹Kyoto University, Kyoto 606-8502, Japan

¹⁰Kyushu University, Fukuoka 812-8581, Japan

¹¹ISAS/JAXA, Sagami-hara 252-5210, Japan

¹²The University of Tokyo, Tokyo 113-0033

¹³Nagoya University, Nagoya 464-8601, Japan.

The distribution of chemical bonds in organic matter (OM) of interplanetary samples (meteorites and micrometeorites) can be efficiently and non-destructively characterized using infrared vibrational spectroscopy (FTIR) [1]. Conventional FTIR microscopy provides a global view of the dust grain physico-chemical composition but remains spatially limited by the diffraction. In state-of-the-art synchrotron-based FTIR microscopy, the typical spot sizes in the mid-IR range can, at best, sample a few μm . This spatial resolution limitation often hampers a direct comparison with complementary techniques such as isotopic imaging with NanoSIMS, transmission electron or X-ray microscopy. Such IR diffraction limitation can be circumvented using AFM-IR microscopy [2]. AFM-IR is now a well-established microscopy technique in the vibrational field, combining an atomic force microscope (AFM) and a tunable IR illuminating source to detect photo-thermal effect and access chemical information. This technique is applied in a wide diversity of scientific fields [3] and we recently used it to analyze various extraterrestrial samples [4-8]. For this study the tunable IR illuminating source is a QCL laser with a spectral range from 1900 cm^{-1} – 900 cm^{-1} with a top-down illumination. This configuration allows two modes of acquisition. In the first one, the wavenumber is fixed and the tip moves along the surface, allowing to acquire simultaneously AFM topography and an IR absorption map of the sample at the selected wavenumber. In the second one, the tip position is fixed on a sample position and the IR laser is tuned to explore the whole available spectral range of the QCL laser, giving access to local IR spectra at the point of interest.

Ryugu samples from chamber A (surface) and chamber C (sub-surface) were received from the “IOM” and “Stone” Hayabusa2 initial analysis teams. Several samples from chambers A and C were prepared by crushing small fragments on diamond windows, down to a thickness of $\sim 1\ \mu\text{m}$. Because of the high resolution of AFM-IR (tens of nanometers), regions of interest were first localized and selected using synchrotron-based FTIR microscopy [8].

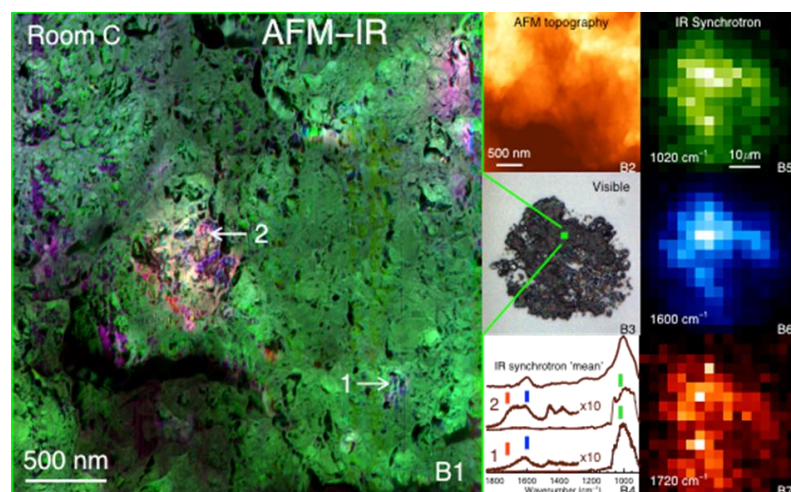


Figure 1: Study of chamber C sample C109-04. B1: $3 \times 3\ \mu\text{m}$ RGB composite image combining the AFM-IR absorption mapping obtained at different wavenumbers corresponding to the absorption of Si-O silicates (1020 cm^{-1} , green), C=C (1600 cm^{-1} , blue) and C=O (1720 cm^{-1} , red). The size of the image here corresponds to the size of one pixel in the synchrotron maps - B2: AFM topography of the $3 \times 3\ \mu\text{m}$ area studied in AFM-IR - B3: optical image - B4: from top to bottom : average IR synchrotron spectra obtained on the whole sample, local spectra obtained by AFM-IR highlighting the presence of OM with and without a C=O signature at 1720 cm^{-1} , on the locations highlighted by arrows in B1. The red, blue and green dashes indicate the wavenumber positions of the IR mapping with the same color - B5-B7: IR maps obtained by transmission synchrotron μFTIR at same wavenumber (and corresponding colors) as the AFM-IR maps. Adapted from [7]

A large-scale map (20 μm x 20 μm) was first recorded to characterize the main components' distribution within the sample with a spatial resolution of ~ 75 nm [8]. As the OM contribution in the IR spectra is weaker than that of minerals, highly spatially resolved maps of 3 x 3 μm in size were acquired with a lateral spatial resolution of ~ 25 nm. It was then possible to localize OM inclusions in the samples (Fig. 1 – B1) by comparing the signal from the Si-O of the silicates (Fig. 1 – B1 in green) and that from the OM contributions of the C=C absorption (Fig. 1 – B1 in blue) and C=O absorption (Fig. 1 – B1 in red). On the larger OM inclusion displayed in Fig. 1 – B1, the OM signal is a mix between C=C and C=O (which appears in purple), but chemical heterogeneities are observed at small scales: parts of the inclusion seem to exhibit local enrichment in C=O (redder) or in C=C (bluer). Local AFM-IR spectra were recorded on these spots, showing locally different C=C and C=O contributions (Fig. 1 – B4) [7].

Based on this first measurement, a more complete analysis of various samples was conducted either on whole-rock samples or on IOM extracted from chambers A and C samples [9]. The results obtained not only confirmed the heterogeneity of the OM distribution already observed but also highlight the fact that OM is mainly distributed in two phases, a diffuse organic component intimately mixed with the mineral matrix and nanoglobule-like organic particles (Fig. 2). These particles are texturally resembling nanoglobules present in primitive meteorites and were identified in both whole-rock and IOM samples from chambers A and C Ryugu samples. The local IR spectra of nanoglobule-like particles also clearly show enhanced carbonyl (C=O) and CH contributions with respect to the diffuse organic matter in Ryugu whole-rock and IOM residue (Fig. 2 – (c)). Such spectra are compatible with that of organic residues formed from UV or ion irradiated ices at low temperatures, simulating the environment of the outer regions of the protoplanetary disk, or in the protosolar cloud.

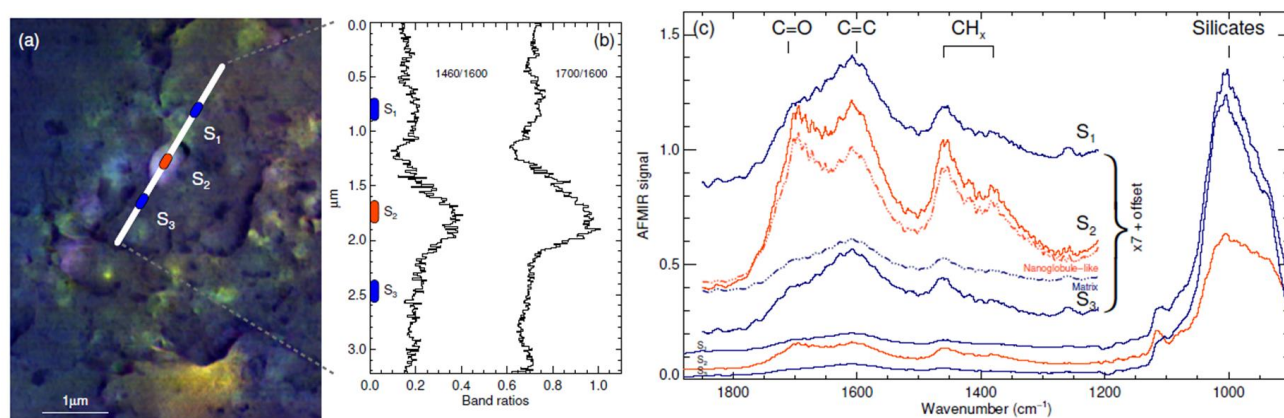


Figure 2: Whole-rock Ryugu sample A0108-19. (a) RGB image of the region including an organic nanoglobule-like particle (C=O at 1720 cm^{-1} in red, C=C at 1600 cm^{-1} in green, CH_x at 1460 cm^{-1} minus 1520 cm^{-1} in blue). The white line shows the location of individual AFM-IR spectra taken across the nanoglobule-like feature. The colored dots (S1 to S3) correspond to average spectra taken on each side (S1 and S3 in blue) and on the nanoglobule-like feature (S2 in red). (b) Intensity ratios corresponding to CH_x/C=C (1460 cm^{-1} /1600 cm^{-1}) and C=O/C=C (1700 cm^{-1} /1600 cm^{-1}) along the white line shown in (a). The location of the S1 to S3 spectra is recalled on the left axis. (c) Average spectra on each side (blue, S1 and S3) and on the nanoglobule-like feature (red, S2). The red dot-dashed line spectrum labelled 'Nanoglobule-like' is obtained by scaling the average of S1 and S3 spectra to the same silicate band intensity as in the S2 spectra, and by subtracting this scaled spectrum from S2. The resulting 'Nanoglobule-like' spectrum is thus freed from the matrix contribution underneath the globule. The nanoglobule-like spectrum shows elevated CH_x signal (intense methyl and methylene deformation modes at ~ 1460 cm^{-1} and ~ 1370 cm^{-1}), as well as high carbonyl contributions around 1700 cm^{-1} . The blue dot-dashed line spectrum labelled 'Matrix' corresponds to the expected contribution from the matrix for equivalent probe depth as for the nanoglobule-like spectrum. Adapted from [9].

AFM-IR measurements demonstrate the presence of organic inclusions intimately mixed with minerals in Ryugu samples at the sub-micron scale. Focusing on the OM-rich zones of Ryugu samples it is possible to unveil, without any chemical treatment, the IR signature in the chemical bondings of chemical OM heterogeneities as well as the sub-micrometric spatial distribution of the different components. This study shows that OM exists in (at least) two forms in Ryugu samples, as a diffuse phase in the minerals matrix, and as isolated inclusions resembling nanoglobules.

References

- [1] Dartois E. et al. 2018 *Astron. Astrophys.*, vol. 609, p. A65. [2] Dazzi A. et al. 2005 *Opt. Lett.*, vol. 30, no. 18, pp. 2388–2390. [3] Dazzi A. and Prater C. B. 2016 *Chem. Rev.*, vol. 117, no. 7, pp. 5146–5173. [4] Mathurin J. et al. 2019 *Astron. Astrophys.*, vol. 622, p. A160. [5] Kerraouch I. et al. 2022 *Geochim. Cosmochim. Acta*, vol. 334, pp. 155–186. [6] Kebukawa Y. et al. 2023 *Icarus*, vol. 400, p. 115582. [7] Yabuta H. et al. 2023 *Science* 80, vol. 379, no. 6634. [8] E. Dartois et al. 2023 *Astron. Astrophys.*, vol. 671, p. A2, Mar. 2023. [9] Mathurin J. et al., in revision.

Sampling and curation of volatile elements in the new era of sample return missions

Guillaume Avice¹, Frédéric Moynier¹, C. Mustin², Jean Duprat³

¹Université Paris Cité, Institut de physique du globe de Paris, CNRS, Paris, France

²IMPMC, Muséum National d'Histoire Naturelle, Sorbonne Université, CNRS, Paris, France

³Centre National D'Etudes Spatiales (CNES), France

The scientific community has been entering a new era of sample return missions with the successful Hayabusa 1&2 (JAXA) and future OSIRIS-REx (NASA) missions, the future missions of samples return from Mars (Mars Sample Return mission, NASA and ESA) and its moon Phobos (MMX, JAXA). Other than their inner scientific values, sample return missions are of key scientific importance as they trigger the development of suites of state-of-the-art analytical techniques in terrestrial laboratories to conduct exhaustive characterization of the returned samples (petrography, mineralogy, chemical analyses etc.). Among these investigations, measuring the elemental and isotopic composition of volatile elements in extraterrestrial samples is a high priority scientific target as they can be used to understand the origin of planetary atmospheres and of water in terrestrial planets (*e.g.*, [1]). More broadly, such measurements could provide answers to the question: Why is the Earth habitable? Such investigations rely on the ability to conduct a proper curation of the samples containing volatile elements. A recent study highlighted the need for developing advanced curation techniques for volatile-rich samples [2] and a recent experiment developed by US-based scientists opened lunar core containers returned to Earth by the Apollo astronauts in order to sample volatile elements (see ref. 3). Developing new curation techniques is also one of the goals of the future curation center CENAME (a Center National for Extraterrestrial Materials) which will be built at the French Musée National d'Histoire Naturelle (MNHN, Paris, France) in collaboration with the Institut de physique du globe de Paris (IPGP, France) (see J. Duprat et al., *this meeting*). This is also one goal of the project MARCUS led by CNES (PI. C. Mustin) and which is part of the new French initiative PEPR Origins: from planets to life.

In 2019, the Hayabusa2 mission successfully sampled over 5 grams of solid samples from the surface and subsurface of the asteroid Ryugu. The preliminary scientific investigations revealed that Ryugu samples are similar to primitive carbonaceous material similar to Ivuna-type meteorites but with less alteration than identified in these meteorites [4]. Having pristine samples from carbon-rich asteroids also allows to put new constraints on the role of these bodies in the delivery of volatile elements to Earth [5]. Recent measurements of the D/H ratio of hydrogen contained in Ryugu samples revealed that carbonaceous-type material could have delivered up to 3% of Earth's water [6]. Importantly, the sealing technique adopted for closing the sample capsule consisted in an aluminum metal seal [7], maximizing the chances to retain extraterrestrial volatile-rich elements such as noble gases. A quick recovery of the sample capsule followed by careful onsite curation protocols [8] allowed to recover the gas originally contained in the sample capsule. Results obtained by a preliminary study reveal that, despite a certain degree of contamination by the Earth's atmosphere, the gas sampled during the mission is extraterrestrial with a clear contribution from solar-wind derived gases [9]. Investigations also revealed that the Al-seal partially re-opened during Earth's entry due to the strong deceleration when the parachute deployed.

The technical developments and sample handling protocols used before, during and after the return of samples by the Hayabusa2 mission are the best and most recent examples of advanced curation techniques for volatile-rich elements collected during space missions [8,9]. Therefore, they represent a reference starting point for improving the current curation protocols and developing new solutions. Ryugu samples are thus providing perfect opportunity to assess the quality of the current techniques of curation of volatile-rich extraterrestrial samples. In this presentation we will show how Hayabusa2 samples have the potential to provide key information on the state-of-the-art of curation techniques and possible improvements.

Gas samples from Ryugu allocated by the JAXA curation center will be delivered to IPGP in fall 2023. Noble gases (Ne, Ar, Kr and Xe) elemental and isotopic composition will be immediately measured in order to : i) evaluate if the different samples prepared by the curation team have the same composition (NT1 vs NT2 sample) ; ii) compare with published data (*e.g.*, [9]) for NT1 sample and evaluate if the composition of the gas has evolved since the preliminary investigations. Samples will then be stored in distinct conditions (closed and exposed to room pressure and temperature for one sample, closed and attached to a turbo molecular pumping station for another sample, closed and exposed to moderate vacuum for another sample). New measurements will then be conducted after 6-9 months to assess which storage conditions is the most appropriate. Results will be shared and discussed with the JAXA curation team the international community concerned on this aspect of the curation of extraterrestrial samples.

Bottle (sample)	Pipette	Measurement/ Storage	Scientific investigations
NT1	new pipette #, container X NT1P#X	immediate measurement and storage at room PT conditions (6-9 months) before second measurement	<ul style="list-style-type: none"> evolution of the gas since Okazaki et al. (2022) study mid-duration (months) storage of gas in shipped containers
	new pipette #, container X NT2P#X	immediate measurement and storage at room PT conditions before second measurement	
NT2	new pipette #, container Y NT2P#Y	container attached 6-9 months to a high vacuum line (10^{-10} torr)	<ul style="list-style-type: none"> differences between NT1/NT2 (sample preparation) optimization of the mid-duration storage (vacuum, moderate vacuum, room PT)
	new pipette #, container Z NT2P#Z	container attached 6-9 months to a moderate vacuum chamber (90% of the pressure inside the cylinder)	
NT5 (blk)	new pipette #, container X NT5P#X	immediate measurement and measurement after 6-9 months of storage in vacuum conditions	<ul style="list-style-type: none"> monitoring of the blank level to decipher the origin of terrestrial contamination

Figure 1: Summary of the sample allocated by the JAXA curation center. The original samples NT1, NT2 and NT5 (bottles, ref. 8) are identified as well as the three different pipettes to be drawn from the bottle by the JAXA curation team. Samples will be measured at different times and stored in different conditions to evaluate curation techniques.

In this presentation we will also describe future long-term developments for the curation of volatile-rich samples. One development will involve testing new materials for the sample containers (*e.g.*, TiN covered Titanium coupons used for the preparation of Perseverance sample tubes and gently provided by colleagues from JPL). We will also improve curation protocols (short- and long-term monitoring) and develop new solutions for vacuum containers.

References

- [1] Avicé G. & Marty B. 2020. Space Science Reviews 216:36. [2] McCubbin et al. 2019. Space Science Reviews 215:48. [3] Parai et al. 2022. Apollo 17 – ANGSA Workshop, LPI Contrib. N°2704:2028. [4] Yokoyama et al. 2022. Science 379:eabn7850. [5] Paquet et al. 2023. EPSL 611:118126. [6] Piani et al. 2023. Astrophysical Journal Letters 946:L43. [7] Okazaki et al. 2017. Space Science Reviews 208:107-124. [8] Miura et al. 2022. Earth Planets Space 74:76. [9] Okazaki et al. 2023. Science 379:eabo0431.

Machine Learning Data Analyses for Asteroid and Micrometeorite Samples

Lewis Pinault¹ and Hajime Yano²

¹*School of Natural Sciences, Birkbeck College, Gower Street, London WC1E 7HX, United Kingdom*

²*Institute of Space and Astronautical Science, Japan Aerospace Exploration Agency, 3-1-1 Yoshinodai, Chuo-ku, Sagami-hara, Kanagawa 252-5210 Japan*

We have developed and trained Machine Learning (ML) convolutional network models on aerogel-captured meteoroid samples of the Tanpopo [1] missions onboard the International Space Station using new camera, recording, and processing techniques that greatly speed and automate their identification and classification. This technique moves beyond datasets that have already been laboriously centred, focused, scaled, imaged, and classified to various types by human researchers, and builds on prior systems [2] to open the door to automated transits by microscope across the Tanpopo aerogel panels at approximately 500x500 pixel increments, at different focal lengths, with images then fed directly into core ML Object Detection programme. The programme then uses its object detection/localisation capabilities to automatically draw bounding boxes around the object or objects of interest in each image, and to automatically run a confidence prediction of which classification of the types it might be, displayed both on the image and as a searchable table [3].

The time-and-manpower gains that can be affected by ML became clear with its further application to the Ryugu A0180 sample. Hundreds of nano-CT scans were conducted to create segmented images [4] whose cross-sections helped reveal characteristic micro-features within the sample such as voids, cracks, and micro-chondrules of particular interest. For an example, human-eye examination of void evidence and 3D distribution in cross-section allowed re-integration of the images to reveal the voids in full dimension. This manual process of identifying and classifying evidence of voids in cross-section is ripe for ML identification, classification, and reintegration using the methods we have developed. Moreover, the data gained by manual imaging of A0180 now forms a robust training data set for applying to more porous and aggregate samples such as unmelted micrometeorites collected in the terrestrial environment.

Thus, 3D optical images, nano-CT data, and external and internal SEM images of Ryugu asteroid samples returned by Hayabusa2 can be archived at international research institutions to create further training data for searching the diversity among different groups of asteroid samples and for practically comparing characteristic micro-structures with the wider suite of micrometeorite collections. In this manner, it may also be possible for the ML modelling to connect evidence found in the Ryugu samples to the potential underrepresentation of particular meteoritic constituents in terrestrial collections.

References

- [1] A. Yamagishi, S. Yokobori, K. Kobayashi, H. Mita, H. Yabuta, M. Tabata, M. Higashide, and H. Yano (2021) Scientific Targets of Tanpopo: Astrobiology Exposure and Micrometeoroid Capture Experiments at the Japanese Experiment Module Exposed Facility of the International Space Station, *Astrobiology*, p1451-1460. <http://doi.org/10.1089/ast.2020.2426>
- [2] S. Sasaki, J. Imani, and H. Yano (2019) Design, Fabrication and Evaluation of an Aerogel Processor CLOXS for the Astrobiology Mission Tanpopo, *Biological Sciences in Space*, 33, p. 7-11.
- [3] L. Pinault, K. Okudaira, H. Kiryu, I. Crawford, and H. Yano (2023, in preparation) Machine Learning Programme for Extraterrestrial Microparticles Using a Custom Machine Learning Model with Mobile Computer Vision and Processing Systems, *Journal title?*
- [4] M.J. Genge, N. Almeida, M. Van Ginneken, L. Pinault, P. Wozniakiewicz, and H. Yano (2023) Ice and Liquid Water in Asteroid Ryugu – Constraints from Sample A0180, this volume.

Characterization of Mg-Fe carbonates in the Ryugu returned samples with MicrOmega

Loizeau, D.¹; Mahlke, M.¹; Pilorget, C.¹; Brunetto, R.¹; Baklouti, D.¹; Ito, M.²; Bibring, J.-P.¹; Le Pivert-Jolivet, T.¹; Aléon-Toppani, A.¹; Riu, L.³; Jiang, T.^{1,4}; Hatakeda, K.⁵; Yogata, K.⁵; Nakato, A.^{5,6}; Carter, J.¹; Yada, T.⁵; Okada, T.⁵; Tahara, R.⁵; Usui, T.⁵; Langevin, Y.¹; Lantz, C.¹; Tomioka, N.²; Yamaguchi, A.⁶; Uesugi, M.⁷; Miyazaki, A.⁵; Nishimura, M.⁵; Nagashima, K.⁵; Kumagai, K.⁵; Hitomi, Y.⁵; Sugiyama, Y.⁵; Nakata, A.⁵

¹*Institut d'Astrophysique Spatiale, Université Paris-Saclay, CNRS, France*, ²*Kochi Institute for Core Sample Research, JAMSTEC, Japan*, ³*ESAC, ESA, Madrid, Spain*, ⁴*School of Earth Sciences, China University of Geosciences, Wuhan, China*, ⁵*Institute of Space and Astronautical Science, Japan Aerospace Exploration Agency, Japan*, ⁶*National Institute of Polar Research, Japan*, ⁷*JASRI/SPRing-8, Japan*

The Ryugu samples brought back by the Hayabusa2 spacecraft in December 2020 have been delivered to the JAXA Extraterrestrial Curation Center [1]. Bulk samples and then sub-bulks and individual grains have been picked up and stored into sapphire dishes, weighed, and analyzed with an optical microscope, FTIR spectroscopy, and MicrOmega hyperspectral imaging [2] for initial description within the curation facility [1]. The MicrOmega instrument used in the JAXA Extraterrestrial Curation Center is a NIR hyperspectral microscope. This configuration allows a mineralogical characterization of pristine Ryugu samples, as they have never been exposed to terrestrial environment.

MicrOmega has a total field of view of 5 mm × 5 mm, with a resolution of ~22.5 μm/pixel in the focal plane. It covers the spectral domain from 0.99 μm to ~3.6 μm. Its capabilities enable the identification of organic matter and different minerals in the returned samples [3]. In particular, carbonates can be detected and characterized in the MicrOmega spectral domain primarily through a strong absorption band at 3.3-3.5 μm, together with shallower specific bands at 2.5 and 2.3 μm, and for some carbonates a large absorption band around 1 μm.

A recently published study [4] based on the analysis of MicrOmega data of ~180 extracted individual grains (a few mm in size) and 14 aggregate samples (all observed with MicrOmega within the Curation Center in 2021) has shown that carbonates are distributed in two main populations. Those populations are different in composition and size/morphology: most detections are made on small grains and inclusions (<100 μm large) with a spectrum similar to dolomite CaMg(CO₃)₂, while for the largest detections, although less numerous, spectra similar to breunnerite (Mg,Fe)CO₃ dominate.

Dolomite is present in many grains as inclusions, and in many aggregate samples, and many occurrences have been reported in recently published studies analyzing some grains in detail [e.g., 5-11]. Breunnerite occurrences have been listed only in studies accessing a larger volume of samples [e.g., 10-13]. However, the large size of breunnerite occurrences [4] makes them a significant component of the returned Ryugu material, showing that it is important to understand when and how they formed compared to the dolomite, and what was the source of Fe and C for this population of carbonates.

The largest breunnerite inclusion was found on grain C0041, covering ~0.25 mm², or ~10% of the visible surface of the grain. This grain is one of the grains with “White regions” described in [5]. This carbonate inclusion shows a complex morphology with three branches, 100s μm long, around a main area, that could point to a formation in a fracture or between grains. In addition, several detached grains of breunnerite, 100s μm long, have been detected in several aggregate samples, indicating possibly many other large inclusions from which those grains were separated.

MicrOmega did not detect any obvious spatial transition from dolomite to breunnerite within a carbonate detection at the surface of grains, which would have indicated a possible gradient during a single formation event, although one observation of dolomite in contact with breunnerite has been made through SEM observations [10]. To better understand formation processes, we are investigating spatial heterogeneity of carbonate composition with a more systematic technique at small scale (few 10s μm) in the MicrOmega data to check for gradients in Mg or Fe content for example: to achieve this, we check for shifts in NIR absorption band positions and shapes at the MicrOmega pixel level. We have also succeeded in extracting one loose grain of breunnerite (in collaboration with the Phase 2 curation Kochi team) and studying it with different techniques (imaging IR spectroscopy, Raman spectroscopy, EDS) that will enable us to check for heterogeneities in carbonate composition of the grain or the presence of other minerals or molecules within the grain at a smaller scale (<10 μm).

The two main populations of carbonates question the formation process or processes that occurred on Ryugu's parent body/bodies, and their respective age of formation. To our knowledge, only one attempt of Ryugu's breunnerite dating has been published so far [6] that does not conclude on a noticeable difference in age of formation between breunnerite and dolomite. More studies of breunnerite occurrences are required to better constrain their age, formation, and carbon sources.

References

- [1] Yada T. et al. (2021) *Nature Astronomy* 6, p.214-220. [2] Pilorget C. et al. (2021) *Nature Astronomy* 6, p.221-225. [3] Pilorget C. and Bibring J.-P. (2014) *PSS* 99, 7-18. [4] Loizeau D. et al., (2023) *Nature Astronomy* 7, 391-397. [5] Nakato A. et al. (2023) *Earth, Planets and Space*, 75(1), 45. [6] McCain K. A. et al. (2023) *Nature Astronomy*, 7(3), 309-317. [7] Fujiya W. et al. (2023). *Nature Geoscience* 16, 675-682. [8] Dartois E., et al. (2023) *Astronomy & Astrophysics*, 671, A2. [9] Nakamura E. et al. (2022) *Proceedings of the Japan Academy, Series B*, 98(6), 227-282. [10] Yamaguchi, A., et al. (2023) *Nature Astronomy*, 7(4), 398-405. [11] Ito, M., Tomioka, N., Uesugi, M. et al. (2022) *Nat Astron* 6, 1163–1171. [12] Yokoyama T. (2022) *Science*, 379(6634), eabn7850. [13] Nakamura T. (2022) *Science*, 379(6634), eabn8671.

Heterogeneity of Ryugu samples due to space weathering effects: near-infrared spectroscopy and fitting analysis

S. Furukawa^{1,2}, T. Okada^{1,2}, K. Yogata², K. Hatakeda^{2,3}, T. Yada², A. Miyazaki², K. Nagashima², R. Tahara², Y. Sugiyama², A. Nakano², T. Ojima², Y. Hitomi^{2,3}, K. Kumagai^{2,3}, M. Nishimura², M. Abe², T. Usui², J.-P. Bibring⁴, C. Pilorget⁴, V. Hamm⁴, R. Brunetto⁴, D. Loizeau⁴, L. Riu⁴, T. Le Pivert-Jolivet⁴,

¹University of Tokyo, Japan, ²Institute of Space and Astronautical Science, JAXA, Japan, ³Marine Works Japan, Yokosuka, Japan, ⁴Institut d'Astrophysique Spatiale, Universite Paris-Saclay, Orsay, France.

Introduction

Hayabusa2 brought back about 5.4 g of Ryugu samples (chamber A: surface samples, chamber C: excavated samples) from the C-type asteroid Ryugu in 2020, and the initial description of the returned samples is ongoing at the Curation Center of the Institute of Space and Astronautical Science (ISAS), JAXA [1][2]. In the initial description, measurements with a near-infrared hyperspectral microscope MicrOmega and spectral analysis are ongoing, and we have developed a fitting analysis method for the asymmetric absorption bands [3].

MicrOmega is a near-infrared hyperspectral microscope developed by the Institut d'Astrophysique Spatiale (IAS) in France, characterized by its ability to acquire spectral data over an area of approximately 5 mm square with a resolution of 22.5 $\mu\text{m}/\text{pix}$ at 0.99-3.65 μm [4]. The measurement results to date have indicated a relatively deep absorption band at 2.7 μm which is thought to originate from the OH group and a slope around 2.0 μm , as common features of most of the Ryugu samples [2].

Methods

In our previous work [3], we developed a fitting analysis method with four Gaussian functions to achieve a more physically accurate analysis for the characteristic 2.7 μm asymmetric absorption band of Ryugu samples. In this study, we applied a fitting analysis with six Gaussian functions after applying baseline estimation and smoothing where necessary [5]. We also applied a fitting analysis with linear functions to the slope around 2.0 μm , which is a characteristic of Ryugu samples, to determine the magnitude of the slope [6].

The spectroscopic data were used in the MicrOmega-Curation DARTS Server (chamber A: 95 spectra, chamber C: 62 spectra).

Results

The results of the fitting analysis are shown in Figure 1 (left) with each Gaussian function, composite waveform, and residuals for the asymmetric absorption band of Ryugu sample A0007 at 2.7 μm . Each of the six Gaussian functions is named f1 to f6 from the short wavelength side, where their peak wavelengths are f1: 2.713 μm , f2: 2.748 μm , f3: 2.786 μm , f4: 2.831 μm , f5: 2.874 μm , and f6: 3.036 μm , respectively.

The results of the fitting analysis using linear functions are shown in Figure 1 (right) for the slope around 2.0 μm .

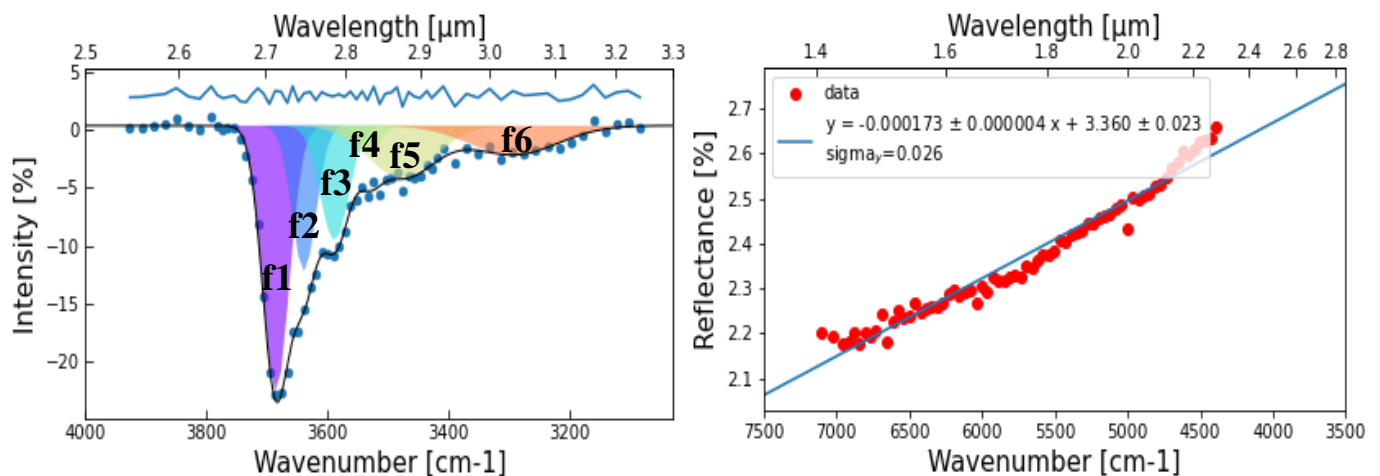


[Figure 1: Results of fitting analysis of spectral data measured by MicrOmega with Ryugu sample A0007 (left: fitting analysis by six Gaussian functions for the asymmetric absorption band at 2.7 μm , right: fitting analysis by linear functions for the slope around 2.0 μm)]

Discussion

The relationship between peak wavelength and depth of the 2.7 μm absorption band (Figure 2 left) shows that the chamber A sample is split into two groups: α , with a shorter peak wavelength and greater depth, and β , with a longer peak wavelength and smaller depth. In contrast, the chamber C sample does not exhibit a clear tendency for such division into two. This dichotomous distribution for the chamber A sample is also present for f1, f2, and f4. Therefore, f1, f2, and f4 are considered to be derived from the same functional OH group. On the other hand, f3, f5, and f6, which do not exhibit dichotomous distribution in the chamber A sample, may be derived from carbonate, carbonyl, and NH groups, respectively, based on the position of the peak wavelengths [2][4][8].

Based on the results of the slope analysis around 2.0 μm , β tends to have a larger absolute value of slope than α , despite within the standard error range, as shown in Figure 2 right (α : $(1.79 \pm 0.501) \times 10^{-4} [\%/ \text{cm}^{-1}]$, β : $(1.84 \pm 0.576) \times 10^{-4} [\%/ \text{cm}^{-1}]$, C: $(1.81 \pm 0.496) \times 10^{-4} [\%/ \text{cm}^{-1}]$). Since the slope of the spectrum is considered to reflect the effect of space weathering, β may be affected by greater space weathering than α [9].

Therefore, in the relationship between peak wavelength and depth in the 2.7 μm absorption band (Figure 2 left), the longer wavelength and smaller depth of the peak position for β compared to α may be due to the greater effect of bond scission related to the OH group caused by space weathering.

In summary, the Ryugu return samples that were measured by MicrOmega were classified into three major groups: α and β in chamber A, and C in chamber C. Also, each of them is considered to be affected by greater space weathering in the order of $\alpha < C < \beta$, respectively.

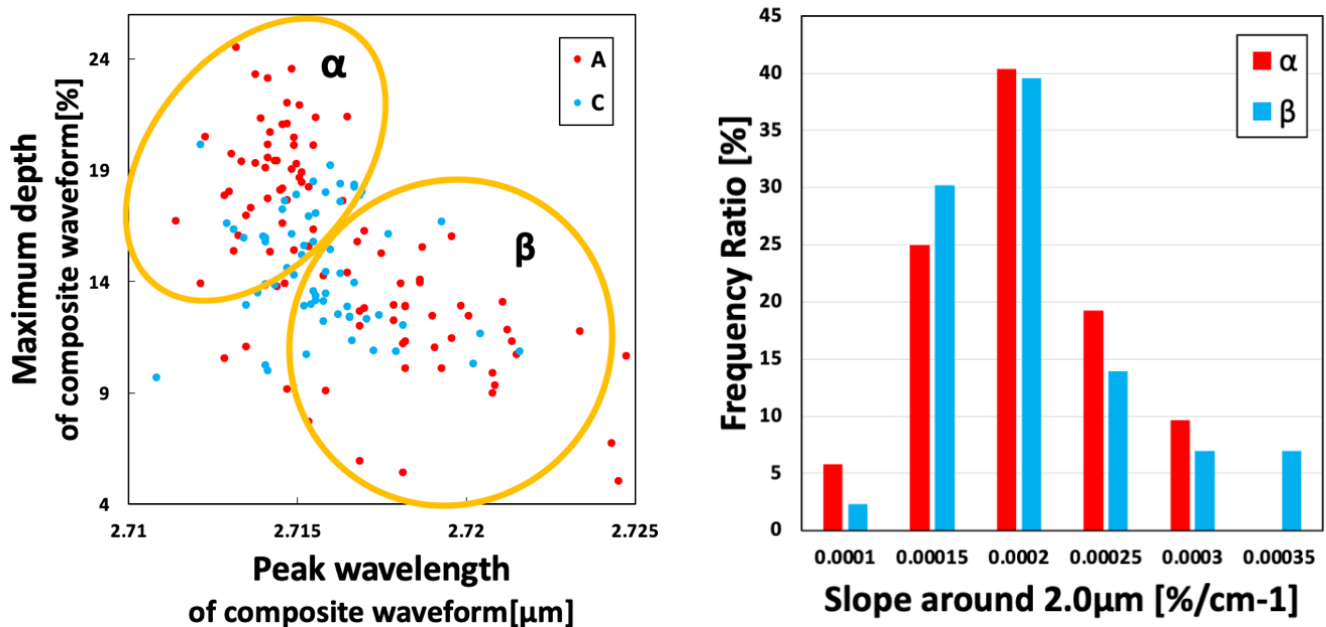


[Figure 2: Left: Relationship between peak wavelength and depth of the composite waveform in the 2.7 μm absorption band, right: slope magnitude around 2.0 μm (chamber A sample: α and β only) versus Frequency ratio]

References

- [1] Yada, T. et al. 2021. Nature Astronomy 6:214.
- [2] Pilorget, C. et al. 2021. Nature Astronomy 6:221.
- [3] Furukawa, S. et al. 2023. Abstract #PPS03-10. JpGU2023.
- [4] Bibring, J.-P. et al. 2017. Space Science Reviews 208:401.
- [5] Eilers, P. H. C. & Boelens, H. F. M. 2005. Leiden University Medical Center report 1:5.
- [6] Furukawa, S. et al. 2023. Abstract #OA-06. JSPS2023 (in Japanese).
- [7] Le Pivert-Jolivet, T. et al. 2022. Abstract #6255. MetSoc2022.
- [8] Loizeau, D. et al. 2023. Nature Astronomy 7:391.
- [9] Morota, T. et al. 2020. Science 368:654.

NH-rich grains detected by MicrOmega in the Ryugu returned samples

Jiang T.^{1,2}, Pilorget C.¹, Loizeau D.¹, Bibring J.-P.¹, Yogata K.³, Hatakeda K.^{3,4}, Brunetto R.¹, Le Pivert-Jolivet T.¹, Lantz C.¹, Riu, L.^{1,5}, Yada T.³, Okada T.^{3,6}

¹IAS, Université Paris-Saclay, CNRS, France, ²School of Earth Sciences, China University of Geosciences, Wuhan, China,

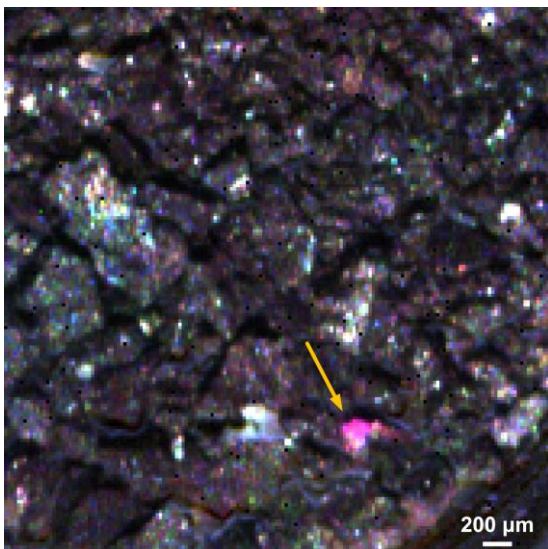
³ISAS Sagamihara Japan, ⁴Marine Works Japan, Ltd, Yokosuka Japan, ⁵ESAC, ESA, Madrid, Spain,

⁶University of Tokyo, Tokyo, Japan

NH-rich compounds have been reported on Ceres [1, 2], Comet 67P [3, 4], and other primitive asteroids [5, 6] thanks to NIR observations. The proposed compositions include ammonium salts, ammoniated phyllosilicates, and ammonia-bearing organics. Investigating their composition and relation with other components can tell us information on how they were formed, what was the environment, and may also indicate the transfer of some volatiles in the Solar System. Similarly, NIR observations of the Ryugu samples obtained at the millimeter scale showed that they exhibit a $\sim 3.06 \mu\text{m}$ shallow feature that was tentatively attributed to NH-rich compounds that would be present at a small scale and spread over the collection [7, 8]. However, one grain (a few hundred microns in size) exhibited a much stronger $\sim 3.06 \mu\text{m}$ feature, coupled with additional features such as $\sim 3.24 \mu\text{m}$ and $\sim 2.72 \mu\text{m}$ bands [7]. Its reflectance ($\sim 10\%$) was also much higher than that of the typical matrix (2-3%). Here we report on our latest analyses to identify grains/inclusions with similar properties (both showing $2.7 \mu\text{m}$ and $3.06 \mu\text{m}$ absorptions).

MicrOmega is an infrared hyperspectral microscope installed inside the Hayabusa2 Curation Facility. It covers the spectral range $0.99\text{-}3.65 \mu\text{m}$ with a pixel size of $\sim 22.5 \times 22.5 \mu\text{m}^2$, and a total field of view covering $\sim 5 \times 5 \text{mm}^2$. From 2021 to July 2023, MicrOmega has measured almost half (in weight) of the Ryugu returned samples in the form of aggregates (~ 50) (small subsets extracted from the bulks, a few tens of mg each) and individual (mm-sized) grains (>500). Here we focus on the aggregate samples, which give access to a large number of grains spread as a thin layer in the sample holders. We use the average spectrum of the grain from the first NH-rich detection in [7] as a reference. After removing the continuum from 2.5 to $3.2 \mu\text{m}$, we calculate the similarities between the reference spectrum and spectra from each pixel, then select the enriched regions with high similarity (strong $3.06 \mu\text{m}$ and $2.7 \mu\text{m}$ bands) and check for consistency at different orientations to avoid biases.

The detections of such areas are quite rare: among all the aggregate samples, we have detected 10 regions of interest (ROIs). The reflectance of the ROIs is generally higher than that of the surrounding material, mostly ranging from $\sim 5\%$ to $\sim 10\%$ but can be up to 15% . The size of the ROIs varies from $\sim 100 \mu\text{m}$ to $\sim 400 \mu\text{m}$, their shape can be from relatively rounded to elongated. Figure 1 shows an RGB image (R $2.01 \mu\text{m}$, G $2.72 \mu\text{m}$, B $3.45 \mu\text{m}$) of an aggregate sample, the pink color area is the ROI, and its average spectrum shows very strong $2.7 \mu\text{m}$ absorption ($\sim 50\%$) and $3.06 \mu\text{m}$ feature ($\sim 10\%$). We will report on the spectral heterogeneity within the ROIs at pixel scale and between different ROIs, in particular their variations in band position, depth, and shape. Since most of the ROI are present as inclusions instead of isolated grains, we will also present their relationship with the surrounding materials.



Such detections highlight the presence of a few particular grains in the Ryugu returned samples that may contribute to understanding the origin and evolution of the N-bearing material in Ryugu's parent body.

Figure 1. RGB image of an aggregate-sample (Sample ID: A0481). R $2.01 \mu\text{m}$, G $2.72 \mu\text{m}$, B $3.45 \mu\text{m}$. The pink region pointed by the yellow arrow is the NH-rich ROI.

References [1] King et al., 1992. *Science* 255, 1551-1553. [2] De Sanctis et al., 2015. *Nature*. 528, 241-244. [3] Poch et al., 2020. *Science*. 367 eaaw7462. [4] Raponi et al., 2020. *Nature Astronomy*. 4, 500-505. [5] Takir and Emery 2012. *Icarus*. 219, 641-654. [6] Rivikin et al., 2022. *Planetary Science Journal*. 3.153 [7] Pilorget et al., 2022. *Nature Astronomy*. 6, 221-225. [8] Yada et al., 2022. *Nature Astronomy*. 6, 214-220.

Nanoscale spectroscopic and microscopic investigation of Ryugu samples

Mehmet Yesiltas¹, Timothy D. Glotch², Yoko Kebukawa³, Paul Northrup², Bogdan Sava⁴, Yasin Durmaz⁴

¹*Kirklareli University, Turkey*, ²*Stony Brook University, USA*, ³*Tokyo Institute of Technology, Japan*, ⁴*Attocube Systems, Germany*

Carbonaceous asteroids are leftover materials from the early solar system. Having escaped harsh planetary processes, they provide clues to understanding the planet formation processes as well as the origin and evolution of the early solar system. The Hayabusa2 spacecraft returned the first samples from the carbonaceous asteroid Ryugu [1,2]. In addition to abundant phyllosilicates (~64–88 vol%), carbonates, sulfides, and magnetite [3], the returned samples provide uncontaminated pristine organic compositions. Macromolecular insoluble [4] and soluble organic matter as well as presolar silicate grains [6,7] have been reported in the Ryugu particles. Extraterrestrial organic matter is typically submicron in size (50–500 nm), and most organic compounds are even smaller [8,9]. Conventional IR methods fail to detect spectral signatures of nanoscale organic matter in extraterrestrial samples because of their insufficient spatial resolutions and other technical limitations.

In this study, we investigated the mineralogy and organic matter content of two Ryugu particles, A0030 (from TD1, chamber A) and C0034 (from TD2, Chamber C), using scattering-type near-field optical microscopy (s-SNOM)-based nanoscale Fourier transform infrared (nano-FTIR) spectroscopy, pseudoheterodyne (PsHet) nanoscale imaging, micro-Raman spectroscopic imaging, and synchrotron-based X-ray microprobe analyses.

Our results show that the two Ryugu particles contain different silicate minerals and organic-rich compositions. The spatial distributions of chemical functional groups and their relations with other components also differ in the studied Ryugu particles. Our results indicate various stages of aqueous alteration and thermal metamorphism processes for Ryugu. The identification of abundant nanoscale organic molecules within the Ryugu grains that could not be identified via micrometer-scale investigations emphasizes the importance of using nanoscale nondestructive methods for studying primitive solar system materials, such as Ryugu particles and those that will be returned soon (such as OSIRIS-REx and MMX samples).

References

[1] Tachibana et al. 2022. *Science* 375, 1011–1016. [2] Yada et al. 2022. *Nat Astron* 6:214–220. [3] Ito et al. 2022. *Nat. Astron.* 6:1163–1171. [4] Yabuta et al. 2023. *Science* 379, eabn9057. [5] Naraoka et al. 2023. *Science*, 379, eabn9033. [6] Barosch et al. 2022. *The Astrophysical Journal Letters*, 935,1. [7] Nguyen et al. 2023. *Science Advances*, 9(28), eadh1003. [8] Garvie et al. 2008. *Meteoritics & Planetary Science* 43, 899-903. [9] Yesiltas et al. 2021. *Scientific Reports* 11, 11656.

Spectroscopic Evidence of Parent Body Aqueous Alteration on Ryugu Sample A0112

A. Maturilli¹, E. Bonato^{1,2}, J. Helbert¹, G. Alemanno¹, Van den Neucker¹, S. Schwinger¹, M. Baqué¹, M. Hamm³, M. D'Amore¹, C. Hamann², K. Mahlow², M. Patzschke³, A. Greshake², L. Hecht^{2,3}

1German Aerospace Center (DLR) – Institute of Planetary Research, Rutherfordstrasse 2, 12489 Berlin, Germany,

2Museum für Naturkunde - Invalidenstrasse 43, 10115 Berlin, Germany,

3Freie Universität Berlin – FB Geowissenschaften – Institut für Geologische Wissenschaften Planetologie and Fernerkundung – Malteserstr. 74 – 100 – 12249 Berlin, Germany.

The Japanese Hayabusa2 sample return mission successfully retrieved fragments from the near-Earth C-type carbonaceous asteroid Ryugu (162173). These fragments share similarities in composition with the Ivuna meteorite, indicating a potential classification as a primitive CI-type asteroid [1]. Among the collected samples, the piece A0112 was sent for spectral analyses at the Planetary Spectroscopy Laboratories (PSL) at the German Aerospace Center (DLR) in Berlin.

The A0112 piece is a relatively large sample collected from the first touchdown site [1]: it weighs 5,1 mg and is 3046x1823 μm in size. The sample was contained in a nitrogen-filled sample holder, free of any form of terrestrial contamination after its retrieval from the asteroid. In order to preserve the sample from external contamination, such as the atmosphere, the first set of analyses were performed with the grain sealed within its sample holder. These analyses employed micro-infrared spectroscopy and Raman micro-spectroscopy. In addition, High-resolution 3D images were taken of multiple sides of the grain with the digital microscope Keyence VHX-7000 and VHX-7100 observation system, which allowed a global view of its surface morphology and topography. This approach enabled the determination of the sample's bulk composition and mineralogy beneath the glass without being influenced by terrestrial alteration.

More than 50 point-localized infrared spectroscopy measurements were performed on the A0112 grain with the Hyperspectral Bruker Hyperion 2000 MicroFTIR to assess the general mineralogy of the fragment through the glass window of the sample holder. MIR (1.3 – 5 μm) reflectance point measurements consisted of 1000-2000 scans at an optical magnification of 15x and a resolution of 4 cm^{-1} . VNIR reflectance spectra were also taken to cover the full spectral range. Raman spectroscopy under neutral atmosphere with the WiTec Alpha 300 confocal Raman microscope [2] was used for organic matter and mineral identification, and to generate elemental maps of the grain.

Through the use of FTIR spectrometers (three identical Bruker Vertex 80V) and a special manufactured sample holder it was possible to measure bi-directional reflectance bulk sample spectroscopy of sample A0112 completely under vacuum in the whole spectral range from UV to FIR (0.25 μm to at least 25 μm spectral range).

From the processed images, the sample can be described as a mostly dark fragment with a few micron-sized, bright inclusions on most of its faces. Micro-FTIR measurements revealed an abundant presence of secondary minerals such as phyllosilicates throughout the sample, with a localized area of approximately 30 μm rich in carbonates. This carbonate-rich region was identified as dolomite due to specific absorbance bands at wavelengths of 1.90, 2.21, 2.73, and 4.4 μm , as well as two distinctive sets of doublets at 3.33, 3.47 μm and 3.81, 3.95 μm [1, 3]. Raman spectroscopy measurements also confirmed the presence of dolomite with spectral bands at 175, 300, 727, and 1098 cm^{-1} . This dolomite inclusion appears to be associated with a vein in the grain. The investigation of hydrated minerals formed through aqueous alteration on the parent body provides valuable insights into the evolution of materials characterizing Ryugu and the protoplanetary disk. The presence of carbonates is particularly significant, suggesting the presence of liquid water within the asteroid, which could potentially play a role in delivering water to Earth or other planets [4]. Furthermore, these results confirm that in-situ point measurements, to localize hydrated minerals and organic matter, are still achievable through the glass window of a sample holder.

The identification of carbonates in the sample provides significant evidence of aqueous alteration processes that occurred on Ryugu's parent body.

References

[1] Nakamura, T. et al. (2022) *Science*. [2] Böttger, U. et al. (2013) *LPS XVIV*, Abstract #2092. [3] Loizeau, D., et al. (2023) *Nat Astron.* 7, 391-397. [4] Ito, M. et al. (2022) *Nat. Astron.* 6, 1-9.

Acknowledgements

The research results have been obtained through the cooperation between DLR and JAXA.

Nitrogen, neon, and argon analysis of a single Ryugu grain by step-heating

J. Gamblin¹, E. Füri¹, B. Marty¹, L. Zimmermann¹, D.V. Bekaert¹, and M.W. Broadley¹

¹Université de Lorraine, CNRS, CRPG, Nancy, France

Introduction: Carbonaceous chondrites are primitive, volatile-rich meteorites, considered to originate from C-type asteroids, which may have contributed to Earth's volatile budget. Studying these objects is key to understand the origin of Earth's volatiles, but terrestrial weathering makes it difficult to distinguish between primary and secondary features. In December 2020, JAXA's Hayabusa2 mission returned to Earth 5.4 g of regolith collected on the C-type asteroid (162173) Ryugu, permitting the analysis of material not altered by terrestrial weathering [1]. The first analyses of noble gases and nitrogen were performed by the 'initial analysis volatile team' [2-3], providing key information about Ryugu, especially its formation, composition, and alteration history. Noble gases were found to be mainly of primordial and presolar origin, with variable contributions from solar wind and cosmogenic components. Nitrogen was present in lower abundances (700 to 900 ppm [2-3]) than in typical CI chondrites, with $\delta^{15}\text{N}$ values ranging from 0.0 ± 0.4 ‰ [2] up to $+43\pm 4$ ‰ [4], indicating sample heterogeneity and the presence of at least two carrier phases: a N-rich phase with $\delta^{15}\text{N}$ up to $+70$ ‰ and a N-depleted phase with $\delta^{15}\text{N}$ near 0 ‰.

Sample and experimental method: For this study, we targeted grain A-0164 (2.6 mg), which was sampled during the first touchdown on the asteroid and corresponds to surface material. The grain was analyzed at the Centre de Recherches Pétrographiques et Géochimiques (CRPG, Nancy, France) by step-heating with a CO₂ laser. By performing a large number of extraction steps, various components of nitrogen and noble gases, carried by different phases, can be distinguished. A total of 85 heating steps were performed at increasing laser power to successively analyze the different phases carrying nitrogen and noble gases. Nitrogen, neon, and argon abundances and isotope ratios were analyzed at each step using a Nu Instruments Noblesse HR mass spectrometer, a state-of-the-art instrument for multi-collection, high-precision, static-vacuum analysis.

Preliminary results:

Noble gases. Neon was mainly released at low temperature steps, whereas Ar was extracted over a wide temperature range. The sample presents a mainly solar wind-like isotopic composition for noble gases, as shown for neon in Figure 1. Step heating allowed us to identify other components, including primordial and presolar components (possibly phase Q and/or HL), as well as a minor cosmogenic contribution.

Nitrogen. Nitrogen is present in higher abundance (1219 ± 113 ppm) than in previous studies, with a bulk $\delta^{15}\text{N}$ value of $+24.4\pm 0.1$ ‰, with significant variations during successive extractions ($+1.0\pm 1.0$ ‰ to $+65.8\pm 1.1$ ‰), pointing to the presence of at least four N-carrier phases.

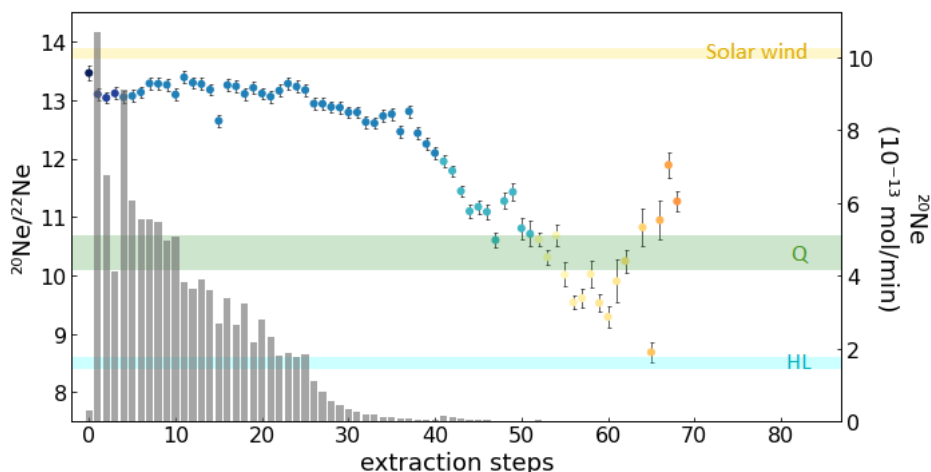


Figure 1. Ne ($^{20}\text{Ne}/^{22}\text{Ne}$) isotope ratio (colored circles) and ^{20}Ne abundance (gray histogram) measured for each of the 85 extraction steps at increasing laser power. The Ne isotopic compositions of the solar wind, Phase Q, and Ne-HL are shown for comparison.

References

- [1] Tsuda Y. et al. 2020. *Acta Astronautica* 171 42:54. [2] Okazaki R. et al. 2023. *Science* 379 6634. [3] Broadley M.W. et al. 2023. *Geochemica et Cosmochimica Acta* 345 62:74. [4] Yabuta H. et al. 2023. *Science* 379 6634.

Chemical composition and variability of Ryugu samples, CI chondrites and Kainsaz assessed by quadrupole ICP-MS analyses

Frank Wombacher

Institute of Geology and Mineralogy, Universität zu Köln, 50674 Köln, Germany.

Introduction. The similar relative abundances of non-atmophile elements between the Sun and rare CI chondrites suggest that CI chondrites represent the most primordial meteorites available for laboratory analyses. Samples returned from asteroid Ryugu by the Japanese Hayabusa2 mission resemble CI chondrites, were not altered on Earth, but affected by aqueous alteration [1-4].

This study aims to provide additional data on the elemental compositions and variabilities and representative sample masses for CI chondrites, Ryugu and the Kainsaz CO3 chondrite.

Samples. Data was obtained for five ~3 mg Ryugu samples from chamber A (1st touchdown), seven ~3 mg chips and 3, 4 and 50 mg bulk powder samples from the Kainsaz CO3 chondrite and ~50 mg powder aliquots from the CI chondrites Ivuna (2 x), Orgueil (3 x) and Y-980115. For quality control, Allende Smithsonian reference powder, JB-2, BHVO-2 and ~3 mg powder test samples from Allende, Ivuna, JB-2 as well as a Perkin Elmer multi element solution were analyzed.

Methods. The ~3 mg samples were digested in HF-HNO₃ at hotplates. The Ryugu samples and 5 out of 7 chips from Kainsaz were not ground before digestion to avoid material loss. Most 50 mg samples were digested in Parr pressure digestion vessels. Methods for quadrupole ICP-MS analyses and data evaluation are given in [5]. Samples were 4000-fold diluted and Rh and Re were used as internal standards. Most elements were determined in kinetic energy discrimination mode using He as a cell gas with CeO/Ce ~ 0.4%. (1.7% in standard mode). For each sample set, three to seven measurement sessions were run. Outliers were removed if > 4 sd and Ta data was rejected from four sessions that yielded unusual low Ta values. Four-point matrix matched calibration [5, 6] yielded a median correlation coefficient of 0.9999 as calculated from all elements and sessions. Repeatability judged from 121 analyses of Ivuna was 3.2% on average with Mn, Co, Cu, Rb, Y, Sr, Pb < 1.5% and 23% for Be being the worst case. In order to rigorously control blank contributions, seven blanks each were prepared along with the Ryugu and Kainsaz samples and four blanks with the 50 mg CI chondrite samples. Median blanks were subtracted. Maximum blanks for ~3 mg samples were: Ryugu and Ivuna: As, Sn and Sb 2 to 6%; Nb 10%; W 16%; Mo 29%; Kainsaz: Zn, As, Cd and Sn <3%; W 15%; JB-2: Zn, Nb, Sn and W 5 to 6 %; Mo 35%.

Results. Most CI chondrite, Allende Smithsonian, JB-2, BHVO-2 and Perkin Elmer solution data agrees within 10 to 20% with reference data [e.g., 7-13]. However, due to problems related to the calibration solutions (as observed in [6]), Sr, Mo, Sb, Ho, Ta, W and Bi are systematically too low. For the basalt reference samples, S, Se, Ag, Ir and Pt were not quantified and Ti, Cr, Ni, Te and As are off by about 20 to 60%. Except for U in Ivuna, results for 3 mg test samples agreed with results for the corresponding 50 mg samples to within better than 10% or within 10 to 20% for Se, Ag, Te (Ivuna), S, Ag, Ir, Pt (Allende) and As and Bi for JB-2 (S, Se, Ag, Ir and Pt not quantified in basalt reference materials). Three mg chips from Kainsaz display some heterogeneity and scatter around the data for the 50 mg bulk sample. However, the 50 mg bulk sample and 3 and 4 mg aliquots from the same powder display fractionated REE. The REE Kainsaz data shows that nugget effects in chondrites can affect larger samples more significantly than small mg samples. The Kainsaz 3 mg chip data displays reproducible, sometimes large enrichments in As, Sb and Pb of unknown origin.

Discussion. Ivuna and Mg normalized data reveal the following: Many elements in CI chondrites agree within ~2 %. Two out of three Orgueil samples display 20 to 50% enrichments in some refractory elements, most notably Zr, Hf, Th and Ba while Y-980115 is depleted in Cd, In, Tl and Bi as observed previously [5]. One Ryugu sample matches the CI chondrite REE pattern, the other four samples are enriched in light over heavy REE with variable REE/Mg. Two Ryugu samples are clearly enriched in Ca and Sr, one in Mn and Fe. Only one out of five Ryugu samples displays contamination of Ta from the projectile. Overall, the 3 mg Ryugu samples from chamber A display a clear CI chondrite affinity, but their chemical compositions are obviously affected by aqueous alteration as previously observed. For CI chondrites, Kainsaz and Ryugu, we estimated the representative sample mass needed to obtain elemental abundances to within 5% at the 95% confidence level, using the formula given in [10]: Representative sample mass = test portion mass * (standard deviation / (mean * standard error of the mean))² * student-t distribution factor.

For CI chondrites (n=4), the median representative sample mass corresponds to 452 mg; for ten elements, including Na, Zr, Hf, Ba, La, Ce and U, the representative sample mass was above 1 g. For Kainsaz, the median representative sample mass equals 74 mg and is above 1 g for S, As, Cd, Sb, Cs and Pb only. The median representative sample mass calculated for Ryugu

corresponds to 99 mg with Mn, Ca and P being the least homogeneous elements with calculated representative sample masses of about 300, 400 and 500 mg. A complete table can be obtained from the author.

Acknowledgements

JAXA for sampling Ryugu and the incredible opportunity to work on these samples. The National Institute of Polar Research (Naoya Imae) for Y-980115, the Smithsonian Institution (Tim McCoy and Glenn MacPherson) for the Allende reference powder, the NHM London (Helena Bates, Natasha Almeida) for Ivuna and Orgueil, the MNHM in Paris (Matthieu Gounelle) and the Universität Münster (Addi Bischoff) for Orgueil. Carsten Münker for lab use; Claudia Funk and Ninja Braukmüller for support in the lab.

References

[1] Yokoyama T. et al. (2022) *Science* 379, [2] Nakamura T. et al. (2022) *Science*, 379, [3] Ito M. et al. (2022) *Nature Astronomy* 6, 1163–1171, [4] Greenwood R. et al. (2023) *Nature Astronomy* 7, 29–38, [5] Bates H. C. et al. (2023) *Meteoritics & Planetary Science*. [6] Braukmüller N. et al. (2018) *Geochimica et Cosmochimica Acta* 239, 17–48, [7] Lodders K. (2021) *Space Science Reviews* 217, 44, [8] Barrat J.A. et al. (2012) *Geochimica et Cosmochimica Acta* 83, 79–92, [9] Jarosewich E. et al. (1987) *Smithsonian Contributions to the Earth Sciences* 27, 49, [10] Stracke A. et al. (2012) *Geochimica et Cosmochimica Acta* 85, 114–141, [11] Wang Z. and Becker H. (2014) *Geostandards and Geoanalytical Research* 38, 189–209, [12] Jochum K. P. et al. (2005) *Geostandards and Geoanalytical Research* 29, 333–338, [13] Braukmüller N. et al. (2020) *Geostandards and Geoanalytical Research* 44, 733–752.

The Mineralogy of Asteroid Ryugu and its Relationship to Highly Altered Extraterrestrial Materials

Ashley King¹, Sara Russell¹, Martin Suttle², Catherine Harrison¹,
Paul Schofield¹, Helena Bates¹, and the Hayabusa2 “Stone” team

¹*Natural History Museum, London, UK (a.king@nhm.ac.uk)*

²*The Open University, Milton Keynes, UK*

The Hayabusa2 mission returned to Earth with ~5.4 g of material collected from two sites on the surface of the Cb-type asteroid (162173) Ryugu [e.g., 1]. In hand specimen, Ryugu particles are dark, often highly friable, and have bulk densities in the range of ~1.2 – 1.8 gcm⁻³ [2–4]. Most Ryugu particles examined to date are breccias consisting of an abundant (~80 – 90 vol.%) fine-grained (<1 µm) matrix of phyllosilicates (interlayered serpentine and saponite) in which coarser (~10’s – 100’s µm in size) grains, fragments, and clusters of oxides (~4 vol.%), sulphides (~3 vol.%), carbonates (~3 vol.%), and phosphates (<1 vol.%) are embedded [2–6]. Several CAI-like fragments (<30 µm) have been identified, as have small (<10 µm), rounded objects with characteristics, such as barred textures, related to melting and crystallisation in chondrules [e.g., 4, 7]. The mineralogy, petrography, and physical properties of Ryugu particles are consistent with them being having formed through near-complete, low temperature (<50°C) water-rock reactions during the first few million years of the Solar System [2–6].

If samples of Ryugu were to land on Earth as meteorites, we could classify them as petrologic type 1 [8]. Such materials were completely altered to secondary mineral assemblages by aqueous processing and contain various phyllosilicates, carbonates, sulphides, and magnetite. Type 1 materials are represented in four meteorite groups (CI, CM, CR, and CY), a handful of ungrouped chondrites (e.g., Flensburg [9]), as xenoliths within meteorites [e.g., 10], and as fine-grained micrometeorites [e.g., 11] and interplanetary dust particles (IDPs) [e.g., 12]. The mineralogy and chemistry of Ryugu particles are closely related to the CI1 (“Ivuna-like”) carbonaceous chondrites, except for the presence of sulphates and ferrihydrite in the latter, which are most likely terrestrial weathering products [13, 14]. However, type 1 samples exhibit a remarkably high diversity of starting materials and alteration conditions, with variations in mineralogy, textures, and oxygen isotopic compositions pointing towards multiple parent bodies. Despite type 1 materials being relatively rare in our collections, in part due to their fragile nature hindering survival during atmospheric entry, highly altered bodies appear to be common throughout the Solar System. These bodies could include primitive asteroids that accreted within the inner and/or outer Solar System, or transition objects such as Main Belt comets or D-type asteroids. Characterising the sources of type 1 materials through laboratory analysis of meteorites and Ryugu particles is therefore an important step towards understanding volatile reservoirs in the early Solar System.

References

- [1] Yada T. et al. 2021. *Nature Astronomy* 6:214. [2] Yokoyama T. et al. 2022. *Science* 379:abn7850 [3] Nakamura E. et al. 2022. *Proc. Jpn. Acad., Ser. B* 98:227. [4] Nakamura T. et al. 2022. *Science* 379:abn8671 [5] Ito M. et al. 2022. *Nature Astronomy* 6:1163. [6] McCain K. et al. 2023. *Nature Astronomy* 7:309. [7] Liu M-C. et al. 2022. *Nature Astronomy* 6:1172. [8] Russell S. et al. 2022. *Meteoritics and Planetary Science* 57:277. [9] Bischoff A. et al. 2021. *Geochimica et Cosmochimica Acta* 293:142. [10] Zolensky M. et al. 1996. *Meteoritics and Planetary Science* 31:484. [11] Kurat G. et al. 1992. 27th LPSC #747-8. [12] Aléon J. et al. 2009. *Geochimica et Cosmochimica Acta* 73:4558. [13] Gounelle M. & Zolensky M. 2001. *Meteoritics and Planetary Science* 36:1321. [14] King A. et al. 2020. *Geochimica et Cosmochimica Acta* 268:73.

Phosphorus, Calcium, and Sulfur in Two Ryugu Samples

George J. Flynn¹, and Paul Northrup²

¹Dept. of Physics, SUNY-Plattsburgh, 101 Broad St., Plattsburgh NY 12901 USA

²Stony Brook University, Stony Brook NY 11794

The Japanese Aerospace Exploration Agency (JAXA) Hayabusa2 spacecraft delivered the first samples of a primitive, carbonaceous asteroid to Earth. One of the objectives of the mission was to use the samples to characterize the formation and evolution of asteroid Ryugu or its parent body. The elemental compositions of some minerals, particularly apatite and, to a lesser extent, carbonate, are reflective of the composition of the fluid from which they were deposited. Because apatite, $\text{Ca}_{10}(\text{PO}_4)_6(\text{OH},\text{F},\text{Cl})_2$, can host F, OH, or Cl in the anion position, its composition is a sensitive probe of the halogen and water content of the hydrothermal fluid from which it was deposited. However, the apatite structure is capable of tolerating relatively large structural distortions, allowing for diverse element substitutions, making other minor and trace elements in apatite a sensitive probe of fluid composition. Carbonate can also be deposited in hydrothermal processing, and some trace element contents can reflect fluid composition. In hydrous meteorites the carbonate crystals are generally much larger than the apatite crystals, so zoning from the interior to the rim in larger carbonates can indicate changes in the fluid composition during the formation. Sulfur, which condenses from the cooling Solar Nebula as schreibersite, an Fe-sulfide, interacts with an oxidizing fluid to alter to Fe-sulfate. In crystals where this alteration is incomplete the sulfide/sulfate ratio can indicate the degree of oxidation by the fluid. We are employing two synchrotron-based instruments to characterize the P, Ca, and S in hydrous meteorites and Ryugu samples to characterize the hydrothermal event(s) that occurred on the Ryugu parent body.

Samples and Instruments: We were loaned five samples of asteroid Ryugu from the Hayabusa2 collection to perform mineral identification, XRF mapping, and P, Ca and S X-ray Absorption Spectroscopy (XAS). The X-ray Fluorescence Microprobe (XFM) Beamline 4-BM of the National Synchrotron Light Source II at Brookhaven National Laboratory is a versatile XRF microscope for the characterization of elemental abundances and chemical speciation in heterogeneous materials, characterizing the K-, or L-lines of the heavier elements. XFM is an imaging beamline designed for spatially-resolved XAS spectroscopy in the 4-20 keV energy range, with a user-tunable spot size from 2 to 10 μm . The Tender Energy Spectroscopy (TES) Beamline 8-BM of the NSLS-II at Brookhaven National Laboratory, has a user-tunable spot size, varying from $10 \times 25 \mu\text{m}$, with a flux of up to 10^{11} photons/s, down to $1 \times 2 \mu\text{m}$, with a flux of up to 10^9 photons/s. A helium sample environment permits XRF element mapping down to 1 eV, for abundance mapping of elements as light as Na. The tunable monochromator (2 to 5 keV) is optimized for K-edge XAS of elements from P to Ca.

Thus far, we have performed XRF maps of the polished surfaces of two of the five Ryugu samples using a 6 μm step size, at two energies; 7 keV, to provide maximum sensitivity for the low-Z elements while avoiding Fe K-edge fluorescence, in order to locate P-, S-, and Ca-bearing phases, particularly hydrothermal alteration products; and 13 keV, accessing heavier elements. The TES microprobe was then used to perform P, Ca, and S micro-XAS on targeted element hot-spots.

Results and Discussion: The initial XFM mapping (Figures 1 and 2) identified several likely effects of hydrothermal processing on the Ryugu parent body, some of which were characterized further by XAS using the TES instrument. The element distributions and associations were very similar to those we previously reported for several CM meteorites [1].

Figure 1: (left) Three color (P, S, Ca) map of Ryugu sample A0055-1, showing multiple Ca-rich grains (blue) including one a $>0.5 \mu\text{m}$ in size, many S hot-spots (green), a few Ca and P bearing grains (purple), and several small P hot spots more easily visible in the enlarged image. **Figure 2:** (right) Three color (P, S, Si) map of Ryugu sample A0026-02.

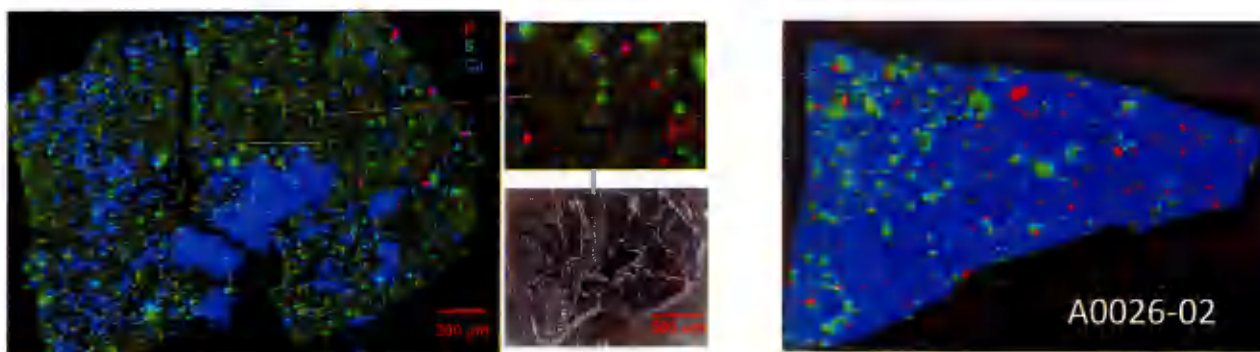
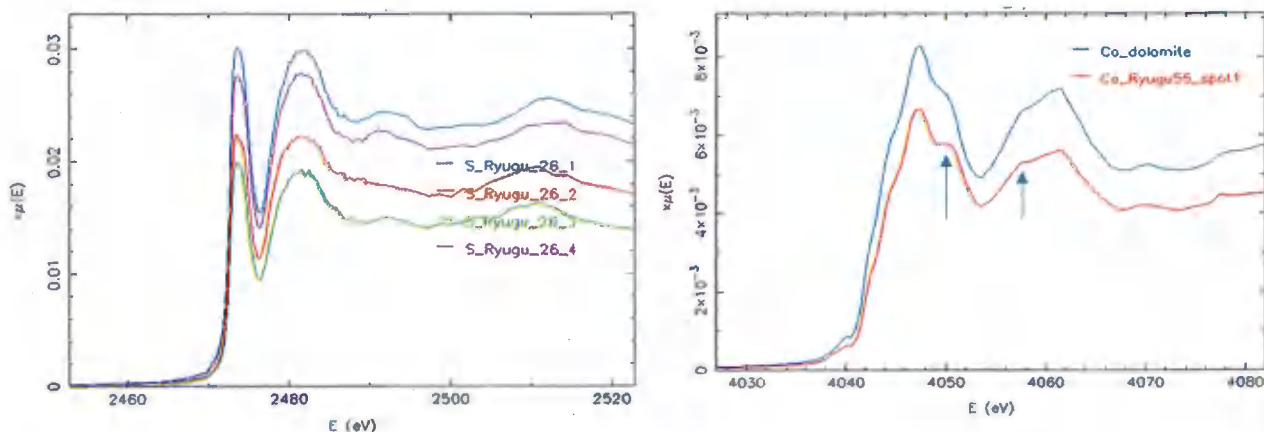


Figure 3: (left) P-XAS of three P hot-spots in A0055-1 that exhibit apatite spectra. Figure 4: (right) Ca-XAS of the large Ca hot-spot in A0055-1. The arrows indicate Ca-XANES features that distinguish dolomite (a bilayered carbonate) from calcite or magnesite (monolayered carbonates).



Apatite: Small P hot-spots were found in both A0026-02 and A0055-1. This P appeared in three distinct element associations (Figure 1): spots with both P and Ca (appearing pink), most likely apatite grains, small P hot-spots without Ca (red in the enlarged insert in Figure 1), which will be further analyzed by XAS, and spots with both S and P (yellowish green), potentially the high-P sulfides found in CM meteorites by Nazarov [2]. Three of the most intense P hot-spots in A0055-01 each have P-XAS spectra consistent with apatite (Figure 3), which is believed to be a hydrothermal alteration product in CM chondrites. These will be studied further to investigate their compositions.

Carbonate: Both samples contained Ca-bearing minerals, most likely carbonates >5 mm in size. One large carbonate, >0.5 mm in size, in A0055-1 was selected for further study. This large carbonate was identified as a dolomite by XAS (Figure 4). The dolomite area of interest contains a significant amount of Mn. Mn-XAS indicated the Mn is in the 2+ oxidation state, consistent with Mn in a bilayered carbonate. Element mapping of this large carbonate will be performed to search for zoning.

Sulfur: Sulfur hot-spots were identified in both samples. All four S hot-spots analyzed thus far in A0026-02 show XAS spectra consistent with pyrrhotite, with no detectable sulfate, consistent with models of Solar Nebular condensation which indicate that S condenses from the cooling gas as an iron-sulfide, resulting in the subsequent incorporation of this iron-sulfide into the Ryugu parent body. However, three of the largest S hot-spots in A0055-1 show mixed sulfide and sulfate in the same grain.

This suggests the sulfides in A0055-1 experienced significant hydrothermal alteration to produce sulfate. This observation is consistent with the alteration of sulfide to sulfate reported in six CM chondrites, where O-isotopic analysis indicated the alteration of sulfide to sulfate occurred on the asteroidal parent body (Airieau et al., GCA, 2005). We also identified an Fe-rich grain in A0055-1 that has an XAS spectrum consistent with magnetite, another mineral believed to be produced by interaction of Fe-metal with an oxidizing fluid. The presence of oxidized S in A0055-1 but only sulfide in A0026-02 may suggest different alteration histories for these two samples collected from the same site.

References

- [1] Flynn, G. J. et al. 2022. Abstract #6290, 85th Annual Meeting of The Meteoritical Society. [2] Nazarov et al. 2008. *Petrology*, 17, 101–123. [3] Airieau et al. 2005. *Geochimica et Cosmochimica Acta*, 69 (16), 4167–4172.

Paleomagnetic Evidence for Formation of Ryugu in the Distal Solar System

Elias N. Mansbach¹, Eduardo A. Lima¹, Michael Sowell², Joseph L. Kirschvink², Jodie B. Ream¹, Roger R. Fu³, Saverio Cambioni¹, Xue-ning Bai⁴, Benjamin P. Weiss¹

¹*Department of Earth, Atmospheric, and Planetary Sciences, Massachusetts Institute of Technology; Cambridge, MA, USA.*

²*Division of Geological and Planetary Sciences, California Institute of Technology; Pasadena, CA, USA*

³*Department of Earth and Planetary Sciences, Harvard University; Cambridge, MA, USA*

⁴*Institute for Advanced Study and Department of Astronomy, Tsinghua University; Beijing, China*

Paleomagnetic studies of meteorites have demonstrated that the solar nebula generated a magnetic field that likely played an important role in accretion during the early solar system [1]. The nebular field reached intensities of $54 \pm 21 \mu\text{T}$ at heliocentric distances of 1-3 AU [2] and $101 \pm 48 \mu\text{T}$ at 3-7 AU [3], and likely decayed by ~ 3 -4 million years (Ma) after the formation of calcium aluminum-rich inclusions (CAIs) [4-7]. However, with the possible exception of Tagish Lake and Wisconsin Range (WIS) 91600, these studies have been restricted to meteorites that formed at distances < 7 AU [8, 9]. Tagish Lake is of particular interest as its arrival to Earth from the asteroid belt implies that its parent body had been inwardly scattered, perhaps due to the formation and migration of the giant planets [9, 10].

The returned samples from asteroid (162173) Ryugu by the Hayabusa2 mission currently provide the best opportunity to study the nebular field in the distal solar system as the parent body may have experienced aqueous alteration at distances up to ~ 20 AU [11]. These particles are also high-quality targets for paleomagnetic investigations as they are: 1) in pristine condition since careful sample handling limits the possibility of magnetic and terrestrial contamination, which can lead to the creation of ferromagnetic minerals that mask the primary record of the particles, and 2) contain single-vortex framboidal magnetite which can retain magnetic records over the age of the solar system [12]. If the magnetite shows evidence of magnetization produced by an ancient field, the source of the field could have been the nebular field or a dynamo on the parent body. The latter case is of particular interest since this would imply that the parent body was partially differentiated with a carbonaceous chondritic crust [13]. Our current understanding of the lifetime of the nebula suggests that if the natural remanent magnetization (NRM) was acquired < 4 Ma, the source of the field was the nebula while a younger age would be indicative of a parent body dynamo. Initial Mn-Cr dating on carbonates that are thought to have formed at the same time as the magnetite yielded an age of 3.1 – 6.8 Ma after the formation of CAIs [14], but more recent dating on carbonates using the same dating system and improved calibrations suggests alteration occurred < 1.8 Ma after CAI formation [15].

An initial paleomagnetic study of two Ryugu particles concluded that the particles formed in a $> \sim 40$ - $400 \mu\text{T}$ nebular field [14, 16]. However, this magnetization may be post-sampling contamination because: 1) magnetite can have coercivities up to 300 mT, but the NRM of previously studied samples were unblocked to only 30 mT; 2) the previously studied samples had been analyzed with an electron microprobe which may have imparted a weak isothermal remanent magnetization (IRM); and 3) initial analysis of MasMag magnetometer data suggested that a boulder on Ryugu did not possess a measurable magnetization ($< 3 \times 10^{-6} \text{Am}^2 \text{kg}^{-1}$ at the m-scale) [17], yet the moment per unit mass of the reported samples is well above this limit ($2.14 \times 10^{-5} \text{Am}^2 \text{kg}^{-1}$).

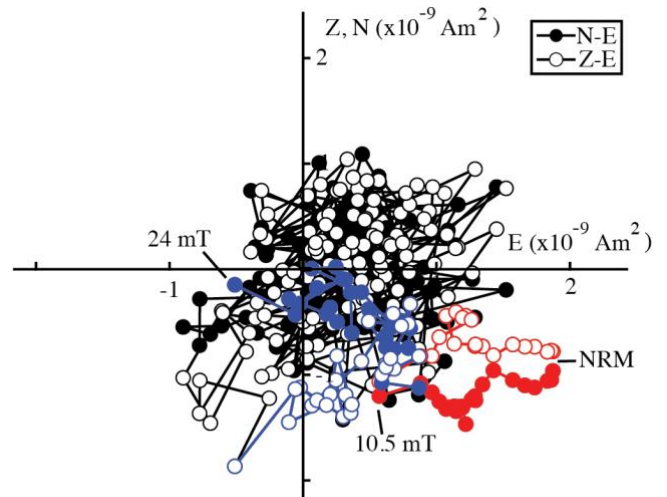


Figure 1: Orthographic projection of endpoints of NRM vectors on the northeast (N-E) and up-east (Z-E) planes during alternating field demagnetization of particle A0397. The LC component is shown in red, the MC component in blue, and the HC range in black. No components are observed > 24 mT.

To address the origin and nature of NRM in Ryugu, we conducted an additional paleomagnetic analysis on three previously unstudied Ryugu particles: A0397, C0085b, and C0006. These samples have not been previously studied using a microprobe or instrument with a strong magnet prior to our paleomagnetic analysis.

Alternating field (AF) demagnetization of the NRM in A0397 to 400 mT in steps of 0.5-1 mT revealed two non-origin trending components (Fig. 1), a low coercivity (LC) component that unblocked between 0 and 10.5 mT and a medium coercivity (MCs) component that unblocked between 11 and 23.5 mT. Above >24 mT is a high coercivity (HC) range in which no NRM components are observed. AF demagnetization of C0085b to 400 mT revealed three NRM components: an LC component that unblocked between 0 and 12.5 mT, and two MC components that unblocked between 13 and 19 mT and 19.5 and 23.5 mT, respectively. The second MC component was origin-trending. As before, above >24 mT is a HC range containing no stable NRM. AF demagnetization of C0006 to 80 mT conducted in 5-10 mT steps revealed a non-origin trending LC component that unblocked between 0 and 20 mT with no apparent components in the HC range above 20 mT.

Paleointensities estimated via the anhysteretic remanent magnetization (100 μ T bias field and 260 mT AC field) method for the LC components are 125.8 ± 28.9 (95% confidence interval, as for all below), 694.6 ± 145.5 and 44.8 ± 69.5 μ T for A0397, C0085b, and C006 respectively. The MC paleointensity for A0397 is 45.6 ± 31.6 μ T, while the two MC paleointensities for C0085b are 36.0 ± 44.4 and 62.3 ± 134.7 . Importantly, the HC paleointensities are all also consistent with null paleofields: 26.4 ± 30.6 μ T for C0085b, 7.4 ± 9.2 μ T for A0397, and 8.8 ± 16.4 μ T for C0006. This indicates that there are magnetic recorders with coercivities >24 mT in the particles that are capable of recording an ancient field but instead formed in the presence of a null or weak field.

Experiments conducted to determine the susceptibility of A0397 to viscous (VRM) remagnetization from prolonged exposure to an Earth-strength field indicate that the total moment gained over 4.5 years (initial sampling to NRM demagnetization) could account for 98% of the combined LC and MC components. We therefore suggest that the source of the LC and MC components in our samples are overprints, most likely a VRM from sitting in Earth's field and the field produced by spacecraft engines (10s of μ T [16]) since sampling. The non-origin trending nature of the two A0397 components further indicate that they are not primary. We suggest that the previously reported strong paleointensities are due to a weak IRM from the electron microprobe as ratio of NRM to saturating IRM is >10% and the components are not origin trending as well.

Our results have profound implications for the history of the Ryugu parent body. Taking the alteration age to be < 1.8 Ma after CAI-formation, our most stringent upper paleointensity limit of 7.4 μ T indicates that alteration occurred at heliocentric distances >15 AU for typical accretion rates during the main lifetime of the nebula of $10^{-8} M_{\odot} \text{ yr}^{-1}$ (and >5 AU for the lower range of accretion rates during the main lifetime of the nebula) (Fig. 2). Given Ryugu's current location (~1 AU), the parent body may have been scattered inward prior to catastrophic disruption, but after experiencing aqueous alteration, due to influence from the giant planets in a similar manner to that proposed for the parent body of Tagish Lake. Our results therefore provide further evidence that the formation and migration of the giant planets led to a major reconstructing of the organization of the solar system.

References

- [1] B. P. Weiss, X. Bai, R. R. Fu. 2021. *Science Advances*. 7. [2] R. R. Fu et al. 2014. *Science*. 346. [3] C. S. Borlina et al. 2021. *Science Advances*. 7. [4] R. R. Fu et al. 2020. *Journal of Geophysical Research: Planets*. 125. [5] J. Gattacceca, B. P. Weiss, M. Gounelle. 2016. *Earth and Planetary Science Letters*. 455. [6] B. P. Weiss et al. 2008. *Science*. 322. [7] B. P. Weiss et al. 2017. *Earth and Planetary Science Letters*. 468. [8] J. F. J. Bryson et al. 2020. *The Astrophysical Journal*. 896. [9] J. F. J. Bryson et al. 2020. *The Astrophysical Journal*. 892. [10] S. N. Raymond, A. Izidoro. 2017. *Sci Adv*. 3. [11] T. Hopp et al. 2022. *Science Advances*. 8. [12] Y. Kimura et al. 2023. *Sci Rep*. 13. [13] B. P. Weiss et al. 2010. *Space Science Reviews*. 152. [14] T. Nakamura et al. 2023. *Science*. 379. [15] K. A. McCain et al. 2023. *Nature Astronomy*. 7. [16] M. Sato et al. 2022. *Journal of Geophysical Research: Planets*. 127. [17] D. Hercik et al. 2020. *Journal of Geophysical Research: Planets*. 125.

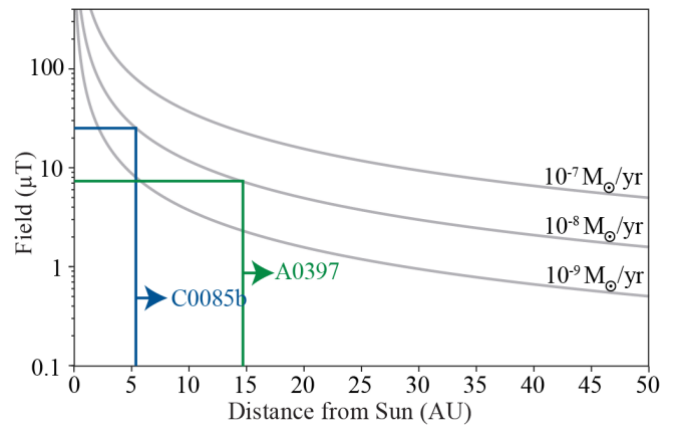


Figure 2: Predicted midplane nebular field assuming accretion around a solar mass star and that the nebular field and disk rotation are aligned. Accretion rates are given at the right-hand side for each curve. Colored lines represent constraints on heliocentric distance at which aqueous alteration occurred based on upper paleointensity limits from particles C0085b and A0397.

Experimental Constraints on the Concentration of Dirac Magnetic Monopoles in Primordial Material returned from Asteroid Ryugu by JAXA's Hayabusa2 Mission

Joseph L. Kirschvink^{1,2}, Michael Sowell¹, Chisato Anai², Atsuko Kobayashi^{1,2}, Yuhji Yamamoto², Elias Mansbach³, Eduardo Lima³, Masahiko Sato⁴, Chie Kato⁵, Hiroshi Ooguri^{1,6}, Tadayuki Takahashi⁶, Thomas Edward Melia⁶, Alexander Kusenko^{6,7}, Volodymyr Takhistov^{6,8}, Tomohiro Usui⁹

¹California Institute of Technology, Pasadena CA, USA

²Kochi Marine Core Research Institute, Kochi University, Japan

³Massachusetts Institute of Technology; Cambridge, MA, USA

⁴University of Tokyo, Tokyo, Japan; ⁵Kyushu University, Fukuoka, Japan

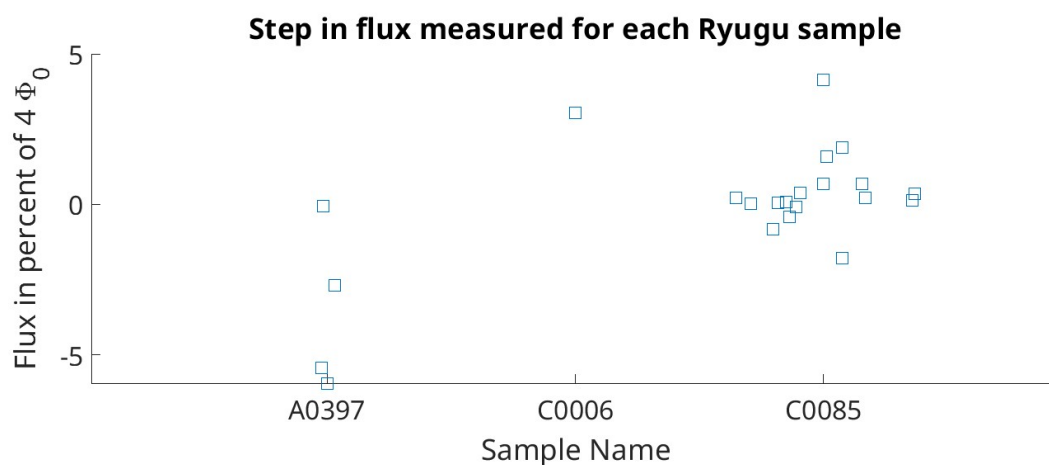
⁶Kavli Institute of Physics and Mathematics of the Universe, University of Tokyo, Tokyo, Japan

⁷University of California at Los Angeles, Los Angeles, CA, USA

⁸High Energy Accelerator Research Organization (KEK), Tsukuba, Japan

⁹JAXA, Kanagawa, Japan

In 1931, Dirac postulated the existence of elementary particles with quantized magnetic charge as an explanation for the observed quantization of electric charge. If found, Dirac magnetic monopoles (DMMs) would require a re-evaluation of electromagnetism and all related theories. However, DMMs have not yet been empirically discovered. Their predicted magnetic charge, multiples of $2\Phi_0$ (where Φ_0 is the magnetic flux quantum: ~ 2.07 fWb), would be detected easily with modern superconducting quantum interference device (SQUID) magnetometers. If cosmic DMMs were trapped on ferromagnetic grains in pre-solar materials, then a promising place to search for them would be in material sampled from primitive small bodies, preferably returned by spacecraft on low-acceleration trajectories, since intense accelerations experienced by meteorites could strip them of DMMs as they enter Earth's atmosphere. By passing material through a 2G SQUID rock magnetometer, a theoretical DMM trapped within ferromagnetic grains would return a change in measured magnetic flux ($\Delta\Phi$) by multiples of $4\Phi_0$, or ~ 8.23 fWb. We performed this experiment on three Hayabusa-2 samples returned from the asteroid Ryugu: samples collected from the sites TD1 (A0397) and TD2 (C0006 and C0085), with a combined mass of 18.7 mg. We measured $\Delta\Phi$ as -0.3 ± 0.2 fWb for A0397, 0.3 ± 0.5 fWb for C0006, and 0.4 ± 1.1 fWb for C0085. Although our numbers were not significantly different from zero and are well below the expected magnetic charge for DMMs, we only sampled 18.7 mg of the ~ 5 g of primitive asteroidal material returned from Ryugu, which is in turn an infinitesimal fraction of the solar system. Due to their importance for all of science, we argue that all primitive materials returned from space missions should be screened routinely for DMMs as part of their initial characterization in the sample receiving laboratories.



Summarized results of 22 pass-through experiments conducted on returned Ryugu samples A0397, C0006, and C0085. Here, $\Delta\Phi$ is expressed as a percentage of $4\Phi_0$ – the minimum quantized change in flux expected by a Dirac magnetic monopole. Since $\Delta\Phi$ of all samples is much lower than $4\Phi_0$, we have not yet detected a magnetic monopole.

Electron holography observation of pseudo-magnetites and metallic iron nanoparticles in space weathered Ryugu sample

Yuki Kimura¹, Takeharu Kato², Satoshi Anada², Ryuji Yoshida², Kazuo Yamamoto², Toshiaki Tanigaki³, Tetsuya Akashi³, Hiroto Kasai³, Kosuke Kurosawa⁴, Tomoki Nakamura⁵, Takaaki Noguchi⁶, Masahiko Sato⁷, Toru Matsumoto⁶, Tomoyo Morita⁵, Mizuha Kikuri⁵, Kana Amano⁵, Eiichi Kagawa⁵, Toru Yada⁸, Masahiro Nishimura⁸, Aiko Nakato⁹, Akiko Miyazaki⁸, Kasumi Yogata⁸, Masanao Abe⁸, Tatsuaki Okada⁸, Tomohiro Usui⁸, Makoto Yoshikawa⁸, Takanao Saiki⁸, Satoshi Tanaka⁸, Fuyuto Terui¹⁰, Satoru Nakazawa⁸, Hisayoshi Yurimoto¹¹, Ryuji Okazaki¹², Hikaru Yabuta¹³, Hiroshi Naraoka¹², Kanako Sakamoto⁸, Sei-ichiro Watanabe¹⁴, Yuichi Tsuda⁸, and Shogo Tachibana^{6,8}

¹*Institute of Low Temperature Science, Hokkaido University, Sapporo 060-0819, Japan.*

²*Nanostructures Research Laboratory, Japan Fine Ceramics Center, Nagoya, 456-8587, Japan.*

³*Research & Development Group, Hitachi, Ltd., Hatoyama, Saitama, 350-0395, Japan.*

⁴*Planetary Exploration Research Center, Chiba Institute of Technology, Narashino 275-0016, Japan.*

⁵*Department of Earth Sciences, Tohoku University, Sendai 980-8578, Japan.*

⁶ *Division of Earth and Planetary Sciences, Kyoto University; Kyoto 606-8502, Japan.*

⁷*Department of Earth and Planetary Science, The University of Tokyo, Tokyo 113-0033, Japan.*

⁸*Institute of Space and Astronautical Science, Japan Aerospace Exploration Agency, Sagami-hara 252-5210, Japan.*

⁹*National Institute of Polar Research, Tashikawa 190-8518, Japan.*

¹⁰*Kanagawa Institute of Technology, Atsugi 243-0292, Japan.*

¹¹ *Department of Natural History Sciences, Hokkaido University, Sapporo 060-0810, Japan.*

¹² *Department of Earth and Planetary Sciences, Kyushu University, Fukuoka 819-0395, Japan.*

¹³ *Graduate School of Advanced Science and Engineering, Hiroshima University, Higashi-Hiroshima 739-8526, Japan.*

¹⁴ *Department of Earth and Environmental Sciences, Nagoya University, Nagoya 464-8601, Japan.*

The traces resulting from space weathering could provide a detailed understanding of interplanetary processes. However, most meteorites are composed of materials produced in the interior of the asteroid and have not undergone space weathering on its surface. Analysis of samples gently collected from the surface of extraterrestrial bodies by spacecraft is therefore useful for studying the details of space weathering [1,2].

Here, we focused on the space weathering of magnetite in samples brought back from the C-type asteroid Ryugu by the *Hayabusa2* spacecraft. Magnetite is an important mineral to record the nebular magnetic field, but studies on its space weathering are limited. Magnetite is universally found in carbonaceous meteorites as a major product of aqueous alteration of asteroids during the early stages of solar system formation. In particular, since most of the samples recovered by the *Hayabusa2* spacecraft were collected from the surface of the asteroid, it is important to understand the degree of space weathering influence on magnetite in order to interpret the origin of remanent magnetization. We have previously studied the magnetic domain structure of framboidal magnetite in recovered samples using electron holography [3,4]. In this study, we report on our newly discovered flamboids, which does not show a typical magnetic domain structure of magnetite.

From an area with relatively abundant Fe and containing many spherical particles similar to framboidal magnetite was selected from the surface of particle A0064-FO007 and an ultrathin section was prepared by focused ion beam (FIB) machining without applying magnetic field greater than that of the Earth. The ultrathin section contained about a dozen framboidal magnetite particles with sizes ranging from 500-900 nm (Fig. 1A). The magnetic domain structures of these particles were observed by electron holography (HF-3300EH; Hitachi High-Tech Corp., Tokyo), and it was found that the magnetic domains of each particle had a concentric magnetic structure typical of submicrometer-sized magnetite particles (Fig. 1B) [5-8].

Ultrathin sections taken from neighboring locations of the same particles also contained flamboidal particles of 400-800 nm in diameter, similar to Fig. 1A (Fig. 1C). The scanning transmission electron microscopy–energy-dispersive X-ray spectrometry analysis of this particle confirmed that it was iron oxide, consistent with magnetite, but electron holography showed no magnetic domain structure. This suggests that the particle is a nonmagnetic mineral and not magnetite. We analyzed the bonding state of iron and oxygen using electron energy loss spectroscopy and found that this nonmagnetic particle exhibited characteristics of both magnetite and wüstite in terms of the bonding state of iron and oxygen. We named such particles that exhibit both features of magnetite and wüstite, and do not show a magnetic domain structure "pseudo-magnetite".

Around the pseudo-magnetite particles, there was a decrease in signal intensity of various light elements in the region of about 2 μm below the surface. In addition, the elemental mapping of iron shows many small iron particles that may have

been released or diffused from the pseudo-magnetite (Fig. 1E). More than 100 metallic iron particles of 30-400 nm were easily counted in an alteration region 2 μm deep, 10 μm long, and 0.1 μm thick from the surface. Assuming that this reduction is due to a micrometeoroid impact and that a 10- μm diameter region is altered to a depth of 2 μm in a single impact, the total number of iron particles produced would be $\sim 10^4$, which could acquire remanent magnetization during an event involving the formation of iron nanoparticles by a micrometeoroid impact. Therefore, the iron particle precipitation associated with a micrometeoroid impact could play an important role as the remanence acquisition event.

Micrometeoroid impacts are thought to have occurred frequently within protoplanetary disks. However, the traces left behind by these impacts are found only on the topmost surfaces of asteroids, so previous studies using meteorites have had limited opportunities to study these traces. Even if a meteorite fell to Earth leaving behind pseudo-magnetite and iron particles, these particles would be oxidized by weathering on the ground afterward. In addition to the samples obtained by the *Hayabusa2* spacecraft, the samples brought back from the asteroid Bennu by OSIRIS-REx will also have a chance to be analyzed. In this process, it is necessary to avoid changes in remanent magnetization due to oxidation of pseudo-magnetite and metallic iron nanoparticles. Although pseudomagnetite may represent only a small percentage of total magnetite, its presence should be considered when analyzing extraterrestrial samples recovered from an asteroid surface. In our presentation, the event and timing of the micrometeorite impact and other suspect magnetite particles will be discussed.

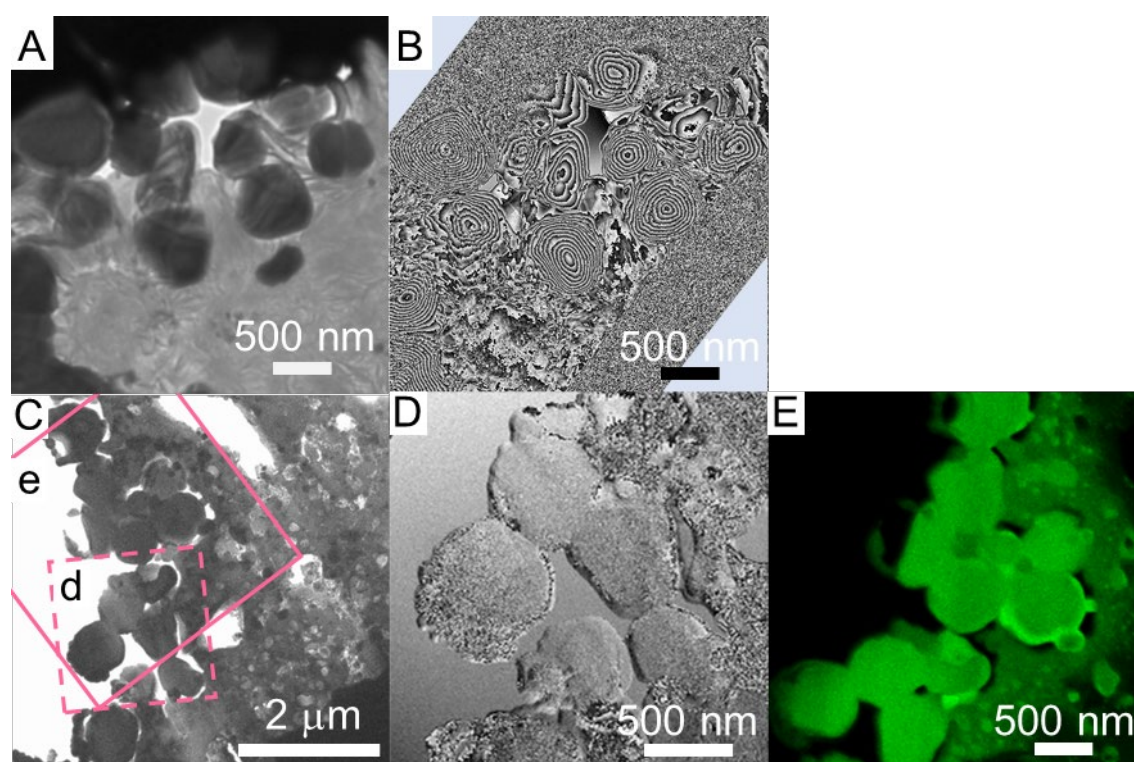


Figure 1. Framboids with and without magnetic domain structures characteristic to magnetite. **A** and **B**. Bright field TEM and the corresponding magnetic-flux-distribution images, respectively, of framboidal magnetite particles in a thin section prepared from the A0064–FO007 sample of asteroid Ryugu. **C**. Bright field TEM image of pseudo-magnetite particles in a thin section prepared from neighboring region of **A**. **D**. Magnetic-flux-distribution image, corresponding to the box **d** in **C**, observed by electron holography. **E**. Elemental mapping of iron corresponding to the box **e** in **C**.

The authors thank the Ministry of Education, Culture, Sports, Science and Technology (MEXT) (grants JPMXS0450200421, JPMXS0450200521) for financial support and JEOL for providing access to the tabletop SEM (JCM-7000, NeoScope). We thank the developers of iSALE, including G. Collins, K. Wünnemann, B. Ivanov, J. Melosh, and D. Elbeshausen. We also thank Tom Davison for the development of pySALEPlot.

References

- [1] Noguchi T. et al. 2011. *Science* 333:1121. [2] Noguchi T. et al. 2023. *Nat. Astron.* 7:170. [3] Nakamura T. et al. 2022. *Science* 379: eabn8671. [4] Kimura Y. et al. 2023 *Scientific Reports* 13:14096. [5] Kimura Y. et al. 2013. *Nat. Commun.* 4:2649. [6] Almeida T. P. et al. 2014. *Nat. Commun.* 5:5154. [7] Almeida T. P. et al. *Geophys. Res. Lett.* 41:7041. [8] Kimura Y., Yamamoto K. & Wakita S. 2021. *Astrophys. J. Lett.* 917:L5.

Characterization Of Early Solar System Aqueous Fluids In Ryugu Samples

Michael Zolensky¹, Robert Bodnar², Andrei Dolocan³, JangMi Han⁴, Romy Hanna³, Iona Gearba³, Queenie Chan⁵, Trevor Ireland⁶, Megumi Matsumoto⁷, Akira Tsuchiyama⁸.

¹NASA JSC, Houston, TX 77058, USA (michael.e.zolensky@nasa.gov); ²Virginia Tech, Blacksburg VA 24060, USA; ³Univ. of Texas, Austin TX 78712, USA; ⁴University of Houston, Houston TX 77204, USA; ⁵Royal Holloway University, Egham Hill, Egham TW20 0EX, UK; ⁶University of Queensland, St Lucia 4072, Queensland, Australia; ⁷Tohoku University, Aoba-ku, Sendai, Miyagi, Japan; ⁸Ritsumeikan Univ., Kusatsu, Shiga, 525-8577, Japan

Introduction: The most direct and convincing evidence for the presence of water and organic molecules on protoplanetary bodies is provided by fluid inclusions trapped in secondary minerals. Our previous research has demonstrated that early solar system fluids have survived as fluid inclusions in a few astromaterials that escaped significant shock, terrestrial alteration, and invasive sample handling [1-3]. We hypothesize that the bulk molecular and isotopic composition of individual fluid inclusions can be measured to provide ground truth for exploring and thermochemical modeling of the compositional and isotopic evolution of fluids in protoplanetary bodies including asteroids, comets and icy moons.

This presentation is an update on our efforts to make measurements of elemental, molecular and isotopic compositions of individual aqueous fluid inclusions in Ryugu samples.

Facilities: For the following XRCT and TOF-SIMS analysis, samples were prepared using the FEI Quanta 3D 600 Dual-beam Focused Ion Beam in the ARES -NASA-JSC Electron Beam Instrument Facility. For the X-ray Computed Tomography (XRCT) scans we used the Zeiss 620 XRM instrument at the University of Texas High-Resolution X-ray Computed Tomography Facility. For the Time of Flight-Secondary Ion Mass Spectrometry (TOF-SIMS) measurements we used the University of Texas Materials Institute's TOF-SIMS 5 and TOF-SIMS 6 instruments (ION-TOF GmbH) equipped with a pulsed Bi⁺ analysis ion beam (30 keV ion energy) and a O₂⁺ sputtering ion beam (1 kV ion energy). The TOF-SIMS instruments are capable of cooling the samples to -160 and -180C, respectively, and without this capability our measurements would be impossible.

Aqueous Fluids: Studies of aqueous alteration in primitive meteorites, based solely on secondary mineral associations, have hinted that this process did not occur under a single set of conditions [4]. The temperatures of alteration that have been suggested are highly variable, from below 0 to ~250°C. The fluid compositions must have likewise varied, though this critical aspect is very poorly understood. Our previous molecular, O and H isotopic measurements of fluids in halite in the Monahans and Zag meteorites [2,5] have shown considerable variation in fluid composition even within individual crystals. For example, we suspect that early solar system aqueous fluids could alternate between being S-rich and S-poor, based on the alternating pyrrhotite-magnetite alteration assemblage observed in the Tagish Lake and Sutter's Mill chondrites [6]. We know from our previous studies of aqueous fluid inclusions in extraterrestrial halite and calcite in the Sutter's Mill C2 chondrite that the mineralizing fluids also contained a significant concentration of mineralizing cations such as Fe, Mg, Ca, and volatiles such as CO₂ and S-bearing compounds in variable abundances (though the abundances are not yet determined) [2,7]. We observed CN⁻, a molecular fragment of a larger nitrogenous compound, in the aqueous fluid inclusions in a Ryugu pyrrhotite crystal [1-3]. Nakamura et al. [3] reported that the earliest formed phyllosilicates in Ryugu were rich in Na, indicating significant compositional changes in the mineralizing fluid.

Ryugu Fluid Inclusion Measurements: Our recent successful, coordinated, XRCT and TOF-SIMS analyses of individual fluid inclusions in a Ryugu pyrrhotite crystal demonstrated that they consist of water, CO₂, sulfur species, and organic material, with H⁻, C⁻, O⁻, S⁻ and OH⁻ as the main fragments detected at these locations [1,3]. In addition, various amounts of F⁻, Cl⁻ and Ni⁻ were found, together with Na⁺, Mg⁺, Al⁺, Cr⁺, K⁺ and Ca⁺. Larger organic fragments such as C₂⁻, C₂H⁻, C₃⁻, CO⁻ and CN⁻ were also detected, indicating the presence in these inclusions of more complex organic molecules containing H, C, N and O. We can expect to see these and additional molecular fragments in other Ryugu fluid inclusions. TOF-SIMS breaks apart molecules - it does not make new ones. Therefore, all these identified species are fragments of once larger molecules which we can identify to some degree.

Measurement of the stable isotopic compositions of aqueous fluid inclusions in Ryugu samples will enable a comparison with our measurements of a few fluid inclusions in carbonaceous chondrites (e.g. [7]), and fluids calculated to have reacted with other primitive samples (CI chondrites, OCs, HEDs, ureilites) which have δD ranging from ~0-3000‰. Actual direct measurements of preserved trapped fluids would thus inform us about fluid changes during aqueous alteration in a large suite of primitive bodies. Russell et al. [8] has suggested that CI materials form

two groups with distinct water/rock ratios, temperature ranges, and hydrogen isotope compositions. Are these truly distinct groups or do these just represent endmembers of a poorly sampled complete range (as also suggested by Russell et al., [8])? Our planned analyses of individual fluid inclusion oxygen and hydrogen isotope compositions in Ryugu samples will settle this issue as we will either observe narrow compositions or a compositional continuum.

Polished Ryugu sample C00025 contains large sulfides, magnesite, magnetite and dolomite crystals (Fig 1). We have already FIBed several foils from this sample and subjected one of the FIB foils to TOF-SIMS measurements. We detected no filled fluid inclusions, however we were limited to analyzing inclusions larger than about 3 μm using the M5 TOF-SIMS instrument, and it appears the inclusions were far smaller (Fig.1). We plan to repeat the measurements of this sample using the newly-installed M6 TOF-SIMS, which has greatly expanded capabilities. We made XRCT scans of two additional Ryugu grains (A0175 and C0043) (Fig 2). From these preliminary measurements we know that A0175 contains numerous pyrrhotite, carbonate, and, probably, apatite crystals with fluid inclusion candidates measuring at least 3-5 μm in diameter, which will permit our planned TOF-SIMS measurements.

The TOF-SIMS analytical data are counts under the peaks for each species. An example of the data is shown in Figure 3, which shows counts for OH- (indicative of H₂O) and C- (here indicative of CO₂). This sample was a synthetic fluid inclusion standard (quartz) prepared by Bob Bodnar where the inclusions contained a 1:1 mixture of H₂O and CO₂. As you can see from the included table, despite the fact that the sensitivity of the technique for CO₂ was much lower than for H₂O, 4/5 of the inclusions showed consistent counts for these species, meaning that with continued calibration we can produce quantitative composition measurements for some species. We note that the signals for CO₂ we observed in the Ryugu pyrrhotite crystal were more pronounced than those we obtained using the 50:50 standard, suggesting a very high abundance of CO₂ in the Ryugu mineralizing fluid. In fact, solid CO₂ sublimed rapidly in a vacuum at our measurement temperature, making quantification very difficult.

In the coming year we will begin isotopic measurements of standards in synthetic fluid inclusions and Ryugu pyrrhotites and carbonates we have already identified, as well as increasing our stock of pre-analyzed Ryugu crystals.

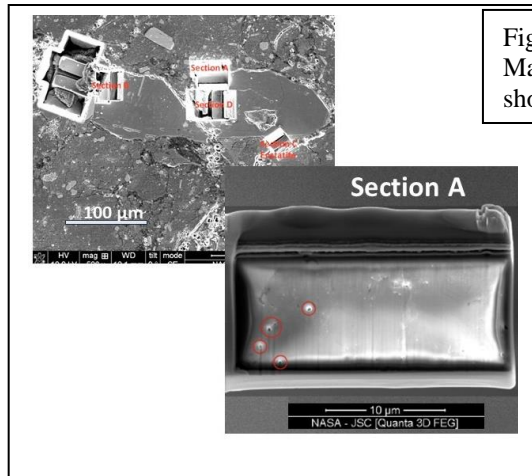
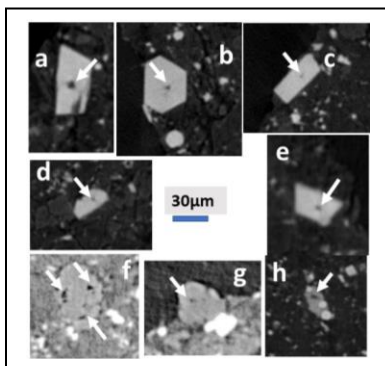


Fig. 1. Magnesite in Ryugu sample C00025 (left) BSE image of Magnesite showing FIB pits. (right) SEI image FIB A foil showing submicron-sized fluid inclusion candidates circled.

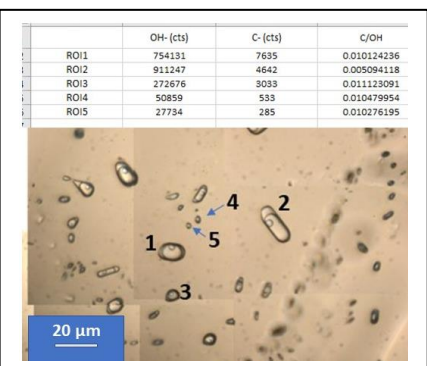
Acknowledgements: We thank JAXA for Ryugu samples, and the NASA Hayabusa2 Participating Scientist Program.

References: [1] Zolensky et al. (2022) *85th Meeting of The Meteoritical Society*. Abstract 6011; [2] Bodnar et al. (2019) *50th LPSC Abstracts*; [3] Nakamura et al. (2022) *Science* **377**, 10.1126/science.abn8671; [4] Brearley (2005) In *Meteorites and the Early Solar System II*. D. S. Lauretta and H. Y. McSween Jr., Eds.; [5] Yurimoto et al. (2014) *Geochemical Journal* **48**, 1-12; [6] Zolensky et al. (2014) *MAPS* **49**, 1997-2016; [7] Tsuchiyama et al. (2021) *Science Advances* **7**, eabg9707; [8] Russell et al. (2022) *MAPS* **57**, 277–301.



(Left) Fig. 2. XRCT “slices” of Ryugu sample A0175. Fluid inclusion candidates are arrowed. (a-e) Pyrrhotite crystals. (f-g) Probable carbonates. (h) Possible apatite crystal.

(Right) Fig. 3. Results of TOF-SIMS measurements of synthetic fluid inclusion standard (quartz), with inclusions that contain a 1:1 mixture of H₂O and CO₂. Inclusions are numbered to match the table (e.g. ROI1=1). Counts = cts.



Three-dimensional description and characterization of lithologies in Ryugu sample

Léna Jossé¹, Zélia Dionnet¹, Alice Aléon-Toppani¹, Rosario Brunetto¹, Andrew King², Emmanuel Gardés³, Eva Heripré⁴,
Donia Baklouti¹, Zahia Djouadi¹, Celine Lantz¹ and Kentaro Hatakeda⁵

¹*CNRS, Institut d'Astrophysique Spatiale, Université Paris-Saclay, Orsay, France*

²*SOLEIL Synchrotron, Gif-sur-Yvette, France*

³*Laboratoire Magmas et Volcans, Clermont-Ferrand, France*

⁴*Procédés et Ingénierie en Mécanique et Matériaux, Paris, France*

⁵*Institute of Space and Astronautical Science, Japan Aerospace Exploration Agency (JAXA), Japan*

Ryugu is a rubble-pile asteroid. Similarly to CI chondrites, the samples returned by Hayabusa2 mission showed the presence of adjoining fragments of different lithologies [1, 2]. These fragments are different in mineralogy, petrology, physical structure (size, porosity) and testify the heterogeneity of Ryugu's asteroid, its complex geological history and evolution [3]. So far, several lithologies have been observed and described partly in polished sections [1, 2, 3]. In this work we used micro-computed tomography (μ -XCT) to observe, analyze and investigate lithologies in 3D. We analyzed their properties (internal structure, shape, size, composition, porosity) and their assemblages with each other in a Ryugu millimeter-sized sample with the objective to better understand Ryugu's heterogeneity and its complexity in term of formation and evolution.

We studied the 3D lithologies of the mm-sized (1.45×2.85×2.1 mm) sample A0159 from Chamber A. Data were obtained at PSYCHÉ beam-line of Synchrotron SOLEIL (France) using a monochromatic X-ray beam operating at 25 keV. Our analysis was conducted on 3D reconstructed images (CT-images, or "slices") with a voxel volume of 1.295 μm^3 and based on the linear attenuation coefficient (LAC). As a first method of data processing, we used pixel segmentation, which classifies each voxel into 5 major domains by its LAC value. The domains are, sorted by increasing LAC, 1-porosity, voids, fractures, 2-matrix, 3-carbonates, 4-sulfides and oxides. Some LAC values were difficult to associate with a specific domain so we classified them as 5-uncharacterized. This method allows us to obtain the proportion of each component within each slice and then in the entire sample, but also the 3D reconstruction of each component.

Contrary to the first method, the local histogram segmentation considers areas of 49×49 voxels. For each area, the calculated histogram of the proportion of pixels for a given LAC value gives access to i) the number of pixels for each of the 5 previously cited domain and ii) the LAC histogram data distribution. Then, each area was locally described in regard to composition and physical properties giving rise to lithologies. This method allowed us to obtain a 3D reconstruction of each lithology in the sample. Tomviz software was used for 3D representation and visualization.

Our preliminary results from the pixel segmentation method showed that, on average, A0159 is made of 42.0±7.0 % of matrix component, 1.2±0.5 % of sulfides and oxides, 4.7±2.8 % of porosity, voids and/or fractures and 27.5±4.7 % of uncharacterized material (undefined components, or technique artifacts). Finally, carbonate components represents 24.1±2.5 % of the sample, a much higher value than previous studies [4]. The 3D reconstruction of carbonates shows a mm-sized vein going through A0159 (fig. 1), indicating important fluid circulation. The vein is about 1100×900×100 μm and it is the largest vein observed so far in a Ryugu sample. Its presence explains the high proportion of carbonate material in A0159. We detected two highly fractured plans along both sides of the vein. The vein ends up with coarse and elongated to rounded carbonate grains with inter-grains voids. In other studies, a complex and elongated structure of size >100 μm was observed in sample C0041 and found to have a wide range of (Mg-Fe)-carbonate composition between siderite–magnesite (or breunnerite) [5, 6]. In sample C0009, [3] found elongated Ca-carbonates forming a chain that they proposed to be a potential remnant of a vein. The detection of a mm-sized vein in

A0159 suggests that Ryugu's parent-body has probably undergone notable water flow through, at least, a mm-sized fracture and that carbonate precipitated as a vein.

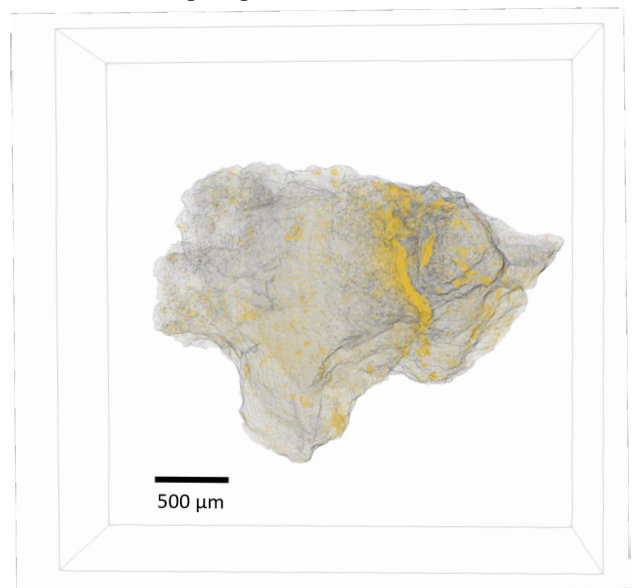


Figure 1: 3D reconstruction of the Ryugu sample A0159 (in grey) combined with the distribution of carbonates (in yellow).

The preliminary results of the second method allowed us to detect several different lithologies. A study is ongoing to determine the exact number of lithologies. These lithologies are mostly composed of matrix with various size and proportion of carbonates, sulfides, oxides, and porosity. One peculiar lithology is made of a compact matrix component, few carbonates, uncharacterized material, sulfides and oxides. This lithology could match the "massive domain" seen by [1] in A0035 or the "fine-grained dark lithology" in C0009 by [3]. The compact lithology is surrounded by long (up to 800 μm) and large fractures (up to 20 μm) and, similarly to [1], some fractures also cross the lithology. Another lithology is rich in rounded and elongated grains of carbonates about 50 μm in size and is located at the end of the vein. This lithology has many small fractures (up to 100 μm long and 10 μm large) which seem to be preferably located around the grains such as in A0037 [3]. However, crossing and surrounding fractures are not present in each lithology. The second method is still ongoing and it is not clear yet whether the carbonate vein crosses a single lithology. However, our preliminary results confirm that Ryugu is a breccia with adjoining fragments of various size (from 100 to 500 μm), composition and physical properties. The analysis of the fractures (distribution, size and shape) strongly indicates a heterogeneity in the mechanical properties of lithologies. All these observations testify the complexity of Ryugu and/or parent-body formation and evolution and its geological past.

References

- [1] E. Nakamura, K. Kobayashi, R. Tanaka, T. Kunihiro, H. Kitagawa, C. Potyszil, T. Ota, C. Sakaguchi, M. Yamanaka, D. M. Ratnayake, *et al.*, "On the origin and evolution of the asteroid ryugu: A comprehensive geochemical perspective," *Proceedings of the Japan Academy, Series B*, vol. 98, no. 6, pp. 227–282, 2022.
- [2] T. Nakamura, M. Matsumoto, K. Amano, Y. Enokido, M. Zolensky, T. Mikouchi, H. Genda, S. Tanaka, M. Zolotov, K. Kurosawa, *et al.*, "Formation and evolution of carbonaceous asteroid ryugu: Direct evidence from returned samples," *Science*, p. eabn8671, 2022.
- [3] A. Yamaguchi, N. Tomioka, M. Ito, N. Shirai, M. Kimura, R. C. Greenwood, M.-C. Liu, K. A. McCain, N. Matsuda, M. Uesugi, *et al.*, "Insight into multi-step geological evolution of c-type asteroids from ryugu particles," *Nature Astronomy*, vol. 7, no. 4, pp. 398–405, 2023.
- [4] C. Pilorget, T. Okada, V. Hamm, R. Brunetto, T. Yada, D. Loizeau, L. Riu, T. Usui, A. Moussi-Soffys, K. Hatakeda, *et al.*, "First compositional analysis of ryugu samples by the micromega hyperspectral microscope," *Nature Astronomy*, vol. 6, no. 2, pp. 221–225, 2022.
- [5] D. Loizeau, C. Pilorget, L. Riu, R. Brunetto, J.-P. Bibring, A. Nakato, A. Aléon-Toppiani, K. Hatakeda, K. Yogata, J. Carter, *et al.*, "Constraints on solar system early evolution by micromega analysis of ryugu carbonates," *Nature Astronomy*, pp. 1–7, 2023.
- [6] A. Nakato, T. Yada, M. Nishimura, K. Yogata, A. Miyazaki, K. Nagashima, K. Hatakeda, K. Kumagai, Y. Hitomi, H. Soejima, *et al.*, "Variations of the surface characteristics of ryugu returned samples," *Earth, Planets and Space*, vol. 75, no. 1, p. 45, 2023.

Size distribution and elemental compositions of anhydrous minerals in the Ryugu samples C0224 and C0260: Implications for radial transport mechanism and source regions of anhydrous minerals

D. Nakashima¹, M. Matsumoto¹, H. Yoshida², T. Mikouchi², T. Nakamura¹

¹Tohoku University, Japan (dnaka@tohoku.ac.jp), ²University of Tokyo, Japan.

Introduction: Samples returned from C-type asteroid Ryugu by the Hayabusa2 spacecraft are mineralogically and chemically similar to CI chondrites [1-4]. It was suggested from the initial analysis of the Ryugu samples that the Ryugu original parent body formed beyond the H₂O and CO₂ snow lines (> 3 – 4 au) in the solar nebula at 1.8 – 2.9 Myr after CAI formation [1]. Nakashima et al. [5] reported elemental compositions and oxygen isotope ratios of chondrule-like objects and Ca-Al-rich inclusions (CAIs) in the Ryugu samples. The objects (< 30 μm) are as small as those from comet Wild2, suggesting radial transport favoring smaller objects from the inner solar nebula (solar neighborhood and chondrule formation regions) to the formation location of the Ryugu original parent body, which is farther from the Sun and scarce in chondrules [5]. Besides chondrule-like objects and CAIs, anhydrous minerals such as olivine, pyroxene, spinel, and hibonite occur in the Ryugu samples and are much more abundant [1]. In the present study, we measured size distribution of anhydrous minerals in the newly allocated Ryugu samples (C0224 and C0260) using FE-SEM and FE-EPMA to test the hypothesis of radial transport favoring smaller objects [5] and elemental compositions to elucidate the source regions of individual anhydrous minerals.

Results: Synchrotron radiation X-ray computed tomography at SPring-8 showed that C0224 has a homogeneous lithology except for the presence of large carbonate crystals of few hundred μm in size and C0260 contains clasts with different lithologies. Three hundred ten anhydrous minerals including chondrule-like objects were found in eight polished sections from C0260 (C0260-01, 02, and 03) and C0224 (C0224-01, 02, 03, 04, and 05), and most of them were from C0260. Polished sections of C0224 were repolished multiple times but only 6 grains were observed. Most anhydrous minerals occur along with calcite, Ca phosphate, and Na-Mg phosphate in FeO-rich phyllosilicate regions, which is characteristic for lithology II clasts (less-altered clasts; [6]). Anhydrous minerals have angular shapes, so that diameters are calculated from surface areas of anhydrous minerals using ImageJ assuming they have spherical shapes. The largest one is 24 μm and smallest one is 0.5 μm. As shown in [Fig. 1a](#), the peak of size distribution of anhydrous minerals including chondrule-like objects occurs at 2 – 3 μm. It should be noted that we counted anhydrous minerals detected by FE-SEM mapping, and therefore there is counting loss of tiny minerals (<< 1 μm). Olivine is most abundant followed by spinel, pyroxene, and hibonite. Mg#’s of olivine are from 89.5 to 99.4, which is consistent with the initial analysis [1]. Low-iron manganese-enriched (LIME) olivine with MnO/FeO ratio (wt%) exceeding 1 [7] is observed. Pyroxene and hibonite grains are too small to obtain precise compositions. Spinel contains variable amounts of Cr₂O₃ (0.21 – 4.0 wt%).

Six chondrule-like objects are observed ([Fig. 1b](#)). They have rounded shapes and mainly consist of FeO-poor olivine with Mg# from 92.0 to 99.2 along with diopside, rounded (oxidized) Fe-Ni metal, and altered phase. The chondrule-like objects are similar to those found in the initial analysis [1,5].

Discussion: Most anhydrous minerals occur in less-altered clasts in the Ryugu samples [1, this study]. The clasts have protected anhydrous minerals from aqueous alteration and brecciation for ~ 4.6 Gyr, so that sizes of the anhydrous minerals reflect those during accretion onto the Ryugu original parent body. Our new data ([Fig. 1a](#)) show that anhydrous minerals in the Ryugu samples (< 24 μm) are smaller than chondrules in chondrites (~ 500 μm; [8]) and isolated olivine in chondrites (> 20 μm; [9]), suggesting radial transport favoring smaller objects to the formation location of the Ryugu original parent body. There are two possible mechanisms for radial transport: a combination of advection and turbulent diffusion [10] and photophoresis [11]. Both mechanisms can transport grains smaller than 30 μm. While the Ryugu original parent body formed at ~ 2 Myr after the CAI formation [1], photophoresis transports 10 μm grains beyond 10 au later than ~ 5 Myr after the CAI formation [11]. Considering the time window, a combination of advection and turbulent diffusion that transports ≤ 20 μm grains beyond 25 au within 1 Myr [10] would be more likely for Ryugu. It will be more plausible by size distributions of anhydrous minerals in other Ryugu samples and CI chondrites.

Olivine in type I chondrules is more enriched in Cr₂O₃ and CaO than olivine in amoeboid olivine aggregates (AOAs) ([Fig. 2a](#)) [5]. ¹⁶O-rich chondrule-like objects, CAIs, and ¹⁶O-rich olivine in the Ryugu samples are distributed in the AOA area, while ¹⁶O-poor chondrule-like object and ¹⁶O-poor olivine are distributed in the type I chondrule area. The difference in the elemental compositions of olivine with different origins is explained by AOA olivine condensation from a residual gas depleted in the refractory elements followed by isolation from the gas before condensation of Cr [5]. Olivine depleted in Cr₂O₃ and CaO may have formed

near the Sun, and olivine relatively enriched in the two elements may have formed in the chondrule formation regions. Thus, it is possible to deduce the source regions of isolated olivine and chondrule-like objects based on the Cr_2O_3 and CaO concentrations. Many of isolated olivine grains and olivine in chondrule-like objects in C0260 and C0224 distribute in the AOA area (Fig. 2b), which is consistent with the FE-EPMA analysis of olivine in CI chondrites [12]. The AOA-like olivine may have formed near the Sun. It is considered from the high abundance of AOA-like olivine in the Ryugu samples and frequent occurrence of ^{16}O -rich olivine in Wild2 particles [13] that olivine formed near the Sun were transported to the outer regions of the early solar nebula and survived due to lack of chondrule forming event that erases ^{16}O -rich signature and original elemental compositions. On the contrary, isolated olivine in chondrites distributes in the type I chondrule area (Fig. 2c), and ^{16}O -rich olivine is rare in chondrites [14]. It is considered that ^{16}O -rich olivine passed the chondrule formation regions and/or melted during chondrule forming events.

Nakashima et al. [5] reported that spinel in the Ryugu CAIs contain small amounts of Cr_2O_3 with < 0.2 wt% and suggested that the CAIs escaped from remelting event and may be as old as the oldest CAIs. Isolated spinel in C0260 show variable Cr_2O_3 concentrations up to 4.0 wt%. Therefore, spinel that acquired Cr by remelting events are also present in the Ryugu samples. Considering the time window of accretion (within ~ 2 Myr after CAI formation; [1]), remelting events may have occurred during that period.

References: [1] Nakamura T. et al. (2022) *Science* 10.1126/science.abn8671. [2] Ito M. et al. (2022) *Nat. Astron.* 10.1038/s41550-022-01745-5. [3] Nakamura E. et al. (2022) *Proc. Jpn. Acad. Ser. B* 98:227. [4] Yokoyama T. et al. (2022) *Science* 10.1126/science.abn7850. [5] Nakashima D. et al. (2023) *Nat. Commun.* 14:532. [6] Mikouchi T. et al. (2022) LPSC LIII, #1935. [7] Klöck W. et al. (1989) *Nature* 339:126. [8] Friedrich J. M. et al. (2015) *Chem. Erde* 75:419. [9] Jacquet E. et al. (2021) *M&PS* 56:13. [10] Hughes A.L.H. & Armitage P.J. (2010) *ApJ* 719:1633. [11] Moudens A. et al. (2011) *A&A* 531:A106. [12] Mikouchi T. et al. (2023) 86th Annual Meeting of The Meteoritical Society, #6178. [13] Nakashima D. et al. (2012) *EPSL* 357-358:355. [14] Tenner T.J. et al. (2018) in *Chondrules: Records of Protoplanetary Disk Processes* 196. [15] Kurat G. et al. (1989) *Meteoritics* 24:35. [16] Jones R. H. et al. (2000) *M&PS* 35:849. [17] Ushikubo T. et al. (2012) *GCA* 90:242. [18] Yamanobe M. et al. (2018) *Polar Sci.* 15:29. [19] Chaumard N. et al. (2021) *GCA* 299:199. [20] Jacquet E. et al. (2021) *M&PS* 56:13. [21] Ushikubo T. & Kimura M. (2021) *GCA* 293:328. [22] Weisberg M. K. et al. (2021) *GCA* 300:279.

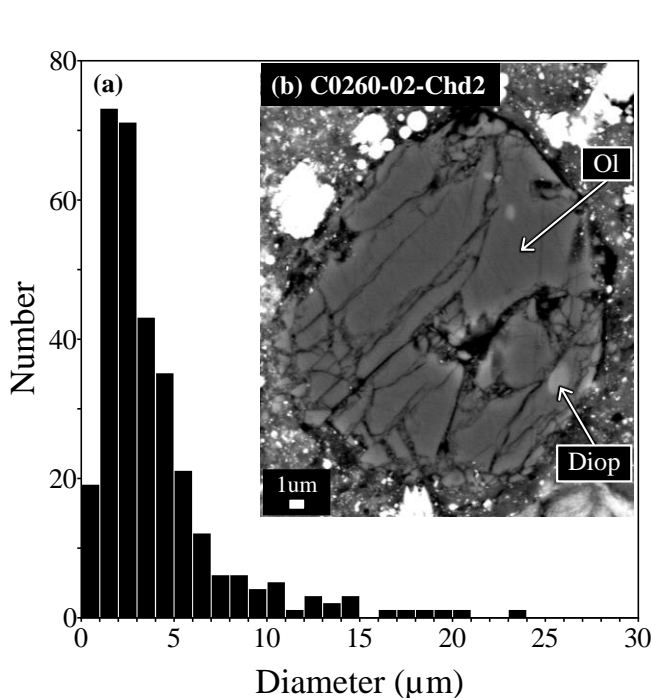


Fig. 1: Size distribution of anhydrous minerals including chondrule-like objects in C0224 and C0260 (a) and backscattered electron image of the chondrule-like object C0260-02-Chd2 (b). Ol, olivine; Diop, diopside.

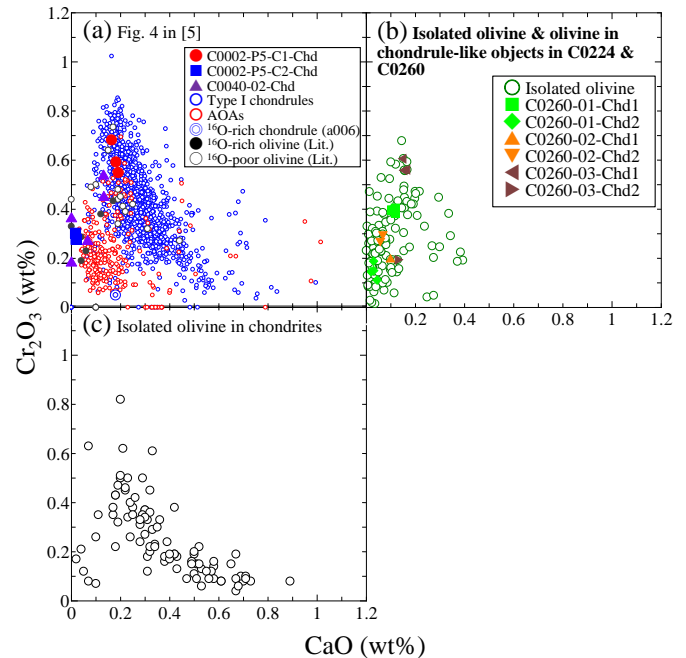


Fig. 2: Comparison of concentrations between Cr_2O_3 and CaO in olivine in chondrule-like objects, type I chondrules, AOAs, ^{16}O -rich and -poor chondrules (a), isolated olivine and olivine in chondrule-like objects in C0224 and C0260 (b), and isolated olivine in chondrites (c). The panel a is from Nakashima et al. [5]. Olivine data in the panel c are from [15-22].

Microstructural and microchemical characteristics of dolomite in Ryugu regolith particles

Falko Langenhorst^{1,2}, Kilian Pollok¹, Tomoki Nakamura³, Tomoyo Morita³, Kana Amano³, Daisuke Nakashima³
and the Hayabusa2 initial analysis core team

¹*Institute of Geoscience, Friedrich Schiller University Jena, Germany*

²*Hawai'i Institute of Geophysics and Planetology, University of Hawai'i at Manoa, USA*

³*Tohoku University, Sendai, Japan.*

Introduction. Previous studies of Ryugu material have reported that the regolith particles record extensive aqueous alteration as the result of water activity in the original parent body [1,2]. The aqueous alteration finally resulted in the almost complete overprint of the primary mineralogical composition and the precipitation of secondary minerals, i.e. phyllosilicates, carbonates, phosphates, sulfides, and oxides. The isotopic $^{18}\text{O}/^{16}\text{O}$ and $^{13}\text{C}/^{12}\text{C}$ signatures of carbonates were recently studied in great detail to obtain information on the conditions of aqueous alteration [3]. Here, we focus on the characterization of the defect microstructures and nanoscale element distributions in dolomite of Ryugu samples to obtain further insights into the formation history and mechanisms of carbonates.

Samples and methods. In the context of the Hayabusa2 initial analysis phase, we have mainly studied polished sections prepared from larger particles recovered in the C chamber, i.e. C0033-01 and C0033-04, and C0055-01 [detailed in 1]. Eleven slices of carbonate-bearing regions were cut from the thin sections by focused ion beam (FIB) preparation on a scanning electron microscope (SEM). Subsequent analytical transmission electron microscopy (TEM) were performed according to the procedure described by [4].

Results and discussion. TEM observations reveal numerous curled dislocations as the most dominant lattice defect in almost all dolomite grains. This shape of dislocation lines indicate that dislocations are not in glide configuration and thus may have been incorporated during imperfect growth from the aqueous fluid. In the vicinity of fractures, sample C0055-01 contains also straight glissile dislocations, which were previously assigned to mild shock [5]. Deformation twins, which are generally regarded as typical for shock-metamorphosed carbonates, are however absent in C0055-01. An explanation for their absence could be that deformation twinning in dolomite requires enhanced temperatures [6], which do not prevail during low shock metamorphism [6].

Mapping of elemental distributions in scanning mode using energy-dispersive X-ray emission spectroscopy show complex and variable zoning of dolomite grains. Many grains show sharp, non-concentric, up to 1 μm thin rims with a significant enrichment in manganese (up to 8 wt% MnO). This observation points, at least, to a second precipitation event, when the fluid became apparently enriched in manganese. A preferential mobilization of manganese might be explained by a (localized) change in the reduction potential. In addition, manganese-enriched dolomites with continuously decreasing manganese concentration from core to rim exist and monitor a gradual change in the fluid chemistry controlled by carbonate growth.

Most interesting is the observation of nanoscale modulations in the rims of dolomite. Such microstructures have also been observed in sedimentary calcian dolomites and are interpreted as growth microstructures [7]. The modulations appear as almost parallel lamellae with regular alternating light and dark contrast, resembling microstructures known for spinodal decomposition. A periodical variation of the fluid composition at the mineral-solution interface during progressing growth is a plausible explanation for this microchemical peculiarity [8].

Acknowledgements. We thank JAXA for providing access to the Ryugu particles. FIB-TEM facilities at FSU Jena were funded by the Gottfried-Wilhelm-Leibniz award to FL (LA 830/14-1).

References

- [1] Nakamura T. et al. 2023 *Science* 379:eabn8671. [2] Nakamura E. et al. 2022 *Proc. Jpn. Acad. Ser. B*:227-282. [3] Fujiya W. et al. 2023 *Nature Geoscience* 16:675-682. [4] Langenhorst F., et al. 2014 *Earth Planets and Space* 66:118. [5] Kikuiiri M. et al. 2022 85th Annual Meeting of The Meteoritical Society:No. 2695. [6] Barber D.J. and Wenk H.R. 1979 *Physics Chemistry Minerals* 5:141-165. [7] Reeder R.J. 1992 In: P. Buseck (editor), *Reviews in Mineralogy* 27:381-424. [8] Ruiz-Agudo E. and Putnis C.V. 2012 *Mineralogical Magazine* 76:227-253.

Investigating the ammonium-bearing phase in Ryugu samples

M. Ferrari¹, L. Folco², S. De Angelis¹, M. Masotta², A. Raponi¹, M.C. De Sanctis¹, E. Mugnaioli²,
R. Borriello², M. Ciarniello¹, E. Ammannito³, E. La Francesca¹, L. Rossi¹, M. Pedone³.

¹INAF-IAPS, Via del Fosso del Cavaliere 100, 00133, Rome, Italy (marco.ferrari@inaf.it); ²Dep. Earth Science, University of Pisa, Via Santa Maria, 53, 56126, Pisa, Italy; ³ASI, Via del Politecnico, 00133, Rome, Italy.

Introduction

The JAXA/Hayabusa2 mission collected 5.4 g of samples from two different sites (i.e., A and C) on the surface of the C-type asteroid (162173) Ryugu [1; 2]. This asteroid is characterized by a low albedo and by the presence of hydrous and carbonaceous materials [3]. The Ryugu surface spectra collected by the Hayabusa2/NIRS 3 spectrometer reveal a narrow absorption feature at 2.72 μm [4] resembling that observed on the surface of Ceres by the Dawn/VIR spectrometer [5; 6]. Laboratory analysis of returned grains confirmed that Ryugu samples contain hydrated silicates, sulfides, oxides, carbonates, and organics and have spectroscopic similarities to CI chondrites [7]. MicrOmega hyperspectral microscope observation [8] revealed the presence of a band at 3.06 μm , indicating the possible presence of NH-bearing phases in most of the returned grains [9]. This ammonium-related absorption feature was confirmed by FTIR measurements [10]. The 3.06 μm band was also observed in the spectra of Ceres by telescopic observations [11] and by the Dawn/VIR spectrometer that accurately characterized its distribution on the dwarf planet's surface [12]. Current interpretations of Ceres spectra suggest that the most likely mineralogical phases hosting ammonium are phyllosilicates [13; 14], but the presence of ammonium salts has also been inferred in specific areas of the Cerean surface [15; 16]. Hydrated silicates represent the main reservoir of water in Ryugu samples, and their presence is indicative of extensive aqueous alteration in the parent body, likely the alteration path that occurred on Ceres. Even if phyllosilicates are the most likely carriers, the specific ammonium-bearing phase determining the 3.06 μm band on Ryugu samples and the surface of Ceres is not fully constrained, nor are the processes that led to ammonium enrichment on these C-type bodies.

Sample selection

Our selection criterion of the samples among those available in the first allocation (2022A) was the presence of the absorption band at 3.06 μm as observed in the spectroscopic data obtained from the preliminary screening by FTIR and MicrOmega. We have considered: 1. Similarities of the 3.06 μm absorption between Ryugu samples and Ceres spectra, in terms of wavelength range and band center position; 2. The presence of surface features or morphological structures suggests some mineralogical diversity.

Through the first allocation, we obtained two samples: A0198 and C0091. The preliminary FTIR data provided by JAXA collected on particle C0091 show the presence of a remarkable absorption close to 3.06 μm . On the contrary, the spectroscopic data collected on particle A0198 show a shallow absorption ascribed to the presence of ammonium and several surface features that comply with our scientific requirements. Moreover, the two assigned samples were collected at different sites which will allow us to make further considerations.

Objectives and research plan

With this work, we aim to contribute to the definition of the physical and mineralogical characteristics of the Ryugu asteroid to understand the initial stages of formation and evolution of C-type bodies; particular attention will be given to the identification of the ammonium-bearing phase(s) and its/their interplay with hydrated silicates. In addition, we aim to define Ryugu's path of alteration and its similarities with Ceres.

The following laboratory analyses will be used to characterize the samples:

- VIS-IR imaging spectroscopy (0.4-5 μm) will be carried out with the SPectral IMager (SPIM) facility [17] on whole samples. Data will allow a first characterization of the mineralogic composition of their external surface, including an assessment of the presence of water, organic matter, and ammonium in addition to the minerals. Furthermore, by using the SPIM facility (i.e., the Dawn/VIR replica), we can perform a compelling comparison between the data collected on the samples with those provided by the Dawn/VIR spectrometer on Ceres;

- X-ray microscopy (XRM). This non-destructive technique has been used to obtain a high-resolution (submicron scale) 3D tomography of the samples, revealing their internal structure (including pore structure and fracturing), as well as the morphology and composition of the individual grains contained in them; XRM data will also enable the location of regions of interest (ROIs) within the samples to be analyzed by transmission electron microscopy (TEM);

- Raman μ -spectroscopy, to obtain compositional maps of the surface of the samples at the micro-metric scale;
- Focused ion beam-field emission gun-scanning electron microscopy (FIB-FEG-SEM) will be used to identify the main mineralogical phases and to extract the electron-transparent lamellae for TEM analyses;
- Transmission Electron Microscopy (TEM), electron diffraction, and energy-dispersive X-ray spectroscopy (EDS) will be used to identify cryptocrystalline mineral phases and crystal defects through high-resolution techniques.

Results

The VIS-NIR spectra obtained with the SPIM facility on the surface of the two particles show the almost ubiquitous presence of a deep V-band centered at lengths slightly above 2.7 μm , and absorptions near 3.4 μm and in the range 3.7-3.9 μm , however, limited at specific points on the surface returning an inhomogeneous surface composition at the scale of ~ 40 μm (SPIM pixel size). These absorption features can be related to the presence of phyllosilicates and carbonates, respectively.

In addition, at some specific points, the band at 3.06 μm is found indicating the presence of ammonium-bearing compounds.

The Raman spectra acquired on the two particles are characterized by a high fluorescence background and by the presence of the Raman D and G-bands related to the presence of poorly ordered carbonaceous matter. The spectral parameters derived from the mathematical fitting of the acquired spectra as band positions, and band intensity ratio do not differ significantly between the two particles. Raman analysis identifies dolomite as the most common carbonate on both particles.

The interpretation of spectral data acquired by both particles is currently in progress. However, at the moment there do not appear to be notable differences in spectral terms (VIS-NIR and Raman) between the two particles coming from the two different sampling sites.

The two samples (A0198 and C0091) are characterized by a generally similar composition in terms of phase abundance and composition. Energy Dispersive X-ray spectroscopic (EDX) data obtained using the FE-SEM confirmed the presence of hydrated silicates, sulfides (Ni-rich and Fe-rich), carbonates, fosfates, and oxides (mainly magnetite). Sulfides form dominantly euhedral grains (up to 5 μm in size), whereas oxides form submicrometric framboid, platy, or columnar structures. The internal distribution of silicates, sulfides, and oxide in the interior of the two samples, as revealed by XRM data, is rather homogeneous. Notably, sample C0091 displays a slightly smaller grain size and a slightly higher porosity compared to particle A0198.

Conclusions

The notable similarities of the spectra of some Ryugu samples with Ceres' average spectrum [18] sparked scientific curiosity. To date, interpretation of remotely sensed data coupled with spectroscopic investigation of analogs has not enabled a full understanding of the mechanisms of ammonium enrichment and the nature of the mineral assemblage hosting ammonium on the surface of C-type objects. Furthermore, studies on meteorites have not provided morphological and compositional information on the mineral phases that preceded the alteration of their progenitor body.

Therefore, we consider that spectroscopic measurements and nanoscale mineralogical investigations that we are conducting on the samples returned from Ryugu represent a unique opportunity to definitively establish the link, if any, between ammonium and the mineralogy of this type of object.

References

- [1] Yada, T. et al. (2021) *Nat. Astron.*; [2] Watanabe, S. et al. (2019) *Science*; [3] Kitazato, K. et al. (2019) *Science*; [4] Kitazato, K. et al. (2021) *Nat. Astron.*; [5] De Sanctis, M.C. et al. (2011) *Space Sci. Rev.*; [6] De Sanctis, M.C. et al. (2015) *Nature*; [7] Tachibana, S. et al. (2022) 53rd LPSC, #1265; [8] Bi-bring, J.-P. et al. (2017) *Astrobiology*; [9] Pilorget, C. et al. (2022) *Nat. Astron.*; [10] Kebukawa, Y. et al. (2022) 53rd LPSC, #1271; [11] King, T.V. et al. (1992) *Science*; [12] Ammannito, E. et al. (2016) *Science*; [13] Ferrari, M. et al. (2019) *Icarus*; [14] De Angelis, S. et al. (2021) *J. Geophys. Res. Planets*; [15] De Sanctis, M.C. et al. (2016) *Nature*; [16] Raponi, A. et al. (2019) *Icarus*. [17] Coradini, A. et al. (2011) EPSC-DPS Joint meeting, #1043. [18] Raponi, A. et al. (2021) *Life*.

Speciation of various elements using scanning transmission/fluorescence X-ray microscopy (STXM/SFXM) and bulk XANES analysis related to aqueous environment in the Ryugu parent body

Takahiro Kawai¹, Keisuke Fukushi², Hiroki Suga³, Masayuki Uesugi³, Shohei Yamashita⁴, Ryoichi Nakada⁵, Mizuho Koike⁶, Hideto Yoshida¹, Masaki Ohura⁷, Megumi Matsumoto⁸, Tomoki Nakamura⁸, Yasuhito Sekine,⁹ and Yoshio Takahashi^{1*}

(*Presenting author)

¹Department of Earth and Planetary Science, Graduate School of Science, The University of Tokyo, ²Institute of Nature and Environmental Technology, Kanazawa University, ³Japan Synchrotron Radiation Research Institute (JASRI), ⁴Photon Factory, Institute of Materials Structure Science, High-Energy Accelerator Research Organization (PF, IMSS, KEK), ⁵Kochi Institute for Core Sample Research, Japan Agency for Marine-Earth Science and Technology (JAMSTEC), ⁶Department of Earth and Planetary Systems Science, Hiroshima University, ⁷RIKEN SPring-8 Center, ⁸Dept. of Earth Sciences, Tohoku University, ⁹Earth-Life Science Institute, Tokyo Institute of Technology

The parent body of the C-type asteroid Ryugu is thought to have been rich in volatile elements and abundant in liquid water, making it an important research target for the origin of water and organic matter on Earth. The water caused various alteration in the surrounding minerals, resulting in layered silicates such as smectite (saponite) and serpentinite being the main constituent minerals of the Ryugu (Nakamura et al., 2023). In this process, the organic matter of the Ryugu parent body also underwent chemical reactions and a wide variety of organic matter was synthesised (Naraoka et al., 2023). It is particularly important to obtain information on the water environment during the aqueous alteration, as the products of chemical reactions of organic matter in water depend on the pH and redox potential (Eh) of the water. In this study, speciation of various elements including iron (Fe), magnesium (Mg), calcium (Ca), and carbon (C) was investigated using scanning transmission X-ray microscopy (STXM) and bulk X-ray absorption near-edge structure (XANES) analysis in the soft X-ray region related to the aqueous environment in the Ryugu parent body. For the elements with concentrations below the detection limit of STXM, scanning fluorescence X-ray microscopy (SFXM), newly developed in SPring-8 and Photon Factory was applied such as nitrogen (N) and sodium (Na). The speciation of these elements in saponite is particularly important, since the Fe oxidation state and chemical composition within the interlayer of the saponite can indicate Eh-pH condition of the Ryugu water.

The Fe(II)/Fe(III) ratio in the octahedral structure of saponite was conducted by STXM. Based on our laboratory experiments, dithionite reduction of natural Fe-bearing saponite corresponding to Eh range from -0.47 to -0.66 (V) at pH = 7 shows the Fe(II)/Fe_{total} ratio around 0.55. The incomplete reduction by dithionite reveals that Fe(II)-bearing saponite is a strong reductant. Assuming that the relationship between the Fe(II)/Fe_{total} ratio and Eh of nontronite in Gorski et al. (2013) is similar to that of saponite, the Fe(II)/Fe_{total} ratio greater than 0.68 measured by STXM indicates that the Eh was less than -0.45 (V).

On the other hand, because saponite has a negative charge in its layered structure, cations from the aqueous phase are adsorbed between the saponite layers during aqueous alteration. In this case, as shown by Fukushi et al. (2019), which cations are retained in the interlayer depends on the concentration of various cations in the coexisting aqueous phase and the selectivity coefficient K. Therefore, the cation composition in the water layer at the time of aqueous alteration can be estimated from the interlayer cation ratio determined by various analytical methods. In this process, speciation of Na, K, and Ca were conducted to obtain their fractions retained in the interlayer. The comparison of the Al content in saponite enables us to estimate the Mg content in the interlayer. Contents of these cations with assumptions of dissolved silica etc. were used to construct an Eh-pH diagram of Mg. We have estimated pH range that can explain the presence of both saponite and dolomite, which are widely distributed in the altered crust in the Ryugu particles. The pH range estimated by the method was pH from 7.8 to 10. Although the range is somewhat wide, the range is consistent with the results suggested in Nakamura et al. (2022).

The combination of Eh around -0.45 (V) and the alkaline pH range estimated above showed that the water was highly reducing, which reveals that H₂ and CH₄ were present in the Ryugu water if we assume the equilibrium condition. Such an alkaline condition is suitable for the polymerisation of amino acids (Kitadai and Maruyama, 2018).

References: Fukushi K. et al. (2019) Semiarid climate and hyposaline lake on early Mars inferred from reconstructed water chemistry at Gale. *Nat. Commun.* **10**, 1–11.; Gorski C. A. et al. (2013) Redox properties of structural Fe in clay minerals: 3. Relationships between smectite redox and structural properties. *Environ. Sci. Technol.* **47**, 13477–13485.; Kitadai N. and Maruyama S. (2018) Origins of building blocks of life: A review. *Geosci. Front.* **9**, 1117–1153.; Nakamura T. et al. (2023) Formation and evolution of carbonaceous asteroid Ryugu: Direct evidence from returned samples. *Science* **379**, eabn8671.; Naraoka H. et al. (2023) Soluble organic molecules in samples of the carbonaceous asteroid (162173) Ryugu. *Science* **379**, eabn9033.

Investigating the organic compounds in the asteroid Ryugu

Imene Kerraouch^{1*}, Rhonda Stroud¹, Larry Nittler², Cassandra Kraver², Jens Barosch^{3,4} and Jianhua Wang³

¹*Buseck Center for Meteorite Studies (BCMS), Arizona State University, USA;* ²*School of Earth and Space Exploration (SESE), Arizona State University, USA;* ³*Earth and Planets Laboratory, Carnegie Institution for Science, USA;* ⁴*Department of Geoscience, University of Wisconsin-Madison, USA.* *ikerraou@asu.edu

Organic compounds in meteorites provide insights into the carbon chemistry present in the interstellar medium and solar nebula and on their alteration on the parent bodies. Further, delivery of these organic compounds could have contributed to Earth's habitability and life. However, studying these compounds in meteorites is complicated by their exposure to terrestrial organic contamination after entering the Earth's atmosphere. As such, one of the goals of the Hayabusa2 sample return mission (asteroid (162173) Ryugu) is to understand the nature, origin, and evolution of organic compounds in the early solar system but from samples free of terrestrial organic contamination. Here, we examine further samples from asteroid Ryugu that were collected during the first touchdown (Chamber A, samples A0079 and A0169; allocated in first Ryugu AO). The goals of our research are to understand diversity, origin, and formation mechanisms of the macromolecular material that dominates Ryugu organics, as well as the secondary processes involved in their modification, such as heating and aqueous alteration.

Fragments of the two Ryugu samples up to a few 10s of microns in size were pressed into Au foils for H, C, and N isotope analysis with the Carnegie NanoSIMS 50L ion microprobe. We used a ~0.4 pA, ~100-nm Cs⁺ primary beam and acquired data for C and N isotopes, including ¹²C₂, ¹²C¹³C, ¹²C¹⁴N, and ¹²C¹⁵N, as well as ¹⁶O, ³²S, and secondary electrons. The prepared samples were then analyzed for ¹H, D, and ¹²C and secondary electrons with a slightly more intense primary beam. C-rich regions of interest (ROIs) were defined in the C-N images and subsequently located and analyzed in the H-D images.

We have analyzed a total area of ~9,000 μm² across the two samples. Data reduction is in progress. The majority of C-rich ROIs appear rounded in the ion images and range from ~100 to 900 nm with some to up to a few μm (e.g., Fig.1). Consistent with previous measurements [2-6], our data shows that the organic material is on average enriched in D and ¹⁵N with most ROIs having compositions consistent within error with average values of δD of a few 100 ‰ and δ¹⁵N ~ +50‰. However, one lath-like rectangular grain was identified in a particle within A0079 (Fig. 1), similar in shape to a grain previously reported in Chamber C [5; Fig.3], but larger. This 4.5 × 1 μm grain has an extreme isotopic composition: δD ≈ 10,000 ‰ and δ¹⁵N ≈ +800‰. In order to clarify the nature and origin of this unusual grain and other select C-rich ROIs, we are currently extracting focused ion beam (FIB) lift-out sections of D and ¹⁵N hotspots. The FIB sections will be studied with transmission electron microscopy, scanning transmission electron microscopy, energy dispersive spectroscopy and electron energy loss spectroscopy at Arizona State University. Results from these investigations will be presented at the symposium.

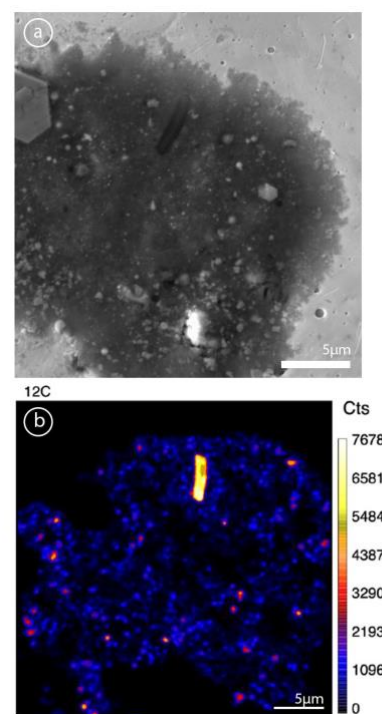


Figure 1. (a) Secondary electron (SE) image of a Ryugu particle from chamber A (A0079) pressed into gold foil. (b) D and ¹⁵N-enriched lath-like (whisker) detected in same particle.

References: [1] Huss G. R. and Draine B. T. 2006. Highlights of Astronomy 2: 353–356. [2] Busemann H. et al. 2006. Science 312, 727–730. [3] Nittler L. R. et al. 2019. Nat. Astron. 3, 659–666. [4] Nittler L. R. et al. 2018). GCA 226, 107–131. [5] Barosch J. et al. 2022. Abstract#2050. 53rd LPSC; [6] Yabuta, H. et al. 2023. Science 379, eabn9057.

Constraining Ryugu's earliest fluid composition by the analyses of phosphates

Nicolas David Greber^{1,2}, Johanna Marin-Carbonne³, Anne-Sophie Bouvier³, James Greenwood⁴, Thomas Bovay³, Martin Robyr³, Cristina Martin Olmos³

¹*Muséum d'histoire naturelle de Genève, Route de Malagnou 1, CH-1208 Genève, Switzerland*

²*Institute of Geological Sciences, University of Bern, Baltzerstrasse 1+3, 3012 Bern, Switzerland*

³*Institute of Earth Sciences, University of Lausanne, CH1015 Lausanne, Switzerland*

⁴*Department of Earth & Environmental Sciences, Wesleyan University, 265 Church Street, Middletown, Connecticut 06459, USA*

Volatile elements and compounds like F, Cl, S, H₂O and CO₂, indisputably exert a strong influence on the nature and evolution of (exo)planets, of which water is arguably the most prominent for the habitability of the Earth. Most volatiles were likely brought to Earth by carbonaceous chondrite-like material, including asteroids, making the undisturbed material of Ryugu key samples to improve our understanding of the distribution of water in our solar system and the origin of water on Earth.

The water concentration in CI chondrites is distinct from that of Ryugu (13 to 20 wt% compared to 6.8 wt%, respectively; [1,2]), which might be explained (i) by loss of water from Ryugu during the disruption of the parent body, (ii) impact heating, (iii) that CI chondrites derive from parent asteroids with higher water content than Ryugu, or (iv) that CI chondrites got contaminated by water during their residence time on Earth [2-4]. Importantly, the apatite grains found in Ryugu likely originate from the aqueous alteration of Ryugu that predates the events that might have lead to the loss of some of Ryugu's water inventory (see points i and ii, [5,6]). Thus, measuring the chemical and isotopic compositions (e.g. H, O, etc) of these apatites will likely help to better constrain the initial composition of Ryugus water, prior to its disruption, which is the aim of different research projects currently ongoing.

We will present the developed method on how we measured the H-isotopic composition of the apatites in Ryugu and discuss this preliminary results in the context of the initial dD value of Ryugu's water.

References

- [1] Palme, H., and J. Zipfel. 2022. *Meteoritics & Planetary Science* 57.2:317-333.
- [2] Yokoyama, et al. 2022. *Science* 379.6634:eabn7850.
- [3] Ito, et al. 2022. *Nature Astronomy* 6.10:1163-1171.
- [4] Kurosawa, et al. 2021. *Communications Earth & Environment* 2.1:146.
- [5] Nakamura, et al. 2022. *Proc. Jpn. Acad. Ser. B* 98
- [6] Sugita, et al. 2019. *Science* 364.6437:eaaw0422.

Interpreting the thermal alteration history from organic matter in Ryugu samples

Queenie Hoi Shan Chan^{1*}, Tomoki Nakamura², Michael Zolensky³, Jangmi Han⁴, Mizuha Kikui², Kana Amano², Ashley King⁵, Charlotte Bays^{1,5}, Peter Krizan¹, Natasha Almeida⁵, Megumi Matsumoto², Akira Tsuchiyama^{6,7,8}, Akira Miyake⁹, Junya Matsuno⁹, Luis Carlos Colococho Hurtarte¹⁰, Rosario Brunetto¹¹, Mark Burchell¹², Vassilia Spathis¹², Ming Chang Liu¹³ and Junko Isa¹⁴, and the Hayabusa2 initial analysis Core team.

¹Centre for Dynamic Earth and the Solar System (CeDESS), Department of Earth Sciences, Royal Holloway University of London, Egham TW20 0EX, UK. ²Department of Earth Sciences, Tohoku University, Tohoku University, Sendai 980-8578, Japan. ³NASA Johnson Space Center; Houston TX 77058, USA. ⁴Department of Earth and Atmospheric Sciences, University of Houston, Houston TX 77204, USA. ⁵Planetary Materials Group, Natural History Museum, London SW7 5BD, UK. ⁶Research Organization of Science and Technology, Ritsumeikan University, Kusatsu 525-8577, Japan. ⁷Chinese Academy of Sciences (CAS) Key Laboratory of Mineralogy and Metallogeny/Guangdong Provincial Key Laboratory of Mineral Physics and Materials, Guangzhou Institute of Geochemistry, CAS, Guangzhou 510640, China. ⁸CAS Center for Excellence in Deep Earth Science, Guangzhou 510640, China. ⁹Division of Earth and Planetary Sciences, Kyoto University, Kyoto 606-8502, Japan. ¹⁰Diamond Light Source, Didcot OX11 0DE, UK. ¹¹Institut d'Astrophysique Spatiale (IAS), Université Paris-Saclay, Orsay 91405, France. ¹²Centre for Astrophysics and Planetary Science, School of Physics and Astronomy, University of Kent, Canterbury CT2 7NZ, UK. ¹³Nuclear and Chemical Sciences Division, Lawrence Livermore National Laboratory, USA. ¹⁴Earth-Life Science Institute, Tokyo 152-8550, Japan.

Introduction: The Hayabusa2 mission visited the near-Earth Cb-type asteroid (162173) Ryugu and has returned to Earth with the surface material of Ryugu. Ryugu is an airless rubble pile asteroid exposed to space weathering [1]. Near infrared remote observations recorded an absorption feature at 2.72 μm indicating the presence of OH-bearing hydrous components. However, the 2.72 μm feature is weak, suggesting that Ryugu was once organic- and water-rich and subsequently dehydrated by a brief period of surficial heating. This feature has also been observed in “thermally metamorphosed carbonaceous chondrites”, “CI-/CM-like”, or “CY” chondrites [2, 3]. Initial examination of the returned samples did not identify any significant heating at >150 °C [4, 5]; however, amino acid analyses suggested similarities to thermally-altered meteorites on the grounds of the predominant straight-chain *n*- ω -amino acid abundances [6]. It remains unclear as to what caused the nonconformal interpretations of the thermal alteration history of Ryugu.

Here we investigate the alteration history of Ryugu by comparing the organic composition of fresh Ryugu samples to that of naturally and experimentally heated chondritic meteorites. This study describes a coordinated effort in analysing organic matter in Ryugu samples using micro-x-ray computed tomography (μ -CT), micro-Raman spectroscopy, focused ion beam (FIB), scanning electron microscopy with energy dispersive X-ray spectroscopy (SEM-EDS), micro-X-ray diffraction (μ -XRD), scanning transmission X-ray microscopy (STXM), X-ray absorption near edge structure (XANES), and synchrotron radiation-based X-ray computed tomography (SR-CT).

Samples and Analytical Techniques: We studied Ryugu samples allocated during the Hayabusa2 preliminary examination (A0063-FC016, A0063-FC017, A0064-FO012, A0067-FC008, C0002-FC014, C0002-FC015, C0025-FC003, C0033-FC003, C0046-FO003) and AO1 (A0009 and C0011), plus raw fragments of naturally long-term (CIs: Orgueil, Ivuna; CMs: Murchison, Murray; CV: Allende; CRs: Grosvenor Mountains 95577; OCs: Yamato (Y)-74191, Queen Alexandra Range 93010) and short-term heated meteorites (Belgica-7904, Jbilet Winselwan, Y-793321, Y-86720, Y-982086) [7, 8]. We also analysed samples of Murchison, Murray and Orgueil experimentally heated to 300, 400, 500, 600, 700 and 900 °C for 1, 10, 50, 100, 500 and 1000 hours. Raman analyses were conducted using a Jobin-Yvon Horiba LabRAM HR Raman microprobe with a 514 nm laser for which the power was maintained at <100 μW at the sample surface. The mineralogy of the raw Ryugu samples was characterised using low-voltage SEM-EDS (FEI Quanta 650) and μ -XRD. We identified regions of interest (ROIs) within A0009 and C0011 by conducting μ -CT analysis using a cabinet-based industrial Zeiss Xradia Versa 520 CT system. Targeted ROIs were picked using sterile tools, pressed into indium, and prepared into electron-transparent sections (~ 100 nm thick) mounted on TEM Cu grids using a FEI Quanta 3D 600 dual beam FIB-SEM, which were studied by STXM-XANES to determine the organic composition. Euhedral sulphide crystals were lifted and mounted on W-needles by the FIB-SEM, and potential fluid inclusions within them were then located by SR-CT conducted at SPring-8 BL47XU at the X-ray energy of 7 keV.

Results and Discussion: Increased heating of carbonaceous materials results in a transition from amorphous to graphitic carbon, and such ordering is traceable using Raman spectroscopy as a cosmo-thermometer [9]. Raman spectroscopic analysis of

the Ryugu samples indicates significant heterogeneity (Figure 1), evident by Raman spectral features that are comparable to the organic matter in both relatively unheated primitive chondrites and those that experienced short duration heating like Y-793321, a Stage II heated chondrite [10].

The Raman spectral features of the organic matter in most of the Ryugu samples are similar to those observed from CIs, consistent with previous studies [11]. However, localised areas within several Ryugu samples show a wider G band, comparable to organic matter processed by short duration heating. The Raman features of the organic matter in broad areas within A0009, A0064 and C0011 clearly deviate from that observed from the other Ryugu samples and Orgueil, with significantly lower D band positions and D band widths that are comparable to chondritic organics that had been heated at elevated temperatures [9], and larger G band widths that are not observed in naturally metamorphosed chondritic meteorites (Figure 1). These trends are similar to those

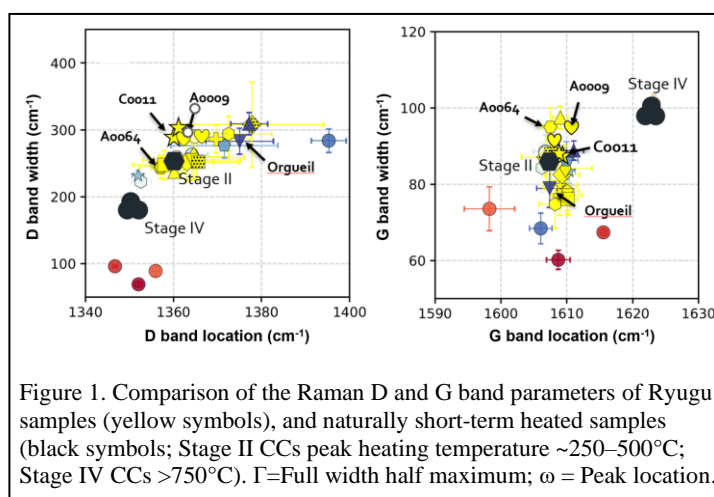


Figure 1. Comparison of the Raman D and G band parameters of Ryugu samples (yellow symbols), and naturally short-term heated samples (black symbols; Stage II CCs peak heating temperature $\sim 250\text{--}500^\circ\text{C}$; Stage IV CCs $>750^\circ\text{C}$). Γ =Full width half maximum; ω = Peak location.

exhibited by astromaterials heated by short-term heating, like interplanetary dust particles [12] and some meteorites [13]. The Raman spectra of A0009, A0064 and C0011 are similar to those of Orgueil experimentally heated to 300°C for 500 h.

Analysis of A0064 by SEM-EDS and μ -XRD shows the presence of hydrated phyllosilicates, suggesting that the particle did not experience significant heating above $\sim 300\text{--}400^\circ\text{C}$. Moreover, the SR-CT data validated the μ -CT scans, and indicate that C0011 contains a sulphide grain hosting an inclusion with X-ray attenuation that is clearly distinct from air (Figure 2). Previous studies have revealed H_2O and CO_2 within such inclusions [14], suggesting that they have not been metamorphosed after aqueous alteration. Analysing these more “evolved” particles with STXM-XANES helped us understand the organic structure corresponding to the Raman features. C-XANES spectra of A0009 and C0011 indicate the presence of aromatic or olefinic groups ($\text{C}=\text{C}$) at $\sim 285\text{ eV}$ and carboxylic groups (COOH) at $\sim 288.5\text{ eV}$ within the matrix associated with carbonate grains (CO_3 absorption at 290.3 eV). While thermally stable oxygenated functional groups were observed in short term (impact induced) heated meteorites [15], the association of the organic matter with carbonates is comparable to the carboxylic-rich diffuse organic matter in CM and CI chondrites [16]. Based on our coordinated investigation, we have drawn two possible scenarios that can explain our observations: (1) some carbonaceous matter in Ryugu had experienced post aqueous alteration short duration heating (impact induced and/or solar irradiation), resulting in the presence of thermally stable oxygenated moieties like furan and phenol that were formed via dehydration and cyclisation of polyalcohols. These “evolved” materials were subsequently disrupted and redistributed by impacts, thermal fatigue, and/or mass wasting processes [17], intermixed with fresh, undisturbed and pristine Ryugu materials. Alternatively, (2) the formation of the macromolecular organic matter occurred at the final stages of aqueous alteration in low-temperature, highly oxidizing fluids, e.g., fluid with OH radicals contributing through H_2O_2 dissociation [18], co-precipitating carboxylic enriched components in the immediate vicinity of carbonate.

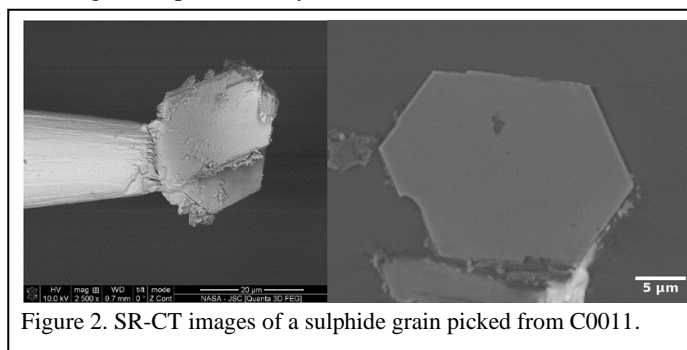


Figure 2. SR-CT images of a sulphide grain picked from C0011.

us understand the organic structure corresponding to the Raman features. C-XANES spectra of A0009 and C0011 indicate the presence of aromatic or olefinic groups ($\text{C}=\text{C}$) at $\sim 285\text{ eV}$ and carboxylic groups (COOH) at $\sim 288.5\text{ eV}$ within the matrix associated with carbonate grains (CO_3 absorption at 290.3 eV). While thermally stable oxygenated functional groups were observed in short term (impact induced) heated meteorites [15], the association of the organic matter with carbonates is comparable to the carboxylic-rich diffuse organic matter in CM and CI chondrites [16]. Based on our coordinated investigation, we have drawn two possible scenarios that can explain our observations: (1) some carbonaceous matter in Ryugu had experienced post aqueous alteration short duration heating (impact induced and/or solar irradiation), resulting in the presence of thermally stable oxygenated moieties like furan and phenol that were formed via dehydration and cyclisation of polyalcohols. These “evolved” materials were subsequently disrupted and redistributed by impacts, thermal fatigue, and/or mass wasting processes [17], intermixed with fresh, undisturbed and pristine Ryugu materials. Alternatively, (2) the formation of the macromolecular organic matter occurred at the final stages of aqueous alteration in low-temperature, highly oxidizing fluids, e.g., fluid with OH radicals contributing through H_2O_2 dissociation [18], co-precipitating carboxylic enriched components in the immediate vicinity of carbonate.

Acknowledgements: We are extremely grateful to the Astromaterials Science Research Group (ASRG) of ISAS/JAXA for providing the Ryugu samples.

Reference: [1] Noguchi, T., et al. *Science*, 2011. **333**: p. 1121-1125. [2] Kitazato, K., et al. *Science*, 2019. **364**: p. 272-275. [3] Vilas, F. *The Astronomical Journal*, 2008. **135**: p. 1101. [4] Naraoka, H., et al. *Science*, 2023. **379**(6634): p. eabn9033. [5] Yabuta, H., et al. *Science*, 2023. **379**(6634): p. eabn9057. [6] Parker, E.T., et al. *GCA*, 2023. **347**: p. 42-57. [7] Tonui, E., et al. *GCA*, 2014. **126**: p. 284-306. [8] Nakamura, T. *JMPS*, 2005. **100**: p. 260-272. [9] Busemann, H., M.O.D. Alexander, and L.R. Nittler. *MAPS*, 2007. **42**: p. 1387-1416. [10] Nakamura, T. *Earth and Planetary Science Letters*, 2006. **242**(1): p. 26-38. [11] Yokoyama, T., et al. *Science*, 2022. **379**(6634): p. eabn7850. [12] Chan, Q.H.S., et al. *MAPS*, 2020. **55**(6): p. 1320-1348. [13] Quirico, E., et al. *GCA*, 2014. **136**: p. 80-99. [14] Zolensky, M., et al., *Hayabusa Symposium*. 2023. [15] Yabuta, H., et al. *MAPS*, 2010. **45**: p. 1446-1460. [16] Le Guillou, C., et al. *GCA*, 2014. **131**: p. 368-392. [17] Morota, T., et al. *Science*, 2020. **368**(6491): p. 654-659. [18] Cody, G.D. and C.M.O.D. Alexander. *GCA*, 2005. **69**: p. 1085-1097.

First direct detection of large aromatic molecules on asteroid (162173) Ryugu sample C0083 and A00145: an interstellar heritage

Hassan Sabbah¹, Ghylaine Quitté¹, Karine Demyk and Christine Joblin¹

¹*IRAP, Université Toulouse III – Paul Sabatier, CNRS, CNES, 31028 Toulouse Cedex 4, France*

Although meteorite analysis has revealed various types of pre-solar grains, the presence of large polycyclic aromatic hydrocarbons (PAHs) of interstellar origin has not been firmly established. Here we present a search for these compounds in the C0083 and A00145 grains from the Ryugu asteroid. The experiment takes advantages of the ultra-sensitivity of the AROMA (Astrochemistry Research of Organics with Molecular Analyzer) setup to target these species.

The AROMA setup was developed specifically for studying the carbonaceous molecular composition of meteorites and cosmic dust analogues [1]. It consists of a laser desorption ionization (LDI) source combined with a segmented linear quadrupole ion trap (LQIT), all connected to an orthogonal time-of-flight mass spectrometer (oTOF). The ion source is at a low pressure of 10^{-6} mbar and can be operated using a two-step laser desorption ionization scheme. This L2MS analysis provides ultra-sensitivity for PAHs and fullerenes as demonstrated in our earlier study [2]. This laser technique also requires little or no sample preparation and uses very little material.

Subsamples of the two Ryugu grains have been isolated and used either as bulk or crushed in the form of powder to improve sensitivity. The data obtained are compared to previous AROMA analyses of carbonaceous chondrites (CCs) such as Murchison and Orgueil. This reveals a number of peculiarities in the distribution of PAHs in Ryugu grains. In particular we report the presence of PAHs containing as much as 50 carbon atoms, which can be considered as interstellar candidates. Moreover, we have identified aromatic compounds that incorporate nitrogen (N) and oxygen (O) heteroatoms, with carbon atoms extending up to 48. These findings impact our view on the complexification of organic matter in the cycle of matter from the interstellar matter to the Solar System. It also motivates the research for these large compounds in other CCs

References

[1] Sabbah et al. 2017. *The Astrophysical Journal*, 843, 34. [2] Sabbah et al 2022. *The Astrophysical Journal*, 931, 91.

FIB Tomography-STXM-TEM on organic material from Hayabusa-2 grain A0083.

H. G. Changela¹, Y. Kebukawa², L. Petera¹, M. Ferus¹, E. Chatzitheodoridis³, L. Nedjl⁴, R. Nebel¹, Z. Hlavenkova⁵, J.

Moravcova⁵, P. Krepelka⁵, R. Holbova⁵, J. Novacek⁵, T. Samoril^{6,7}, K. Sobotkova⁶, H. Tesarova⁶ and D. Zapotok⁸

¹ J'Heyrovski Institute of Physical Chemistry, Czech Academy of Sciences, Prague, Czechia. ² Tokyo Institute of Technology, Tokyo, Japan. ³ National Technical University of Athens, Greece. ⁴ Bruno University of Technology, Czechia. ⁵ Central European Institute of Technology Masaryk University, Brno, Czechia. ⁶ Central European Institute of Technology Nano, Brno, Czechia. ⁷ TESCAN GROUP a.s., Brno, Czechia. ⁸ TESCAN USA Inc, Pennsylvania, USA. Email: changela@unm.edu

Introduction The success of the *Hayabusa-2* mission provides unique insight into prebiotic evolution from a known asteroid free from terrestrial contamination. Asteroid 16273Ryugu (Ryugu here on in) is of CI (Ivuna-type) composition, lacking any distinct chondrules and calcium aluminium inclusions, and is composed mainly of secondary minerals including phyllosilicate, carbonates, (Fe, Ni) sulphides, Fe-oxides and phosphates [1]. Organic material (OM) also pervades Ryugu, characteristic of OM found in primitive chondrite matrices. Micron to submicron organic particles (OPs) – macromolecular organic objects completely surrounded by inorganic material – make up the major mass fraction of OM [e.g. 2], consistent with insoluble organic matter (IOM). A volumetrically diffuse organic component aromatic-poorer and carboxylic-richer than OPs found within chondritic hydrated silicates [3] also occurs in Ryugu [4]. This study is on a grain from the 1st touch-and-go (TAG) site on Ryugu, characterising the distribution, functional chemical variation and mineral setting of OM *in situ*.

Samples & Methods Grain A0083 (Radegast here on in) is a 1.3 and 1.7 mm grain from Chamber A of the *Hayabusa-2* collector TAG site. Radegast was prepared and analyzed taking an approach of minimal damage and material loss for characterisation. Radegast was picked up with vacuum tweezers and placed on a clean Au base with an ~2 mm divot, mounted on an Al stub. An ~1.5 mm circular hole in clean Al foil was placed over the top of Radegast and fastened at the edge of the stub, exposing the grain out of the hole and securing it. This has the advantage that the grain can be turned over by lifting the foil for any further characterization whilst leaving the grain intact. Focused Ion Beam (FIB) ~100 nm lamella of Radegast were prepared for Scanning Transmission X-ray (STXM) and Transmission electron Microscopy (TEM). The TESCAN *AMBERX* and *LYRA3* at TESCAN GROUP and the Central European Institute of Engineering & Technology (CEITEC)-nano, respectively, were used to compare the effects of Xe⁺ plasma FIB with Ga⁺ FIB lamella preparation on the STXM measurements of OM in the samples. To minimize sample information losses by destruction from the traditional FIB lamella sample preparation, FIB tomography was performed from the edge of the grain during milling prior to lift-out. Grains of Ivuna were also embedded in molten S for ultramicrotome using methods in [5]. 110 nm samples were cut using a Leica UC7 at CEITEC-Muni to compare the STXM measurements between Xe-, Ga- FIB lamella and microtome samples. Scanning Transmission X-ray Microscopy (STXM) measurements were made at BL 19A at the Photon Factory, Japan. S/TEM was performed with the CEITEC-MUNI Thermofisher *Talos F200C*, and the J'Heyrovski Institute's JEOL 2100.

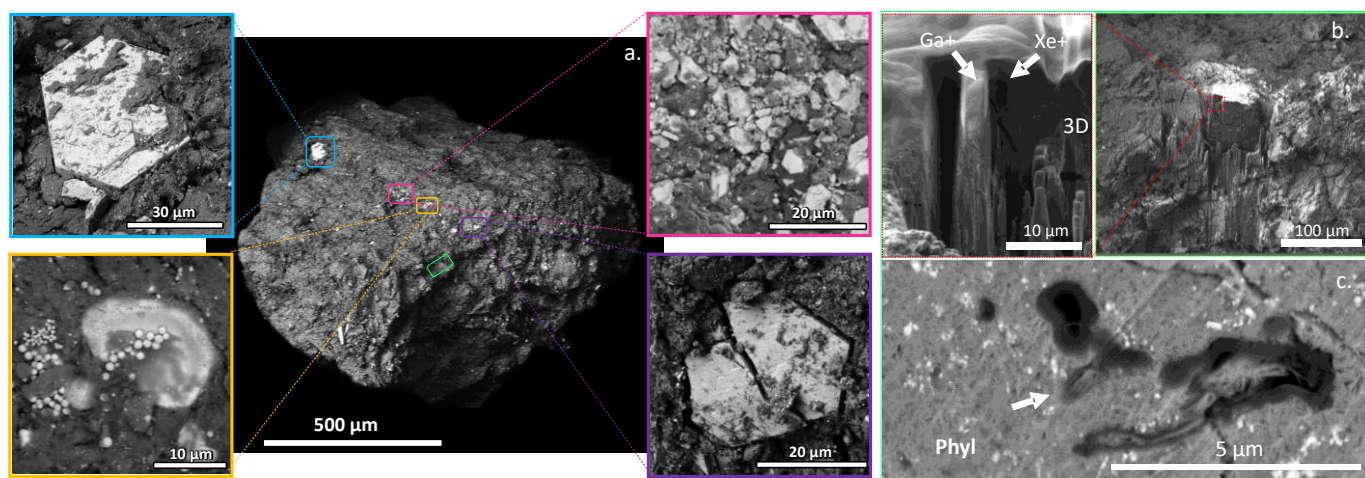


Figure 1. BSE images of particle A0083 (Radegast). (a) Entire image of Radegast. Insets show various phases on the top of the particle. Blue and purple are Fe-Sulphides (probably hexagonal pyrrhotite) Yellow is Fe-oxides (magnetite). Pink is a mixture of minerals. Green rectangle shows the region of tomography from the top edge of Radegast. (b) Tomography and Lamella liftout regions. Inset show the milled regions for tomography and lamella liftout made between Ga⁺ (*LYRA3*) and Xe⁺ (*AMBERX*) FIB instruments. (c) A Coarse grained organic particle (arrowed) from 1st cross section of tomography volume.

Results & Discussion Radegast displays CI composition similar to samples from both TAG sites, suggesting widespread alteration across the asteroid. Organic particles are mostly submicron with IOM morphology. Some coarser OPs identified in the tomography completely surround phyllosilicate, suggesting post-formation of the primary mineralogy within them (Fig. 2).

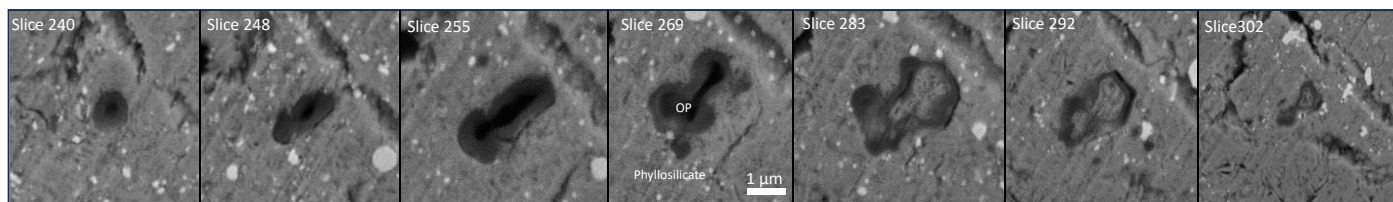


Figure 2. FIB Tomography slices of a coarse-grained organic particle in Radegast.

Organic particles and diffuse OM are consistent between FIB and microtome samples of Ivuna (diffuse OM in microtome samples have not been previously reported), implying that both Ga⁺ and Xe⁺ FIB preserve the functional chemistry of OPs and diffuse OM (Fig. 3). Carbon-XANES shows that individual OPs in closer proximity to one another are more equilibrated, suggesting that the alteration recorded in the grain was a common process evolving them. They have aromatic-rich, 3-peak spectra similar to the ‘aromatic’ particles in [4]. Notably, OPs in Ivuna are aromatic poorer, with lower aromatic/ketone ratios than those in Radegast and other Ryugu samples. Aromatic-rich OPs are however in higher abundance in the CR1 GRO 95577 [2] and Orgueil [3] than the type 2/3 carbonaceous chondrites. Diffuse OM (aromatic-poorer and aliphatic/carboxylic-rich OM than OPs) in Radegast is also more similar to diffuse OM found in Ivuna (Fig. 3) and GRO 95577 [2], with higher carboxyl/aromatic peak ratios than type 2/3. It is also similar by being in phyllosilicate rather than amorphous hydrated silicates found in type 2/3 chondrites. SEM and TEM (Fig. 5) shows coarse and finer domains of phyllosilicate. Diffuse OM occurs in both domains of phyllosilicate but is less concentrated in the coarse domains than the finer ones that are also intermixed mostly with Fe and Fe,Ni-rich sulphides (Fig. 3a). HRTEM shows the coarse domains as mixed layers of serpentine and smectite, consistent with previous studies [6].

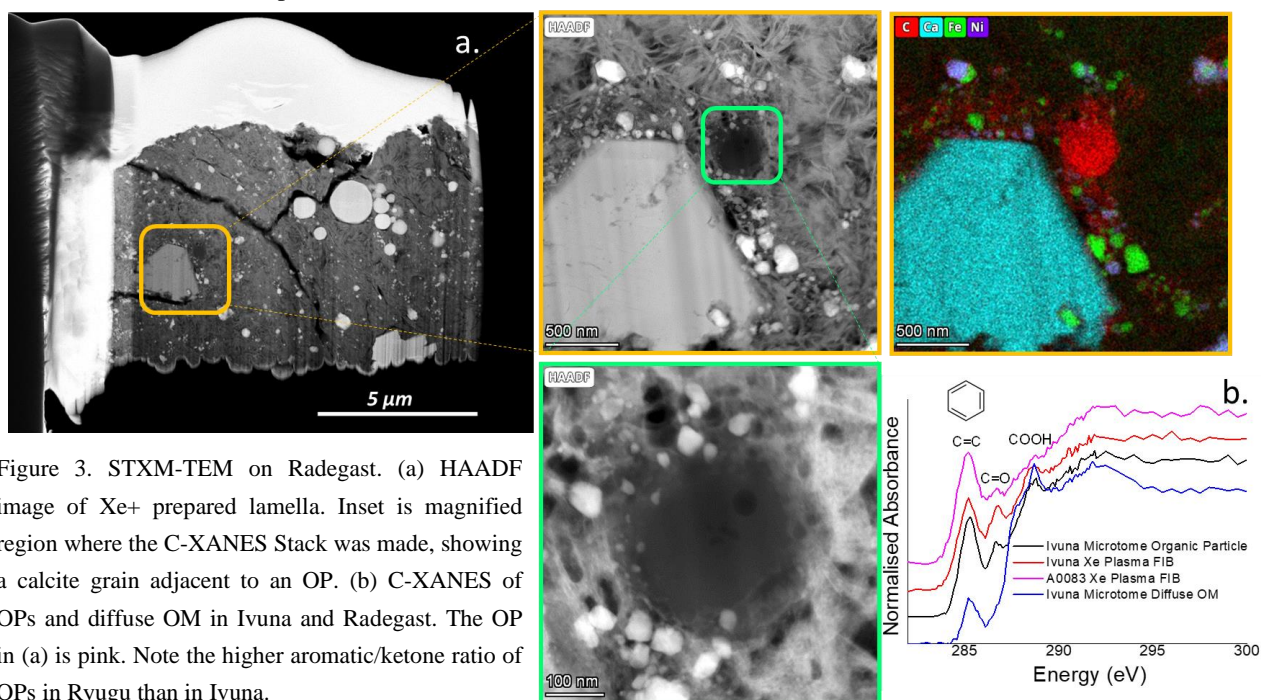


Figure 3. STXM-TEM on Radegast. (a) HAADF image of Xe⁺ prepared lamella. Inset is magnified region where the C-XANES Stack was made, showing a calcite grain adjacent to an OP. (b) C-XANES of OPs and diffuse OM in Ivuna and Radegast. The OP in (a) is pink. Note the higher aromatic/ketone ratio of OPs in Ryugu than in Ivuna.

Conclusion Organic material in Radegast evolved into aromatic-rich organic particles and aliphatic/carboxyl-rich diffuse OM by alteration on Ryugu, similar to those found in type C1 planetary materials.

References [1] Nakamura T. et al. 2022 *Science* 379: eabn8671. [2] Changela. H. G. et al. 2018 *Meteoritics & Planetary Science* 53:1006-1029. [3] Le Guillou C. et al. 2014 *Geochimica Cosmochimica Acta* 131: 368-392. [4] Yabuta H. et al. 2023 *Science* 679: 6634. [5] Noguchi T. et al. 2020 *Life* 10(8):135. [6] Ito M. et al. 2022 *Nature Astronomy* 6(10): 1-9.

Acknowledgements This research was funded by the Czech Science Foundation Project Reg. No. 21-11366S with financial support by ERDF/ESF Centre of Advanced Applied Sciences (CZ.02.1.01/0.0/0.0/16_019/0000778). We acknowledge CF CryoEM of CIISB, Instruct-CZ Centre, supported by MEYS CR (LM2023042) and European Regional Development Fund-Project UP CIISB (No. CZ.02.1.01/0.0/0.0/18_046/0015974). We thank Takis Theodossiou of the Greek Meteorite Museum for the curation of the Ivuna meteorite.

New view on the paleomagnetic record of samples from asteroid Ryugu

C. Maurel¹, J. Gattacceca¹, M. Uehara¹

¹CNRS, Aix Marseille Université, IRD, INRAE, CEREGE, Aix-en-Provence, France

The JAXA Hayabusa 2 mission returned ~5 g of material from the C-type asteroid Ryugu. Ryugu material contains abundant magnetite and pyrrhotite, formed during aqueous alteration on its parent body. The timing of aqueous alteration is not yet well constrained, with estimates ranging between 1.8 and 6.8 Myr after CAI formation (Yokoyama et al., 2022; McCain et al., 2023). Given these uncertainties, aqueous alteration on Ryugu's parent body may have occurred during the lifetime of the solar nebula magnetic field (i.e., up to ~5 Myr after CAI formation; Weiss et al., 2017). Magnetite and pyrrhotite may therefore carry a chemical remanent magnetization reflecting the intensity of this field.

Rock magnetic and paleomagnetic data of Ryugu samples were recently published (Nakamura et al. 2022; Sato et al., 2022). The authors measured the NRM of two samples (0.425 mg and 1.556 mg) and demagnetized the NRM using alternating fields (AF). They identified stable remanence components in both samples up to 24 mT and 32 mT, respectively, which they interpreted as evidence that Ryugu material experienced a 41- to 390- μ T solar nebula field.

We conducted a new paleomagnetic investigation of two other Ryugu samples with mass 0.8 mg and 20.8 mg. Data are very consistent among our two samples, but their mass-normalized NRM intensities are 20 to 100 times weaker than the published ones. NRM demagnetization data exhibit a poorly defined low-coercivity component up to ~8 mT, but become completely erratic at higher AF field steps. A similar demagnetization behavior is found after applying anhysteretic remanent magnetizations (ARM) acquired in bias fields up to 10 μ T. For ARM bias fields of 20 μ T and greater, we can identify a component of the magnetization in the coercivity range 10-50 mT. Although further analyses are being conducted, this favors the idea that the samples experienced magnetic fields < 17 μ T in intensity, assuming the sample acquired a chemical remanent magnetization. This upper limit is compatible with both (i) the nebula field intensity estimated from other meteorites with similar age of the NRM, and (ii) the absence of field.

We suspect that the samples used by Nakamura, Sato and colleagues may have been contaminated by exposure to strong magnetic fields up to ~20 mT. We will discuss how such a contamination can be identified using measurements that are non-destructive for the NRM. This highlights the need for extreme caution to avoid magnetic contamination during handling of returned extraterrestrial material. Our data show, however, that the samples were not remagnetized *en masse* during sampling on the asteroid, in transit in the spacecraft or during curation preceding any measurements.

We are very grateful to JAXA for the allocation of the Ryugu samples A0154 and C0005.

References

Yokoyama, T., et al. (2023) *Science* 379, eabn7850; McCain, K. A., et al. (2023) *Nat. Astro.* 7, 309-317; Weiss, B. P., et al. (2017) *Earth Planet. Sci. Lett.* 468, 119-132; Nakamura, T., et al. (2022) *Science* 379, eabn8671; Sato M., et al. (2022) *J. Geophys. Res. Planets* 127, e2022JE007405

Cosmogenic Radionuclide Records of Hayabusa Aggregate and Particle Samples

Kunihiko Nishiizumi¹, Marc W. Caffee², Keisuke Nagao³, Kees C. Welten¹, Jozef Masarik⁴

¹Space Sciences Laboratory, Univ. of California, Berkeley, CA 94720-7450, USA., ²Dept. of Physics & Astronomy, Purdue Univ., West Lafayette, IN 47907-2036, USA., ³Div. of Polar Earth-System Sci., KOPRI, Incheon 21990, Korea, ⁴Faculty of Math. & Physics, Comenius Univ., SK-842 15, Bratislava, Slovakia

Hayabusa2 arrived at the C-type asteroid 162173 Ryugu in June 2018, and successfully collected surface samples from two sampling sites, returning ~5.4 g of material to Earth on December 6, 2020. The surface samples stored in Chamber A were collected by the 1st touchdown (TD) on Ryugu's surface on February 21, 2019. A crater (diameter of ~14 m) on Ryugu's surface was made using a collision device - denoted "Small Carry-on Impactor (SCI)" - on April 5, 2019 [1]. The samples in Chamber C were collected proximal to the north side of this artificial crater by the 2nd TD on July 11, 2019 and possibly contain ejecta from the crater [2]. Distance between TD1 and TD2 is ~820 m.

Our studies are based on the measurement of those nuclides produced in asteroidal surface materials by cosmic rays - both solar (SCR) and galactic cosmic rays (GCR). Cosmic-ray-produced (cosmogenic) nuclides are used to determine the duration and nature of the exposure of materials to energetic particles. Our goals are to understand both the fundamental processes on the asteroidal surface and the evolutionary history of its surface materials. For Hayabusa2 samples, there are several specific questions we aim to address: (1) are the Chamber C samples, collected during the 2nd TD ejecta deposits from the artificial crater, (2) if so, what is the original depth of each recovered sample in the Ryugu regolith, and (3) what is the surface exposure time, mixing rate, and erosion/escape rate of Ryugu's surface? To answer these questions, we were allocated and received particles from Chamber A and Chamber C for measurements of cosmogenic radionuclides and noble gases as a part of initial analysis of Ryugu. We have measured cosmogenic ¹⁰Be ($t_{1/2} = 1.36 \times 10^6$ yr), ²⁶Al (7.05×10^5 yr), ³⁶Cl (3.01×10^5 yr), and stable noble gases in those samples [3-5]. Based on noble gas analysis of ~2 dozen Ryugu samples, we found that cosmic ray exposure (CRE) ages of Chamber A (surface) samples, A0105, range from 2.9 to 7.5 Myr and Chamber C (sub-surface) samples, C0106, range from 1.6 to 5.8 Myr based on ²¹Ne concentrations [3, 6]. We also found that four C0106 particles were exposed at depth of ~50, 110, 130, and 145 g/cm² respectively and had different CRE ages based on cosmogenic nuclide measurements [3, 5].

To further study of the exposure condition of Ryugu surface materials, we obtained one grain, A0130, from Chamber A and 3 grains, C0012, 0162, and 0182 from Chamber C. In addition, we obtained two aggregate samples, A0221 and C0212, in order to determine average exposure ages and depths for both Chamber A and C samples. As shown above, each grain had different exposure histories (age and depth). This is similar to what we found for exposure histories of individual grains of lunar core samples. While cosmogenic radionuclides of lunar bulk soils show smooth depth profiles, the measured radionuclide concentrations of individual rock fragments at the same depth show deviations from the smooth depth profiles [7].

Each sample was gently crushed by a mortar and pestle made from sapphire and then divided into two fractions, one fraction for cosmogenic radionuclides (this work) and one for noble gases measurements [8]. The samples were individually transferred to a small Al weighing boat and the masses were determined using an ultra-micro balance. For cosmogenic radionuclide analysis, the sample was transferred to a Teflon bomb and dissolved with HF and HNO₃ mixture in the presence of Be and Cl carriers. After Cl was separated as AgCl for ³⁶Cl measurements, a small analysis aliquot was taken for chemical analysis by ICP-OES. Beryllium, Al, and Mn were separated by ion chromatography, using anion and cation ion exchange columns, and Be and Al were purified for AMS measurements. To serve as a baseline comparison, a few grains of the Orgueil CI chondrite were analyzed using the same protocols. Beryllium-10 and ²⁶Al AMS analyses were performed at PRIME Lab, Purdue University [9]. Measured isotopic ratios were normalized by AMS standards [10, 11] and converted to radionuclide concentrations (dpm/kg).

Chemical compositions in Ryugu samples measured by ICP-OES are shown in Table 1. Since sample sizes are slightly larger than previous Ryugu initial analysis, data show less scatter. Bulk chemical compositions of samples from TD1 and TD2 determined using ICP-MS [12] are also shown in the table. Our analysis of A0221 and C0212 are in good agreement with analysis of TD1 and TD2 samples determined by [12]. Noticeably, both our two samples and published analysis of TD1 and TD2 samples [12] were obtained from aggregate samples and not individual grains. Although [12] concluded that there are no systematic differences in chemical composition between the samples from TD1 and TD2 sites, our limited measurements indicate that Ca is slightly higher and Fe is lower in TD1 samples than that of TD2.

Table 1. Chemical compositions in Ryugu samples and Orgueil CI chondrite.

Sample	Mg (%)	Al (%)	K (ppm)	Ca (%)	Ti (ppm)	Mn (ppm)	Fe (%)	Co (ppm)	Ni (%)
A0130	9.32	0.94	720	1.45	520	1990	18.39	540	1.13
A0221	10.84	0.90	520	1.69	530	3040	19.76	560	1.20
C0012	10.54	0.91	600	1.09	460	2020	21.15	600	1.31
C0012	10.74	0.91	580	1.18	490	2340	20.11	560	1.21
C0162	10.81	0.90	570	1.08	570	2120	20.75	560	1.26
C0182	9.36	0.84	400	0.95	510	1510	18.63	520	1.13
C0212	10.77	0.98	550	1.18	510	2370	20.53	590	1.26
Ryugu (TD1)*	10.69	0.86	520	1.63	480	3000	19.49	550	1.18
Ryugu (TD2)*	10.42	0.90	600	1.37	470	2490	20.22	590	1.22
Orgueil CI	7.37	0.64	440	0.60	340	1380	14.23	400	1.18
Orgueil CI [#]	9.63	0.60	530	0.76	-	1680	17.76	540	1.04

*[12], [#]Previous measurement (unpublished 2003)

Cosmogenic nuclide ¹⁰Be and ²⁶Al concentrations in Ryugu samples are shown in Table 2 along with that of Orgueil CI chondrite. Using the MCNP Code System [13], we calculated the GCR production rates of ¹⁰Be and ²⁶Al by spallation reactions for a body having a 2 π geometry with Ryugu's chemical composition [12]. Based on the comparison of the observed radionuclide concentrations with model calculated ¹⁰Be and ²⁶Al production rate depth profiles, assuming the radionuclide concentrations in Ryugu are saturated, we obtained the first order estimation of exposure depth of each sample and shown in Table 2. Based on those depths we calculated ²¹Ne production rates and calculated ²¹Ne CRE ages in each sample [8]. The calculated exposure depths and CRE ages of each grain obtained by TD2 scatter, in similar fashion as previous works [3, 5]. The preliminary estimation of average exposure depth of aggregate sample A0221 is somewhat deeper than those of each grain obtained from TD1. The depth range of aggregate sample C0212 collected by TD2 is estimated to be 110 - 140 g/cm² based on ¹⁰Be concentration. The ²⁶Al concentration of C0212 indicates much shallow depth of 10 - 90 g/cm². One possible explanation is that C0212 contains a small amount of surface material that contains high SCR produced ²⁶Al. The measurement of thermal neutron-capture produced ⁴¹Ca ($t_{1/2} = 1.0 \times 10^5$ yr) - in progress - is critical to further constrain the exposure depth of each sample.

Table 2. Cosmogenic nuclide ¹⁰Be and ²⁶Al concentrations in Ryugu samples and Orgueil CI chondrite.

Sample	Mass (mg)	¹⁰ Be (dpm/kg)	²⁶ Al (dpm/kg)	Depth (g/cm ²)
A0130	0.676	9.94 ± 0.29	29.2 ± 1.3	10 - 70
A0221	10.718	11.23 ± 0.10	27.4 ± 0.6	70 - 100
C0012	4.200	7.50 ± 0.10	24.3 ± 0.8	90 - 140
C0012	7.274	7.43 ± 0.15	23.3 ± 0.8	110 - 150
C0162	1.531	7.58 ± 0.21	24.6 ± 1.0	95 - 145
C0182	0.983	6.28 ± 0.15	25.3 ± 1.3	85 - 135
C0212	8.406	9.06 ± 0.09	29.3 ± 0.6	110 -140
Orgueil CI	6.000	14.91 ± 0.31	35.9 ± 1.2	-
Orgueil CI [#]	52.60	21.19 ± 0.36	40.4 ± 0.8	-

[#]Previous measurement (unpublished 2003)

Acknowledgments: We thank Hayabusa2 project team and Hayabusa2 curation members. Orgueil was obtained from MNHN-Paris. This work was supported by NASA's LARS program.

References:

- [1] Arakawa M. et al. (2020) Science. 368, 67-71. [2] Tsuda Y. et al. (2020) Acta Astronautica. 171, 42-54. [3] Nagao K. et al. (2022) Meteor. Planet. Sci. 57, A337 #6320. [4] Nishiizumi K. et al. (2022) Lunar Planet. Sci. LIII, #1777. [5] Nishiizumi K. et al. (2022) Hayabusa Symposium 2022. S21-08. [6] Okazaki R. et al. (2022) Science. 379, eabo0431. [7] Nishiizumi K. et al. (1985) Lunar Planet. Sci. XVI, 620-621. [8] Nagao K. et al. (2023) Hayabusa Symposium 2023 (this meeting). [9] Sharma P. et al. (2000) Nucl. Instrum. Methods Phys. Res. B 172, 112-123. [10] Nishiizumi K. (2004) Nucl. Instrum. Methods Phys. Res. B223-224, 388-392. [11] Nishiizumi K. et al. (2007) Nucl. Instrum. Methods Phys. Res. B258, 403-413. [12] Yokoyama T. et al. (2022) Science. 379, eabn7850. [13] Masarik J. and Reedy R. C. (1994) Geochim. Cosmochim. Acta. 58, 5307-5317.

Noble Gases of the 1st and 2nd AO Ryugu Samples Collected by the Hayabusa2 Spacecraft

Keisuke Nagao^{1*}, Kunihiko Nishiizumi², Marc W. Caffee³, Hwayoung Kim¹, Changkun Park¹, Jong Ik Lee¹, Jozef Masarik⁴
¹KOPRI, Incheon 21990, Korea, ²Space Sciences Laboratory, Univ. of California, Berkeley, CA 94720-7450, USA, ³Dept. of Physics & Astronomy, Purdue Univ., West Lafayette, IN 47907-2036, USA, ⁴Comenius Univ., Bratislava, Slovakia, *present address: Seki 2082, Maniwa-shi, Okayama 719-3156, Japan. knagao520@gmail.com

Hayabusa2 arrived at the C-type asteroid 162173 Ryugu in June 2018, and successfully collected surface samples from two sampling sites, returning ~5.4 g of samples to Earth on December 6, 2020. Surface samples stored in Chamber A were collected during the 1st touchdown (TD) on Ryugu's surface on February 21, 2019. A crater (diameter of ~14 m) on Ryugu's surface was made using a collision device - denoted "Small Carry-on Impactor (SCI)" on April 5, 2019 [1]. Samples in Chamber C were collected proximal to this artificial crater and are possibly ejecta from the north side of the crater by the 2nd TD on July 11, 2019 [2].

Our studies on the Hayabusa2 samples are based on the measurement of those nuclides produced in asteroidal surface materials by both solar (SCR) and galactic cosmic rays (GCR). Cosmic-ray-produced (cosmogenic) nuclides are used to determine the duration and nature of the exposure of materials to energetic particles [3]. Our goals are to understand both the fundamental processes on the asteroidal surface and the evolutionary history of its surface materials. These processes occur over timescales spanning the present to 10⁹ yrs into the past, and are important not only for understanding the history of Ryugu's surface but also for studies of asteroid-meteoroid evolutionary dynamics. For Hayabusa2 samples, there are several specific questions we aim to address: (1) are the Chamber C samples, collected during the 2nd TD, ejecta deposits from the artificial crater, (2) if so, what is the original depth of each recovered sample grain in the Ryugu regolith, and (3) what is the average surface exposure time, mixing rate of regolith materials, and erosion/escape rate of Ryugu's surface? We investigate and utilize cosmogenic radionuclides (¹⁰Be, ²⁶Al, ³⁶Cl, and ⁴¹Ca) and noble gases, especially cosmogenic ²¹Ne in Ryugu samples. Expected maximum cosmogenic nuclide concentrations in millimeter-sized (~1 mg in mass) Ryugu sample are a few times 10⁵ - 10⁷ atoms or lower. These values are higher than the present detection limits of accelerator mass spectrometry (AMS) and noble gas mass spectrometry, but 2 orders of magnitude smaller than normal studies of cosmogenic nuclide measurements in meteoritic materials.

We present here the noble gas isotopic compositions of 6 samples (Table 1) allocated as the 1st and 2nd AO. Noble gases were measured with the system of modified-VG5400 mass spectrometer at Korea Polar Research Institute (KOPRI). The noble gas system had been used to measure the Itokawa samples at the University of Tokyo [4], and then moved to KOPRI afterward in 2015. Noble gases were extracted from each sample using a miniature furnace specially designed for small samples, using a Ta-tube with a Mo-crucible. A sample dropped into the crucible is heated from outside of the Ta-tube by a W-heater. Electric current applied to the W-heater is controlled by a computer program monitoring the heating temperature with a W-Re thermocouple. Samples were installed in a glass-made sample holder, which was set on the furnace and preheated for a day at about 120°C to remove atmospheric noble gas contamination adsorbed on the samples. Stepwise heating was applied to extract noble gases, i.e., 200, 900, and 1700°C for small samples (A0130, C0162, and C0182), and 200, 600, 900, 1200, and 1700°C for larger samples (A0221, C0012, and C0212). The extracted noble gases from each sample were purified and separated into 5 fractions, i.e., He, Ne, Ar, Kr, and Xe, then measured isotope abundances and isotopic ratios for each fraction.

Total values of concentrations of ⁴He, ²⁰Ne, ³⁶Ar, ⁸⁴Kr, and ¹³²Xe, and isotope ratios of He, Ne, and Ar obtained by the stepwise heating method are presented in Table 1. Data of Orgueil CI chondrite measured in this work are also presented for comparison. Solar He and Ne with very high concentrations of ⁴He (14.9 and 9.3×10⁻⁴ cm³STP/g) and ²⁰Ne (2.0 and 1.5×10⁻³ cm³STP/g) were observed for the aggregate samples A0221 and C0212, respectively. These samples showed ²⁰Ne/²²Ne ratios of 12.8–13.7 in the temperature range of 200–900°C. The ratios are close to the value of 13.78 for solar wind (SW) [5]. Release peaks of ⁴He for these samples were at the heating temperature of 600°C, for which ³He/⁴He was 3.9×10⁻⁴, slightly lower than the SW value of 4.64×10⁻⁴ [5]. Smaller amounts of SW He and Ne are also indicated in A0130. Neon isotopic compositions for other samples are a mixture of several primitive components, e.g., P1 (Ne-Q), P3 (presolar diamond), and Ne-E(H) (SiC) [6]. Xe isotopic ratios, e.g., ¹³⁰Xe/¹³²Xe, ¹²⁹Xe/¹³²Xe, and ¹³⁶Xe/¹³²Xe, indicate that trapped Xe is mostly Q-Xe component, with a small or negligible contribution of cosmogenic and HL or fissiogenic Xe.

Concentrations of cosmogenic ³He were difficult to calculate, because only a small excess of cosmogenic ³He was observed at the low heating temperatures at 200–900°C for some samples (³He/⁴He = 5.2, 7.3, 4.9, and 4.8×10⁻⁴ for A0221, C0012, C0162, and C0212, respectively), and most ³He/⁴He ratios were between 1.23×10⁻⁴ for trapped Q-He [6] and 4.64×10⁻⁴ for SW [5]. Neon isotopic compositions are a mixture of several primitive components, e.g., SW [5], P1 (Ne-Q), P3 (presolar diamond), and Ne-E(H) (SiC) [6], to which a small contribution of cosmogenic ²¹Ne was detected. Calculated concentrations of

cosmogenic ^{21}Ne in excess of the assumed trapped $^{21}\text{Ne}/^{22}\text{Ne} = 0.029$ are presented in Table 1. The concentrations of cosmogenic ^{21}Ne are $(4.06\text{--}11.9)\times 10^{-9}$ $\text{cm}^3\text{STP/g}$. The concentrations of 11.9 and 9.83×10^{-9} $\text{cm}^3\text{STP/g}$ for aggregate samples A0221 and C0212, respectively, are higher than those observed for the initial analysis samples, $(1.6\text{--}7.8)\times 10^{-9}$ $\text{cm}^3\text{STP/g}$ [7, 8]. Exposure depths were estimated from preliminary measurements of ^{10}Be and/or ^{26}Al in same samples. Then, each production rate P_{21} was obtained by new calculation using the MCNP Code System. Calculated cosmic ray exposure (CRE) ages are shown in Table 1. CRE ages calculated for the samples from Chamber-A are roughly 4 and 11 Myr for A0130 and A0221, respectively. CRE ages for 3 samples from Chamber-C, C0012, C0162, and C0182, are in the range of 3–5 Myr, while C0212 has longer CRE age of 8–9 Myr. The CRE ages of 3–5 Myr for the samples from Chamber-A and -C are similar to the reported ages for initial analysis samples, 3–5 Myr [7] and ~5 Myr [8]. Contrary to these grain samples, two aggregate samples A0221 and C0212 with longer CRE ages are enriched in SW-Ne. Samples measured in the present work must have been irradiated heterogeneously by both GCR and SW on the Ryugu's surface before sampling by the Hayabusa2.

Sample	Mass mg	Stepwise heating ²⁾	⁴ He	²⁰ Ne	³⁶ Ar	⁸⁴ Kr	¹³² Xe	³ He/ ⁴ He	²⁰ Ne/ ²² Ne	²¹ Ne/ ²² Ne	³⁸ Ar/ ³⁶ Ar	⁴⁰ Ar/ ³⁶ Ar	²¹ Ne _{cosm}	P_{21} ³⁾	T_{21} ³⁾
			$10^{-9}\text{cm}^3\text{STP/g}$						10^{-4}						$10^{-9}\text{cm}^3\text{STP/g}$
A0130	0.2086	3 steps	219000	1230	1600	15.9	19.3	3.84	10.54	0.0654	0.1858	1.79	4.41	1.10–1.20	3.7–4.0
A0221	1.6610	5 steps	1490000	20400	3430	16.9	18.5	3.54	12.85	0.0362	0.1842	0.485	11.9	1.20	9.9
C0012	2.2179	5 steps	97700	472	1530	15.9	19.6	3.59	8.27	0.0978	0.1861	0.419	4.06	1.12–1.20	3.4–3.6
C0162	0.1886	3 steps	118000	706	1430	15.3	17.7	4.46	8.68	0.0984	0.1867	1.34	5.83	1.13–1.17	5.0–5.2
C0182	0.2768	3 steps	93800	432	1370	20.5	17.0	3.80	8.09	0.1280	0.1876	1.18	5.45	1.15–1.20	4.5–4.7
C0212	0.8232	5 steps	932000	15200	2720	16.1	18.7	3.89	12.95	0.0371	0.1849	0.427	9.83	1.12–1.17	8.4–8.8
Orgueil(CI)	1.7205	3 steps	672000	1130	1260	13.0	15.7	3.51	10.08	0.1099	0.1856	2.37	9.37	2.22 ⁴⁾	4.22

¹⁾ Isotopic ratios of Kr and Xe are not presented.
²⁾ Heating temperatures are 200, 900, and 1700°C for 3 steps, and 200, 600, 900, 1200, and 1700°C for 5 steps.
³⁾ Each depth was estimated based on preliminary measurements of cosmogenic radionuclides. The production rates and CRE ages were not included $\pm 5\%$ uncertainty of our new calculations and experimental errors.
⁴⁾ Production rate in 4π -geometry for CI chondrites [9].

Acknowledgment: We thank Hayabusa2 project team, especially the curation members. We also thank HMNH-Paris for providing Orgueil sample.

References

- [1] Arakawa M. et al. 2020. Science 368, 67–71
- [2] Tsuda Y. et al. 2020. Acta Astronautica 171, 42–54
- [3] Reedy R. C. et al. 1983. Annu. Rev. Nucl. Part. Sci. 33, 505–537.
- [4] Nagao K. et al. 2011. Science 26, 1128–1131.
- [5] Heber V. S. et al. 2009 Geochim. Cosmochim. Acta 73, 7414–7432.
- [6] Ott U. (2002) Noble gases in Geochem. and Cosmochem., Rev. in Mineral. Geochem. 47, 71–100.
- [7] Nagao K. et al. 2022. Meteoritical Soc. Meeting, Abstract #6134.
- [8] Okazaki R. et al. 2023. Science 379, 788.
- [9] Eugster O. 1988. Earth Planet Sci. Lett. 52, 1649–1662.

Insights into Early Solar System Isotopic Reservoirs Inferred from Ryugu

Quinn R. Shollenberger¹, Jan Render¹, and Gregory A. Brennecka¹

¹Lawrence Livermore National Laboratory

Introduction: Returned primitive Solar System material presents a unique opportunity to address multiple important planetary science questions. Recent work has demonstrated that material returned from the Japan Aerospace Exploration Agency's (JAXA) Hayabusa2 mission from Cb-type asteroid (162173) Ryugu is most closely related to Ivuna-type (CI) carbonaceous chondrites [e.g., 1-2], which have a chemical composition similar to that of the Sun's photosphere. The pristine nature and CI-like chemical composition of Ryugu samples allows researchers to use bulk-rock nucleosynthetic isotope anomalies to establish genetic relationships to planetary bodies and to refine our knowledge of the isotopic evolution of the Solar System, as well as the accretion history of the terrestrial planets [e.g., 1-6].

The initial isotopic study of four Ryugu particles found it has an indistinguishable Fe isotope composition from CI chondrites—which is itself different from all other carbonaceous chondrites [2]. This led to the conclusion that a third isotopic reservoir may have existed in the early Solar System for CI and CI-like bodies to form separate from the carbonaceous and non-carbonaceous reservoirs. However, the existence of a third isotopic reservoir has recently been challenged through two different models [7-8], and those studies have shown that the isotopic dichotomy between carbonaceous and non-carbonaceous meteorites extends to Fe isotopes. These authors suggest that the appearance of an apparent third isotopic reservoir in the meteorite record reflects a lack of Fe isotope data from carbonaceous achondrites [8]. Here we report Fe and Ti isotopic analyses with the addition of Ni isotope compositions on a bulk sample from Ryugu to shed new light on the isotopic reservoirs present in the early Solar System.

Methods: Ryugu particle A0208, provided by JAXA, was analyzed in this study. This particle was part of a surface sample that was collected in Chamber A during the first touchdown of the Hayabusa2 spacecraft. Approximately 8 mg of Ryugu particle A0208 was weighed and dissolved in a pre-cleaned PFA vial using a combination of concentrated HF:HNO₃, followed by aqua regia. Two procedural blanks as well as the geostandards BCR-2 and BHVO-2 were processed alongside our Ryugu sample for all procedures. Following dissolution, we obtained major and trace element concentrations using a Thermo Scientific Element XR ICP-MS at Lawrence Livermore National Laboratory (LLNL) following previously published methods [9].

All samples were processed through multiple chemical separations to purify the elements of interest using previously established procedures. The first separation was to isolate Fe from the sample matrix [10] followed by purification of Ti [e.g., 11] and Ni [e.g., 12]. Yields of our procedures were >80% and the blanks were negligible considering the total amount of material processed for Fe, Ti, and Ni. Iron and Ni isotopic analyses were performed on a Thermo Scientific Neptune *Plus* MC-ICPMS at LLNL while Ti isotopes were measured on a Thermo Scientific Neoma MC-ICPMS at LLNL [e.g., 2, 11-12].

Results and Discussion: Whereas the previously analyzed Ryugu particles were all around 25 mg or less [1-2], our particle A0208 weighed only 8 mg. Despite this difference and the limited masses in general, we observe that our Ryugu particle exhibits elemental concentrations comparable to what has been reported in previous work (Fig. 1). Shown in figure 1 are major and trace element concentrations obtained for particle A0208 against the average concentration data from the initial Ryugu study [1], demonstrating overall excellent agreement. A few small differences exist between the two works (the most notable being Be), which are readily explained by heterogeneities at these small sample scales (< 25 mg).

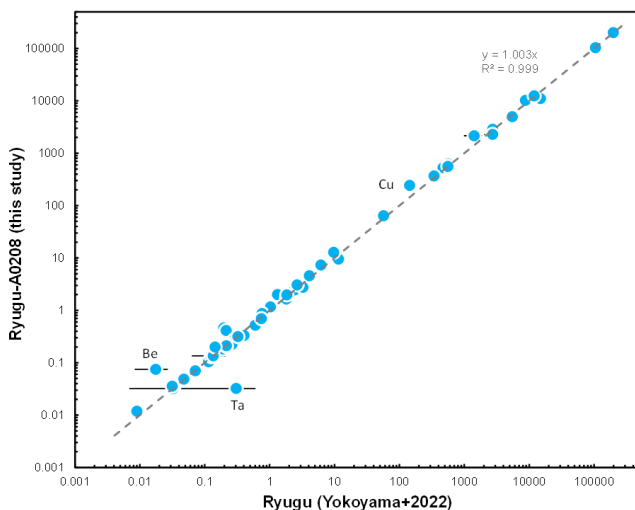


Figure 1. Major and trace element abundances of Ryugu A0208 particle of this work plotted against the average concentrations determined for Ryugu particles A0106, A0107, and C0108 from [1]. With a few exceptions, most elements are in good agreement between the two studies. Uncertainties for ICP-MS data from this study are estimated to be $\pm 5\%$, whereas error bars shown for data from [1] are two standard deviations of the two ICP-MS measurements reported in that work.

Figure 1. Major and trace element abundances of Ryugu A0208 particle of this work plotted against the average concentrations determined for Ryugu particles A0106, A0107, and C0108 from [1]. With a few exceptions, most elements are in good agreement between the two studies. Uncertainties for ICP-MS data from this study are estimated to be $\pm 5\%$, whereas error bars shown for data from [1] are two standard deviations of the two ICP-MS measurements reported in that work.

Shown in Figure 2 are select Ti, Fe, and Ni isotope data commonly used for genetic comparison of meteoritic materials. Our measured Fe and Ti isotopic compositions are indistinguishable from other Ryugu particles as well as from CI chondrites [1-2]. The overlapping Fe and Ti isotopic compositions of our Ryugu particle with previous measurements indicate that sample heterogeneity is not a big concern for major elements analyzed here. Although specific values and uncertainties were not provided in [13], our Ni isotope data from Ryugu particle A0208 appear to be consistent with these previous Ni isotope measurements as well as CI chondrites (Fig. 2). This result offers further support to the interpretation that Ryugu is most closely related to CI chondrites [1-2, 13].

The new Ti, Fe, and Ni isotopic data obtained in this study demonstrate that Ryugu and CI chondrites may plot on a continuation of a trend defined by the carbonaceous chondrites. Previous studies have suggested that CI chondrites and Ryugu may have formed at greater heliocentric distances compared to other carbonaceous chondrites [e.g., 2, 13-14] and our data are supportive of this interpretation given that Ryugu and CI chondrites are an endmember in the carbonaceous reservoir. While our data do not clearly provide evidence for the existence of a third isotopic reservoir in the early Solar System as previously suggested [2], this is not ruled out, either. Additional isotopic measurements are underway at LLNL for Cr and any finalized data and further interpretations will be reported at the meeting.

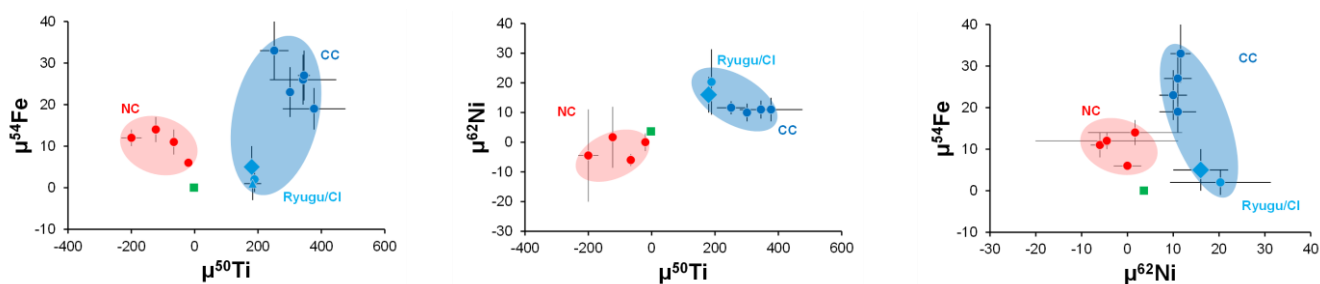


Figure 2. Plots of $\mu^{54}\text{Fe}$ vs. $\mu^{50}\text{Ti}$, $\mu^{62}\text{Ni}$ vs. $\mu^{50}\text{Ti}$, and $\mu^{54}\text{Fe}$ vs. $\mu^{62}\text{Ni}$, where μ designates parts per million deviation from a terrestrial standard. Ryugu particle A0208 from this study is the large light blue diamond, previous Ryugu measurements are shown as a light blue triangle, average CI chondrite as a light blue circle, carbonaceous chondrites (CC) as dark blue circles, non-carbonaceous meteorites (NC) in red circles, and Earth as a green square. Iron and Ti isotopic data from [2]. Ni isotopic data compiled from [15-19].

Acknowledgements: The authors thank JAXA for providing Ryugu particle A0208 that was used in this study. This work was performed under the auspices of the U.S. DOE by LLNL with contract DE-AC52-07NA27344 with release number LLNL-ABS-848622. This work was funded by the Laboratory Directed Research and Development program of Lawrence Livermore National Laboratory (23-LW-015).

References

- [1] Yokoyama T. et al. (2022) *Science* 10.1126/science.abn7850. [2] Hopp T. et al. (2022) *Science Advances* 8, eadd8141. [3] Fischer-Gödde M. & Kleine T. (2017) *Nature* 541, 525-527. [4] Burkhardt C. (2021) *Science advances* 7, eabj7601. [5] Schiller M. et al. (2020) *Science Advances* 6, eaay7604. [6] Burkhardt C. et al. (2019) *Geochimica et Cosmochimica Acta* 261, 145-170. [7] Marrocchi Y. et al. (2023) *The Astrophysical Journal Letters* 954, L27. [8] Yap T. & Tissot F.L.H. (2023) *Icarus* 405, 115680. [9] Wimpenny J. et al. (2022) *Earth & Planetary Science Letters* 578, 117318. [10] Rolison J. M. et al. (2019) *Applied Geochemistry* 103, 97-105. [11] Shollenberger Q. R. et al. (2022) *Geochimica et Cosmochimica Acta* 324, 44-65. [12] Render J. et al. (2018) *The Astrophysical Journal* 862, 26. [13] Spitzer F. et al. (2023) LPSC #2488. [14] Desch S.J. (2018) *The Astrophysical Journal* 238, 11. [15] Steele R.C.J. et al. (2012) *The Astrophysical Journal* 758, 59. [16] Tang H. & Dauphas N. (2012) *Earth & Planetary Science Letters* 359-360, 248-263. [17] Tang H. & Dauphas N. (2014) *Earth & Planetary Science Letters* 390, 264-274. [18] Regelous M. et al. (2008) *Earth & Planetary Science Letters* 272, 330-338. [19] Burkhardt C. et al. (2017) *Meteoritics & Planetary Science* 52, 807-826.

Nickel isotopic composition of Ryugu and the link between CI and other carbonaceous chondrites

T. Kleine F. Spitzer¹, C. Burkhardt¹, the Hayabusa2-initial-analysis chemistry team, and the Hayabusa2-initial-analysis core
¹Max Planck Institute for Solar System Research, Justus-von-Liebig-Weg 3, 37077 Göttingen, Germany

The initial analyses of samples returned from Cb-type asteroid 162173 Ryugu by JAXA's Hayabusa2 mission provided isotopic, mineralogical, and chemical evidence for a close link of Ryugu to CI chondrites [1,2]. A subsequent study has shown that Ryugu and CI chondrites share the same nucleosynthetic Fe isotope signatures, which are distinct from those of other carbonaceous chondrites [6]. This not only demonstrates that Ryugu and CI chondrites are genetically linked, but also that they derive from another reservoir than all other carbonaceous chondrites [3]. However, the origin of these distinct Fe isotopic compositions of CI chondrites/Ryugu compared to other carbonaceous chondrites is not well understood. Nickel isotopes hold considerable promise to further investigate the genetic link between Ryugu and CI chondrites. When normalized to $^{61}\text{Ni}/^{58}\text{Ni}$, CI chondrites do not only display the largest $\mu^{62}\text{Ni}$ and $\mu^{64}\text{Ni}$ anomalies among carbonaceous chondrites (where $\mu^i\text{Ni}$ is the parts-per-million deviation from terrestrial standard values), but they also have a distinct $\mu^{60}\text{Ni}$ composition compared to all other known carbonaceous chondrite-like materials. We obtained four Ryugu samples (A0106–A0107, A0106, C0108, C0107) along with six carbonaceous chondrites including the CI chondrites Orgueil and Alais, which have been chemically processed alongside the Ryugu samples [2]. In addition, we also measured several grouped and ungrouped carbonaceous chondrites. Chemical purification of Ni involved a 3-step ion-exchange chromatographic procedure that achieves sufficiently low $^{58}\text{Fe}/^{58}\text{Ni}$ and $^{64}\text{Zn}/^{64}\text{Ni}$ ratios in the final purified Ni cuts to allow for accurate and precise correction of isobaric interferences. All isotope measurements were performed on the Thermo Scientific NeptunePlus MC-ICP-MS at the Institut für Planetologie, University of Münster. Instrumental mass bias is corrected by internal normalization to either $^{61}\text{Ni}/^{58}\text{Ni}$ or $^{62}\text{Ni}/^{61}\text{Ni}$ using the exponential law. All data are reported in the μ -notation as the parts per 10^6 deviation relative to the standard.

The new Ni isotopic data for CM, CO, CV, and CR chondrites agree well with those reported in previous studies and reveal that these chondrites are characterized by negative $\mu^{60}\text{Ni}$ and positive $\mu^{62}\text{Ni}$ and $\mu^{64}\text{Ni}$ values (Fig. 1). The two ungrouped carbonaceous chondrites Tagish Lake (TL) and Tarda, for which no Ni isotopic data have been reported previously, have Ni isotope anomalies similar to those carbonaceous chondrites. By contrast, CI chondrites display distinct Ni isotopic compositions and particularly distinctly larger $\mu^{64}\text{Ni}$ and $\mu^{60}\text{Ni}$ compared to other carbonaceous chondrites (Fig. 1). Importantly, the Ni isotopic compositions of all four Ryugu samples overlaps with those of the CI chondrites, indicating distinct Ni isotopic compositions of CI chondrites/ Ryugu compared to all other carbonaceous chondrites (Fig. 1). This is consistent with the nucleosynthetic Fe isotope variations among carbonaceous chondrites, which also reveal a uniquely distinct composition for CI chondrites and Ryugu [3].

Isotopic variations among carbonaceous chondrites are thought to reflect variable proportions of three main components having distinct isotopic compositions: refractory inclusions (e.g., CAI), chondrules/chondrule precursors, and CI chondrite-like matrix [4, 5]. The incorporation of CI chondrite-like matrix in other groups of carbonaceous chondrites is consistent with systematic variations of (i) volatile element contents, (ii) mass-dependent isotope fractionations of moderately volatile elements, and (iii) nucleosynthetic ^{54}Cr anomalies with the fraction of matrix in each chondrite. However, in Ni isotope space, CI chondrites (and Ryugu) are offset from the composition of other carbonaceous chondrites, indicating that CI chondrites are not fully representative of the matrix in other groups of carbonaceous chondrites. Instead, this matrix appears to have formed from different precursor material than CI chondrites, either because it formed in a different area of the disk or because it was modified by processes in the disk prior to its incorporation in carbonaceous chondrites.

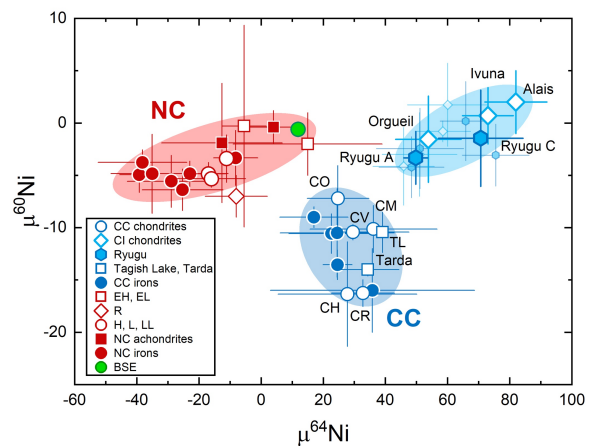


Fig. 1: $\mu^{60}\text{Ni}$ versus $\mu^{64}\text{Ni}$ for non-carbonaceous (NC) and carbonaceous (CC) meteorites. CI chondrites and Ryugu have distinct Ni isotopic compositions compared to NC and CC meteorites.

References

- [1] Yada T. et al. 2022. Nature Astronomy 6:214–220.
- [2] Yokoyama T. et al. 2022. Science abn7850.
- [3] Hopp T. et al. 2022. Science Advances 8:8141.
- [4] Alexander 2019. Geochimica et Cosmochimica Acta 254:277-309.
- [5] Hellmann et al. 2023. Astrophysical Journal Letters 946: L34.

The magnesium isotope composition of samples returned from asteroid Ryugu

Martin Bizzarro^{1,2*}, Martin Schiller¹, Tetsuya Yokoyama³ and the Hayabusa2 Initial Analysis Team

¹*Centre for Star and Planet Formation, Globe Institute, University of Copenhagen, Copenhagen, K 1350, Denmark. *email: bizzarro@sund.ku.dk*

²*Université Paris Cité, Institut de Physique du Globe de Paris, CNRS, 75005 Paris, France*

³*Department of Earth and Planetary Sciences, Tokyo Institute of Technology, Tokyo 152-8551, Japan.*

The nucleosynthetic isotope composition of planetary materials provides a record of the heterogeneous distribution of stardust within the early Solar System. Thus, nucleosynthetic signatures can be used to infer genetic relationships between early formed bodies and, ultimately, provide constraints on their accretion regions. In December 2020, the Japan Aerospace Exploration Agency Hayabusa2 spacecraft returned to Earth the first samples of a primitive asteroids, namely the Cb-type asteroid Ryugu. This provides a unique opportunity to explore the kinship between primitive asteroids and carbonaceous chondrites. Based on chemistry, mineralogy, petrology and isotope systematics of various elements, it has been proposed that Ryugu samples are closely related to Ivuna-type (CI) carbonaceous chondrites. Indeed, the bulk nucleosynthetic isotope composition for tracers like ⁵⁴Cr and ⁵⁰Ti as well as the chemical abundances of most elements are within the range of CI chondrites. Moreover, like CIs, Ryugu samples experienced extensive aqueous alteration in the presence of water and mainly consist of hydrous silicates (serpentine and saponite) and other secondary minerals (i.e., carbonate, magnetite, and sulfide) interpreted to have formed during asteroidal fluid circulation.

High-precision Mg isotope measurements can provide a novel perspective on the kinship between Ryugu with CI chondrites and, by extension, the accretion region of Cb-type asteroids. Magnesium isotope variability in Solar System materials can originate from the decay of the short-lived ²⁶Al nuclide as well as primary nucleosynthetic processes. Moreover, Mg isotopes can also be fractionated according to their masses by high-temperature events in the protoplanetary disk or, alternatively, by low-temperature parent body secondary. Thus, the combination of high-precision mass-independent and mass-dependent Mg isotope compositions is useful to understand genetic relationships and accretion history of planetary materials.

Here, we report high-precision $\mu^{26}\text{Mg}^*$ and $\mu^{25}\text{Mg}$ values of Ryugu samples together with those of CI, CM, CV and ungrouped carbonaceous chondrites. The stable Mg isotope composition of Ryugu aliquots define $\mu^{25}\text{Mg}$ values ranging from -160 ± 20 ppm to -272 ± 30 ppm, which extends to lighter compositions relative to Ivuna-type (CI) and other carbonaceous chondrite groups. We interpret the $\mu^{25}\text{Mg}$ variability as reflecting heterogeneous sampling of a carbonate phase hosting isotopically light Mg ($\mu^{25}\text{Mg} \sim -1400$ ppm) formed by low temperature equilibrium processes. After correction for this effect, Ryugu samples return homogeneous $\mu^{26}\text{Mg}^*$ values corresponding to a weighted mean of 7.1 ± 0.8 ppm. Thus, Ryugu defines a $\mu^{26}\text{Mg}^*$ excess relative to the CI and CR chondrite reservoirs corresponding to 3.8 ± 1.1 and 11.9 ± 0.8 ppm, respectively. These variations cannot be accounted for by in situ decay of ²⁶Al given their respective ²⁷Al/²⁴Mg ratios. Instead, it requires that Ryugu and the CI and CR parent bodies formed from material with a different initial ²⁶Al/²⁷Al ratio or that they are sourced from material with distinct Mg isotope compositions. Thus, our new Mg isotope data challenge the notion that Ryugu and CI chondrites share a common nucleosynthetic heritage.

Oxygen isotope systematics of crystalline silicates in comet Wild 2: Comparison to anhydrous minerals in Ryugu and CI chondrites

Noriko T. Kita¹, Mingming Zhang¹, Donald E. Brownlee² and David J. Joswiak²

¹*WiscSIMS, Department of Geoscience, University of Wisconsin-Madison*

²*Department of Astronomy, University of Washington*

Initial analyses of Ryugu returned samples indicated that they are similar to CI (Ivuna-type) carbonaceous chondrites, which mainly consist of minerals that formed by parent body aqueous alteration [e.g., 1-5]. Discovery of CO₂ bearing fluid inclusions in Ryugu pyrrhotite suggests that the Ryugu parent body accreted in the outer solar system beyond the CO₂ and H₂O snowlines (>3-4 au [2]). Kawasaki et al. [6] conducted oxygen isotope analyses of anhydrous minerals, such as olivine and pyroxene that are extremely rare in Ryugu and CI chondrite Ivuna. They examined the distribution of mass-independent fractionation factors of oxygen 3-isotopes, expressed by $\Delta^{17}\text{O}$ ($= \delta^{17}\text{O} - 0.52 \times \delta^{18}\text{O}$), in olivine grains from Ryugu and CI chondrites, and found them to be similar to those of comet Wild 2 from the NASA Stardust mission [7-12]. They suggested that the formation region of the Ryugu asteroid could have been farther into the outer solar system than most carbonaceous chondrites and closer to the accretion region of comets.

Here, we summarize oxygen isotope data of olivine and pyroxene from comet Wild 2. To date, ~90 relatively coarse-grained particles (>2 μm to upto 60 μm) have been analyzed for oxygen isotopes, including ~20 from the literature [7, 9-13] and ~70 from recent studies [14-16]. These latter studies include more than 50 particles extracted from the longest type B Stardust track (~17 mm) T227, which contains numerous relatively coarse (>2 μm up to 20 μm) particles in the bulb region in addition to at least four terminal particles (TP). The largest TP measures 60 μm in diameter and has a porphyritic chondrule-like texture [16]. The majority of Wild 2 particle analyses were conducted at the WiscSIMS IMS 1280 using a 2 μm -sized primary beam [7, 9, 12-16]. Oxygen isotope data of individual olivine and pyroxene particles are shown in the plot of $\Delta^{17}\text{O}$ versus Mg# (molar $[\text{Mg}]/[\text{Mg}+\text{Fe}]$) in Figure 1. This diagram has been used for the studies of meteoritic chondrules to understand the isotope signatures of precursors and redox states during their formation [e.g., 17]. We also summarize published oxygen isotope analyses of olivine and pyroxene from Ryugu [6, 18] and other CI chondrites [6, 19-20] for comparison (Figure 2).

Wild 2 olivine and pyroxene show a wide range of Mg# ranging from 100 to 50 and are evenly distributed (Figure 1). The $\Delta^{17}\text{O}$ values are bimodal where most particles are ¹⁶O-poor with $\Delta^{17}\text{O}$ values ranging from -7‰ to +7‰ and others with $\Delta^{17}\text{O}$ of ~-22‰, values similar to CAIs in carbonaceous chondrites. The latter ¹⁶O-rich particles are either LIME (low iron and Mn-enriched) olivine, nearly pure forsterite, or enstatite, all which are with highest Mg#>98. They are likely early solar nebula condensates similar to those in AOAs [9,12]. In addition, rare occurrences of ¹⁶O-rich relict olivine have been identified, such as in the chondrule-like object Gozen-sama, studied by [7]. The ¹⁶O-poor particles show a general tendency of a slight increase in $\Delta^{17}\text{O}$ values with decreasing Mg# (Figure. 1). The majority of Wild 2 particles (60-70%) are FeO-rich (Mg#<90) and many of them show zero to slightly positive $\Delta^{17}\text{O}$ values. Similar results have been obtained from Giant Cluster IDP U2-20GCA [21], which is considered to be of cometary origin [22]. They overlap with data from CR chondrite chondrules [16, 23-25], suggesting a genetic relationship between CR chondrites and cometary particles [e.g., 9], though FeO-rich chondrules are uncommon in CR chondrites and do not show $\Delta^{17}\text{O}$ values higher than 1‰ [12, 16, 21].

Olivine and pyroxene data from Ryugu and CI chondrites are summarized in Figure 2. Most grains have high Mg# (≥ 98) with bimodal $\Delta^{17}\text{O}$ values of ~-5‰ and -22‰ and minor FeO-rich grains show $\Delta^{17}\text{O}$ values of ≤ 0 ‰. Similar to Wild 2 particles, ¹⁶O-rich olivine grains are often Mn-rich [6, 18, 20] and may be related to AOAs (e.g., [26]). However, the majority of ¹⁶O-poor olivine and pyroxene in Ryugu and CI chondrites cluster at the $\Delta^{17}\text{O}$ values of -5‰, which are uncommon among Wild 2 particles. Ryugu and CI data are more similar to chondrule data in major carbonaceous chondrites, such as CMs and CVs (e.g., [27-28]). Rare chondrule-like objects were identified in Ryugu [29], though they are substantially smaller than typical chondrules in carbonaceous chondrites.

Several Wild 2 particles are chondrule-like objects containing plagioclase and glass [7, 9-11, 16, 30]. Two of them were studied for ²⁶Al-²⁶Mg chronology, but do not show any resolvable excess ²⁶Mg [9, 31], suggesting that they formed later than 3-4 Ma after CAI formation (by assuming homogeneity of ²⁶Al in the solar system). In contrast, the Ryugu and CI chondrite parent bodies might have accreted much earlier ~2 Ma after CAIs and experienced aqueous alteration by the heat generated from ²⁶Al decay [2]. Thus, a major difference between anhydrous minerals in comets and CI chondrites could be related to the timing of accretion in the outer solar system. Comet Wild 2 contains late-forming (>3 Ma) chondrule-like materials, which may have formed in the outer solar system [16]. They were not present in the Ryugu and CI chondrite-forming regions at the time of the CI chondrite parent body accretion.

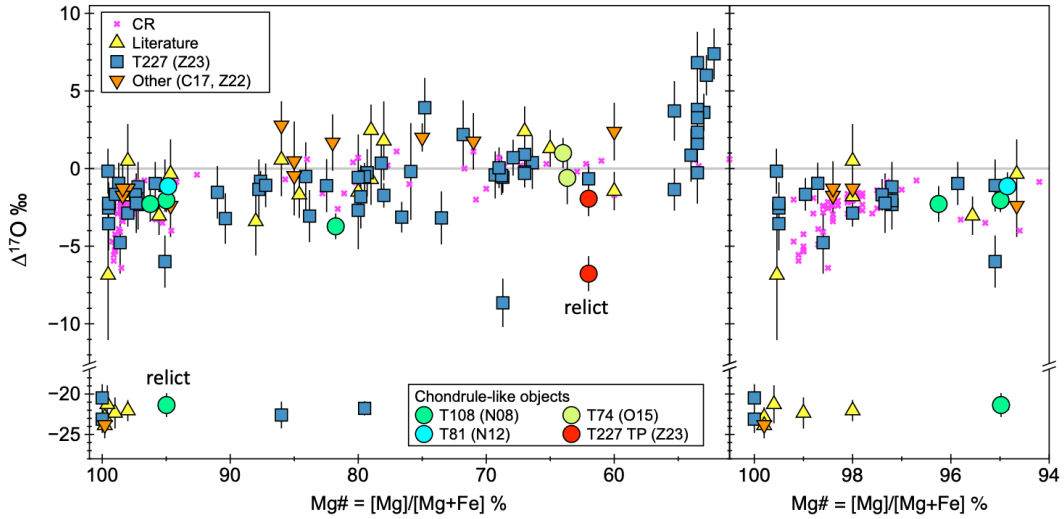


Figure 1. Mg# vs. $\Delta^{17}\text{O}$ relationship among olivine and pyroxene particles in comet Wild 2 (after Zhang et al. [16]). Data sources: Literature [7, 9-13], T227 [16] and others [14-15]. Data from CR chondrules [17, 23-25] are plotted for comparison (error bars are ignored). Chondrule-like objects are shown as circles [7, 9, 11, 16] including ^{16}O -rich relict olivine data [7, 16].

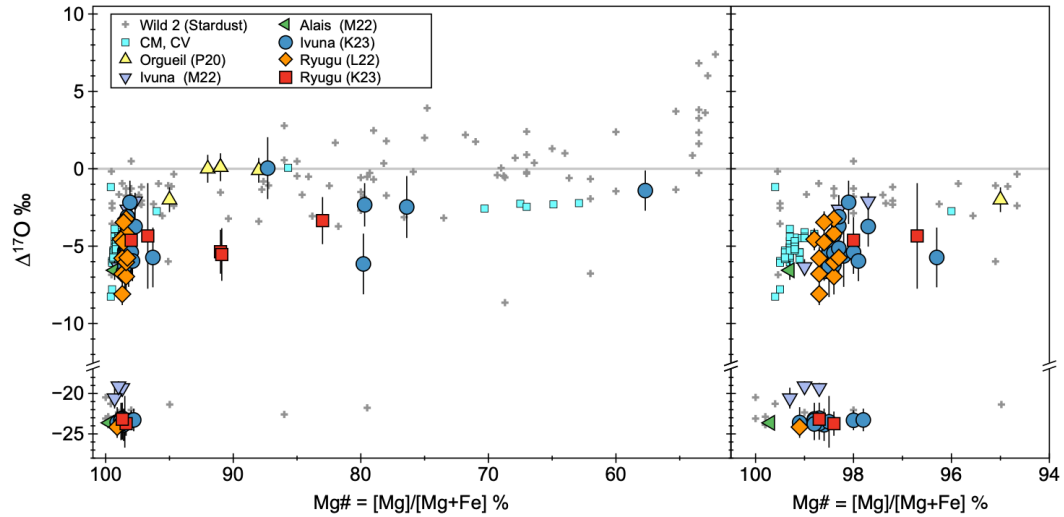


Figure 2. Mg# vs. $\Delta^{17}\text{O}$ relationship among olivine and pyroxene grains in Ryugu (K23 [6]; L22 [18]) and CI chondrites Orgueil (P20 [19]), Ivuna (K23, M22 [20]), and Alais (M22). The Wild 2 comet data (Figure 1) and CM and CV chondrite chondrule data [27-28] are shown for comparison (error bars are ignored). Majority of ^{16}O -poor Ryugu and CI chondrite data show systematically lower $\Delta^{17}\text{O}$ and higher Mg# than those of Wild 2.

References [1] Yokoyama T. et al. 2023. *Science* 379:eabn7850. [2] Nakamura T. et al. 2023. *Science* 379:eabn8671. [3] Ito M. et al. 2022. *Nat. Astron.* 6:1163–1171. [4] Nakamura E. et al. 2022. *Proc. Jpn. Acad., Ser. B* 98:227–282. [5] Yamaguchi A. et al. 2022. *Nat. Astron.* 7:398–405. [6] Kawasaki N. et al. 2022. *Sci. Adv.* 8:eade2067. [7] Nakamura T. et al. 2008. *Science* 321:1664–1667. [8] Nakamura-Messenger K. et al. 2011. *MaPS* 46:1033–1051. [9] Nakashima D. et al. 2012. *EPSL* 357–358:355–365. [10] Ogliore R. C. et al. 2012. *ApJ*. L745:L19. [11] Ogliore R. C. et al. 2015. *GCA* 166:74–91. [12] Defouilloy C. et al. 2017. *EPSL* 465:145–154. [13] Joswiak D. J. et al. 2014. *GCA* 144:277-298. [14] Chaumard N. et al. 2018. Abstract #2163. 49th LPSC. [15] Zhang M. et al. 2022. Abstract #1057. 53rd LPSC. [16] Zhang M. et al. 2023. Abstract #. 1711. 54th LPSC. [17] Tenner T. J. et al. 2015. *GCA* 148:228-250. [18] Liu M. et al. 2022. *Nat. Astron.* 6: 1172–1177. [19] Piralla M. et al. 2020. *GCA* 269: 451-465. [20] Morin G. L. F. et al. 2022. *GCA* 332: 203-219. [21] Zhang M. et al. 2021. *EPSL* 564:116928. [22] Joswiak D. J. et al. 2017. *MaPS* 52:1612-1648. [23] Connolly H. C. and Huss G. R. 2010. *GCA* 74:2473–2483. [24] Schrader D. L. 2013. *GCA* 101:302-327. [25] Schrader D. L. 2014. *GCA* 132:50-74. [26] Mikouchi T. et al. 2022. Abstract #. 1935. 53rd LPSC. [27] Chaumard M. et al. 2018. *GCA* 228: 220-242. [28] Hertwig A. T. et al. 2018. *GCA* 224:116-131. [29] Nakashima D. et al. 2023. *Nat. Commun.* 14:532. [30] Joswiak D. J. et al. 2012. *MaPS* 47:471-524. [31] Nakashima D. et al. 2015. *EPSL* 410:54-61.

Oxygen isotopic composition of dolomite in Ryugu: New insights into the thermal history of the Ryugu parent body.

Wataru Fujiya¹, Takayuki Ushikubo², Shingo Sugawara¹, Akira Yamaguchi³, Kohei Fukuda⁴, Martin R. Lee⁵, Kentaro Terada⁴, Phillip A. Bland⁶ and Bryan J. Travis⁷

¹Faculty of Science, Ibaraki University, 2-1-1 Bunkyo, Mito, Ibaraki 310-8512, JAPAN (wataru.fujiya.sci@vc.ibaraki.ac.jp),

²Kochi Institute for Core Sample Research, JAMSTEC, ³National Institute for Polar Research, ⁴Osaka University, ⁵Glasgow University, ⁶Space Science and Technology Centre, Curtin University, ⁷Planetary Science Institute

Introduction: Ryugu samples underwent extensive aqueous alteration, and a variety of secondary minerals such as phyllosilicate, oxide, sulfide, and carbonate formed during water-rock interaction [1-5]. Among the secondary minerals, carbonates are of particular interest because their O and C isotopic compositions reflect the conditions of aqueous alteration, and because they can be dated using the ⁵³Mn-⁵³Cr systematics. Previous studies of the O and C isotopic compositions of dolomite (CaMg(CO₃)₂) in Ryugu have suggested that it formed at temperatures lower than 80 °C [1,2,6,8] when the system was approaching equilibrium [7,8]. The ⁵³Mn-⁵³Cr dating of Ryugu carbonate suggests that their formation may have spanned as much as 5 Myr [1,6]. Therefore, Ryugu carbonate potentially helps us decipher the thermal history of the Ryugu parent body. However, it is unclear whether Ryugu carbonate formed during prograde alteration when temperature was increasing or during retrograde cooling, which makes it difficult to establish a realistic thermal history model. In this work, we investigated the O isotopic compositions of dolomite in Ryugu samples A0203 and C0192 to further constrain its formation conditions. Also, we will measure the O isotopic compositions of magnetite in these samples to estimate the O isotopic equilibrium temperatures between dolomite and magnetite.

Experimental: Prior to isotope work, the microstructures of dolomite grains in samples A0203 and C0192 were characterized by Transmission Electron Microscopy (TEM) using a FEI T20 operated at 200 kV. The *in-situ* O-isotope analyses on two and six dolomite grains from A0203 and C0192, respectively, were performed using CAMECA IMS 1280-HR [9]. Negative ions of ¹⁶O⁻, ¹⁷O⁻, and ¹⁸O⁻, produced by a focused Cs⁺ primary ion beam (~30 pA, 3-4 μm in diameter), were simultaneously detected with a Faraday cup (FC) for ¹⁶O⁻ signals and two electron multipliers (EMs) for ¹⁷O⁻ and ¹⁸O⁻. Instrumental mass fractionation was corrected using a series of dolomite-ankerite standards [10]. The uncertainties on δ¹⁷O, δ¹⁸O, and Δ¹⁷O values were typically ±1.12, ±0.86, and ±1.35‰ (2σ), respectively.

Results and discussion: TEM showed that dolomite grains in A0203 and C0192 differ in their crystal size and habit, with those in A0203 typically being 1-2 μm size euhedral crystals whereas C0192 dolomite is coarser and anhedral. The analyzed dolomite grains have only a small variation in δ¹⁸O values as observed by previous studies [1,6-8]. The δ¹⁸O values of A0203 and C0192 dolomite are at the higher and lower end of those reported previously and clustered at 32.91 ± 0.47‰ (N = 6; 2SE) and 26.54 ± 0.58‰ (N = 2; 2SE), respectively. Notably, the Δ¹⁷O values of A0203 and C0192 dolomite are also systematically different (-1.13 ± 0.82‰ and 0.46 ± 0.36; 2SE). A similar anti-correlation between δ¹⁸O and Δ¹⁷O values can also be recognized for the previous data, implying that Ryugu dolomite with higher δ¹⁸O values tends to have lower Δ¹⁷O values [6-8]. The Δ¹⁷O, and possibly, δ¹⁸O values of aqueous fluids are expected to have decreased during progressive aqueous alteration because of the O-isotope exchange between water and anhydrous rock which initially had higher and lower Δ¹⁷O (and δ¹⁸O) values [11,12]. Thus, the A0203 dolomite with lower Δ¹⁷O values likely precipitated from more evolved fluids that underwent O-isotope exchange to a greater extent than the C0192 dolomite. On the other hand, the equilibrium O isotopic fractionation between water and dolomite is larger at lower temperatures with the δ¹⁸O values of dolomite being higher than those of water [13]. Therefore, the A0203 dolomite with higher δ¹⁸O values likely precipitated at lower temperatures than the C0192 dolomite. These observations may suggest that Ryugu dolomite formed during retrograde cooling. This argument is in line with the small variation in δ¹³C values observed for Ryugu dolomite, which suggests its formation in higher O fugacity at the later stage of aqueous alteration [7]. For further information regarding the formation conditions of dolomite, we plan to measure the ⁵³Mn-⁵³Cr ages of dolomite in A0203 and C0192.

References:

- [1] Yokoyama T. et al. 2022. Science 379: eabn7850. [2] Nakamura E. et al. 2022. Proc. Jpn. Acad., Ser. B 98: 227-282. [3] Ito M. et al. 2022. Nat. Astron. 6: 1163-1171. [4] Nakamura T. et al. 2022. Science 379: eabn8671. [5] Yamaguchi A. et al. 2023. Nat. Astron. 7: 398-405. [6] McCain K. A. et al. 2023. Nat. Astron. 7: 309-317. [7] Fujiya W. et al. 2023. Nat. Geosci. 16: 675-682. [8] Kita N. T. et al., submitted. [9] Fujiya W. et al. 2020. Geochim. Cosmochim. Acta 274: 246-260. [10] Śliwiński, M. G. et al. 2016. Geostand. Geoanal. Res. 40: 157-172. [11] Clayton & Mayeda 1984. Earth Planet. Sci. Lett. 67: 151-161. [12] Marrocchi et al. 2018. Earth Planet. Sci. Lett. 482: 23-32. [13] Zheng Y.-F. et al. 1999. Geochem. J. 33: 109-126.

Numerical Simulation of Ryugu’s Thermophysical Properties using the Discrete Element Method

B. Agrawal¹, M. Grott¹, J. Knollenberg¹, J. Biele², B. Gundlach³, J. Blum⁴

¹German Aerospace Center, Berlin, Germany, ²German Aerospace Center, Köln, Germany, ³Westfälische Wilhelms-Universität Münster, Germany, ⁴Technische Universität Braunschweig, Germany

Between June 2018 and November 2019, the Hayabusa2 mission [1] investigated the near-Earth asteroid (162173) Ryugu. The main objective of the mission was to study this pristine C-type asteroid to better understand the origin and evolution of materials in the early solar system. Hayabusa2 deployed the MASCOT lander in October 2018 and following a detailed remote sensing and in-situ investigation, Hayabusa2 returned samples to Earth in December 2020. A summary of main findings of the mission was recently reviewed by [2], who also compared results obtained during the remote sensing, in-situ, and sample analysis phases.

The detailed study of Ryugu over scales ranging from the micro (sample) scale to global remote sensing data revealed that while several properties derived from remote sensing and in-situ analysis agree very well with results obtained from the sample analysis, some discrepancies exist [2]. These scale dependent effects include properties like reflectance and thermophysical properties. Here, we focus on the derived thermal properties, which were determined using MASCOT’s MARA radiometer [3], the Hayabusa2 orbiter’s TIR thermal infrared imager [4], as well as the returned samples [5]. While in-situ and remote sensing data roughly agree, yielding thermal inertias of $282_{-25}^{+93} \text{ Jm}^{-2}\text{K}^{-1}\text{s}^{-1/2}$ [6, 7] and $225 \pm 45 \text{ Jm}^{-2}\text{K}^{-1}\text{s}^{-1/2}$ [4, 8], respectively, sample analysis indicates values of $890 \pm 45 \text{ Jm}^{-2}\text{K}^{-1}\text{s}^{-1/2}$ [5], which are thus about three times as large.

The reason for the observed scale dependence of the thermophysical properties remains unknown, but it has been proposed that the difference could be caused by a thermal shielding effect on intermediate scales [5]. Cracks may, for example, be generated by thermal fatigue and a conceptual model of how these cracks may be distributed inside boulders is shown in the left panel of Fig. 1. Thermal fatigue would extend to a few skin depths $d_\epsilon = \sqrt{\kappa P/\pi}$, where $\kappa = k/\rho c_p$ is thermal diffusivity, ρ is density, c_p is specific heat, and P is the period of the forcing (a day-night cycle). Remote sensing instruments like MARA and TIR are sensitive to material over a similar depth range, while samples could contain considerably less cracks.

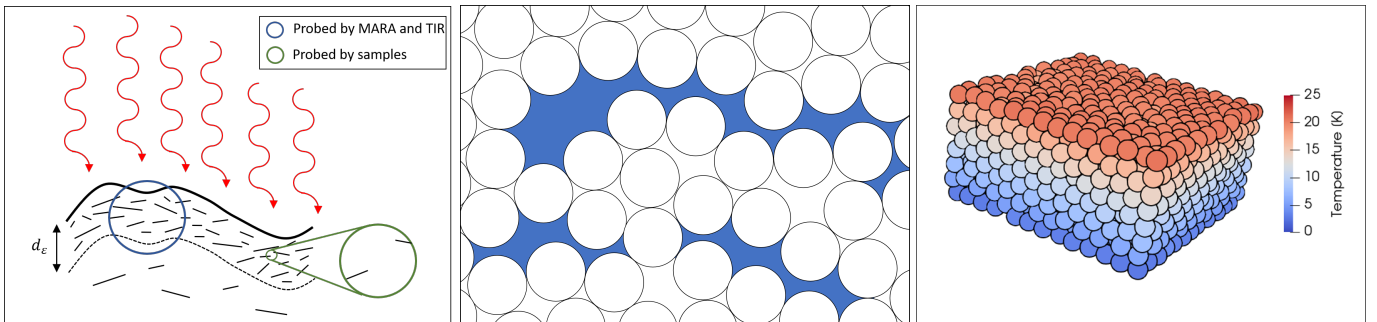


Figure 1: Left: Conceptual model of scale dependence of thermophysical properties. The range of materials sampled by the in-situ and remote sensing instruments MARA and TIR is indicated in blue, while the returned samples are indicated in green. On large scales, the material may exhibit abundant cracks due to insolation induced fatigue, while samples may contain only few cracks. Middle: Modeling approach including cracks induced by thermal fatigue using discrete elements. Fatigue induced cracks separating particles are indicated in blue. Right: First results of simulating heat flow through a bed of monodisperse particles without cracks. Colour represents particle temperatures going from red (hot) to blue (cold).

Our project focuses on exploring this discrepancy and formulating a thermophysical model of the boulders including cracks and sintering. To understand the thermophysical properties of asteroids, we base our model on the LIGGGHTS(R)-PUBLIC package [9]. It is an open source discrete element method particle simulation software built for simulating general granular motion and atomic/molecular dynamics. The program integrates Newton’s equations of motion for a large collection of spherical particles which interact via short or long range forces. The inter-particle forces are determined based on a user selected contact model which can encompass interactions such as elastic (contact) forces, rolling friction, cohesion and surface geometry of particles. In addition to mechanical interactions, the package can also be used to study the thermal energy transport between particles in contact. This is governed by

the thermal conductivities of the particles and their contact areas. Here we specify contact areas as the cross section of the geometrical overlap of two spherical particles. Upon introducing cracks in a random packing of monodisperse particles (middle panel in Fig. 1), we intend to study the thermal properties of the bulk material.

As a benchmark test for the numerical code we calculate the steady-state heat flow through a particle-bed to reproduce the relation between thermal conductivity, contact areas, and particle radii. Once in thermal equilibrium, thermal conductivity of the bed can be calculated given the specified temperature boundary conditions and resulting heat flux through the bed. This can then be compared to analytical and experimental results for monodisperse particles [10]. First results of the simulation are shown in the right hand panel of Fig. 1 where heat is flowing vertically downwards through a bed of cohesion-less particles with adiabatic boundary conditions elsewhere.

Once the numerical method has been benchmarked using monodisperse cohesion-less particles, we will include polydisperse particles and a parameterized description of enhanced heat transport through inter-particle bonds. Using the contact area as a tuning parameter we fit the numerical results to the thermal properties, as derived from sample analysis [5]. Then, cracks will be introduced as outlined in the middle panel of Fig. 1 and the associated reduction in thermal conductivity will be investigated. In this way, we will systematically study the amount of material disruption necessary to match the remote sensing observations [7, 6, 4].

References

- [1] Sei-ichiro Watanabe et al. In: *Space Science Reviews* 208.1 (July 2017), pp. 3–16.
- [2] Katharina Otto et al. In: *Earth, Planets and Space* 75.1 (Apr. 2023), p. 51.
- [3] M. Grott et al. In: *Space Science Reviews* 208.1 (July 2017), pp. 413–431.
- [4] Tatsuaki Okada et al. In: *Nature* 579.7800 (Mar. 2020), pp. 518–522.
- [5] T. Nakamura et al. In: *Science* 379.6634 (2023), eabn8671.
- [6] Maximilian Hamm et al. In: *Planetary and Space Science* 159 (2018), pp. 1–10.
- [7] M. Grott et al. In: *Nature Astronomy* 3.11 (Nov. 2019), pp. 971–976.
- [8] Yuri Shimaki et al. In: *Icarus* 348 (2020), p. 113835.
- [9] Christoph Kloss et al. In: *Progress in Computational Fluid Dynamics* 12.2-3 (2012), pp. 140–152.
- [10] N. Sakatani et al. In: *AIP Advances* 7.1 (Jan. 2017), p. 015310.

Defect and exsolution microstructures in four pyroxene-rich grains from Itokawa

Falko Langenhorst^{1,2}, Agnese Fazio¹, and Dennis Harries³

¹*Analytical Mineralogy of Nano- and Microstructures, Institute of Geoscience, Friedrich Schiller University Jena, Germany*

²*Hawai'i Institute of Geophys. and Planetology, School of Ocean and Earth Science and Technology, University of Hawai'i at Manoa, USA*

³*European Space Resources Innovation Centre, Luxembourg Institute of Science and Technology, 41 rue du Brill, L-4422Belvaux, Luxembourg*

Introduction: In 2010, the Hayabusa spacecraft returned precious regolith grains from the rubble pile asteroid 25143 Itokawa. Subsequent investigations confirmed the link between LL4-6 ordinary chondrites and the S-type asteroid Itokawa and revealed its eventful past [1, 2]. The processes reported in regolith grains comprise thermal annealing in the original parent body and the full range of space weathering effects from surface amorphization by ion bombardment to collisional fragmentation [2-6]. Pyroxenes, the second most abundant phase in ordinary chondrites, are an important source of information on these processes, as they develop various process-indicative defects. Thus, we pursued here a systematic study of the microstructures in ortho- and clinopyroxene grains from Itokawa and discuss the results in terms of thermal metamorphism and space weathering.

Samples and methods: In the context of the 4th International Announcement of Opportunity for Hayabusa sample investigation, we have obtained four pyroxene-containing Itokawa particles: RB-QD04-0092, RA-QD02-0205, RB-CV-0192, and RB-CV-0144 [7]. These grains were cut by focused ion beam (FIB) preparation on a scanning electron microscope (SEM) and then studied by analytical transmission electron microscopy (TEM), following the procedure described by [6].

Results: *RB-QD04-0092* is a flat grain (29 x 26 x 12 μm) consisting of orthopyroxene ($\text{En}_{78}\text{Fs}_{21}\text{Wo}_1$) and olivine (Fo_{71-78}). Both olivine and orthopyroxene show defects that are compatible with local shock metamorphism, i.e. olivine contains [001] dislocations, while orthopyroxene is pervaded by multiple (100) clinoenstatite lamellae. The regolith grain shows a 40-70 nm wide continuous damaged rim due to solar wind irradiation.

RA-QD02-0205 is a prismatic grain (55 x 43 x 15 μm) that only consists of a single crystal orthopyroxene ($\text{En}_{74}\text{Fs}_{24}\text{Wo}_2$). The dominant defects are also pervasive (100) clinoenstatite lamellae, which are decorated by partial dislocations. The grain is surrounded by a 50 nm thin polynanocrystalline rim.

RB-CV-0192 is also prismatic in shape (19 x 10 x 8 μm), and contains both orthopyroxene ($\text{En}_{76}\text{Fs}_{23}\text{Wo}_1$) and clinopyroxene ($\text{En}_{50}\text{Fs}_7\text{Wo}_{43}$). Adjacent olivine, plagioclase, and whitlockite were detected, too. Besides (100) clinoenstatite lamellae in orthopyroxene there are no other defects. The solar wind damaged polynanocrystalline rim is up to 50 nm thick.

RB-CV-0144 is 17 x 12 x 5 μm in size and contains both orthopyroxene ($\text{En}_{79}\text{Fs}_{20}\text{Wo}_1$) and clinopyroxene ($\text{En}_{50}\text{Fs}_6\text{Wo}_{44}$). The pyroxenes possess subgrain boundaries and are traversed by thin (up to 10 nm) (100) exsolution lamellae. One side of the entire regolith grain displays a polynanocrystalline and layered rim of up to 60 nm thickness.

Discussion: The presence of amorphous to nanocrystalline rims documents the solar wind damage of Itokawa grains. Moreover, the occurrence of shock defects in localized areas of olivine and pyroxenes (clinoenstatite lamellae and dislocations) as well as the absence of microcraters on their surfaces indicate that cascades of collisions took place in the regolith. As consequence of active space gardening the effective exposure time of regolith grains must have been reduced. Of particular interest is the observation of thin exsolution lamellae in pyroxene, whose width of up to 10 nm points to slow cooling rates of < 1 $^{\circ}\text{C}$ per 1000 years at peak temperatures of 800°C [2, 8].

Acknowledgements: We thank JAXA for providing access to the Itokawa particles. FIB-TEM facilities at FSU Jena were funded by the Gottfried-Wilhelm-Leibniz award to FL (LA 830/14-1). AF is grateful to the Alexander von Humboldt Foundation for a postdoctoral grant.

References

- [1] Noguchi T., et al. 2011 Science 333:1121. [2] Nakamura T. et al. 2011 Science 333:1113. [3] Keller L.P. and Berger E.L. 2014 Earth Planets and Space 66:71. [4] Noguchi T., et al. 2014 Meteoritics & Planetary Science 49:188. [5] Harries D. and Langenhorst F. 2014 Earth Planets and Space 66:163. [6] Langenhorst F., et al. 2014 Earth Planets and Space 66:118. [7] Fazio et al. 2020 Vol.14, EPSC2020-645. [8] Weinbruch S. and Müller W.F. 1995 Geochimica et Cosmochimica Acta 59: 3221.

Asteroid Itokawa ... but when did form exactly?

F. Jourdan¹, N.E. Timms¹, T. Nakamura², W.D.A. Rickard¹, C. Mayers¹

¹*Curtin University, Perth, GPO Box U1987, WA, Australia*

²*Tohoku University, Aoba, Sendai, Miyagi 980-8578, Japan*

Rubble pile asteroids consist of reassembled fragments from shattered monolithic asteroids and are much more abundant than previously thought in the solar system. In earlier studies (*1, 2*), we analysed five regolith dust particles recovered by the Hayabusa space probe from the rubble pile asteroid 25143 Itokawa, using a workflow of microstructural analysis by electron backscatter diffraction (EBSD), element mapping by time-of-flight secondary ion mass spectrometry (ToF-SIMS \pm atom probe) and $^{40}\text{Ar}/^{39}\text{Ar}$ geochronology. We showed that Itokawa must have formed before or at ca. ≥ 4.2 Ga and concluded that rubble pile asteroids can survive ambient solar system bombardment processes for extremely long periods. Here, we continue our quest to understand the bombardment history of Itokawa with the so far seemingly elusive goal of precisely pinpointing the age and nature of the catastrophic breakup of Itokawa's parent body. Only through a larger number of $^{40}\text{Ar}/^{39}\text{Ar}$ ages on single particles and U/Pb ages on phosphate grains (*3*) coupled with careful particle characterizations, will we be able to achieve this goal. With that in mind, we analysed three new particles.

RA-QD02-0300 (dia. = 190 μm) is composed of olivine, plagioclase, with minor troilite. EBSD and ToF-SIMS analyses show that the plagioclase in this particle is distributed in vein-like structures and has a fine polycrystalline texture of <10 μm grains with abundant inclusions and K-rich exsolutions. This suggests it represents recrystallised melt domains. Olivine crystals show no sign of shock deformation. We obtained a plateau age of **4130 \pm 33 Ma** ($P = 0.55$). Noticeably, this age is very similar to previous results from other particles at 4219 ± 35 and 4149 ± 41 Ma (*1*), indicating an age concentration around that time. Could it be that the parent body of Itokawa broke up at ca. 4.2 Ga while some of the impact heated material slowly cooled down inside the newly formed insulating rubble pile asteroid over ca. 100 million years? This scenario is tantalizing as it would be similar to the scenario proposed by (*4*) for the breakup of an initially hot chondritic parent body at 4.5 Ga and with subsequent debris cooling at rates of ca. 1 to 10 $^{\circ}\text{C}/\text{Ma}$ inside the rubble pile asteroids.

RA-QD02-0306 (160 μm) is composed of olivine and plagioclase with minor troilite and chromite. This particle is the only $^{40}\text{Ar}/^{39}\text{Ar}$ -dated particle which contains measurable solar wind, with a $^{38}\text{Ar}/^{36}\text{Ar}$ ratio of 0.188 ± 0.049 (2σ) that is indistinguishable from modern solar wind value. Along with the presence of abundant micro-craters, melt drop and blisters observed on the surface of the particle observed by (*5*), this indicates that this particle spent some time directly at the surface of the asteroid. This particle shows a structured $^{40}\text{Ar}/^{39}\text{Ar}$ age spectrum, with two different portions attributed to the gas released by the plagioclase and olivine phases. Plagioclase yielded a mini-plateau (59 % ^{39}Ar released) age of **4557 \pm 61 Ma** ($P = 0.71$) similar to the U-Pb phosphate age of 4640 ± 360 Ma obtained by (*3*) on another particle, suggesting that it recorded the initial cooling deep inside Itokawa's parent asteroid and was not affected by heat during the breakup process. This demonstrates that, during the breakup of Itokawa's parent body, part of the asteroid experienced minimum to negligible shock pressure and temperature increase. This is similar to the conclusions reached via impact modelling calculated for the rubble pile asteroid Ryugu (*6*). This is also in excellent agreement with breakup models of structurally weakened monolith asteroids that do not require a particularly large impactor to shatter (*7*).

RA-QD02-0311 (108 μm) is composed of olivine, Ca-rich pyroxene, plagioclase and troilite. Elemental maps show that this particle contains very little plagioclase compared to the other particles and most of the K is contained in a rim-like structure exposed at the edge of the particle. Olivine crystals show no sign of shock deformation, yet $^{40}\text{Ar}/^{39}\text{Ar}$ dating reveals a complex age spectrum with maximum weighted-mean age of 705 ± 53 Ma ($P=0.39$) including 47% of ^{39}Ar released and indicating an impact ≤ 0.7 Ga. This maximum age, coupled

with an available impact age of 2291 ± 139 Ma (2) and maximum age estimates (1, 8), suggests that impact events happened many times during the history of Itokawa and that the high porosity of the rubble pile material was able to convert low-shock events into high temperature spikes, sufficient to reset and/or partially reset the $^{40}\text{Ar}/^{39}\text{Ar}$ chronometer (2) in some material.

In summary, we propose that Itokawa's parent body was disrupted ca. 4.2 billion years ago in a process involving heterogenous temperature distribution during the impact. Some of the heated material, mixed with cold material, cooled down inside a larger version of Itokawa, possibly over a period of ca. 100 Ma. Itokawa kept being bombarded and eroded by small impactors since its formation with some of these events recorded by the $^{40}\text{Ar}/^{39}\text{Ar}$ system.

References

[1] Jourdan et al. 2023. *Proceedings of the National Academy of Sciences* **120**, e2214353120. [2] Jourdan et al., 2017. *Geology* **45**, 819-822. [3] Terada et al., 2018. *Scientific Reports* **8**, 11806. [4] Lucas et al., 2020. *Geochim Cosmochim Acta* **290**, 366-390. [5] Matsumoto et al., 2018. *Icarus* **303**, 22-33. [6] Nakamura et al., 2022. *Science* **379**, eabn8671. [7] Michel et al. 2004. *Icarus* **168**, 420-432. [8] Park et al., 2015. *Meteoritics and Planetary Science* **50**, 2087-2098.

Characterization of a mass movement site in Benu’s Bralgah Crater and implications for other asteroids

Yuhui Tang¹, D.S. Lauretta¹, R.-L. Ballouz², D.N. DellaGiustina¹, C.A. Bennett¹, D.R. Golish¹

¹*Lunar and Planetary Laboratory, University of Arizona, Tucson, AZ, USA.*

²*The Johns Hopkins University Applied Physics Laboratory, Laurel, MD, USA.*

Near-Earth asteroids such as Benu and Ryugu have boulder-covered surfaces and latitude-dependent slope distributions, signifying that mass movements of boulders perform significant roles in the surface evolution of these small bodies. The OSIRIS-REx (Origins, Spectral Interpretation, Resource Identification, and Security–Regolith Explorer) mission [1] documented numerous locations on Benu exhibiting evidence of mass movements of surface material, mostly towards the lower elevation equatorial region [2]. One such location, contained within Bralgah Crater, was considered (but not used) by the mission as a candidate site for sample collection; thus, high-resolution images collected during reconnaissance of this area allow a more detailed survey than would be possible elsewhere [3] [Fig. 1]. An apparent flow “wake” downhill from a 4.8-m-diameter central boulder in the area, where medium-sized boulders are much less prevalent than in the surrounding terrain, provides an opportunity to investigate the characteristics of mass flow on the asteroid. Through boulder mapping and topographic analysis, we found evidence of a pileup behind the central boulder, as well as a strong orientational preference of the boulders in this area [Fig. 2]. This preferential long-axis orientation exhibits the same westward deflection from the expected downslope direction that we observed at another mass movement site in Benu’s northern hemisphere [4], implying that a global mechanism with effects mirrored between the northern and southern hemispheres is affecting the mass flows.

We performed dynamical simulations of seismic shaking using the discrete-element N-body code PKDGRAV [5–8] to better constrain the conditions that may have formed the landscape. In these simulations, we used boulder sizes similar to those surveyed at the Bralgah Crater site and an environment with a similar 4.8-m-diameter central boulder. We were able to replicate the pileup of material uphill from the central boulder and the wake downhill from it, producing similar elevation profiles created by a lack of downflowing material in the wake area [Fig. 3].

Simulations also showed a preferential orientation emerging, with a strong possibility for preferential orientation parallel to direction of motion. Combined with the orientational preference observed in this and other studies of Benu’s landscape, this indicates that the Coriolis effect could be a major factor in the mass movement of boulders and would help to explain the westward deflection of the boulders’ long-axis orientation. Numerical simulations show that the Coriolis effect is strong enough to induce an east-west displacement of the boulders, which can amount to 10% of the downslope displacement, which could lead to the observed orientational preferences. This effect would be expected to occur on other fast-spinning asteroids, such as Ryugu, where this hypothesis predicts a similar orientational preference, with eastward deviation from the poleward migration of the boulders.

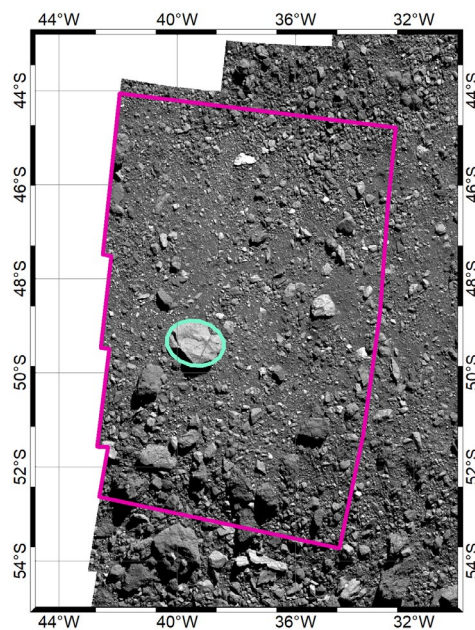


Figure 1. A map of the survey area (magenta outline) within Bralgah Crater, projected in ArcGIS, with the central boulder (long axis, 4.8 m) highlighted by the light blue best-fit ellipse. The downhill direction is north in this area.

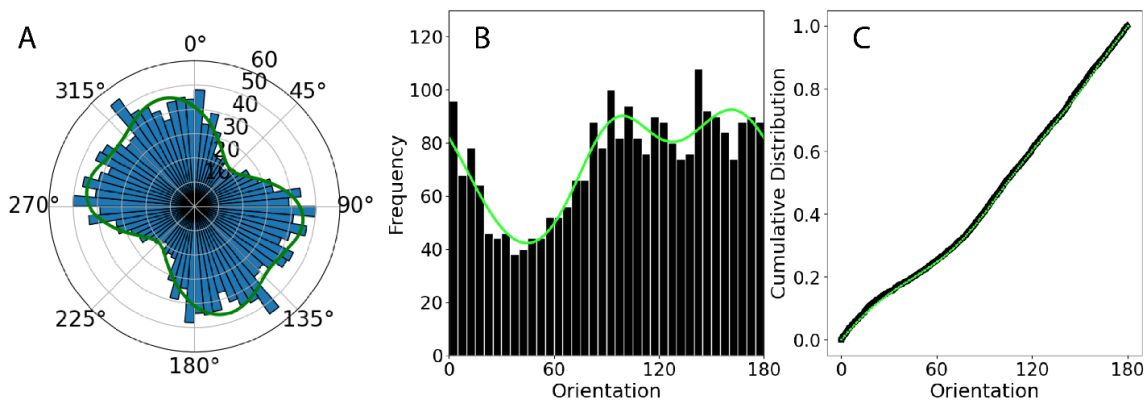


Figure 2. Orientations of the surveyed boulders as a rose diagram (A) and histogram (B), with the data best fitted by a bimodal von Mises distribution (green) with peaks at 94.1° and 164.2° (p -value = 0.839). (C) The empirical distribution function (black line) and cumulative distribution function (green line) of the orientations, used for the K-S tests to derive the p -values.

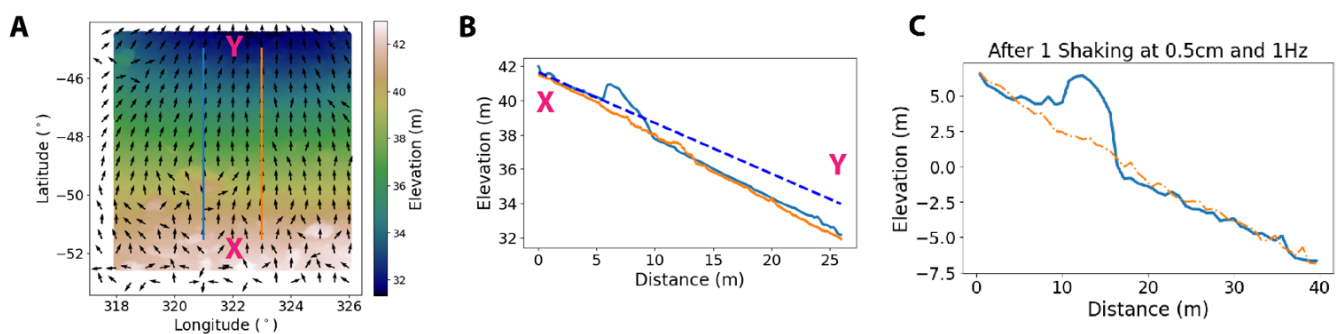


Figure 3. (A) Elevation map of the study site, overlaid with arrows indicating the direction of greatest slope, with the locations of the elevation profiles along longitudes 321°E and 323°E marked in cyan and orange, respectively. (B) The elevation profiles indicated in (A), with the 321°E line profile (cyan) crossing the middle of the central boulder. The blue dashed line represents the best-fit slope of the pileup area uphill from the central boulder, extrapolated across the entire mass movement length. The extrapolated profile ranges from 0.8 to 1.6 m above the actual elevation profile downhill from the central boulder, with greater differences further north (downhill). (C) Elevation profile of simulations after one shaking. The cyan solid line shows elevation along the center of the wake, and the orange dashed-dot line shows the elevation along a parallel transect away from the wake.

References

- [1] Lauretta, D. S., et al. (2017). OSIRIS-REx: Sample Return from Asteroid (101955) Bennu. *Space Science Reviews*, 212(1–2), 925–984. <https://doi.org/10.1007/s11214-017-0405-1>
- [2] Jawin, E. R., et al. (2020). Global Patterns of Recent Mass Movement on Asteroid (101955) Bennu. *Journal of Geophysical Research: Planets*, 125(9). <https://doi.org/10.1029/2020JE006475>
- [3] Lauretta, D. S., et al. (2021). OSIRIS-REx at Bennu: Overcoming challenges to collect a sample of the early Solar System. In *Sample Return Missions* (pp. 163–194). Elsevier. <https://doi.org/10.1016/B978-0-12-818330-4.00008-2>
- [4] Tang, Y., et al. (2023). Simulating impact-induced shaking as a triggering mechanism for mass movements on Bennu. *Icarus*, 395, 115463. <https://doi.org/10.1016/j.icarus.2023.115463>
- [5] Ballouz, R.-L. (2017). Numerical Simulations of Granular Physics in the Solar System [Ph.D., University of Maryland, College Park].
- [6] Richardson, D. C., Quinn, T., Stadel, J., & Lake, G. (2000). Direct Large-Scale N-Body Simulations of Planetesimal Dynamics. *Icarus*, 143(1), 45–59. <https://doi.org/10.1006/icar.1999.6243>
- [7] Schwartz, S. R., Richardson, D. C., & Michel, P. (2012). An implementation of the soft-sphere discrete element method in a high-performance parallel gravity tree-code. *Granular Matter*, 14(3), 363–380. <https://doi.org/10.1007/s10035-012-0346-z>
- [8] Zhang, Y., et al. (2017). Creep stability of the proposed AIDA mission target 65803 Didymos: I. Discrete cohesionless granular physics model. *Icarus*, 294, 98–123. <https://doi.org/10.1016/j.icarus.2017.04.027>

Photometry of Ryugu and SCI crater as inferred by ONC images

A. Longobardo¹, M. Angrisani¹, E. Palomba¹, F. Dirri¹, Y. Yokota², T. Kouyama³, R. Honda⁴ and the Hayabusa2/ONC Team

¹ INAF-IAPS, via Fosso del Cavaliere 100, 00133 Rome, Italy

² JAXA-ISAS, 3-1-1 Yoshinodai, Chuo-ku, Sagami-hara City, Kanagawa Prefecture, 252-5210, Japan

³ National Institute of Advanced Industrial Science and Technology, Umezono 1-1-1, Tsukuba, 305-8568, Japan;

⁴ Kochi, University, Kochi, Japan

The JAXA/Hayabusa2 rendezvoused with the Ryugu asteroid from June 2018 to November 2019, performing an artificial impact experiment on 5th April 2019.

The goal of this work is to study the photometric properties' variation of the target area (latitude 4.5-10°N; longitude 299-305°E) after the artificial impact experiment. This is done by applying an empirical method based on the statistical analysis of the ONC camera's dataset (in particular, the v band, centred at 0.55 μm), similar to that applied to several asteroids (e.g., Longobardo et al., 2014; 2018) and to the NIRS3 dataset of Ryugu (Longobardo et al., 2022).

The method has been firstly applied on the entire dataset acquired between March and April 2019, covering most of the Ryugu surface. The first step was the retrieval of the equigonal albedo, by applying the Akimov disk function. The obtained equigonal albedo is independent of incidence and emission angle when phase angle is lower than 60°, while a slight dependence is still present for larger phase angles.

Then, the average phase function of Ryugu was obtained. This is very similar to that obtained on the NIRS3 dataset (i.e., in a different spectral range), according to our expectations.

Then, we calculated two photometric parameters $R20$ (i.e., the radiance factor at 20° phase) and PCS_{1540} (i.e., the phase function steepness between 15° and 40° phase angles) and compared them to photometric parameters calculated on phase functions of other asteroids visited by space missions and on both disk-integrated and disk-resolved phase functions of Ryugu obtained by Tatsumi et al. (2019). The disk-resolved phase functions by Tatsumi et al. (2019) and obtained in this work are in good agreement.

Nevertheless, the Ryugu's disk-resolved phase function is much flatter than other dark asteroids. Otherwise, the disk-integrated phase function of Ryugu is in good agreement with other dark asteroids. This is ascribed to the fact that dark bodies' phase function flattens with improving spatial resolution due to the reducing role of shadowing. A similar behaviour was observed on other dark asteroids, i.e., Ceres (Longobardo et al., 2019) and Bennu (Golish et al., 2021).

Finally, we focused the analysis on the artificial impact area by comparing phase curves before and after the impact. Currently, the only variations observed are within uncertainties, but we need to enlarge the dataset before to give any definitive conclusion.

Acknowledgements. We thank the ONC development/operations Team.

References

- Golish et al. (2021), *Icarus* 357, 113724
Longobardo et al. (2014), *Icarus* 240, 20-35
Longobardo et al. (2019), *Icarus* 320, 97-109
Longobardo et al. (2022), *A&A* 666, A185
Tatsumi et al. (2019), *A&A* 639, A83

The shape distributions of sub-mm-sized impact experiment fragments from Allende meteorite

Tatsuhiko Michikami¹, Akira Tsuchiyama^{2,3,4}, Axel Hagermann⁵, and Sunao Hasegawa⁶

¹Faculty of Engineering, Kindai University, Hiroshima Campus, 1 Takaya Umenobe, Higashi-Hiroshima, Hiroshima 739-2116, Japan, (michikami@hiro.kindai.ac.jp), ²Research Organization of Science and Technology, Ritsumeikan University, 1-1-1 Nojihigashi, Kusatsu, Shiga, 525-8577, Japan, ³CAS Key Laboratory of Mineralogy and Metallogeny/Guangdong Provincial Key Laboratory of Mineral Physics and Materials, Guangzhou Institute of Geochemistry, Chinese Academy of Sciences (CAS), 511 Kehua Street, Wushan, Tianhe District, Guangzhou, 510640, China, ⁴CAS Center for Excellence in Deep Earth Science, Guangzhou 510640, China, ⁵Luleå University of Technology, Space Campus, 981 28 Kiruna, Sweden, ⁶Institute of Space and Astronautical Science, Japan Aerospace Exploration Agency, Sagamihara, Kanagawa 252-8510, Japan.

Several spacecraft have shown that kilometer-sized or smaller asteroids, such as Itokawa, Ryugu and Bennu, are covered with regolith particles. The shapes of regolith particles are considered clues to understanding their formation and evolution on asteroid surface. Ryugu particles are likely fragments resulting from impacts on the asteroid's surface. However, there has been a lack of laboratory impact experiments specifically examining the shapes of fragments in carbonaceous chondrites, which originate from carbonaceous asteroids like Ryugu and Bennu. In this study, we take the first step towards a better understanding of the shapes of impact fragments in carbonaceous chondrites. We conducted an impact experiment on the carbonaceous meteorite Allende and investigated the shape distributions of sub-mm-sized impact fragments using X-ray microtomography. As a result, we observed many fragments cross-sections along the chondrule boundary. In addition, these fragments tended to be rounder than previously observed impact fragment shapes. However, because the total number of these fragments is relatively small, the overall shape distribution of the fragments was found to be the same as that of previous impact fragment shapes. This finding will be useful for understanding the formation process of regolith layers on the asteroid surface, Itokawa particles, Ryugu particles, and Bennu particles scheduled to return to Earth.

Spectral characterization of (98943) 2001 CC21, fly-by target of Hayabusa2#

Perna D.¹, Barucci M.A.², Belskaya I.^{2,3}, Birlan M.^{4,5}, Bourdelle de Micas J.¹, Dotto E.¹, Fornasier S.², Hasegawa S.⁶, Ieva S.¹, Inasaridze R.⁷, Ishiguro M.⁸, Kitazato K.⁹, Krugly Yu.³, Kuroda D.¹⁰, Mazzotta Epifani E.¹, Palomba E.¹¹ and Yoshikawa M.⁴

¹INAF – Rome Observatory, Italy. ²LESIA – Observatoire de Paris, France. ³Kharkiv National University, Ukraine. ⁴IMCCE – Observatoire de Paris, France. ⁵Astronomical Institute of the Romanian Academy, Romania. ⁶ISAS-JAXA, Japan. ⁷E. Kharadze Georgian National Astrophysical Observatory, Abastumani, Georgia. ⁸Seoul National University, South Korea. ⁹Aizu University, Japan. ¹⁰Japan Spaceguard Association, Japan. ¹¹INAF-IAPS, Italy

To help solving uncertainties about the surface composition and possible heterogeneity of asteroid (98943) 2001 CC21, next fly-by target of Hayabusa2#, we acquired new visible and NIR photometric and spectroscopic data.

Visible (BVRI) spectrophotometry was obtained on November 2022 in the framework of the European NEOROCKS project, using the 1.2-m telescope located at the Haute-Provence observatory in France. Details of the observations and data reduction are given in [1]. The measured colors are within the range of values typical for S-complex. Figure 1 shows a comparison of the spectral behaviors of 2001 CC21 and templates of Sq, Sr, L and K-types according to the Bus-DeMeo classification scheme [2]. Our observations are well consistent with Sq or Sr types and do not support a L-type classification. This result is in agreement with recently published data on polarimetry and near-infrared spectrometry of this asteroid [3].

On January-February 2023, we also used the 2.6-m NOT telescope (La Palma, Canary Islands, Spain) to acquire visible spectra and NIR photometry of 2001 CC21 at different rotational phases. These data, currently under reduction, will allow us to further constrain its surface composition and possible heterogeneity.

On January 22, 2023 we observed 2001 CC21 in R band and covered the whole rotational period (Fig.2). The CCD observations were carried out using the 0.7-m telescope at the Abastumani Astrophysical Observatory, Georgia. The lightcurve amplitude is 0.75 mag and $P_{rot} \sim 5.03$ hours.

Preliminary results confirm the S-complex taxonomy, and suggest a subtle spectral variation with the rotational phase. An overview of our results will be presented and discussed at the Symposium.

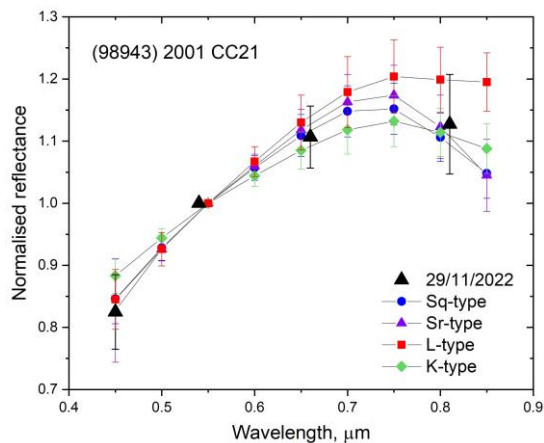


Figure 1. Comparison of 2001 CC21 obtained data with different asteroid taxonomic templates [4].

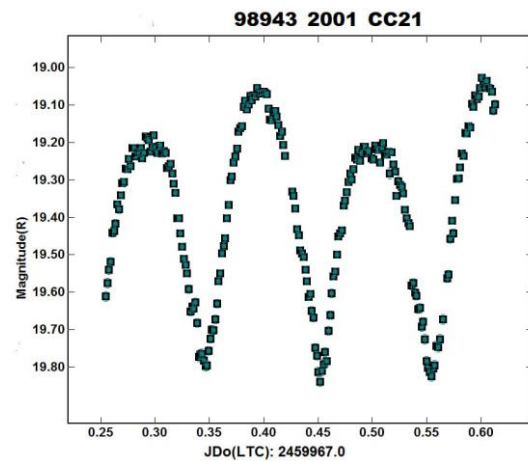


Figure 2. Lightcurve obtained on Jan 22, 2023.

References

[1] Hromakina et al. 2021. MNRAS 520:3143. [2] DeMeo F. et al. 2009. Icarus 202:160. [3] Geem J. et al. 2023. MNRAS 525:L17. [4] Barucci et al. 2023. Abstract #2015, ACM 2023.

Asteroid (142) Polana at 3 μm and its Connection to Primitive Near-Earth Asteroids

Driss Takir¹

¹Jacobs, NASA JSC

Introduction: Impacts between asteroid-sized objects have dominated the solar system's history and played a significant role in forming asteroid families. The New Polana family is a low-inclination and the most prominent low-albedo family within the inner Main Belt between the ν_6 secular resonance at ~ 2.0 AU and the 3:1 mean-motion resonance with Jupiter at ~ 2.5 AU [1]. This family formed over 2000 Myr ago and is parented by the B-type asteroid (142) Polana [1]. [2] and [3] found that primitive near-Earth asteroids (NEAs), including Hayabusa2's asteroid target (162173) Ryugu and OSIRIS-REx's asteroid target (101955) Bennu, are likely disrupted fragments that originated during the formation of the New Polana family. Other possible sources of primitive NEAs in the inner Main Belt include the Clarissa, Erigone, Polana, and Sulamitis, families and the collisionally evolved background asteroids outside these families [2, 4].

The age of the solar system is longer than the collisional lifetime of asteroid Bennu [5], a rubble pile asteroid with a mean diameter of 490.06 ± 0.16 m [6] and a spinning top-like shape [7]. Asteroid 142 Polana, the largest remnant of the New Polana family [1], has been spectrally (~ 0.5 - 2.5 μm) and dynamically linked to asteroid Bennu [e.g., 2]. Bennu's spectra were measured over the wavelength range from 0.4 to 4.3 μm with OSIRIS-REx Visible and InfraRed Spectrometer (OVIRS) [8]. Here, we investigate the compositional linkage of asteroids Polana and Bennu using 3- μm Polana spectra measured at the Infrared Telescope Facility (IRTF).

Results: Polana's prism (0.7- 2.5 μm) spectra exhibit a broad concave feature centered ~ 1.21 μm with a band depth of $\sim 11\%$. The spectrum has a slight positive slope toward wavelengths greater than 1.2 μm . We acquired two Prism sets of Polana, the first at 12:32 UTC and the second at 12:48 UTC on July 2nd, 2023. Spectra of the two prism sets are similar, showing no compositional heterogeneity in the observed surface of Polana. On the other hand, Polana's LXD (1.9– 4.2- μm) spectra do not reveal any pronounced spectral features in the ~ 2.0 - 4.0 - μm spectral range, suggesting that this asteroid is not hydrated (Figure 1).

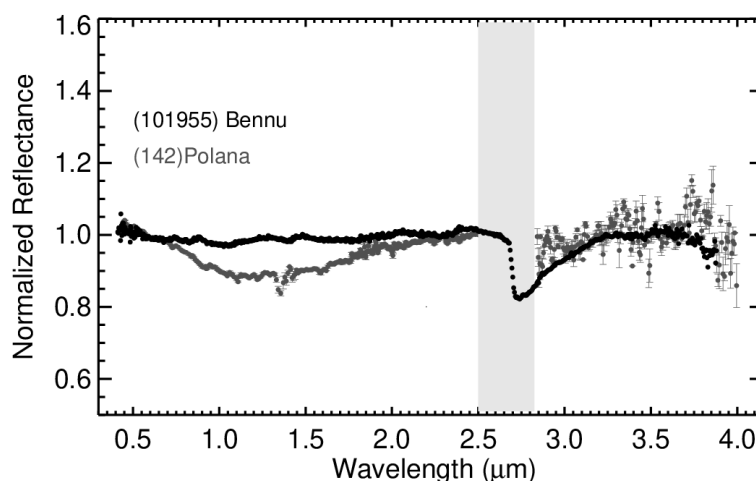


Figure 1. Spectra of asteroids Bennu and Polana. The ~ 1.2 - μm band in Polana is more pronounced than in Bennu. Bennu's spectrum is an average spectrum measured at the 10:00 a.m. station. Unlike Bennu, Polana does not show a pronounced feature at ~ 3 - μm . Slope-removed spectra are normalized at 2.2 μm .

Discussion: Prism's spectrum of Polana shows a broad feature centered around 1.2 μm (Figure 1), possibly due to amorphous iron-rich silicates abundant in least-processed CO carbonaceous chondrites that experienced minimal aqueous alteration and thermal metamorphism [10, 11]. Magnetite was also suggested to cause the 1.2- μm feature in B-type asteroids [12]. The 1.2- μm feature in the Polana spectrum is much deeper and more pronounced than Bennu's, suggesting that Polana has more abundant amorphous silicates or magnetite on its surface than Bennu. Polana was previously observed by [13], and its spectra SNR did not allow the authors to confirm the presence of a feature at ~ 3 - μm . In this work, the LXD spectrum of Polana was found to be featureless (does not exhibit a 3- μm feature within two sigma), suggesting that Polana's surface is much less hydrated than Bennu's. Bennu's spectra were measured by OSIRIS-REx's OVIRS spectrometer, revealing that this primitive asteroid is hydrated (the 3- μm band has a depth of $\sim 20\%$) consistent with CM-, CI-, or CR-type carbonaceous chondrites [9]. In addition, Polana's LXD spectra do not indicate the presence of organics and/or carbonates, unlike Bennu, whose spectra were found to be consistent with carbonates dominated by calcite and aromatic and aliphatic organics with CH bonds [14, 15].

The lack of pronounced water (OH/H₂O), organic materials, and carbonates features on asteroid Polana could be related to the degree of heating produced by shock metamorphism during the New Polana family-forming event and the ejecta reaccretion that contributed to additional heating. To lose most of its surface hydrated minerals, including serpentines, Polana had to be exposed to impact temperatures higher than ~ 800 K [16]. Heating generated by disruptive collisions (families forming events) is substantial, where the temperature of almost all the parent bodies increases from 300 K (initial temperature) to 700 K [17]. [18] concluded that the hydration state of the members of a collisional family is heterogeneous and mainly depends on the impact energy level within the family.

Several factors can affect the degree of heating and shock metamorphism during family-forming events, including the impactor velocity and size, porosity within the asteroid's parent body, and material ejection efficiency. [19] found that in rubble-pile asteroids, the impactor velocity and size are the main factors responsible for high-grade shock metamorphism in impacts occurring in the Main Belt. According to these authors, changing the porosity, responsible for the overall energy

absorption within the parent body, from 10% to 30% in their simulations only slightly decreases the shock pressure and temperature.

Another possibility for explaining the discrepancy between Polana and Bennu in the 3- μm band could be that the New Polana family-forming event exposed the parent body's deep interior. The dislodged Bennu fragment from the parent body contains phyllosilicates, organics, and carbonate, unlike the exposed interior of the parent body that does not include these materials.

Laboratory experiments on carbonaceous chondrites have shown that space weathering can also affect the spectral characteristics of these chondrites [20, 21]. For example, irradiating these carbonaceous chondrites can cause their near-infrared spectra to become bluer and brighter or redder and darker depending on several factors, including their initial albedo. Space weathering can also cause the band depth of mineral absorptions at 0.7 and 3.0 μm to decrease respectively by 12 % to 50% [22]. Space weathering could cause the band depth at 3.0 μm to degrade significantly over time. The New Polana is one of the older families in the Main Belt (~2000 Myr, [1]). Near-Earth asteroids' lifetimes are ~10 Myr [3]; therefore, Bennu would have been less exposed to space weathering than Polana was.

Exogenic materials and breccias are common in NEAs (e.g., [23]). Exogenous basaltic materials were discovered on the rubble pile asteroid Bennu, linked to inter-asteroid mixing that occurred at macroscopic scales after the end of the planetesimal formation [24]. It is possible that exogenic hydrated (in addition to basaltic) materials landed on Bennu, contributing to its hydration level.

Remote sensing observations of the primitive NEAs Ryugu and Bennu suggested that these two asteroids experienced different aqueous alteration histories, as revealed by the characterization of their surface composition using the 3- μm band. The NIRS3 instrument on board Hayabusa2 detected a weak and narrow absorption feature centered around 2.27 μm across the observed Ryugu's surface, attributed to hydroxyl-bearing minerals [25]. Returned samples from Ryugu confirmed that this asteroid has a similar composition to CI-type carbonaceous chondrites [26]. OSIRIS-REx's OVIRS detected a broader and deeper 3- μm band in Bennu compared to NIRS3 observations of Ryugu. Based on their 3- μm hydration features, it is more likely that Ryugu and Bennu came from different parent bodies with distinct aqueous alteration and thermal histories. With the current ground-based observations of Polana and due to strong Earth atmospheric absorptions that affect the ~2.7- μm region, it is not feasible to fully assess if this asteroid has a 3- μm band like the narrow and subtle band found in Ryugu. An approved JWST program to observe Polana (with the NIRSpec and MIRI instruments) will allow us to further investigate Polana's connection to Bennu and Ryugu.

References: [1] Walsh, K.J et al. 2013. *Icarus* 225, 283–297. [2] Campins, H. et al. 2010, *ApJ*, 721, L53. [3] Bottke, W. F et al. 2015, *Icarus*, 247, 191. [4] Arredondo, A. et al. 2021. Volume 368, 1. *Icarus*. [5] Bottke, W. F. 2015 et al. *Icarus* 247, 191–271. [6] Barnouin, O. S. et al. 2019. *Nat. Geosci.* 12, 247–252. [7] Lauretta, D. S. et al. 2019 *Nature* 568, 55–69. [8] Reuter, D. C. et al. 2018. *Space Sci. Rev.*, pp. 214, 54. [9] Hamilton, V. E et al. 2019, *Nat. Astron.*, 3, 332. [10] Cloutis, E.A. et al. 2012. *Icarus* 220, 466–486. [11] McAdam, M. and Gustafsson, A. 2021. *Icarus* 369 (2021) 114592. [12] Yang, B., Jewitt, D. 2010. *The Astronomical Journal*, 140:692–698. [13] Rivkin, A. S. et al. 2022 *Planet. Sci. J.* 3, 15. [14] Kaplan, H. H. et al. 2020, *Science*, 370, eabc3557. [15] Kaplan, H.H. et al. 2021. *A&A* 653, L1. [16] Nakamura, T. Yamato 2016. *Earth Planet. Sci. Lett.* 242, 26–38. [17] Davison, T.M et al. 2010. *Icarus* 208 468–481. [18] Michel, P. 2020. et al. *Nature Communications* volume 11, Article number: 2655. [19] Guldemeister et al. 2022. *The Planetary Science Journal*, 3:198 (12pp). [20] Lantz et al. 2018. Space weathering trends on carbonaceous asteroids: possible explanation for Bennu's blue slope? *Icarus* 302, 10–17. [21] Thompson, M. S. et al. *Icarus* 319, 499–511. [22] Matsuoka, M. et al. *ApJL* 890 L23. [23] Bischoff, A. et al. 2010. *Meteorit. Planet. Sci.* 45, 1638–1656. [24] DellaGiustina et al. *Nature Astronomy*, 5, January 2021 | 31–38. [25] Kitazato et al. 2019. Vol 364, Issue 6437 pp. 272–275. [26] Yada et al. 2021. *Nature Astronomy* volume 6, pages 214–220.

Unveiling dark objects in Solar System: grain size effects on the infrared spectrum of mineral mixtures in presence of opaque components

G. Poggiali^{1,2}, L. Fossi², A. Wargnier¹, J. Beccarelli³, J.B. Brucato², M.A. Barucci¹, P. Beck⁴, M. Matsuoka⁵, T. Nakamura⁶, M. Pajola³, S. Fornasier^{1,7}, F. Merlin¹, A. Doressoundiram¹, T. Gautier⁸ and G. David¹

¹LESIA-Observatoire de Paris, Université PSL, CNRS, Sorbonne Université, Université de Paris Cité, 92195 Meudon Principal Cedex, France (giovanni.poggiali@obspm.fr)

²INAF-Astrophysical Observatory of Arcetri, Firenze, Italy

³INAF-Astronomical Observatory of Padova, Padova, Italy

⁴Institut de Planétologie et d'Astrophysique de Grenoble, OSUG/CNRS, Grenoble, France

⁵The Geological Survey of Japan, National Institute of Advanced Industrial Science and Technology, Tsukuba, Japan

⁶Department of Geophysics, Tohoku University, Sendai Miyagi, Japan

⁷Institut Universitaire de France (IUF), 1 rue Descartes, F-75231 Paris Cedex 05, France,

⁸LATMOS, CNRS, Sorbonne Université, Université Versailles St-Quentin, Guyancourt, France

Dark surfaces characterize several bodies in the Solar System: from primitive carbonaceous asteroids to the enigmatic surface of Phobos and Deimos, our knowledge on the spectroscopic behaviour of low albedo surfaces is still incomplete. A dark surface can be related to multiple factors, for example presence of opaque material [1] or strong surface alteration [2]. In order to interpret remote sensing data, laboratory studies remain a pivotal tool to unveil the surface physical state and composition. Several processes can be simulated in the laboratory, but the preparation and analysis of complex mixing of analog material is one of the most fundamental tool and, at the same time, one of the most complex study when multiple components are used. In this work, we aim to study how dark material mixed with basaltic material at different grain sizes can affect the spectroscopic features from near- to mid-infrared (1.25-25 μm).

Our sample set includes four series of basaltic mix (feldspar and pyroxene), at different grain sizes from $< 50 \mu\text{m}$ to $1000 \mu\text{m}$, mixed with amorphous carbon at increasing weight percentages from 1% to 50%. We analysed several features on the spectrum of each mineral mixture: (i) near infrared slope; (ii) $2.7 \mu\text{m}$ OH-stretching band; (iii) Christiansen features; (iv) Reststrahlen band and Transparency feature. Measurements presented in this work [3], for the first time take into account a large wavelength range and point towards a critical effect of dark material with a different outcome for each grain size. Some of the most interesting results involved the slope and the different behaviour of the Reststrahlen band. This dataset will be a good support in the interpretation of upcoming data from Phobos Martian Moon eXploration mission, as well as in understanding of previous data from dark surfaces in the Solar System like Ryugu and Benu.

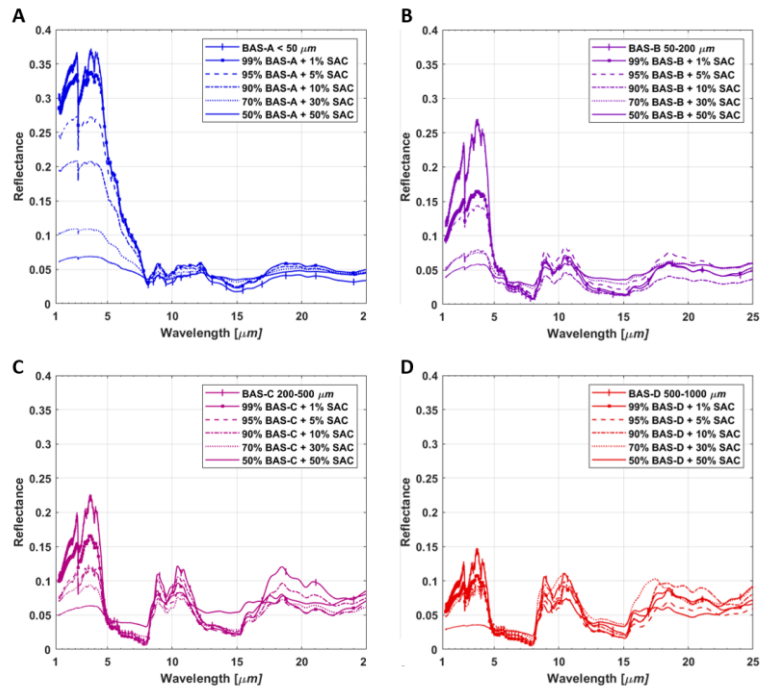


Figure 1. Infrared spectra of basaltic mixtures [BAS] at different grain sizes, < 50 , $50-200$, $200-500$ and $500-1000 \mu\text{m}$, with addition in different proportions, from 1 to 50%, with synthetic amorphous carbon [SAC].

References

[1] Cloutis et al 1990, Icarus, 84 (2), 315-333 [2] Hasegawa et al 2022, The Astrophysical Journal Letters, 939, L9 [3] Poggiali et al 2023, Astronomy & Astrophysics (submitted)

Investigating the effects of space weathering in Ryugu samples using coordinated microanalyses.

L. E. Melendez¹, M. S. Thompson¹, L. P. Keller², S. A. Eckley³, and C. J. Snead²

¹*Department of Earth, Atmospheric, and Planetary Sciences, Purdue University, West Lafayette, IN (melendl@purdue.edu)*

²*ARES, NASA Johnson Space Center, Houston, TX*

³*Jacobs, NASA Johnson Space Center, Houston, TX.*

Introduction: Airless planetary surfaces are characterized by a distinct lack of an atmosphere or magnetic field, leading to direct exposure to the effects of hypervelocity micrometeoroid impacts and solar wind ion irradiation [1]. These processes, cumulatively known as space weathering, gradually alter the microstructural and chemical properties of the grains on airless surfaces. Signatures of space weathering include vesiculated textures, amorphous grain rims (upper ~100 nm), solar flare tracks, and Fe-bearing nanoparticles (npFe) [2,3]. The accumulation of these microstructural space weathering characteristics, particularly the presence of npFe, alters the spectral properties of airless regoliths resulting in changes in spectral slope and reflectance of the surfaces, and the attenuation of characteristic absorption bands in the visible to near-infrared (Vis-NIR) wavelengths. These spectral changes complicate our ability to accurately interpret the mineralogy of airless bodies via remote sensing spectroscopy [1,4]. Studies of space weathering have primarily focused on anhydrous silicate minerals, reflecting the main components of the available returned samples from the Moon and S-type asteroid Itokawa [3,5,6]. However, our understanding of space weathering of primitive, organic-rich carbonaceous materials is still a work in progress. The Japan Aerospace Exploration Agency (JAXA)'s Hayabusa2 mission offered the first opportunity to directly investigate carbonaceous asteroids by returning samples from C-type asteroid (162173) Ryugu. Initial studies of Ryugu samples show mineralogical similarities to CI chondrites along with surface modifications consistent with space weathering. These surface modifications are primarily in the form of μm -thick silicate melts, amorphized phyllosilicates, glassy spherules, and burst vesicles [3,7]. Here, we report results from coordinated microanalytical techniques to further our understanding of the mineralogy and space weathering of carbonaceous materials.

Samples and Methods: We have been allocated two Ryugu particles returned by Hayabusa2; one particle collected at each of the two touchdown sites (A0152 and C0178). To understand the internal microstructure, mineralogy, and surface morphology of the two particles, we used X-ray computed tomography (XCT) to scan the samples using the Nikon XTH 320 micro-XCT at NASA Johnson Space Center (JSC) (Fig. 1). We also completed a higher-resolution sub-volume scan on the Zeiss Xradia 620 Versa at the University of Texas at Austin High Resolution X-ray CT Facility (UTCT) (Fig. 1). We segmented the dataset to identify different phases (e.g., sulfide minerals) and their spatial distribution using Dragonfly software. Due to the friable nature of the sample, small fragments were shed from the main mass during sample transport. We transferred $<500 \mu\text{m}$ fragments of each particle to SEM mounts covered with carbon tape and coated the fragments with evaporated carbon. The stubs were characterized using the Quanta 3D FEG focused ion beam scanning electron microscope (FIB-SEM) at NASA JSC using both backscatter (BSE) and secondary electron (SE) imaging detectors along with a 70 mm^2 SDD energy dispersive X-ray spectroscopy (EDS) detector (Fig. 2).

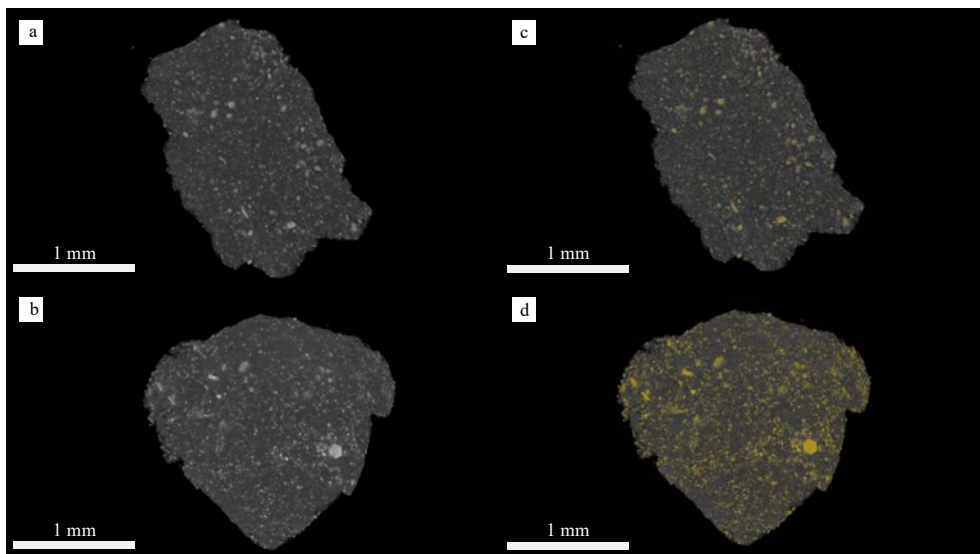


Figure 1. XCT scan of grain A0152 (a) and C0178 (b) with a resolution of $2.15 \mu\text{m}$ per voxel. Volume renderings with bright (higher relative Z number) phases (i.e., pyrrhotite and magnetite) in yellow for A0152 (c) and C0178 (d).

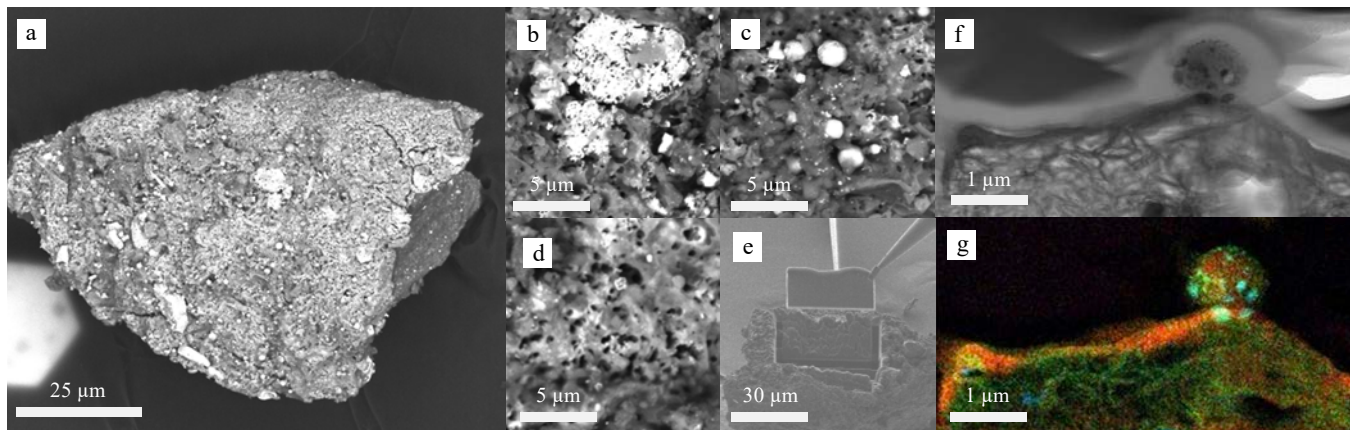


Figure 2. (a) Backscattered electron image (BEI) of one of the subparticles from A0152 with Fe_{1-x}S (e.g., pyrrhotite (b)) and characteristic signatures of space weathering, including (c) melt droplets and (d) vesicular textures. This melt deposit was targeted for further analysis in the TEM, with electron transparent thin sections prepared using FIB-SEM (e). The BF STEM image from the resulting FIB section (f) shows a region with a sub- μm impact spherule on the surface on top of a darker melt layer. The composite RGB image (g) shows Mg (red), Fe (green), and S (blue), revealing a Mg-rich melt layer and a spherule with nanophase Fe and FeS inclusions.

Particles from chamber A that displayed vesicles or melt textures on their surface (indicators of micrometeoroid bombardment) were targeted for the preparation of three focused ion beam (FIB) sections for further analysis in the scanning transmission electron microscope (STEM). Particles from chamber C reflected the expected mineralogy of Ryugu but evidence of space weathering has not been identified on these grains. Two FIB sections were extracted from the phyllosilicate matrix and magnetite grains for comparison to the space-weathered regions of A0152. Bright field (BF) and dark field (DF) STEM images and chemical maps of the FIB sections were acquired using the JEOL 2500SE STEM equipped with a 60 mm^2 ultra-thin window silicon drift energy-dispersive EDS detector at JSC.

Discussion and Conclusions: XCT results indicate that the grain is a micro-breccia, and that hexagonal sulfide grains (likely pyrrhotite) are ~ 10 to ~ 200 μm wide and are distributed throughout the fine-grained phyllosilicate and carbonate-rich matrix. Magnetite (Fe_3O_4) particles were also observed in both samples, exhibiting both framboidal and plaquette morphologies. 3D shape (SPO) and crystallographic (CPO) preferred orientations of sulfides (Fig. 1b) are being analyzed using Blob3D and 3DGrainMapper software, respectively. Currently, surface mesh renderings of A0152 and C0178 are being explored for evidence of impact cratering events, following [8]. SEM analysis of fragments from A0152 revealed vesiculated melt layers and frothy melt textures with melt spherules with embedded nanoparticles, resembling the deposits observed in simulated micrometeoroid bombardment [9]. STEM imaging confirmed the presence of Mg-rich phyllosilicates (serpentine and saponite), magnetite with variable morphologies, sulfides, and dolomite, consistent with previous studies of Ryugu samples indicating a low temperature aqueous alteration history [10, 11]. EDS analyses of these FIB sections of these regions revealed impact spherules and melt layers (up to 200 nm thick) containing abundant nanophase Fe-S and Fe-Ni-sulfides. Many of the nanoparticles are polyphasic, as opposed to the monomineralic nanoparticles observed in experimental samples. The melt layers have varying compositions depending on the underlying grain matrix: phyllosilicate grains have Ni-rich and Fe-poor melt layers while carbonate grains have Fe-, Mg- and O-rich melt layers. None of the particles analyzed thus far from C0178 exhibit textures characteristic of space weathering, which may be due to the comparatively ‘fresh’ nature of the subsurface sampling site, but we plan on proposing for additional grains for further analysis. We will continue to analyze these samples to better understand the effects of space weathering on carbonaceous regolith in preparation for the analysis of returned samples from asteroid Benu by OSIRIS-REx this year.

References

- [1] Pieters C. M. and Noble S. K. (2016) *Journal of Geophysical Research* 121(10): 1865–1884. [2] Keller L. P. and McKay D. S. (1997) *Geochimica et Cosmochimica Acta* 61:2331–2341. [3] Noguchi T. et al. (2014) *Meteoritics & Planetary Science* 49:188–214. [4] Chapman C. R. (2004) *Annual Review of Earth and Planetary Sciences* 32:539–567. [5] Taylor L. A. et al. (2001) *Journal of Geophysical Research: Planets* 106:27985–27999. [6] Nakamura, T. et al. (2011) *Science* 333: 1113–1116. [7] Matsumoto, T. et al. (2021) *Hayabusa Symposium 2021*. NIPR.[8] Hamann, C. et al. (2023) *86th Annual Meeting of the Meteoritical Society Conference* Abstract 2692. [9] Thompson M.S. et al. (2019) *Icarus* 319: 499–511. [10] Matsumoto T. et al. (2021) *Nature Communications* 11:1–8. [11] Nakamura T. et al. (2022) *Science* 379: 6634–6785. [12] Tomioka et al. (2023) *Nature Astronomy* 7: 669–677.

Impact-induced melting and fragmentation of C-type asteroid regolith inferred from impact craters on a large Ryugu sample

C. Hamann¹, E. Bonato², A. Maturilli², K. Mahlow¹, M. Patzschke³, R. Luther¹, K. Kurosawa⁴, G. Alemanno², S. Schwinger², A. Van den Neucker², M. Baqué², L. Hecht^{1,5}, A. Greshake¹, and J. Helbert²

¹Museum für Naturkunde Berlin, 10115 Berlin, Germany. ²German Aerospace Centre, 12489 Berlin, Germany. ³Bruker Nano Analytics, 12489 Berlin, Germany. ⁴Planetary Exploration Research Center, Chiba Institute of Technology, Narashino 275-0016, Japan. ⁵Institute of Geological Sciences, Freie Universität Berlin, 12249 Berlin, Germany.

The surfaces of airless planetary bodies are continually exposed to hypervelocity impacts of micrometeoroids and the influx of solar-wind ions as well as electromagnetic radiation emitted from the sun or other galactic sources [1,2]. Over time, these processes gradually alter the morphologies, microstructures, and chemical compositions of regolith grains exposed to space [3–7], which is collectively known as space weathering. Because space weathering alters the optical properties of space-exposed regolith (e.g., [2]), understanding space weathering of various types of planetary surfaces is critical for interpretation of remote-sensing data obtained from such surfaces and for matching various meteorite types to potential parent bodies. However, while the effects of space weathering on anhydrous regolith materials is well understood on the basis of samples returned from the Moon (e.g., [3,4]) and S-type asteroid Itokawa (e.g., [5–7]), space weathering of hydrous, carbonaceous-chondrite (C-type) like asteroidal surfaces is poorly understood so far. Samples returned by JAXA's Hayabusa2 mission from C-type near-Earth asteroid Ryugu (e.g., [8,9]) allow us to directly study the processes and products of space weathering of C-type asteroid regolith. Previous studies demonstrated that the uppermost surfaces of regolith grains returned from Ryugu's surface are amorphous and dehydrated due to influx of solar-wind ions [10,11]. In addition, small microcraters typically less than 10 μm across and splashes of quenched melt—presumably impact melts—have been reported from several Ryugu samples [10,12]. To better understand the role of micrometeoroid impacts in space weathering of C-type asteroids, we studied the impact-crater population on Ryugu sample A0112, which is a large (3.0×1.8 mm) regolith grain collected at the first touchdown site from the asteroid's immediate surface.

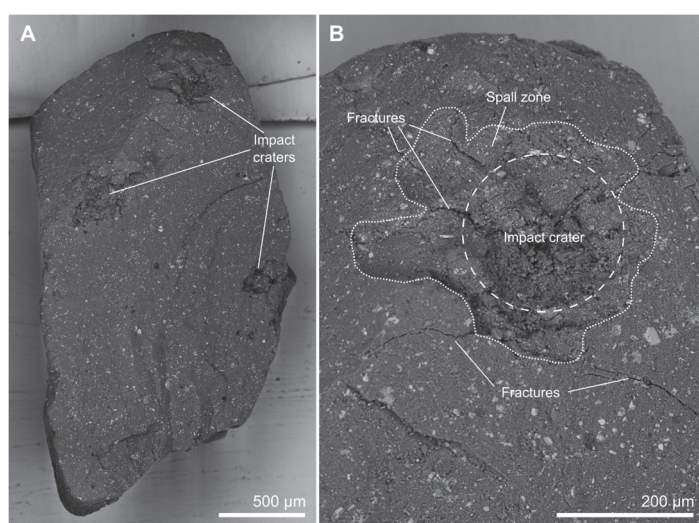


Figure 1. SEM-BSE images of the crater-covered side of A0112 (A) and the largest impact crater surrounded by a spall zone and surface-related, impact-produced fractures (B).

Scanning electron microscopy (SEM) at Museum für Naturkunde Berlin, Germany and Bruker Nano Analytics, Berlin, Germany as well as X-ray micro-computed tomography (μCT) at Museum für Naturkunde Berlin revealed the presence of three large, crater-like depressions of 150–270 μm diameter as well as of several smaller, circular pits of between 5 and 20 μm diameter on one of the surfaces of A0112 (Fig. 1). High-magnification SEM imaging furthermore revealed the presence of frothy, highly vesicular materials that are interpreted as quenched impact melts (cf. [10]) lining the bottoms and walls of the large and many of the small crater-like depressions (Fig. 2). Reflectance spectra obtained at German Aerospace Centre, Berlin, Germany from the frothy material lining the largest crater-like depression are almost featureless between 2 and 4 μm (Fig. 3) and resemble those obtained from the CI chondrite Ivuna heated to 700 $^{\circ}\text{C}$ [13]. Control

spectra obtained from the non-crater-bearing sides of A0112 are consistent with infrared spectra of other Ryugu samples (e.g., [14]) and showed pronounced spectral features at 2.71 μm and 3.32 and 3.46 μm that correspond to OH-bearing phyllosilicates and carbonates, respectively. Elemental analysis by energy dispersive X-ray spectroscopy (EDS) and EDS element distribution maps showed that the frothy materials are quenched silicate–sulfide emulsions, which suggests that the crater-like depressions and pits are impact craters. Quenched melt splashes up to 300 μm across exist not only on the crater-bearing side of A0112, but also on an additional side of the sample. These are similar in chemical composition to the frothy layers described recently from other Ryugu samples [10] and invariably comprise silicate–sulfide emulsions. High-resolution EDS element distribution maps furthermore suggest that the quenched melts contain immiscible FeNi metal droplets (cf. [11]). In terms of major-element

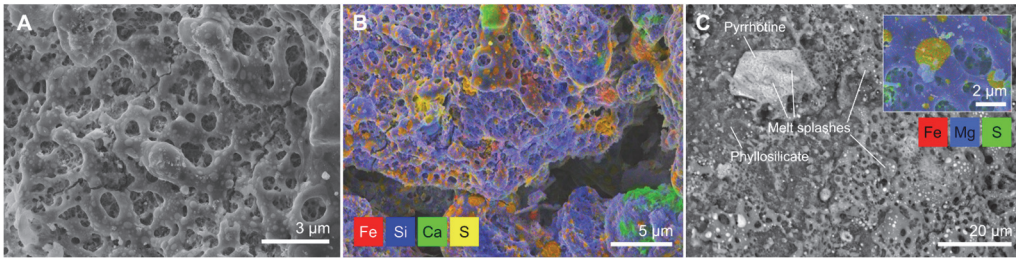


Figure 2. SEM-SE image (A) and element distribution map (B) of quenched impact melts lining the bottoms of the large impact craters on A0112. (C) SEM-BSE image of quenched melt splashes on the surface of A0112. A high-magnification element distribution map of the quenched melt splashes is shown in the inset.

subsurfaces adjacent to and below the large craters are intensely fractured; in particular, we observed fracture patterns resembling radial, concentric, and spallation fractures known from impact experiments in the strength regime (e.g., [17] and references therein). Consistent with lunar microcraters [17], large craters >150 μm are surrounded by irregular spallation zones whereas small craters <40 μm are almost perfectly bowl-shaped.

While investigations on the impact craters and quenched melts on A0112 are ongoing, our preliminary results provide information on the nature and magnitude of impact-induced processing of C-type asteroid surfaces in relation to solar wind-induced space weathering. Sample A0112 appears to be the most intensely shocked Ryugu sample investigated so far—the majority of smaller Ryugu samples were so far reported to be either essentially unshocked [18] or only marginally affected by micrometeoroid impacts, with solar wind-derived modifications dominating over impact-induced modifications [10–12]. Our findings of relatively large craters and abundant quenched impact melts on A0112 suggests that micrometeoroid impacts play an equally important role in space weathering of C-type asteroid regoliths as solar-wind induced modifications do. Impact-induced fracturing and spallation associated with the large craters on A0112 also informs on the efficiency of impact-induced fragmentation of grains in C-type asteroid regoliths [19]: Our observations suggest that spallation zones of micrometeoroid impact craters are likely sources of hydrated carbonaceous micrometeoroids arriving on Earth, contradictory to recent proposals based on unshocked to mildly shocked Ryugu grains [18]. This hypothesis is based on the fact that spall fragments ejected from spall zones surrounding hypervelocity impact craters are typically unshocked (e.g., [20]), but detailed numerical models using the iSALE shock physics code are currently being computed to probe peak pressures and temperatures in the spall zones surrounding the craters on A0112. If A0112's microcrater population is representative of Ryugu's surface, our results have relevance for evaluation of the relative roles of thermal [21,22] vs. impact-triggered [17] comminution of, and dust production from, C-type asteroid regolith.

Acknowledgments: We thank JAXA for allocation of Ryugu sample A0112.

References

- [1] Hapke B. 2001. *Journal of Geophysical Research Planets* 106: 10039–10073.
- [2] Pieters C. M. and Noble S. K. 2016. *Journal of Geophysical Research Planets* 121: 1865–1884.
- [3] Keller L. P. and McKay D. S. 1997. *Geochimica et Cosmochimica Acta* 64: 2331–2341.
- [4] Pieters C. M. et al. 2000. *Meteoritics & Planetary Science* 35: 1101–1107.
- [5] Noguchi T. et al. 2011. *Science* 333: 1121–1125.
- [6] Noguchi T. et al. 2014. *Meteoritics & Planetary Science* 49: 188–218.
- [7] Thompson M. S. et al. 2014. *Earth, Planets and Space* 66: 89.
- [8] Yokoyama T. et al. 2023. *Science* 379: eabn7850.
- [9] Nakamura T. et al. 2023. *Science* 379: eabn8671.
- [10] Noguchi T. et al. 2023. *Nature Astronomy* 7: 170–181.
- [11] Melendez L. E. et al. 2023. Abstract #6286. 86th Meteoritical Society Meeting.
- [12] Nakato A. et al. 2023. *Earth, Planets and Space* 75: 45.
- [13] Hiroi T. and Pieters C. M. 1996. Abstract #551. 27th LPSC.
- [14] Pilorget C. et al. 2022. *Nature Astronomy* 6: 221–225.
- [15] Genge M. H. and Grady, M. M. 1999. *Meteoritics & Planetary Science* 34: 341–356.
- [16] Zolensky M. et al. 2022. *Meteoritics & Planetary Science* 57: 1902–1919.
- [17] Hörz F. et al. 2020 *Planetary and Space Science* 194: 105105.
- [18] Tomioka N. et al. 2023. *Nature Astronomy* 7: 669–677.
- [19] Flynn, G. J. 2009. *Planetary and Space Science* 57: 119–126.
- [20] Melosh H. J. 1984. *Icarus* 59: 234–260.
- [21] Delbo M. et al. 2014. *Nature* 508: 233–236.
- [22] Delbo M. et al. 2022 *Nature Geoscience* 15: 453–457.

chemistry, the melt splashes on A0112 match fusion crusts around the CI chondrites Orgueil and Alais [15] and resemble a quenched melt particle of likely impact-melt origin recently reported from Orgueil [16]. Furthermore, μCT scans revealed that the

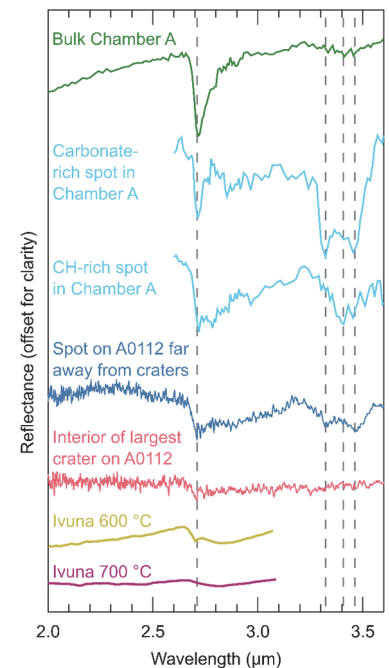


Figure 3. Reflectance spectra obtained from the largest impact crater on A0112 (red) compared against a spot far away from the craters (blue). Also shown are spectra of bulk A particles (green; [14]), carbonate- and CH-rich spots on Chamber A particles (light blue; [14]), and heated Ivuna CI chondrite (yellow and pink; [13]) for comparison.

Temporal variability of thermal-cycling induced fracturing in chondrites

N. Latsia¹, J. Borg¹, E. Kaufmann¹, M. Granvik^{1,2} and A. Hagermann¹

¹*Luleå University of Technology*

²*University of Helsinki*

Regolith on asteroid surfaces was thought to be a result of micrometeoroid impacts [1], but some recent studies [2,3] claim that thermal fatigue is the dominant regolith production process on airless bodies. Thermal fatigue is produced by diurnal and/or annual variations on the surface temperature of asteroids and its efficiency depends on the heliocentric distance, the rotation period, and the thermal inertia of the asteroid's surface. A fundamental assumption of previous studies is that thermal fatigue remains effective over thousands, or even millions, of thermal cycles. However, the Kaiser effect, extensively studied in the field of fracture mechanics on terrestrial rocks, states that fracturing on materials ceases when previously exerted load levels are not exceeded [9]. Previous research has demonstrated that the thermal properties of CM2 chondrites depend on their mineralogy [11]. Thus, the thermal expansion coefficient of each mineral at specific temperature changes can be translated into different mechanical loads resulting from thermal fatigue.

We aim to observe the time-resolved crack propagation induced by thermal stresses over subsequent thermal load cycles in meteorites – acting as asteroid analogues – in order to understand the role of thermal fatigue in eroding asteroid surfaces. According to several studies, Ryugu is similar to CI [5,6,7,8] and CM [8] carbonaceous chondrites, and hence provides ground truth observations for these samples. We investigate CI, CM, and, for comparison, LL chondrites to examine the behaviour of thermal fatigue on different petrographic types of meteorites. The samples are subjected to a minimum of 100 cycles at $\Delta T=210\text{K}$ as the temperature variation of C-type NEAs is 200K [2]. To identify the spatial occurrence of pre-existing and propagating cracks, the samples are scanned using X-ray tomography.

We aim to use non-destructive testing (NDT) methods to detect the time and frequency of crack initiation and propagation. NDT methods are used in many industries to identify and characterize the integrity of a material's surface and interior without interfering with its destruction [10]. The Kaiser effect predicts a decrease in the number of produced stresses as the number of thermal cycles increases, considering that the previous maximum and minimum temperatures of each cycle remain constant at 170C° and -40C° respectively. If the Kaiser effect is applicable, we expect to see the effects of thermal fatigue wane after a few thermal cycles, suggesting that other mechanisms, such as chemical alteration, are contributing to the breakdown process of asteroids.

References

[1] Housen K.R. et al. 1979. *Icarus* 39(3) 317-351. [2] Delbo M. et al. 2014. *Nature* 508(7495) 233-236. [3] Molaro J.L. et al. 2015. *JGR Planets* 120(2) 255-277. [4] Sakatani N. et al. 2021. *Nature Astron* 5(8) 766-774. [5] Yokoyama T. et al. 2022. *Science* 379(6634) abn7850. [6] Yada et al. 2022. *Nature Astron* 5(3) 214-220. [7] Kitazato K. et al. 2021. *Nature Astron* 5(3) 246-250. [8] Grott M. et al. 2020. *JGR* 125(12) e2020JE006519. [9] Kaiser J. 1950. A study of acoustic phenomena in tensile heat (PhD Thesis). [10] Dwivedi K. S. et al. 2017. *Materials Today* 5(2) 3690-3698. [11] Opeil C.P. et al. 2020. *MAPS* 55(8).

CALICO – an ESA M7 proposal to Explore Dwarf Planet Ceres

Axel Hagermann¹, Stefan Schröder¹ and the CALICO Consortium
¹*Luleå University of Technology*

Dwarf planet Ceres was the first member of the asteroid belt to be discovered. It is much richer in water than the other objects in the asteroid main belt, which suggests an origin elsewhere. Ceres' surface also shows clear signs of recent, possibly ongoing, geological activity and is regarded as the closest ocean world to Earth. The ocean worlds of the outer Solar System are of extreme interest for their potential to support biological activity over geological timescales. Unsurprisingly, the exploration of these enigmatic bodies is one of the priorities of ESA's Voyage 2050 strategy.

One region on Ceres of particular interest is Occator crater with its bright evaporite deposits, the so-called faculae. Formed by the extrusion of subsurface liquids, these deposits offer a window into Ceres' interior. In response to ESA's call for an M7 mission the international CALICO consortium, led by Luleå University of Technology, proposed CALICO (Ceres Autonomous Lander Into Crater Occator), a mission that will land in Occator crater and analyse the salt- and organics-rich deposits of Vinalia Faculae.

CALICO's science questions cover three themes:

1. Ceres as an active ocean world
2. Ceres' potential for habitability
3. Ceres' origin and evolution

CALICO will investigate carbon and organic material in the subsurface brine to assess the potential for complex organic chemistry, it will determine the physicochemical conditions to assess habitability. It will look for the chemical elements required for the building blocks of life and the elements required for biological energy production.

In order to unravel Ceres' origin and evolution, CALICO will pay special attention to the role of ammonia in its interior and the origin of Ceres' water as well as its magnetic history. CALICO will investigate the links between Ceres, asteroids, comets and carbonaceous chondrites.

In this talk, the mission concept and science payload of the CALICO mission will be presented, with a brief overview of the evolution and status of the proposal.

Next Generation small body Sample Return mission: a concept study for a future Japanese mission to a comet

Hiroyuki Kurokawa¹, Yuri Shimaki², Naoya Sakatani², Ryota Fukai², Tatsuaki Okada², Yoko Kebukawa³, Jun Aoki⁴, Atsushi Kumamoto⁵, Taichi Kawamura⁶, Satoshi Tanaka², Eri Tatsumi², Seitaro Urakawa⁷, Yuichi Tsuda², Osamu Mori², Takanao Saiki², The Next Generation Small Body Sample Return WG

¹*University of Tokyo*, ²*Japan Aerospace Exploration Agency*, ³*Tokyo Institute of Technology*, ⁴*Osaka University*, ⁵*Tohoku University*, ⁶*Université Paris Cité/Institut de Physique du Globe de Paris, CNRS*, ⁷*Japan Spaceguard Association*

The Next Generation small body Sample Return (NGSR) mission is a future solar-system exploration mission for sample return from a solar system small body under consideration. In February 2023, we newly launched the Science Working Group (WG) for the NGSR mission. The Science WG studies science goals and mission payloads of the NGSR. In collaboration with the Engineering WG, the Science WG aims to propose the NGSR as a strategic large-class mission which will be launched in 2030s by ISAS, JAXA. The strategic large-class mission will be selected in late 2024.

The NGSR targets a comet to bring back its subsurface materials and to explore its surface and internal structure. The Science WG defined the NGSR as a mission to unveil the origin of the solar system, namely, I) the origin of the solar-system “materials” in galactic evolution and II) the origin of the solar-system “bodies” to form planetesimals. For those science goals, we categorize science objectives as follows: Science objective I-1) unveiling the types of parent stars of the solar-system materials and their fractions, I-2) elucidating the origins of cometary organic matters, II-1) clarifying whether comets are rubble-pile or a pebble-pile bodies, and II-2) elucidating the formation environment of comets.

Science Goal I can be mainly achieved by sampling and analysis of subsurface materials of the target comet. In contrast to surficial materials that experienced alteration caused by space weathering and cometary activities, subsurface materials are thought to be pristine record of the original solar-system building blocks and, consequently, of the evolution of materials in our galaxy. Excavating and sampling subsurface materials are needed. Moreover, we are planning to install a mass spectrometer for in situ analysis of volatile materials that will potentially be altered and/or lost before the sample recovery.

Science Goal II can be mainly achieved by physical explorations of the interior structure with a radar and/or seismometer. Pebble-pile bodies (pristine first-generation of planetesimals) and rubble-pile bodies (disrupted and re-accreted planetesimals) should have different interior structures; only the latter are thought to possess meter-scale internal voids. The meter-scale heterogeneity can induce different propagation and reflection patterns for both radio and seismic waves.

Intermediate bodies of Asteroids and the Moon from an Earth 3GMS model

Yasunori MIURA

Department of Earth System Sciences, Faculty of Science, Yamaguchi University

Introduction: Previous formation model of active water planet Earth has been static description of three material states (3MD) from various planetary and Earth sciences, which have been studied in details for more description as public definition from scientific researched fields to public library and museum for educated words. On the other hands, there are two unsolved items of 1) formation of active Earth planet, and 2) formation of inactive Asteroids and the Moon-Mars comparatively in the Earth-type planetary bodies. The main purpose of the paper is to new active Earth formation model called here as Active Three Material States (A3MS) to be continued to be young products on global and local sites of the planet now [1,2] (Table 1).

Problem and characteristics of the previous 3MD model: The previous 3MD model shows typical merits for the definition of each terminology word on educational sites of school, library, book and museum sites, though it shows some demerits for static description (without previous and future changes in details). This is mainly because planet Earth is not static but so active globally and locally as complicated phenomena to be changed one direction in wide Universe totally. In fact, we meet difficult spots (totally inactive with old history of primordial ages) to explain the details and comparison of extraterrestrial bodies of many Asteroids and the Moon and Mars even in neighbor celestial bodied in the Earth-type planetary bodies of the Solar System. We have to make more detailed figure of active planet Earth from various academic fields of geology, rocky minerals, mixed rocks, physics-chemistry-biology contently with news sciences of environmental and computer information. It is herewith keeping unsolved problem for many academic researched fields separated into individual academic fields [3,4].

New model of present S3MS model: It might be difficult to young scientists who study one of many academic fields preciously for present wide points of academic fields to be explained. However, new wider scientists (even older scientists) from fundamental Earth sciences (mineral-rock chemistry, micro-observation analyses and wide geological sciences) are possibly solved totally, where they should be studied also wide planetary fields of planet, physics-chemistry and active shock wave fields of quake-volcano-impacts (QVI) processes comparatively [5,6].

Main points of new A3MS model: The present A3MD model shows possible explanation for active process of rocky solid system of Earth which are activated energy naturally to change rocks from older to newer ages among three material states of solid, fluid liquid-to vapor air (SLV), which we can see younger trends of Earth totally. Compared short human life age, the solid of Earth are surely changed with longer times (due to life with light elements from carbon organic molecules with fluid system, compared with rocky system of Earth with longer ages of change comparatively with continued change processes).

Meaning of existences of Atmosphere and Ocean systems on rocks (VLS) to Earth: On primordial period of Earth, natural activation energy (QVI) has been started from no ocean system by gravitational quake (tidal) and rocky system to be found three planets and the Moon and Asteroids on the Earth-type planetary zone. However present earth site has change to produce, keep in side fluid and solid rock inside as mixture of fluids and vapors for some geological periods to be more active on dried primordial Earth with huge collisions (*i.e.* planetary-planetary, and/or multiple asteroids collision, where might be the most big chance of formation of global ocean mixed fluid system, where characteristic aspects of fluid liquid phases are showing boundary as image boundaries with irregular round shapes and light molecules with many elements involving between solid (rock) and vapor (air) phases formed as global ocean system on water planet Earth during decreased temperatures and continuous lower temperature among three material states (VLS) with new formed active phenomena of plate quake and volcano locally to keep moderate temperature kept in Earth system as moderate complex processes on active Earth now [2-4].

Comparative differences of Earth and other celestial bodies: The present A3MS model can be explained younger planet Earth

by natural active phenomena QVI events, which can be shown by major differences between young Earth and other bodies beyond Earth. The Mineral crystals defined from small to large sizes with colorful units of Earth can be formed by ocean plate activities of quake and volcano with interior magmatic melting with irregular but continuous movements under room-temperature condition of water-Earth, though inactive celestial bodies of Asteroids and the Moon show tiny assemblages of rocks with primordial ages. Continuous magma melting and metamorphic events are used to be formed final pure and large mineral crystal of quartz SiO_2 and CaCO_3 calcite carbonates (gem mineral) only water planet Earth. Ocean fluids are water mixed with many tiny elements from light to heavy metals brought by many asteroid impacts on ocean for longer geological periods, where as in similar process of mixed rocks to pure mineral crystal the mixed fluid of ocean water can be produces to pure water of rain and underground water or glacier ice globally as small percentage as pure products on active Earth. Life shows the similar A3MS assemblages on the rocks of water planet earth corporately as shown in different paper. This suggest comparatively organic life works can be seen in the complicated and continuous A3MS process discussed in this paper shortly, which it suggests that life system of organic compounds can be existed and continued the A3MS system on active Earth as we can observed clearly.

Intermediate steps of various Asteroids 1M to the Moon 1M , and Mars 2MS from active planet Earth A3MS: From whole differences between inactive 1MS (one material state) of Asteroids compared with 2MS (two material states) , the Asteroids show initial collision aggregates with various grains and rocks of Si-system (mountain rocks), Ca system (ocean rocks) and Fe-group system (heavy iron) with some contents of non-mineral elements of CO(HN)-systems synthesized in organic compounds on active planet Earth. From active A3MS model, products of non-mineral CHO-system are obtained in continuous and active planet Earth easily. For inactive Asteroids and the Moon, light element CHO-system groups are easily formed from products contained carbon elements (cf. steel parts) with impacted sample collections and/or analytical procedures by **collision less-shock** wave reactions by electron, ion and laser beam bombardments in analytical chambers are extremely carefully to be interpreted on the paper [5]. In short, many joined aggregates can be observed in many parts of the Asteroids before forming the Moon or Mars planet as intermediate solid-aggregated rocks before forming the water planet Earth with other active group of life-A3MS system groups [2].

Table.1 Comparison of material states MS of Earth, Asteroid and other extraterrestrial bodies.

Celestial bodies	Mineral or Rocks	Organic Life System
Earth (water planet)	Active three material states (A3MS) system	Non-mineral light elements (CHON) system
Asteroids, the Moon (Mars)	A material state (1MS) Intermediate mixture	Store in solid interior (mixture), Contamination?

Summary: The present work has been summarized as follows.

- (1) Active planet model A3MS can be explained on Earth, but others inactive bodies are 3MS on the Solar System.
- (2) This model can explain younger rock of Earth and older rocks of other bodies of Asteroids.
- (3) New large crystals and life system on Earth and mixed rocks on Asteroids might be explained in the model.
- (4) Aggregates observed in the Asteroids before forming the Moon or Mars planet as intermediate solid-aggregated rocks before forming the water planet Earth with other active groups of life system groups.

References: [1] Miura Y. (2018) IMA-22,1189. [2] Miura Y. (2023) JAMS. E5-15. [3] Wilson J.T. (1965) Nature, 207 (4995), 343-347. [4] Miura Y. (1996) Shock-Wave Handbook (SV, Tokyo),1073-1209. [5] Miura Y. and Kato T. (1993) AIP, 283, 488-492. [6] Miura Y. (1992) Celestial Mechanic. & Dynamical Astro. (KA), 54, 249-253.

Chrome-spinel in Hayabusa particles: Recorders of Asteroid Itokawa's thermal history

Jemma Davidson^{1,2}, Devin L. Schrader^{1,2}, Thomas J. Zega³, Pierre Haenecour³, Kenneth J. Domanik³, Kazuhide Nagashima⁴, Noriko Kita⁵ and Philipp Heck^{6,7}.

¹*Buseck Center for Meteorite Studies, Arizona State University, AZ 85287, USA*

²*School for Earth and Space Exploration, Arizona State University, AZ 85287, USA*

³*Lunar and Planetary Laboratory, University of Arizona, AZ 85721, USA*

⁴*Hawai'i Institute of Geophysics and Planetology, University of Hawai'i at Mānoa, HI 96822 USA*

⁵*WiscSIMS, University of Wisconsin-Madison, Madison WI 53706, USA*

⁶*Robert A. Pritzker Center of Meteoritics and Polar Studies, Negaunee Integrative Research Center, Field Museum of Natural History, Chicago, IL 60605, USA*

⁷*Department of the Geophysical Sciences, University of Chicago, Chicago, IL, USA*

Introduction: Chrome-spinel, which includes chromite (FeCr_2O_4) and Cr-rich spinel ($[\text{Mg,Fe}][\text{Al,Cr}]_2\text{O}_4$), records both pre- and post-accretionary formation conditions while remaining resilient to extensive alteration (e.g., [1–5]). They are found in a wide variety of astromaterials, including chondrites, as well as Hayabusa [6] and Stardust [5] returned samples. The morphologies, chemical compositions, and O-isotope compositions of chrome-spinel minerals in returned samples provide important information on their primary formation conditions in the nebula (temperature, time, oxygen fugacity) and on the secondary alteration conditions on the parent body (thermal metamorphism).

Chrome-spinel and olivine in FeO-rich chondrules in carbonaceous and ordinary chondrites are very sensitive indicators of thermal metamorphism [1,4]. We compare the compositions, textures, and O-isotope compositions of chrome-spinel from asteroid 25143 Itokawa with those from ordinary chondrites to investigate correlations between formation mechanism, oxygen fugacity, and formation/alteration temperatures. Studying chrome-spinel in Hayabusa particles constrains the parent body formation and alteration conditions of asteroid 25143 Itokawa and provides information about the variety of material present on this asteroid (e.g., [6]).

Samples and analytical procedures: We were allocated three Hayabusa-returned particles during the Hayabusa AO7 (Table 1; Fig. 1a–c). Two of the allocated samples contain olivine-chrome-spinel pairs, while the third is solely chrome-spinel. All samples are large enough for multiple *in situ* O-isotope analyses.

Table 1. Hayabusa-returned samples for study.

Sample	Size (diameter)	Phases
RA-QD02-0316	117 × 51.5 μm	olivine, chr
RB-CV-0091	29.88 × 14 μm	olivine, chr
RB-CV-0262	39.2 × 23.3 μm	chr

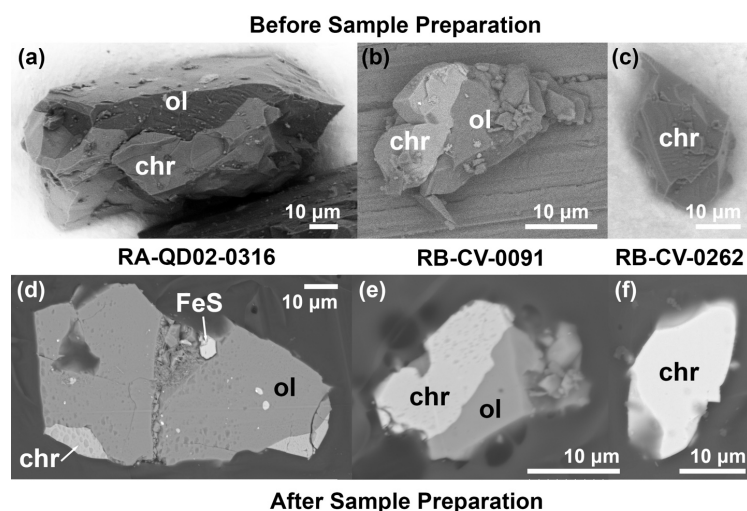


Figure 1. Hayabusa particles studied here (a, b, c) before, and (d, e, f) after sample preparation (i.e., mounting in epoxy and microtoming). (a–c) Backscattered electron (BSE) images modified from the JAXA Hayabusa particle catalogue used for preliminary identification of phases. (d–f) BSE images showing flat surfaces created by microtoming after mounting in epoxy. The orientation of RA-QD02-0316 changed slightly after mounting in epoxy, resulting in a smaller area of exposed spinel. Where chr = chrome-spinel, ol = olivine, and FeS = iron sulfide.

Sample preparation: The Itokawa samples were prepared at the University of Arizona's Lunar and Planetary Laboratory (LPL) following a modified version of the method presented in [7]: the particles were mounted on the top of epoxy bullets, which were then trimmed and sliced using a Leica EM UC7 ultramicrotome with two diamond knives (a trim knife and a cutting knife) to create flat surfaces that were suitable for microbeam analysis. The progressive excavation of each Itokawa grain was monitored using a Keyence VHX-7000 4K digital-optical microscope at LPL to ensure that overlying epoxy was removed to reveal

sufficient sample area for further analysis while preserving as much of the particle as possible. Analysis in 3D microscopy mode confirmed that the microtome method created smooth, flat surfaces ideal for EPMA and *in situ* O-isotope analysis.

Electron microscopy: The prepared samples were then carbon-coated and imaged in backscattered electron (BSE) mode in a Hitachi TM4000Plus II Tabletop scanning-electron microscope (SEM) at LPL Kuiper-Arizona Laboratory for Astromaterials Analysis facility (K-ALFAA) to verify that the microtome method created smooth, flat surfaces required for subsequent microprobe analysis (Fig. 1d–f). We then determined the major and minor element compositions of olivine and chrome-spinel in each of the Itokawa particles using the Cameca SX-100 EPMA at LPL K-ALFAA.

Results: Olivine-spinel thermometry: The olivine-spinel geothermometer was used to calculate closure temperatures for the two Itokawa particles that contain olivine and chrome-spinel mineral pairs (RA-QD02-0316 and RB-CV-0091). Quantitative compositional analyses were performed via EPMA at the edges of mineral pairs to determine the major and minor element compositions of both phases. Olivine-spinel temperatures were then determined using these data and an Excel version of the MELTS calculator [9]. Temperatures were determined at a pressure of 1 bar, which is a reasonable approximation for asteroids [10]. These calculations yielded closure temperatures of $\sim 610 \pm 50$ °C (1 sigma, 1σ) to $\sim 710 \pm 50$ °C for the different particles, which agree within a 2σ error. Assuming the olivine and spinel pairs in Itokawa particles originated from chondrules, these temperatures do not reflect the conditions of chondrule crystallization but rather closure temperatures after thermal metamorphism (e.g., [11]), consistent with temperatures recorded by olivine-spinel pairs in LL3.5–6 chondrites [8]. Temperatures indicative of crystallization in the chondrules of LL3.00–3.3 chondrites are typically >1000 °C [8].

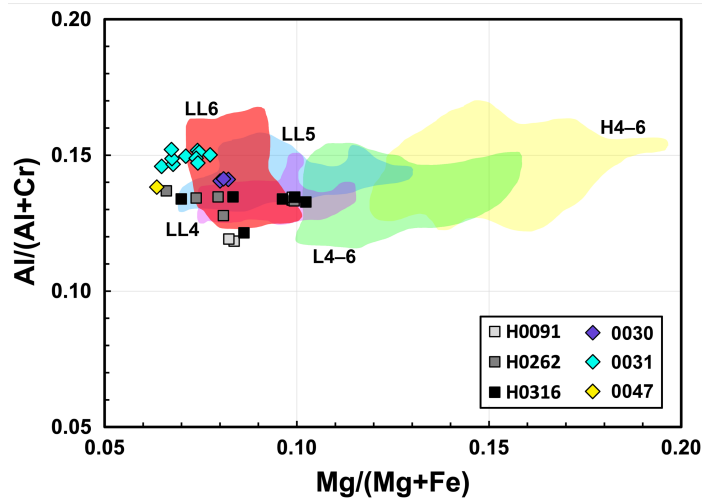


Figure 2. Chromite compositions for Hayabusa particles studied here (H0091, H0262, and H0316; squares) and from [6] (RA-QD02-0030, -0031, and -0047; diamonds) compared to those from ordinary chondrites (fields drawn from data in [6] and [8]).

Major and minor element compositions: The major and minor element compositions of each of the Itokawa chrome-spinels show that they have $\text{Cr}/(\text{Cr}+\text{Al}) > 0.8$, indicating that they are all chromite (i.e., FeCr_2O_4). Their $\text{Mg}/(\text{Mg}+\text{Fe})$ and $\text{Al}/(\text{Al}+\text{Cr})$ ratios cover a broader range than chromite compositions reported from three other Itokawa particles (RA-QD02-0030, -0031, and -0047) [6] (Fig. 2).

Since olivine-spinel geothermometry indicates that the Itokawa chromites studied here originate from thermally metamorphosed material, their compositions are compared with those from type 4–6 ordinary chondrites (LL, L, and H) (Fig. 2). The Itokawa chromites appear to be slightly less equilibrated than those previously reported by [6], which best match LL5 and LL6 chondrites, and cover similar compositions to chromites from LL4–6 chondrites (see comparison of OC data from [8] in Fig. 2).

Discussion: Due to the significant overlap between the major and minor element compositions of chromite from LL4–6 chondrites, it is not possible to match the Itokawa chromites studied here with specific petrologic types. Future work will include performing *in situ* O-isotope analyses of both olivine and chrome-spinel phases in each sample. This will enable us to constrain the specific meteorite petrologic type matches to the Itokawa chromites. However, the presence of Itokawa chromites covering the same range as LL4–6 chondrites is consistent with Itokawa being a breccia of LL4–6 materials [6].

References: [1] Johnson and Prinz 1991. *Geochimica et Cosmochimica Acta* 55:893–904. [2] Krot et al. 1993. *Earth & Planetary Science Letters* 119:569–584. [3] Kimura et al. 2006. *Geochimica et Cosmochimica Acta* 70:5634–5650. [4] Davidson et al. 2011. Abstract #5319. *Meteoritics & Planetary Science Supplement*. [5] Gainsforth et al. 2015. *Meteoritics & Planetary Science* 50:976–1004. [6] Nakamura et al. 2011. *Science* 333:1113–1116. [7] Che and Zega 2023. *Nature Astronomy* DOI:10.1038/s41550-023-02012-x. [8] Kimura et al. 2006. *Geochimica et Cosmochimica Acta* 70:5634–5650. [9] Sack and Ghiorso 1991. *American Mineralogist* 76:827–847. [10] Benedix et al. 2005. *Geochimica et Cosmochimica Acta* 69:5123–5131. [11] Wlotzka 2005. *Meteoritics & Planetary Science* 40:1673–1702.

Coordinated Analyses of Hayabusa particles RB-CV-0234, RB-QD04-0039, and RA-QD02-0310: Constraints on asteroid Itokawa formation from sulfides and silicates

Devin L. Schrader¹ and Thomas J. Zega²

¹*Buseck Center for Meteorite Studies, School of Earth and Space Exploration, Arizona State University, Tempe, AZ 85287-1404, USA (devin.schrader@asu.edu),*

²*Lunar and Planetary Laboratory, University of Arizona, Tucson, Arizona 85721, USA (tzega@arizona.edu)*

Introduction: Sulfides are important phases in planetary materials because their compositions, textures, and crystal structures can be used to constrain oxygen fugacity of formation, shock stage, and aqueous-, thermal-, and cooling-histories [e.g., 1–8]. The pyrrhotite-group sulfides are largely nonstoichiometric and have a range of compositions (typically $0 \leq x \leq 0.125$, but x can be ≤ 0.2 ; i.e., FeS [troilite] to $\text{Fe}_{0.8}\text{S}$) and distinct crystal structures (polytypes). The stoichiometric end members are 2C (troilite; FeS, hexagonal) and typically 4C (Fe_7S_8 , monoclinic) pyrrhotite. There are also pyrrhotites of intermediate compositions with $0 \leq x \leq 0.2$ (all hexagonal), including the non-integral NC-pyrrhotites and the integral 5C (Fe_9S_{10}), 6C ($\text{Fe}_{11}\text{S}_{12}$), and 11C ($\text{Fe}_{10}\text{S}_{11}$) pyrrhotites [e.g., 9–11]. Geothermometry of pyrrhotite-pentlandite intergrowths in meteorites shows that most formed via primary cooling from high temperature (i.e., chondrule cooling in the protoplanetary disk) or thermal alteration on the parent body [e.g., 12–14]. Sulfides in the LL4 to LL6 chondrites typically equilibrated $\leq 230^\circ\text{C}$, consistent with formation during cooling after thermal metamorphism [2]. Analyses of Hayabusa particles identified asteroid 25143 Itokawa as LL4–6 chondrite material ($\sim 10\%$ LL4 and $\sim 90\%$ LL5–6) [e.g., 15–18] that was thermally metamorphosed between ~ 780 and 840°C [15]. Itokawa particles were found to record shock stages between S2 and S4, with most particles around S2 [19,20]. Sulfides in Hayabusa particles [e.g., 15,21,22] may record additional and/or complementary information on the formation conditions of asteroid Itokawa.

We performed coordinated analyses of the Hayabusa particles RB-CV-0234, RB-QD04-0039, and RA-QD02-0310, allocated in Hayabusa AO5. Preliminary analysis by JAXA's Hayabusa examination team via scanning electron microscopy (SEM) determined that particle RB-CV-0234 (25.9 μm in diameter) consists of FeS, Fe, FeNiS, and CuS, making it an ideal target potentially containing both pyrrhotite group sulfides [(Fe,Ni,Co,Cr) $_{1-x}\text{S}$] and the rare Ni-rich sulfide, pentlandite [(Fe,Ni,Co,Cr) $_9\text{S}_8$]. In addition, JAXA's Hayabusa examination team determined that particle RB-QD04-0039 (52 μm in diameter) consists of olivine, low-calcium pyroxene, and troilite, and that particle RA-QD02-0310 (127 μm in diameter) consists of olivine, plagioclase, and troilite. These two Hayabusa particles provided excellent opportunities to identify sulfides with petrographic context and to analyze their adjoining silicate minerals, unlike RB-CV-0234 that only contained sulfides. Here, we compared in situ analyses of these particles to the results from LL3–6 chondrite silicates and sulfides [e.g., 1,2], with the goal of further constraining the formation and alteration conditions of asteroid Itokawa. Preliminary analyses from RB-CV-0234 and RB-QD04-0039 were presented in [23,24,25].

Samples and Analytical Procedures: We mounted RB-CV-0234, RB-QD04-0039, and RA-QD02-0310 each on epoxy bullets, using a method modified from [21], and microtomed them in preparation for analysis and sample extraction using the FEI Helios NanoLab 660 focused-ion-beam-SEM (FIB-SEM) at the University of Arizona (UAz). X-ray element maps and high-resolution images of the microtomed RB-CV-0234 and RB-QD04-0039 were obtained with the FIB-SEM prior to extraction of a $\sim 10 \times 10 \mu\text{m}$ sections from each particle, which were then thinned to electron transparency ($< 100 \text{ nm}$) following the methods of [26]. The FIB sections were then analyzed using the 200 keV aberration-corrected Hitachi HF5000 scanning transmission electron microscope (S/TEM) at UAz. After a FIB section of the sulfide from RB-QD04-0039 was obtained, RB-QD04-0039 was analyzed on the Cameca SX-100 electron microprobe (EPMA) at UAz. Microtome preparation of RA-QD02-0310 did not reveal sulfides for further structural analyses via TEM, but the compositions of its silicates were determined via EPMA at UAz.

Results: FIB-SEM X-ray element maps showed that the microtomed surface of RB-CV-0234 consisted entirely of pyrrhotite. However, X-ray element maps of the extracted FIB section, determined via TEM analysis, revealed a single large grain of pyrrhotite and a single smaller grain of pentlandite ($4.8 \times 1.3 \mu\text{m}$) at the bottom of the section (**Fig. 1**). Selected-area electron-diffraction (SAED) patterns of the pyrrhotite and pentlandite grains index to 2C pyrrhotite (troilite) and pentlandite along the [110] zone axis (i.e., they are crystallographically oriented), respectively. The compositions of RB-CV-0234 via quantitative

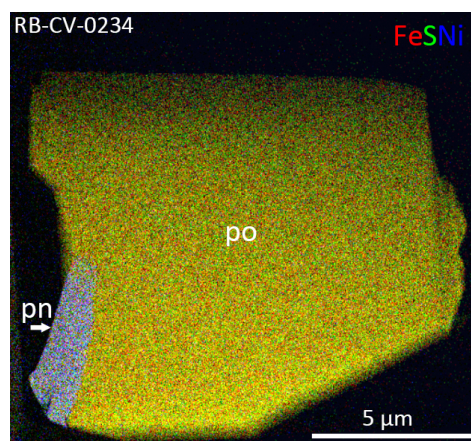


Figure 1. Composite TEM X-ray element map (RGB=FeSNI) of RB-CV-0234 FIB Section; where po = pyrrhotite and pn = pentlandite.

energy-dispersive X-ray spectroscopy [27] are 35.2 wt.% S and 64.8 wt.% Fe for pyrrhotite, and 32.4 wt.% S, 49.4 wt.% Fe, and 18.2 wt.% Ni for pentlandite. The microtomed surface of RB-QD04-0039 showed a single sulfide grain, as well as olivine (Fa28.1–29.5, Fa28.9±0.5 [1 σ]; n = 7) and low-calcium pyroxene (Fs23.8–24.9, Fs24.3±0.6, Wo1.1±0.1 [1 σ]; n = 3) (**Fig. 2**). A FIB section of the sulfide grain in RB-QD04-0039 revealed it to be troilite. The microtomed surface of RA-QD02-0310 showed a grain of olivine (Fa28.9–31.3, Fa30.2±0.8 [1 σ]; n = 12), with two chrome-spinels.

Discussion: The sulfides in RB-CV-0234 are most consistent with it being a sulfide grain from an LL6 chondrite, similar to the sulfides from Saint-Séverin studied by [1,2]. We infer this because: (1) the Ni content of pentlandite is consistent with the characteristic Ni contents of LL chondrite pentlandite [2,14]; and (2) based on results from the LL3–6 chondrite sulfides we previously studied [1,2,14], sulfide grains in Saint-Séverin (LL6, S2 [2,28]) contain a similar pentlandite/pyrrhotite morphology (i.e., blocky pentlandite in pyrrhotite) and 2C pyrrhotite (troilite) with pentlandite [1]. The other LL chondrites we studied contained either a distinct morphology (e.g., pentlandite lamellae) and/or multiple polytypes of pyrrhotite [1,2]. The compositions of pyrrhotite and pentlandite in RB-CV-0234 are consistent with equilibrating <300°C, perhaps as low as 230°C, similar to that of LL4–6 chondrites [2,25]. The olivine grain in RB-QD04-0039 contains planar fractures, indicating a shock stage of at least S3 and minimum shock pressures of 5–10 GPa [29]. The silicate compositions of both RB-QD04-0039 and RA-QD02-0310 (Fa28.9±0.5 and Fa30.2±0.8, respectively) are consistent with that of equilibrated LL chondrites, consistent with that found by [15] for Hayabusa particles. Relative to the iron-wüstite (IW) buffer, the oxygen fugacity constraints on the formation of troilite [30] and of pentlandite [14] indicates that RB-CV-0234 and RB-QD04-0039 were likely altered between approximately IW–2.2 and IW, consistent with that found for LL5 and LL6 chondrites by [14]. Therefore, the morphology and chemical compositions of sulfides and silicates of RB-CV-0234, RB-QD04-0039, and RA-QD02-0310, as well as inferred sulfide equilibration temperature and oxygen fugacity constraints are consistent with equilibrated LL chondrites.

Acknowledgements: We thank JAXA for the loan of the Hayabusa particles used in this study through the 5th International Announcement of Opportunity, and NASA grant NNX17AE53G (DLS PI, TJZ Co-I) for funding this research.

References

- [1] Schrader D. L. and Zega T. J. 2017. Abstract #6347. 80th MetSoc. [2] Schrader D. L. and Zega T. J. 2019. *Geochim. Cosmochim. Acta* 264:165. [3] Arnold R. G. 1967. *Can. Min.* 9:31. [4] Kissin S. A. and Scott S. D. 1982. *Econ. Geol.* 77:1739. [5] Raghavan V. 2004. *J. Phase Equilib.* 25:373. [6] Wang H. et al. 2006. *J. Sulfur Chem.* 27:1. [7] Harries D. and Langenhorst F. 2013. *Meteorit. Planet. Sci.* 48:879. [8] Bennet M. E. and McSween Jr. H. Y. 1996. *Meteorit. Planet. Sci.* 31:255. [9] Morimoto N. et al. 1975. *Econ. Geo.* 70:824. [10] Wang H. et al. 2006. *J. Sulfur Chem.* 27:1. [11] Harries D. et al. 2011. *Am. Min.* 96:716. [12] Jamsja N. and Ruzicka A. 2010. *Meteorit. Planet. Sci.* 45:828. [13] Schrader D. L. et al. 2015. *Meteorit. Planet. Sci.* 50:15. [14] Nakamura T. et al. 2011. *Science* 333:1113. [15] Schrader D. L. et al. 2016. *Geochim. Cosmochim. Acta* 189:359. [16] Noguchi T. et al. 2014. *Earth, Planets, and Space* 66:124. [17] Tsuchiyama A. et al. 2011. *Science* 333: 1125. [18] Tsuchiyama A. et al. 2014. *Meteorit. Planet. Sci.* 49:172. [19] Noguchi T. et al. 2011. *Science* 333:1121. [20] Zolensky M. E. et al. 2012. Abstract #1477. 43rd LPSC. [21] Berger E. L. and Keller L. P. 2015. *Microscopy Today* 23:18. [22] Harries D. and Langenhorst F. 2014. *Earth, Planets, and Space* 66:163. [23] Schrader D. L. and Zega T. J. 2018. *Hayabusa 2018, 6th Symposium on Solar System Materials*. [24] Schrader D. L. and Zega T. J. 2019a. *Lunar Planet. Sci. L*, Lunar Planet. Inst., Houston, #2009. [25] Schrader D. L. and Zega T. J. 2019b. Abstract #6400. 82nd MetSoc. [26] Zega T. J. et al. 2007. *Meteorit. Planet. Sci.* 42:1373. [27] Zega T. J. et al. 2018. Abstract #2084. *Microsc. Microanal.* 24 (Suppl. 1). [28] Rubin A. E. 2004. *Geochim. Cosmochim. Acta* 68:673. [29] Stöffler D. et al. 2018. *Meteorit. Planet. Sci.* 53:5. [30] Schrader D. L. et al. 2021. *Geochim. Cosmochim. Acta* 303:66.

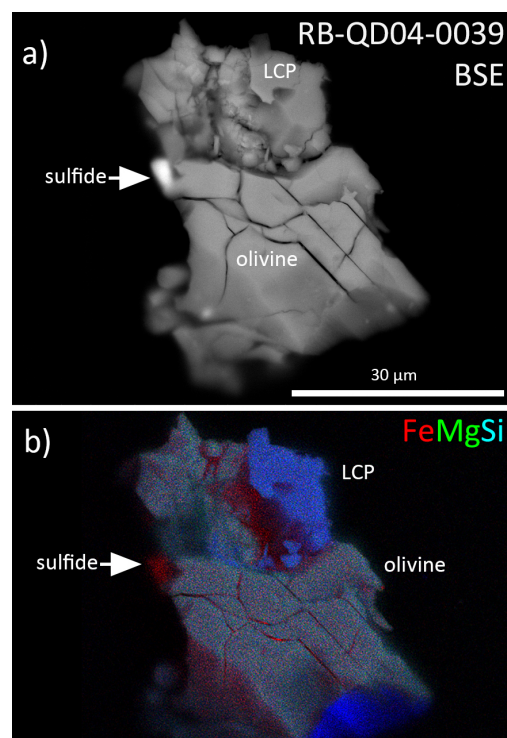


Figure 2. (a) Back scattered electron (BSE) image and composite EPMA X-ray element map (RGB=FeMgSi) of RB-QD04-0039; LCP = low-calcium pyroxene.

Are there 100s of ppm water in nominally anhydrous minerals of non-carbonaceous asteroids?

Dennis Harries¹

¹*European Space Resources Innovation Centre (ESRIC), Luxembourg Institute of Science and Technology, 41 rue du Brill, L-4422 Belvaux, Luxembourg*

Non-carbonaceous (NC) asteroids of mainly the S type comprise a large fraction of objects in the main asteroid belt and among the near-Earth asteroid population. Materials represented by them have played significant roles in the accretion of the terrestrial planets, but generally NC materials have been considered essentially dry relative to carbonaceous chondrites (CC). In consequence, NC planetesimals were usually not considered as carriers of H₂O delivered to the early Earth. Recently, SIMS studies of regolith particles returned by JAXA's Hayabusa mission from S-type/LL-group asteroid 25143 Itokawa have reported 240 to 990 ppm H₂O in the nominally anhydrous minerals (NAMs) orthopyroxene, olivine, and albite [1,2]. Additional data has indicated similar contents in NAMs of equilibrated chondrites of the L and LL groups [1,3] and in NAMs of unequilibrated chondrites [4].

H₂O contents on the order of 100s of ppm in NAMs of ordinary chondrites would have substantial implications for the early accretion of H₂O to the proto-Earth and would also imply high lithostatic pressures during thermometamorphism within chondritic planetesimals not consistent with current size estimates. Moreover, high water-to-rock ratios during metamorphism could indicate much higher bulk H₂O contents of pristine equilibrated chondrites beyond the defect-bound hydroxyl component, e.g., in the form of fluid inclusions. This would have considerable implications for the targeting of S-type near-Earth asteroids for in-situ space resources utilization (ISRU).

In order to shed more light on the H₂O contents in asteroidal NAMs, we have conducted a survey of H₂O in equilibrated chondrites and achondrites using the NanoSIMS 50L at the Open University, UK [5]. This contribution serves to place these results in perspective with other recent findings. The NAMs studied comprise olivine and orthopyroxene from a set of equilibrated ordinary chondrites of the L and LL groups (Baszkówka, Bensour, Kheneg Ljouâd, and Tuxtuac) and several ultramafic achondrites (Zakłodzie, Dhofar 125, Northwest Africa [NWA] 4969, NWA 6693, and NWA 7317). For calibration we used terrestrial olivine and orthopyroxene with H₂O contents determined by Fourier transform infrared spectroscopy. Our 99.7% (~3SD) detection limits achieved were 3.6 to 5.4 ppm H₂O for olivine and 7.7 to 10.9 ppm H₂O for orthopyroxene.

Our survey did not identify any meteorite sample that consistently showed H₂O contents in NAMs above our detection limits. Other recent SIMS studies of H₂O in NAMs of ungrouped achondrites and acapulcoites/lodranites, including NWA 6704 (paired with our sample of NWA 6693) and Dhofar 125, did not detect H₂O above 2.1 ppm [6] and 6.6 ppm [7], respectively. SIMS analyses of NAMs in unequilibrated chondrites by have also indicated very low H₂O contents of 8 to 14 ppm in these materials [8].

Finding H₂O contents one to two orders of magnitude lower than previously reported suggests that the parent planetesimals of the highly metamorphic chondrites, primitive achondrites and ultramafic achondrites studied were efficiently degassed during metamorphism and melting, if they initially had held substantial amounts of volatiles [5,6]. The discrepancies between SIMS analyses of Itokawa samples/equilibrated chondrites showing 100s of ppm H₂O on the one hand and equilibrated chondrites showing hardly any detectable H₂O on the other hand may stem from two contributions: Systematic errors of the analyses and/or heterogeneity of the samples. Sample contamination leading to systematically biased H₂O contents is a major suspect. It appears more likely to occur than H₂O loss from the strongly bound hydroxyl defects in NAMs, which requires substantial or prolonged heating to diffusively remove H₂O. The studies available rarely analysed the same samples or meteorites, rendering it difficult to rule out sample heterogeneity. However, there is currently no other indication to support the hypothesis that common equilibrated chondrites underwent metamorphism under vastly different peak pressures and H₂O fugacities, leading to heterogeneous H₂O contents in NAMs among different meteorites.

Hence, the presence of 100s of ppm H₂O in samples of asteroid Itokawa and equilibrated non-carbonaceous chondrites is doubtful and the role of their parent bodies in delivering water to the terrestrial planets needs to be questioned.

References

- [1] Jin Z. and Bose M. 2019. *Science Advances* 5:eaav8106.
- [2] Chan Q.H.S. et al. 2021. *Scientific Reports* 11:5125.
- [3] Jin Z. et al. 2021. *Planetary Science Journal* 2:244.
- [4] Stephant A. et al. 2017. *Geochimica et Cosmochimica Acta* 199:75–90.
- [5] Harries D. et al. 2023. *Meteoritics & Planetary Science* 58:705–721.
- [6] Newcombe M.E. et al. 2023. *Nature* 615:854–857.
- [7] Stephant A. et al. 2023. *Earth and Planetary Science Letters* 615:118202.
- [8] Shimizu K. et al. 2021. *Geochimica et Cosmochimica Acta* 301:230-258.

Development of Nondestructive X-ray CT Imaging Techniques to Identify and Locate Presolar Grains in Meteorite Sample Jbilet with Application to Ryugu Samples

D. Z. Shulaker¹, M. Ferrucci², B. M. Rogers², M. R. Savina¹, B. H. Isselhardt¹, Q. Shollenberger¹

¹*Nuclear and Chemical Sciences Division, Lawrence Livermore National Laboratory, CA (shulaker1@llnl.gov)*

²*Materials Engineering Division, Lawrence Livermore National Laboratory, CA.*

Introduction: The development of non-destructive analytical methods of precious material from sample-return missions is necessary to preserve as much material as possible, including presolar grains. Most commonly, an entire sample is dissolved to isolate presolar grains from the sample matrix. However, dissolving an entire meteorite or material from a sample-return mission also dissolves essentially everything but presolar SiC, graphite, and nanodiamonds. This results in the loss of precious material and presolar silicates. In attempt to save sample material, previous studies target presolar graphite and silicon carbide (SiC) grains using nanoscale secondary ion mass spectrometry (NanoSIMS), scanning electron microscopy (SEM), and/or focused ion beam (FIB) to image regions of meteorite fragments or thin sections [1–6]. When compared to traditional dissolution of meteorite fragments, these methods preserve grains and textural information. However, these methods are exceptionally time consuming, cover very little sample surface area, and often result in locating few presolar grains.

X-ray computed tomography (CT) is a non-destructive imaging technique that generates a three-dimensional representation of a sample in terms of an X-ray attenuation image. X-ray CT is used extensively in many fields of research and in industry, though its application to locating and identifying graphite and SiC grains in meteorites and other precious samples from sample-return missions is limited. X-ray CT is promising for this task because of its potential to locate and identify 10s to 100s of presolar grains while preserving the sample. The X-ray CT images can also be used to efficiently target specific regions in the sample for more precise characterization by NanoSIMS or for subsequent analyses, such as by resonance ionization mass spectrometry (RIMS). In this work, we present ongoing work in the development of an X-ray CT based paradigm for imaging fragments of meteorite sample Jbilet Winselwan (hereafter referred to as Jbilet) to locate and identify presolar grain types. Ultimately, X-ray CT will be used to image Ryugu fragments to locate and identify presolar grains and place presolar grains in mineralogical context. The X-ray CT image of the full Ryugu fragment will be used to intelligently target smaller regions of interest for subsequent isotopic analyses by NanoSIMS and RIMS.

Methods: To develop X-ray CT imaging techniques, a ~150 μm diameter fragment of Jbilet was mounted on carbon tape on an SEM stub. This was imaged on a Zeiss Xradia 510 Versa using a conventional acquisition and subsequent tomographic reconstruction by cone-beam filtered back projection. The reconstructed image consists of a three-dimensional array of volumetric picture elements (voxels), each assigned a gray value corresponding to the attenuation of X-rays by the material(s) contained within the voxel. The ability to distinguish features in the sample is dependent on the ability to detect changes in the reconstructed gray values. X-ray attenuation is a function of material composition (namely, atomic number, and physical density) and photon energy. Conventional cabinet X-ray systems typically use vacuum tube X-ray sources, which generate polychromatic ‘bremsstrahlung’ X-rays, i.e., characterized by a broad range of photon energies. However, since conventional reconstruction algorithms assume monochromatic X-rays, changes in the reconstructed gray values are not linearly related to changes in atomic number and/or physical density. The absence of sensitivity to photon energy in conventional X-ray CT imaging means that it is difficult to distinguish features with similar material properties, such as presolar grains.

One of our long-term objectives is to perform multi-spectrum acquisitions for direct material characterization by leveraging so-called ‘dual-energy’ acquisitions: two datasets acquired under distinct X-ray spectra, and a home-grown algorithm for decomposing the acquired data into voxel-wise effective atomic number and electron density [7]. As a precursor to our long-term objective, in this study we performed a conventional ‘single-spectrum’ acquisition at 40 kV tube acceleration voltage with a voxel size of 240 nm (Fig. 1). The reconstructed image was subsequently analyzed with VGStudio (Volume Graphics GmbH) and its foam/powder analysis functionality to identify individual particles and to extract their morphological and gray value statistics.

Results: Despite the previous caveat on relating gray value changes to material differences, features with substantially different attenuation properties could be distinguished using the mean gray value of the voxels contained within the particle regions. Furthermore, we can compare the extracted particle morphology, such as sphericity, diameter, and volume, to expected morphology for each grain as an additional criterion for particle classification. Based on these criteria, we make the following observations: (1) pores are typically less than 15 μm in diameter; (2) larger spherical voids approximately 20 μm in

diameter are surrounded by purportedly concentric shells of high attenuation particles with a finer particle size compared to the matrix, and (3) particles with the highest mean attenuation values are highly spherical and generally less than 5 μm in diameter. Using the data collected in this study in concert with previous studies of Jbilet [8,9], we hypothesize the identification of various discrete particles. For instance, that the larger, spherical features could be chondrules or chondrules with alteration phases and smaller high mean grey value spherical particles could be metal blebs.

Future work: We have identified several ways to overcome identified limitations with X-ray CT, such as reducing imaging artifacts, improving image quality, and spatial and attenuation resolution. For instance, without energy sensitivity in the acquisition and subsequent reconstruction, it is difficult to separate grains with similar morphology but distinct material properties, like SiC and graphite. Beam-hardening artifacts (such as false high gray value regions due in large part to the absence of energy sensitivity observed at the exterior edge of the meteorite as shown in Fig. 2) can interfere with the correct identification of features. By imaging a thinner fragment, we can use lower energy photons, which will result in reduced beam hardening artifacts and increased sensitivity to small changes in material properties within the sample.

We will also investigate the inclusion of external material references, such as synthetic SiC and graphite, into the measurement volume to serve as gray value benchmarks for identifying the same materials inside the sample.

Acknowledgments: We thank G. Brenneka for the Jbilet Winselwan meteorite sample and A. Mohan for reconstruction assistance. This work was performed under the auspices of the U.S. Department of Energy by Lawrence Livermore National Laboratory under Contract DE-DEAC52-07NA27344 and was supported by the Laboratory Directed Research and Development Program at LLNL under project 20-ERD-030 and 23-LW-015. LLNL-ABS-854399.

References: [1] Nguyen A. N. et al. (2007) *ApJ*, 656, 1223–1249. [2] Keller L. et al. (2012) *MicroSC*, 18, 1704–1705. [3] Davidson J. et al. (2014) *GCA*, 139, 248–266. [4] Sanghani M. N. et al. (2021) *ApJS*, 352, 1–26. [5] Barosch J. et al. (2022) *ApJL*, 935, 1–12. [6] Nguyen A. N. et al. (2023) *Sci. Adv.*, 9, eadh1003. [7] Azevedo S. G. et al. (2016) *IEEE Trans Nucl Sci*, 63, 341–350. [8] Friend P. et al. (2018) *Meteorit. Planet. Sci.*, 53, 2470–2491. [9] King A. J. et al. *Meteorit. Planet. Sci.*, 54, 521–543.

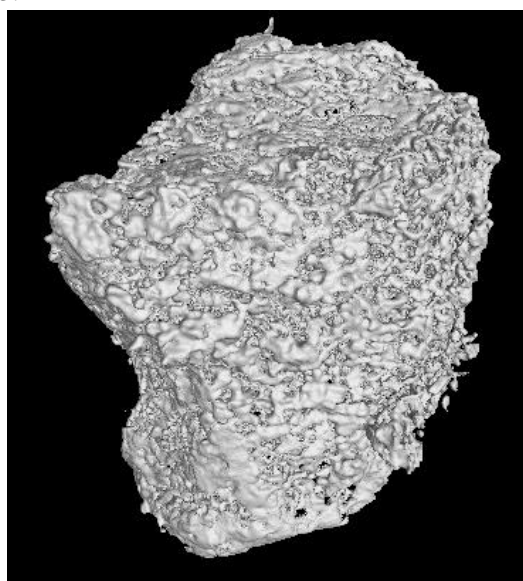


Figure 1. X-ray CT image of a $\sim 150\ \mu\text{m}$ diameter Jbilet fragment.

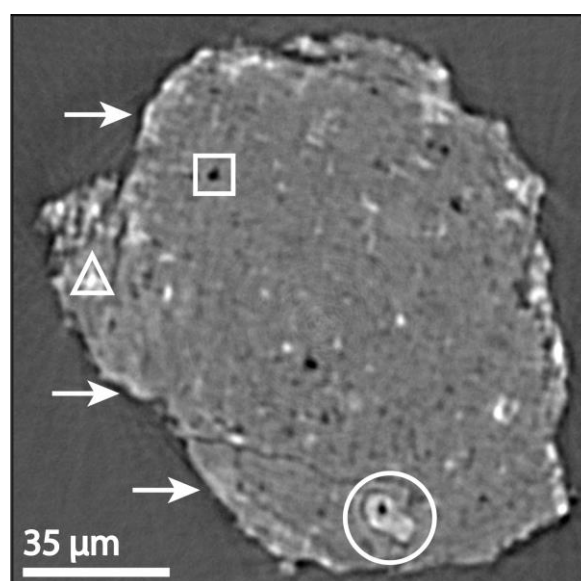


Figure 2. Cross section slice through a reconstructed X-ray CT image of Jbilet fragment. Examples of observed characteristics: square is a pore, triangle is metal bleb, and the circle is a chondrule. Arrows point to the “beam hardening” artifact that appears around the meteorite edge.

X-ray nano-CT and TEM-EDS Analyses of Impact Melt Splashes on Ryugu Samples

Megumi Matsumoto^{1*}, Junya Matsuno², Akira Tsuchiyama^{2,3}, Tomoki Nakamura¹, Yuma Enokido¹, Masahiro Yasutake⁴, Kentaro Uesugi⁴, Akihisa Takeuchi⁴, Satomi Enju⁵, Shota Okumura⁶, Itaru Mitsukawa⁶, Mingqi Sun³, Akira Miyake⁶, and the Hayabusa2 initial analysis team.

¹Department of Earth Sciences, Tohoku University, Tohoku University, Miyagi 980-8578, Japan. ²Research Organization of Science and Technology, Ritsumeikan University, Shiga 525-8577, Japan. ³Chinese Academy of Sciences (CAS) Key Laboratory of Mineralogy and Metallogeny/Guangdong Provincial Key Laboratory of Mineral Physics and Materials, Guangzhou Institute of Geochemistry, CAS, Guangzhou 510640, China. ⁴Japan Synchrotron Radiation Research Institute (JASRI), SPring-8, Hyogo 679-5148, Japan. ⁵Earth's Evolution and Environment Course, Department of Mathematics, Physics, and Earth Science, Ehime University, Ehime 790-8577, Japan. ⁶Division of Earth and Planetary Sciences, Kyoto University, Kyoto 606-8502, Japan.

Introduction: Ryugu samples are chemically and mineralogically similar to CI chondrites, and consist mainly of Mg-rich phyllosilicates, Fe-Ni-sulfides, magnetite, carbonates, hydroxyapatite, organic matters, and other minor minerals [1–5]. Some Ryugu particles experienced space weathering on the asteroid surface and exhibit amorphized and melted sample surfaces formed by solar wind irradiation and micrometeoroid bombardments [6]. A0067 and A0094 particles are among the space weathered Ryugu samples [6] and have flat sample surfaces which exhibit a lot of microcraters and impact melt splashes. In the present study, we investigated one relatively large microcrater (A0067-crater#1) and two impact melt splashes (A0067-melt#1 and A0094-melt#1) on the two particles (Fig. 1) by scanning electron microscope equipped with energy dispersive X-ray spectroscopy (SEM-EDS), X-ray nano-tomography (XnCT), and scanning transmission electron microscope (STEM) equipped with EDS to unveil the nature of the impactors hit on the asteroid Ryugu.

Results and Discussion: A0067-melt#1 shows round shape (~20 μm in diameter) and is composed of a Mg-Fe-rich glassy silicate main body and an Fe-rich opaque drop (~10 μm) attaching on the glassy silicate. It was extracted from the A0067 particle using focused ion beam technique and analyzed by XnCT and STEM-EDS. The analyses revealed that A0067-melt#1 is attached onto the saponite-rich coarse phyllosilicate layer (~1–4 μm in thickness) [2] developed along with the A0067 main body surface. Some gaps occur between the phyllosilicate sheets. These probably formed from shrinking of the phyllosilicate layers associated with volatile losses caused by the attaching of the hot impact melt splash. The glassy silicate in A0067-melt#1 has homogeneous Mg-Fe-rich composition with the ratio Mg/(Mg+Fe) in atom (hereafter Mg#) of ~0.64 and contains only small amounts of Fe-Ni metal-sulfide spherules (<100 nm). The Fe-rich opaque drop consists of dendritic crystals of α -(Fe-Ni) (~200–300 nm) embedded in the matrix composed mainly of troilite and minor pentlandite, and probably formed by a rapid cooling of an Fe-S-Ni melt.

A0094-melt#1 shows hourglass-like morphology (~15 \times 5 μm) and is probably made of two Mg-Fe-rich glassy silicate drops connected to each other. XnCT-STEM-EDS analyses revealed that A0094-melt#1 is compositionally inhomogeneous and shows patchy structure with Fe-rich (Mg# 0.52–0.55) and Fe-poor (Mg#~0.79) glassy silicate regions (2–5 μm in size). The boundaries between the regions are unclear. Spherical voids (a few tens of nanometers to ~2 μm) are abundant both in the Fe-rich and the Fe-poor regions. The Fe-poor region contains almost no crystalline phase whereas the Fe-rich region contains spherical and irregular-shaped Fe-Ni sulfides (<500 nm) and olivine grains (1–2 μm). Some aggregates (0.3–1 μm) consisting mainly of spongy inorganic carbon, irregular-shaped Fe-Ni sulfides, and Mg-rich silicates were also observed in A0094-melt#1. The aggregates are textually similar to primitive organic materials reported in anhydrous chondritic IDPs and carbonaceous chondrites [7], and might have formed from such primitive organic matters through volatile losses caused by impact induced heating.

A0067-crater#1 is ~5 μm in diameter. XnCT-STEM-EDS analysis revealed that A0067-crater#1 is ~4 μm in depth and traps small amount of mixture of glassy silicate

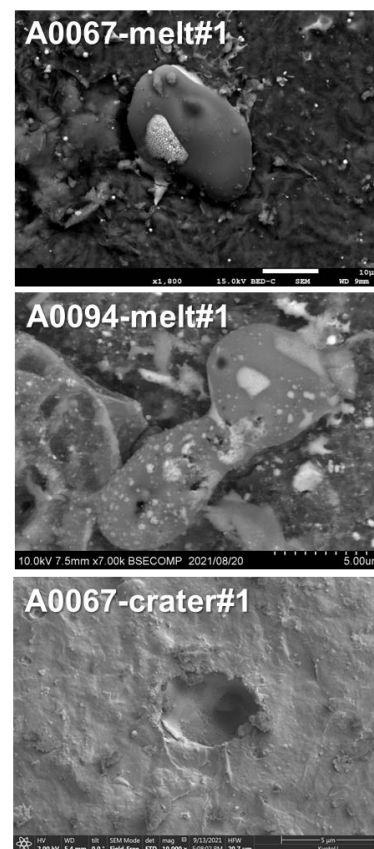


Fig. 1. FE-SEM images of A0067-melt#1, A0094-melt#1, and A0067-crater#1.

and troilite. The mixture should be an impact melt and shows flow structure consisting of glassy silicate and troilite layers (30–250 nm in thickness) stacking with each other. The glassy silicate layer is compositionally inhomogeneous and separated into Si-poor and Si-rich glasses. Both the silicate glasses contain spherical voids (<200 nm) and Fe-Ni sulfide spherules (<100 nm). The Si-poor glass (Mg#~0.72) is abundant compared to the Si-rich glass and compositionally similar to the glassy silicates in A0067-melt#1 and A0094-melt#1. The Si-rich glass selectively occurs along with the crater wall and probably formed *in-situ* from a Si-rich source material originally distributed on the A0067 particle surface. In the present study, we observed thin (<100 nm) Si-rich layers on A0067 and A0094 particle surfaces. These might correspond to the Si-rich vapor deposits previously reported on surfaces of some space weathered Ryugu particles [6] and may be the source of Si-rich glass in A0067-crater#1.

In the impact melts, different source materials such as impactors and Ryugu surface materials would have been mixed. The impact melts studied consist mainly of Mg-Fe-rich glassy silicate parts whose major element compositions (including Fe-Ni sulfide and olivine grains) are plotted along with an extension of a line connecting the CI (solar) composition [8] and the Fe-vertex in a (Si+Al)–Mg–Fe ternary diagram (Fig. 2). This suggests the impact melts studied have common source materials and the compositional trend seems to represent a mixing line of the source materials. A0094-melt#1 shows compositional inhomogeneity suggesting an incomplete mixing of the source materials, and the Fe-poor and the Fe-rich regions might be proximate to the original source materials. The Fe-poor region is compositionally similar to the Mg-rich phyllosilicate matrix in the Ryugu samples (Fig. 2) [2], which consists >80 vol.% of Ryugu samples, and probably sourced from Ryugu surface materials. On the other hand, the Fe-rich region has CI-like composition which deviate from the compositions of Ryugu’s phyllosilicates and other Ryugu components (Fig. 2). This suggests that Ryugu is not the source of the Fe-rich region and that the Fe-rich region was probably sourced from the impactors. The known small planetary materials having CI-like compositions are interplanetary dust particles (IDPs) and micrometeorites derived from asteroids and comets. Among those, anhydrous chondritic IDPs have bulk compositions which match well with the compositional range of the impact melts studied (Fig. 2) [9], and might be the source of the Fe-rich region. This is consistent with the presence of the carbonaceous aggregates, which might have formed from primitive organic matters, in A0094-melt#1. These mean that the impact melts studied might have formed by anhydrous chondritic-IDPs impacts on the Ryugu’s surface. Further study of many more impact melt splashes and microcraters will give important information about the variation and flux of the impactors that hit on asteroid Ryugu.

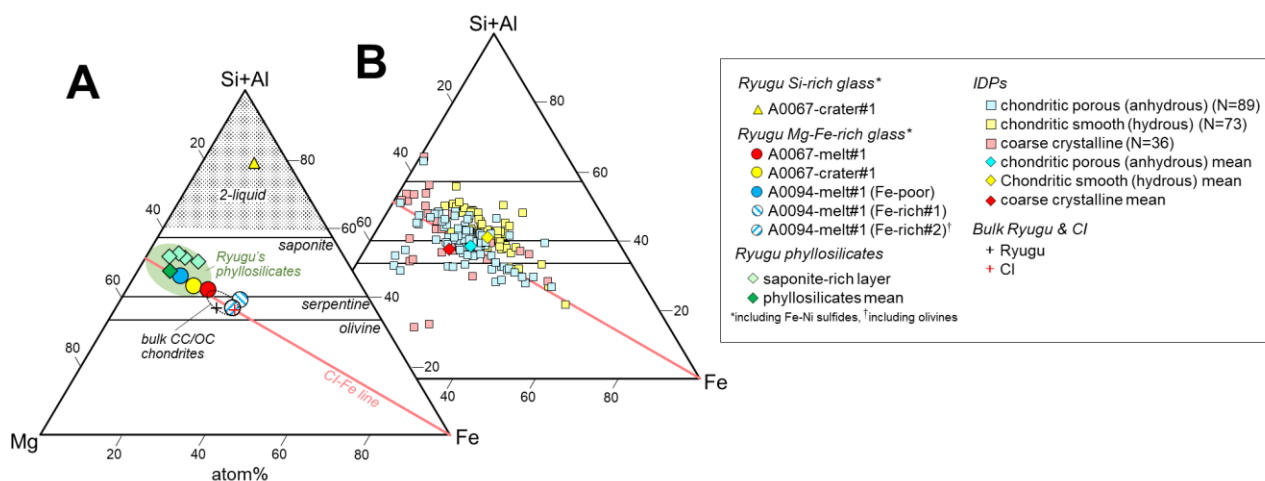


Fig. 2. (Si+Al)–Mg–Fe atom% ternary diagram of compositions of the melt splashes. (A) The major element compositions of the melt splashes studied and (B) those of IDPs. The compositions of IDPs are from [9], Ryugu’s bulk composition is from [1], and the composition of the phyllosilicates in the Ryugu samples is from [2]. The compositional field of Ryugu phyllosilicates (774 analyses) [2] is shown as a green colored oval.

Reference: [1] Yokoyama et al. (2023) *Science*, **379**, eabn7850. [2] Nakamura et al. (2023) *Science*, **379**, eabn8671. [3] Ito et al. (2022), *Nat. Astron.* **6**, 1163–1171. [4] Nakamura et al. (2022) *Proc. Jpn. Acad. Ser. B* 98:227. [5] Yamaguchi et al. (2023), *Nat. Astron.* **7**, 398–405. [6] Noguchi et al. (2023) *Nat. Astron.* **7**, 170–181. [7] Matrajt et al. (2012) *Meteorit. Planet. Sci.* **47**, 525–549. [8] Lodders (2021) *Space Sci. Rev.* **217**, 44. [9] Schramm et al. (1989) *Meteoritics* **24**, 99–112.

Comparison of Thermal Diffusivity between Ryugu grains and Carbonaceous Chondrites

Takuya Ishizaki¹, Ryota Fukai¹, Rei Kanemaru¹, Keisuke Onodera², Yoshinao Yasuda³,
Toru Yada¹, Masanao Abe¹, Tatsuaki Okada¹, Tomohiro Usui¹

¹Japan Aerospace Exploration Agency, 3-1-1 Yoshinodai, Sagamihara, Kanagawa 252-5210, Japan

²The University of Tokyo, 7-3-1 Hongo, Bunkyo-ku, Tokyo 113-0033, Japan

³Kwansei Gakuin University, 1-155 Uegahara Ichiban-cho, Nishinomiya, Hyogo 662-8501, Japan

Introduction: According to the general planetary formation scenario, the Solar System bodies evolved over a long period of time through repeated collision, fragmentation, and aggregation of planetesimals formed in the solar nebula. Thermal evolution, which induces various physicochemical reactions such as aqueous alteration, thermal metamorphism, and volcanism, is important for the evolution of planets. The temperature history inside the planetesimals followed in thermal evolution can vary greatly depending on when and how large they agglomerate and their effective thermal conductivity. Therefore, it is essential for the theory of planetary system formation to know the thermal conductivity of asteroids and meteorites, especially those that are thought to have existed since the early stages of planetary system formation.

The Ryugu sample brought back in 2020 by Hayabusa2 was found to be a primitive Ivuna-type carbonaceous chondrite, which is close to the average chemical composition of the Solar System [1]. Additionally, the elastic properties of the Ryugu grains were found to be similar to those of the Tagish Lake meteorite [2]. On the other hand, the thermophysical properties of Ryugu grains were found to vary widely from grain to grain [3]. Although this is the most important parameter in understanding the thermal history of asteroidal parent bodies, the cause of this variation has not been clarified. In this study, we measured the thermal diffusivities of Ryugu particles and carbonaceous chondrites using the lock-in thermography (LIT) periodic heating method [3], which was also used for the initial analysis of Ryugu grains to evaluate how the thermal properties of Ryugu grains are related to those of other carbonaceous chondrites.

Samples and Methodology: In this study, the thermal diffusivities of Ryugu and the carbonaceous chondrites were measured. A breakdown of the samples is as follows: three grains of Ryugu (A0172, A0038, and C0054), three grains of Ivuna (CI), one grain of Murchison (CM2), one grain of Tarda (C2-ungrouped), three grains of Tagish Lake (C2-ungrouped), and two grains of Allende (CV3). Bulk densities of the sample were also measured by obtaining weights and volumes of the sample. The volume was obtained by using an X-ray computed tomography (X-CT) device (SKYSCAN 1272). The X-CT images were also utilized to avoid cracks inside the sample, because the cracks may specifically affect to the results of the thermal diffusivity measurements.

In the measurement by the LIT periodic heating method, a spot on the sample is periodically heated using a laser, and the temperature response is measured by LIT to obtain the phase lag distribution on the sample surface. Then, the thermal diffusivity is analyzed from the gradient of the phase lag according to this equation; $D = \pi f / (d\theta/dr)^2$. Here, D is thermal diffusivity, f is heating frequency, θ is phase lag and r is distance from heating point. A measurement apparatus was originally constructed by combining a LIT (InfraTec ImageIR® 8350hp) with InSb cooled detector and 3x objective lens which provides a spatial resolution of 5 μm , optics, and a diode laser (633 nm, less than 10 μm of focus diameter). The laser beam was modulated according to the synchronized periodic signal from LIT, and an average power was estimated to be less than 10 mW. The schematic of the measurement is shown in Figure 1.

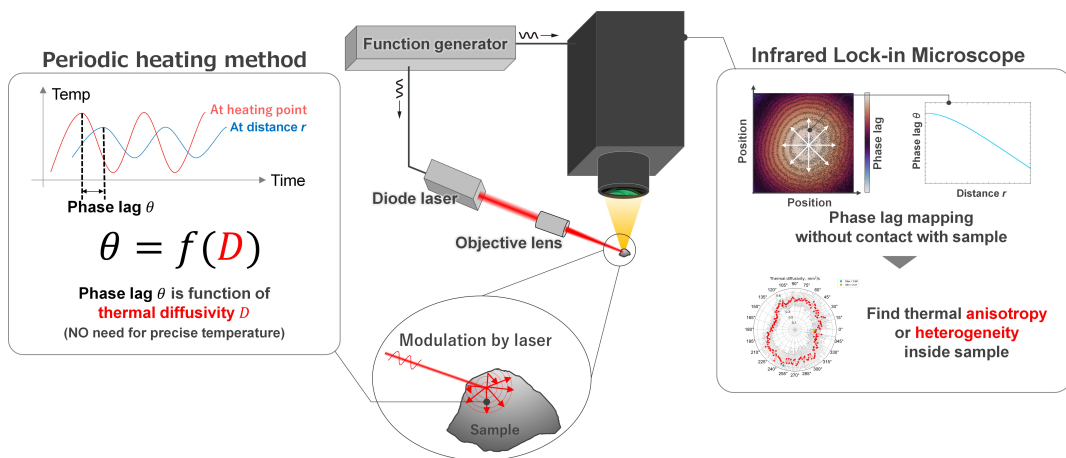


Figure 1 Schematic of the measurement.

The heating frequency was selected according to the sample size to avoid the influence of reflected temperature waves at the sample edge, and then measurements were performed at 20 Hz. The samples were measured under vacuum conditions of a pressure less than 10^{-4} Pa to refrain the effect of the surrounding air because the air causes the overestimate of the thermal diffusivity in the case of the low thermal diffusivity material.

Results and Discussion: The average value of the measured directional distribution of the thermal diffusivities of the Ryugu grains were $(1.5\text{--}3.7) \times 10^{-7} \text{ m}^2/\text{s}$. The thermal diffusivity of A0308 was particularly low, averaging $1.5 \times 10^{-7} \text{ m}^2/\text{s}$, which is the lowest value among all the Ryugu grains ever measured. The thermal diffusivities of the ten grains of carbonaceous chondrites were $(1.5\text{--}5.1) \times 10^{-7} \text{ m}^2/\text{s}$, with the Allende meteorite having a definitely higher value and the Tagish Lake meteorite having a definitely lower value than that of the others. The results for the other meteorites coincided within the margin of error.

Figure 2 shows the relationship of the thermal diffusivity and bulk density for each sample. Figure 1 also includes the results of the initial analysis of Ryugu [3], and reference values of Allende (CV3) measured by Soini et al. [4], and Murchison (CM2), Murray (CM2), Cold Bokkeveld (CM2), Jbilet Winselwan (CM2) and NWA 7309 (CM2) by Opeil et al. [5] are also shown as square plots. The results show a positive correlation between thermal diffusivity and bulk density, which is in agreement with reference values, except for Jbilet Winselwan and NWA 7309. Tagish Lake and Ryugu have the smallest thermal diffusivity and density among the groups that experienced the aqueous alteration, including Ryugu. On the other hand, the density and thermal diffusivity of Allende are confidentially larger than the other carbonaceous chondrites and Ryugu. There are several possible causes explaining the variation: (i) thermal diffusivities and densities of Ca- and Al-rich inclusions and chondrules are possibly larger than those of the matrix and Allende has a larger volume fraction of them [6]; (ii) the thermal diffusivity of the matrix possibly to be larger when olivine content is higher; (iii) the thermal diffusivity may be reduced by pores and cracks in the matrix developed during an aqueous alteration. We still have no clear conclusion for the cause of variation. Nevertheless, the variation of the thermal diffusivity and relationship with the density is critical for the thermal evolution of the planetesimals.

Also, Ryugu grains show a thermal diffusivity-bulk density relationship more similar to the Tagish Lake than to the Ivuna sample, which has a similar elemental composition to Ryugu. This result is in agreement with the elastic properties measured by Onodera et al. [2] and suggests that in carbonaceous chondrites with petrological classifications 1 or 2, thermo-mechanical properties may be dominated by mechanical and structural features consisting of the matrix, inclusions, and voids inside the grain. The grain of the lowest thermal diffusivity in Ryugu samples do not have a smaller bulk density than that of other Ryugu grains. Furthermore, the results of the thermal diffusivity distribution analysis indicate that the decrease

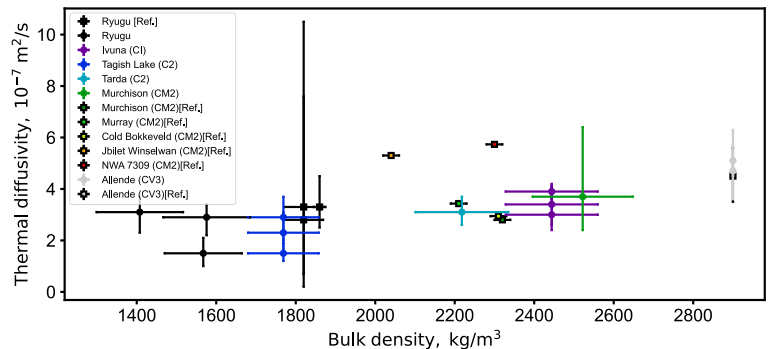


Figure 2 Thermal diffusivity vs. bulk density of Ryugu and carbonaceous chondrites.

in thermal diffusivity is unlikely due to cracking because the angular distribution of the thermal diffusivity seemed almost isotropic. In other words, this suggests the possibility that there is a heterogeneous distribution of the pore structure or tiny inclusions that reduce the thermal diffusivity while maintaining the bulk density.

To investigate the relationship between elastic wave velocity and thermal diffusivity, we additionally measured the primary elastic wave (P-wave) velocities of some samples as follows: one grain of Ivuna (CI), one grain of Murchison (CM2), one grain of Tarda (C2-ungrouped), and three grains of Tagish Lake (C2-ungrouped). The pulse transmission method was used for the measurements. Details of the measurements of the P-wave velocity are described in a previous report [7]. The result is shown in Figure 3, and the reference value of Ryugu is from Ref. [3, 5]. Figure 3 shows that there is a positive correlation between thermal diffusivity at the range of 0–2 km/s for the P-wave velocities. However, for P-wave velocities above 2.0 km/s, the thermal diffusivity tends to approach a constant value for P-wave velocity. Although the number of measurements is insufficient to clearly understand the cause of this trend, since the thermal diffusivity is more susceptible for the structural factors than the elastic wave velocity, it is possible that the structural factors in the grain may differ around the P-wave velocity of 2.0 km/s (e.g., whether the cracks are in a contact or non-contact at interface). The relationship between thermal diffusivity and elastic wave velocity will be able to provide an effective basis for understanding the internal structure of Ryugu and chondrite grains, by increasing sampling numbers for the carbonaceous chondrites in petrological classifications 1 or 2 and 3.

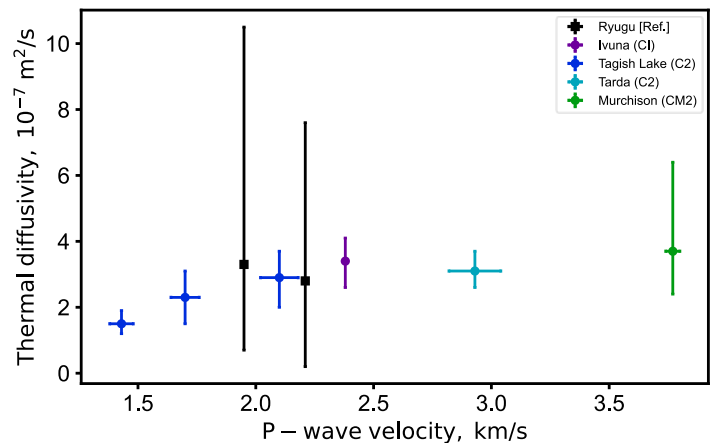


Figure 3 Thermal diffusivity vs. P-wave velocity of Ryugu and carbonaceous chondrites.

References

- [1] T. Yokoyama et al., *Science*, abn7850 (2022).
- [2] K. Onodera et al., *ESS Open Archive*, May 25 (2023).
- [3] T. Ishizaki et al., *Int. J. Thermophys.*, 44(4), 51, 2023.
- [4] Soini et al., *Meteorit. Planet. Sci.* 55, 402–425 (2020).
- [5] Opeil et al., *Icarus*, 208(1), 449–454, (2020).
- [6] H. Y. McSween, Jr. and G. R. Huss, “*Cosmochemistry*,” Cambridge Univ. Press, 169 (2010).
- [7] Onodera et al., *Proc. Jpn. Soc. Planet. Sci. Fall Mtg.* 2023 (2023).

Spatial relationship between macromolecular organic matter and organic-bearing phyllosilicates in Ryugu grain.

Toru Matsumoto¹, Takaaki Noguchi², Tohru Araki³, Takuji Ohigashi⁴, Yohei Igami², and Akira Miyake²

¹*The Hakubi center for Advanced Research, Kyoto University.* ²*Division of Earth and Planetary Sciences, Kyoto University,*
³*Institute for Molecular Science,* ⁴*High Energy Accelerator Research Organization.*

Introduction: Regolith samples recovered from the C-type asteroid Ryugu show chemical and petrological characteristics similar to those of CI carbonaceous chondrites [e.g., 1-3]. They consist of primitive components of the early solar system, including water and organic matter, but are highly modified in the parent body by aqueous alteration. Insoluble organic macromolecules (IOM) in Ryugu grains are the dominant components of organic matter in Ryugu's materials [3]. The chemical structures, distributions, and morphologies of the macromolecular organic matter can be tracers of the evolution of organic materials in the interstellar medium, the protosolar disk, and the aqueous environment in the parent body of Ryugu [3]. Recent analysis of the interlayer spaces of phyllosilicate minerals in Ryugu grains suggested the presence of organic molecules in clay structures [4, 5]. The infrared absorption band at around 3 μm obtained from Ryugu grains may come from N-H bearing molecules trapped in the interlayers of phyllosilicates [6]. These results suggest that phyllosilicates have been affected by organic matter during the aqueous alteration. Detailed investigation of the interlayer spaces of phyllosilicates and their spatial association with macromolecular organic matter will provide insight into the interaction between minerals, water, and organic matter in the parent body of Ryugu. In this study, we focused on carbon-rich regions in a Ryugu grain and examined the spatial relationship between organic materials and phyllosilicates, together with their chemical features.

Methods: A Ryugu grain from the chamber A (grain No. A0142) was distributed by JAXA as a sample for the international announcement of opportunity and was used in this study. The surface features of the grain was observed using a field-emission (FE)-scanning electron microscope (SEM) (JSM-7001F). Electron-transparent sections were extracted from the regions of interest using a focused ion beam system (FIB Helios NanoLab G3 CX). Scanning transmission X-ray microscopy (STXM) imaging was performed to obtain X-ray absorption near edge structure (XANES) spectra from the sections. The bonding structure of carbon was investigated using XANES spectra at the carbon K-edge (at 280 eV-320 eV). After STXM analysis, the sections were observed using field-emission transmission electron microscope (TEM) (JEOL JEM2100F).

Results: Backscattered electron images of the grain surface show the concentration of organic matter embedded in the phyllosilicate matrix (Fig. 1a). Several carbon-rich spots were found on the grain surface. We investigated the largest carbon-rich region with approximately $17 \times 8 \times 9 \mu\text{m}$ in size (Fig. 1ab). Carbon-XANES spectra of the carbon-rich region include major peaks of aromatic carbon (285 eV) and carboxyl carbon (288.5 eV), and those of phyllosilicate matrix in the vicinity of the carbon-rich region show peaks of aromatic carbon (285 eV), carboxyl carbon (288.5 eV), aliphatic carbon (287.5 eV), and carbonates (290.4 eV). TEM analysis showed that organic materials and fibrous phyllosilicates are finely intermixed in the carbon-rich region. Hereafter, we call the carbon-rich region as the carbon-phyllosilicate aggregate (CPA). Distinct morphologies of organic materials, such as the organic globules, were not identified in the CPA. The surrounding matrix consists mainly of fibrous phyllosilicates, magnetite, iron sulfides, and carbonates. High-resolution TEM images showing layered structures of the fibrous phyllosilicates (Fig. 1c) enabled us to investigate the interlayer distance of the phyllosilicates. The majority of the fibrous phyllosilicates in the CPA and the matrix have interlayer distances of 0.7~0.75nm, and 1.0-1.2nm. These values correspond to typical interlayer distances of serpentine and saponite in Ryugu samples, respectively [2]. On the other hand, fibrous phyllosilicates with interlayer distances of 1.23-1.35 nm were occasionally observed in the CPA and in the matrix close to the carbon-rich region (Fig. 1c).

Discussion: The enrichment of aromatic and carboxylic carbon in the XANES spectra from the CPA is similar to the spectral features of highly-aromatic or aromatic macromolecular carbon in Ryugu samples [3]. The concentration of aromatic organic matter may have occurred by redistribution and/or synthesis of organic matter during fluid activity in the parent body. It is also possible that large chunks of organic matter have been incorporated during the initial accretion of the parent body, in the form of primitive materials originated from the outer solar system [7]. The appearance of aliphatic carbon in the matrix is consistent with the previous XANES study of Ryugu samples, in which aliphatic organics were detected in association with phyllosilicates [8]. Previous X-ray diffraction measurements of Ryugu samples detected 001 reflection of smectite at 1.26 nm [4]. The relatively large interlayer distance was interpreted as the expansion of the interlayer space due to the presence of organic molecules [4]. Accordingly, the interlayer distances of 1.25-1.35 nm found in our sample suggest that organic species

are intercalated into the phyllosilicates. The spatial relationship between the CPA and the possibly organic-bearing phyllosilicates suggests that macromolecular organic matter could have interacted with surrounding phyllosilicates during aqueous alteration, as suggested by analyses of carbonaceous chondrites [9, 10].

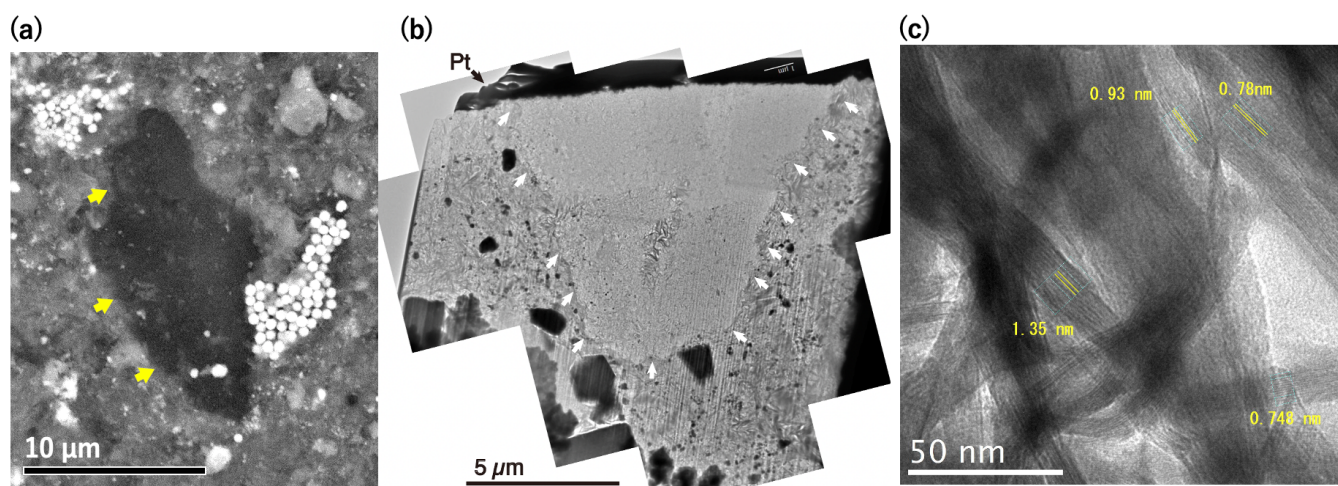


Figure 1. SEM and TEM analysis of the carbon-rich region of Ryugu grain (A0142). Backscattered electron image (a) and bright-field TEM image (b) of the carbon-phyllsilicate aggregate (CPA). Arrows indicate the interface between the CPA and surrounding phyllosilicate matrix. (c) High-resolution TEM image of fibrous phyllosilicates near the CPA. Interlayer distances are shown in the figure.

References: [1] Yokoyama et al. 2022. *Science* 379.6634, eabn7850. [2] Nakamura et al. 2022. *Science* 379.6634, eabn8671. [3] Yabuta et al. 2023. *Science* 379. 6634, eabn9057. [4] Viennet et al. 2023. *Geochem. Persp. Let.* 25, 8-12. [5] Damien et al. 2023. *Meteoritics & Planetary Science* under review. [6] Pilorget et al. 2022. *Nat. Astron.* 6, 221-225. [7] Duprat et al. 2010. *Science* 328, 742-745. [8] Ito et al. 2020. *Nature Astron.* 6:1163-1171. [9] Garvie and Buseck, 2007. *Meteoritics & Planetary Science* 42, 2111-2117. [10] Guillou et al. 2014. *Geochim. Cosmochim. Acta*, 131, 368-392.

Analysis of a thermal correction method for the MIRS infrared spectrometer: preparation for the future observations of the Martian moons Phobos and Deimos

G. David¹, M. Delbo², A. M. Barucci¹, F. Merlin¹, P. Beck³, S. Fornasier¹ and G. Poggiali¹

¹ *LESIA, Observatoire de Paris, Université Paris Cité, Université PSL, Sorbonne Université, CNRS, Meudon, France*

² *Laboratoire Lagrange, Observatoire de la Côte d'Azur, Université Côte d'Azur, CNRS, Nice, France*

³ *Institut de Planétologie et d'Astrophysique de Grenoble, OSUG/CNRS, 122 rue de la piscine, F-38000 Grenoble, France*

Introduction: The Martian Moon eXploration (MMX) mission is scheduled to be launched to the Martian system in 2024 [1]. The scientific payload will include the MMX InfraRed Spectrometer (MIRS, [2]), an instrument dedicated to the study of Mars and its satellites: Phobos and Deimos. MIRS data will contribute, together with the other instruments and the sample return analysis, to understand the origin of the two Martian moons. It will help to decipher whether they are captured asteroids or rather formed by accretion from a debris disk, the latter resulting from a giant impact between Mars and a planetesimal. In the spectral range covered by MIRS (0.9-3.6 μm), several components of geological interest will be studied through their spectral properties such as anhydrous and hydrous silicate minerals, water ice, or organic matter. Constraining the presence and relative abundance of these phases will help to determine the Martian moons' formation processes. However, several absorption bands associated with these compounds are in the spectral region beyond $\sim 2.5 \mu\text{m}$, where the signal collected by the instrument is a combination of reflected sunlight and thermal emission from the observed surfaces. The thermal emission - the so-called thermal tail - can strongly modify the continuum of the spectra and the width of the absorption bands. Consequently, before proceeding to the mineralogical analysis and interpretation of future MIRS data, a thermal emission correction is needed. In this study, a simple method of thermal emission correction is tested on synthetic data to evaluate its potential and limitations.

Method: The thermal tails of spectra are mainly controlled by the surface's temperatures, roughness and emissivity. For airless bodies, such as Phobos and Deimos, the surface conditions can be highly fluctuating, between $\sim 130 \text{ K}$ and $\sim 300 \text{ K}$ [3]. Temperature and emissivity are often not well-constrained on planetary surfaces, but they can be estimated directly from the infrared spectra. In this work, we deliberately explored a simple empirical method of thermal tail removal, based on Planck blackbody fit, owing to the MIRS instrument will provide a large amount of data and a method running quickly will save computing time and make it easier data interpretation during MMX flight operations. We used the approach from [4], which was originally developed to correct the Moon Mineralogy Mapper (M^3) observations onboard the Chandrayaan-1 spacecraft. This approach is iterative and uses the assumption that the continuum of the reflected solar component is approximately linear beyond $2.5 \mu\text{m}$. The signal at short wavelengths (with no thermal contribution) is used to extrapolate the reflected component in the thermal tail part of the spectra at a given wavelength. The differences between the projected reflectance and the original spectra, corresponding to the thermal contribution, are then fitted with a blackbody Planck function radiation, and a temperature can be derived. Emissivity (ϵ) is determined by using the projected I/F (the signal collected by the instrument normalized to the solar flux) at a specific wavelength and Kirchhoff's law ($\epsilon=1-I/F$). Here, we perform two iterations to adjust the temperature, using in the second run the previous corrected spectra. While in the first iteration, emissivity is considered as constant with wavelength, the second iteration will consider a wavelength-dependent emissivity (i.e., the Kirchhoff's law is used for each wavelength).

Synthetic data: Different spectral datasets were generated for the purpose of this study by means of a thermophysical model [5], which calculates thermal infrared spectra of airless bodies or sub-portions thereof as a function of several physical parameters such as albedo, roughness, thermal inertia, rotation period, direction of the rotation axis, as well as illumination and viewing geometry. The first dataset corresponds to seven synthetic reflectance spectra thought to be reasonably analogous to Phobos, for which thermal contribution at different temperatures from 262 K to 329 K has been added. In this first set of simulations, the scene corresponds to a flat facet of the Phobos shape model in nadir view. The second dataset includes the same parameters but this time, roughness has been generated by adding hemispherical section craters into the facet. This makes such that sub-facets with different inclinations with respect to the sun and the instrument compose the field of view. Each sub-facet contributes to the thermal infrared flux with its own temperature, which depends on the geometry relative to the sun. Finally, the last dataset is similar to the previous one but includes a fictitious absorption band centered at $3.2 \mu\text{m}$, to study its effect on thermal correction. In all our simulations, ϵ has been set to 0.9, which is thought to be consistent with the Martian moon surfaces.

Results: The first dataset is used to test the consistency between the temperature retrieved by the thermal correction model and the temperature used as input by the thermophysical model. Our results show that the first iteration gives an average of $\sim 0.8 \text{ K}$ of difference from the true temperature, while the second iteration increases the error on temperature retrieval with an average of $\sim 1.4 \text{ K}$ of difference. These results are consistent with the experiment made by [4], who found that the derived temperature by this approach of heated basalt in the laboratory was around 1 degree of the true measured temperature. The emissivity predicted by the model is also very consistent with the one used in the thermophysical model ($\epsilon=0.9$) to generate the

data. The first iteration predicts $\varepsilon \sim 0.88$ for all temperatures, whereas the second iteration predicts emissivity within 0.86-0.88. To determine the efficiency of the thermal correction, we calculated the mean absolute percentage error (MAPE), which quantifies the difference between each corrected spectrum and its spectrum of reference (i.e. spectrum generated without thermal contribution) that can be expressed as $MAPE = \sum_{\lambda > 2.5 \mu m}^n \left| \frac{y_{\lambda} - x_{\lambda}}{y_{\lambda}} \right| \frac{100}{n}$, where y_{λ} and x_{λ} are the I/F values of the reference and corrected spectra for each wavelength in the thermal part (i.e., $\lambda > 2.5 \mu m$). For the first data set, we found that corrected spectra have respectively MAPE scores of $\sim 1.25\%$ ($\sigma = 0.5\%$) and $\sim 0.21\%$ ($\sigma = 0.2\%$) on average for the first and second iterations, which is pretty good. For the second dataset, including roughness in the simulated scene, the complexity of the data slightly degrades the thermal correction (Figure 1, left panel). For all spectra, a small rise in reflectance can be observed after the thermal correction at the edge of the spectra due to an under-correction. Nevertheless, this residual thermal contribution is quite negligible as expressed by the good MAPE scores. On average, they are respectively equivalent to $\sim 3.1\%$ ($\sigma = 1.1\%$) and $\sim 1\%$ ($\sigma = 0.49\%$), for the first and second iterations, which is satisfying. Emissivity predicted by the model ($\varepsilon_{\text{iteration 1}} \sim 0.88$, $\varepsilon_{\text{iteration 2}} = 0.86-0.88$) is still very consistent with the reference and is similar to the emissivity guessed for the first dataset.

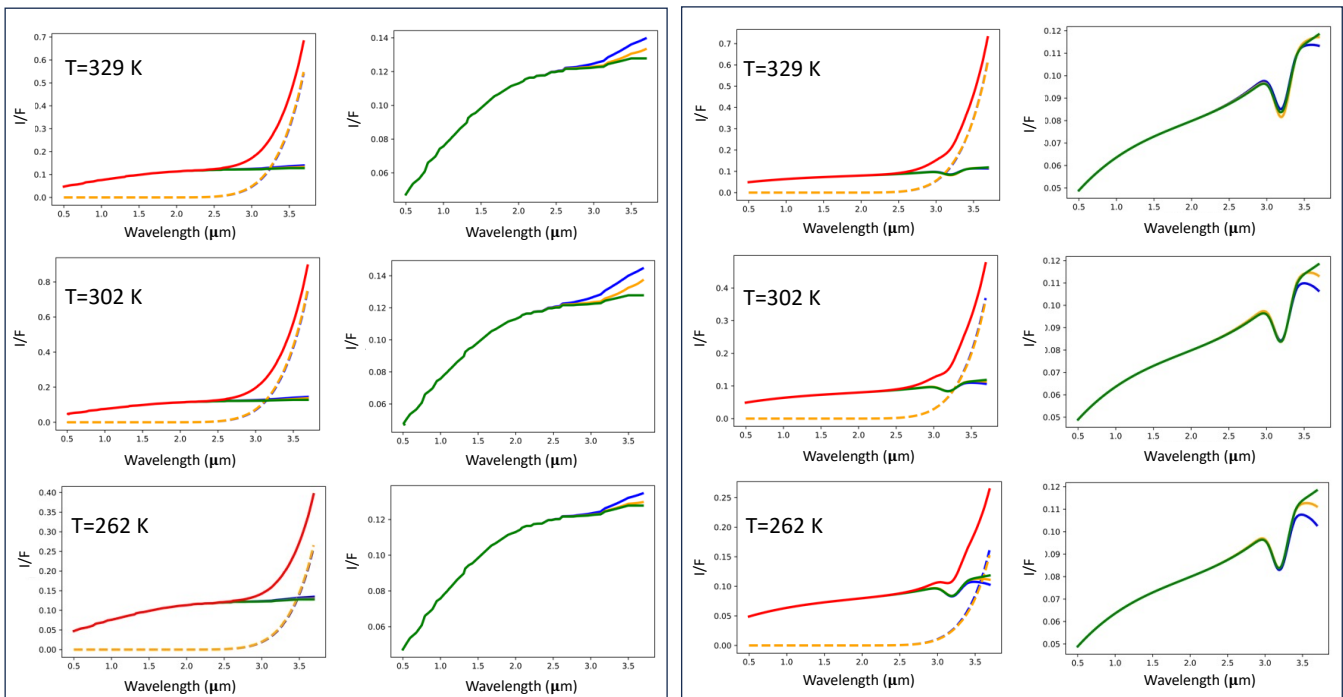


Figure 1. Results of thermal correction of several synthetic reflectance spectra of Phobos generated by means of a thermophysical model [5]. Spectra with thermal emission (red lines) are compared to the two iterations of thermal removal (first and second iterations are represented respectively in blue and orange). Green spectra correspond to the synthetic spectra simulated without the thermal contribution and they serve as a benchmark. Dash lines correspond to the Planck functions of the first and second iterations (respectively in blue and orange). The left panel shows the results for the second set of synthetic data, whereas the right panel corresponds to the third dataset with absorption bands.

For the synthetic spectra containing a synthetic absorption band at $3.2 \mu m$, the model of thermal correction seems to be still efficient (Figure 1, right panel). The MAPE scores of these spectra remain quite good with an average of $\sim 1.6\%$ ($\sigma = 0.61\%$) and $\sim 0.8\%$ ($\sigma = 0.01\%$). Emissivity is still overall in line with the one used to generate the data ($\varepsilon_{\text{iteration 1}} \sim 0.92$, $\varepsilon_{\text{iteration 2}} = 0.89-0.92$). Despite the relatively good MAPE scores, a drop in reflectance can be observed at the edge of the spectra (beyond $3.45 \mu m$), which was also observed in the work made by [4]. In terms of band depths, the differences with the references are in averages respectively equivalent to $\sim 7.3\%$ ($\sigma = 0.96\%$) and $\sim 4.7\%$ ($\sigma = 4.2\%$) for spectra corrected with one and two iterations.

Conclusion: In this study, we tested on simulated data of Phobos, the thermal correction method developed by [4]. Our results show that this method appears to be usable for the thermal correction of future MIRS observations. The correction seems to be efficient, especially for high surface temperatures. Moreover, by improving each time the MAPE scores with the second run of the data treatment, we confirmed the efficiency of the iterative approach. We also quantified the impact of the thermal correction on the absorption bands and found an overestimate of the band depths limited to a few percent. This is an ongoing work to improve the thermal tail removal in preparation for the planned activity of MIRS during the orbital phase of MMX mission.

References: [1] Kuramoto, K., et al., (2021), Earth Planets Space. 74(1), 1-31. [2] Barucci, M. A., et al., (2021), Earth, Planets, and Space. 73-211. [3] Giuranna, M., et al. (2011), Planetary and Space Science. 59(13), 1308-1325. [4] Clark, R. N., et al., (2011), Journal of Geophysical Research: Planets, 116(E6). [5] Delbo, M., et al., (2015), Asteroids IV, 1, 107-128.

A Comparative Carbon-XANES and -EELS study of Organic Material from Asteroid 162173 Ryugu and Ivuna.

H. G. Changela^{1,2}, L. Petera^{1,3}, J. C. Bridges⁴, Y. Kebukawa⁵, L. Hicks⁶, N. Topping⁴, C. S. Allen⁷, E. Chatzitheodoridis⁸, M. Ferus¹

1 Department of Spectroscopy, J. Heyrovsky Institute of Physical Chemistry, Czech Academy of Sciences, Czechia. 2 Department of Earth & Planetary Science, University of New Mexico, New Mexico, USA. 3 Department of Inorganic Chemistry, Charles University in Prague, Czechia. 4 Space Research Centre, School of Physics and Astronomy, University of Leicester, UK. 5 Department of Earth & Planetary Sciences, Tokyo Institute of Technology, Japan. 6 School of Geology, Geography, and the Environment, University of Leicester, UK. 7 electron Physical Science Imagine Centre, Diamond Light Source, Oxford, UK. 8 School of Mining, National Technical University of Athens, Greece. Email: changela@unm.edu

Introduction The arrival of samples from carbonaceous asteroids 16273Ryugu [1] 101955Bennu [2] provide a window into early Solar System organic evolution on a known asteroid. Organic material (OM) from carbonaceous asteroids is currently most accurately characterised *in situ* by coordinating synchrotron based scanning transmission X-ray microscopy (STXM) with transmission electron microscopy (TEM) on samples. Organic functional chemical variations can be measured by Carbon K-edge X-ray absorption near edge structure (XANES), whilst organic morphology and its mineral setting is characterised by subsequent TEM. Carbon-energy electron loss spectroscopy (EELS) offers the same possibility as C-XANES but with the advantage of being performed in a stand-alone TEM. Here we compare C-EELS with -XANES on OM from Asteroid Ryugu and the Ivuna CI chondrite prepared by dual beam focused ion beam (FIB)- scanning electron microscopy (SEM) and ultra microtome to assess the effects of electron beam dosage by all techniques.

Methods Two adjacent ~100 nm thick lamella were prepared using FIB-SEM (Fig. 1). Lamella 1 was prepared using Xe-plasma FIB-SEM with the Helios 5 Hydra DualBeam (CEITEC, Masaryk University (MUNI), Czechia) and analysed by TEM-C-EELS with the JEOL ARM200CF (ePSIC, Diamond Light Source, UK), followed by STXM-XANES at Beamline BL19A of the KEK Photon Factory, Japan. Lamella 2 (Fig. 1) was prepared by Xe-plasma FIB-SEM with the TESCAN AMBER X (TESCAN ORSAY holding a.s., Brno, Czechia) followed by STXM-XANES (i.e. no TEM) at the photon factory. Microtome samples of Ivuna were prepared using methods in [3] at CEITEC-MUNI with a Leica UC7. Organic material in a lamella from Ryugu grain C0105-03500000 provided by the Hayabusa-2 preliminary examination SAND team prepared using the University of Leicester's FEI Quanta 3D was also measured by C-EELS at ePSIC.

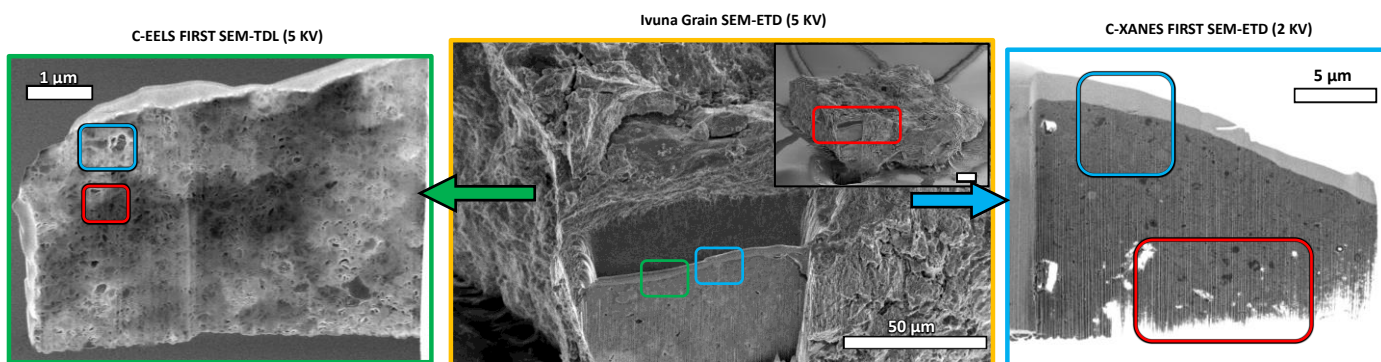


Figure 1. SE image of a grain of Ivuna on carbonate sticky and coated with 5 nm Au. Large cross section at the front of the grain was the location where 2 adjacent FIB lamella were extracted: one with C-K edge EELS then XANES (left extraction) and the other direct XANES (right lamella). Blue and red rectangle mark the ROIs where the EELS and XANES maps were taken (Fig. 2).

Results Electron beam exposure to chondritic OM during SEM, TEM and EELS changes its functional chemistry, in both its macromolecular and particularly in soluble/insoluble form within phyllosilicate (Fig. 2). A peak at ~290.4 eV attributed to carbonate -O-C=O-O- bonds is observed under 200 KV electron doses by TEM, STEM imaging and by EELS spectral mapping. This feature is absent from microtome samples measured by XANES. A bulge in the EELS spectra consistent with amorphous an carbon σ^* peak (~288 – 315 eV) is found in organic particles. The carboxylic (288.5 eV) peak found in diffuse OM within phyllosilicates (e.g. Graph 2) is replaced by the carbonate one at 290.4 eV (Graphs 1 & 4).

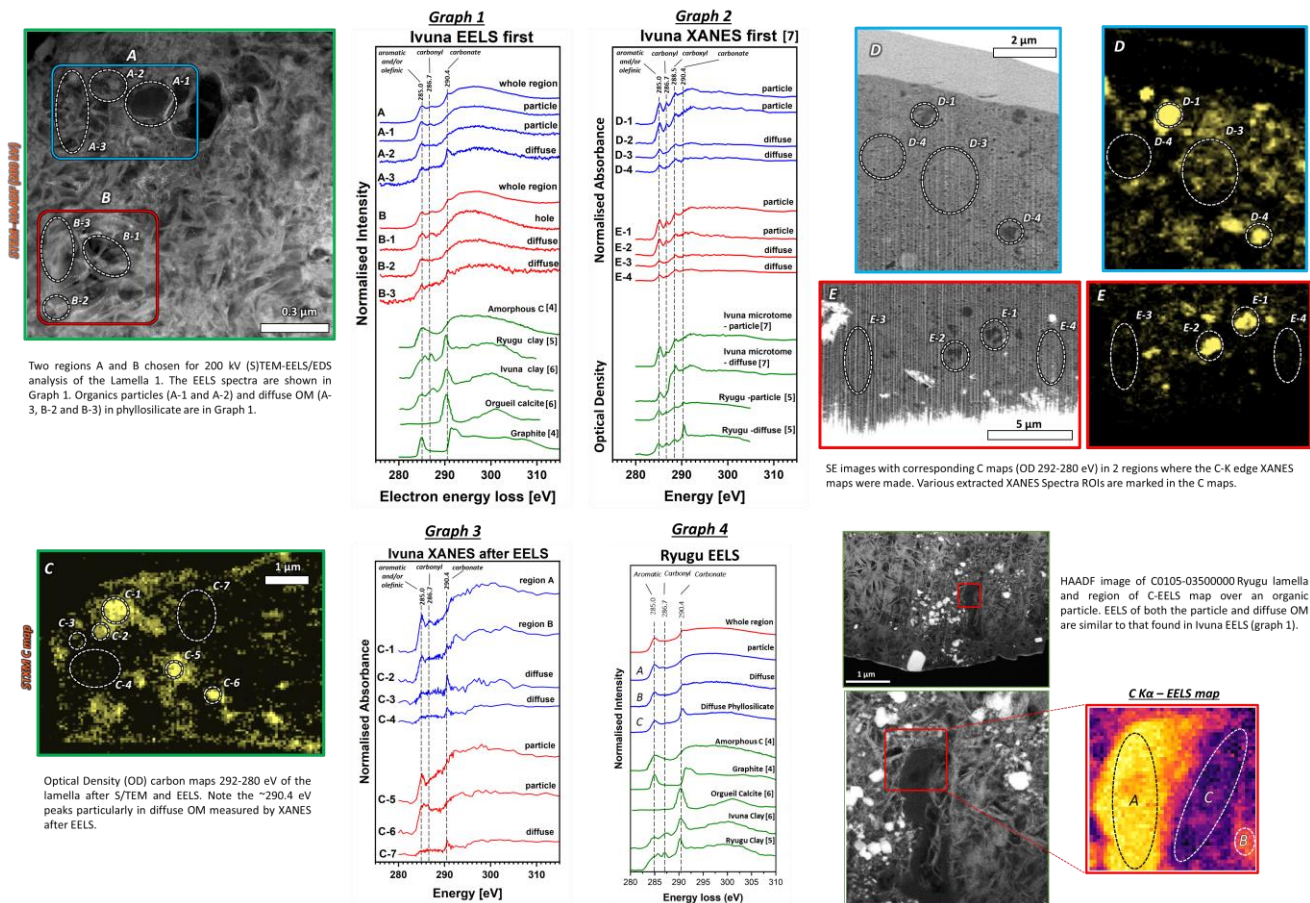


Figure 2. Carbon-EELS and -XANES on the Ivuna lamella and Ryugu sample.

Discussion The amount of radiation damage has been shown much lower in STXM-based XANES spectroscopy than in TEM-based EELS [8]. Our observations particularly of organo-carbonate bonding in diffuse OM shows its formation sensitive to e-beam exposure rather than X-ray exposure. This was also identified by [9] in terrestrial coals imaged with 5KV SEM during FIB lamella preparation. Furthermore, Yabuta et al. 2023 [5] reported the lack of any carbonate peak in microtome samples measured by XANES, but occurring in FIB sections with organic particles and diffuse OM in Ryugu samples (referred to as clay bound OM in their study). Our microtome samples of CI chips also lack this peak in any XANES measurements, suggesting that e-beam exposure during FIB-SEM preparation also formed the organo-carbonate bonds observed in previous STXM studies [e.g. 10] and recently in [5]. However, potential mixture of indigenous organo-carbonate cannot be ruled out.

Conclusions Chondritic OM is sensitive to electron radiolysis particularly by the formation of organo-carbonate bonding, although the formation mechanism is unclear. Carbon-EELS of organic particles also convolute the 288.5 eV carboxyl peak by an amorphous bulge. This means that synchrotron XANES coordinated with subsequent TEM more accurately provides a measure of functional chemical variation of chondritic OM than EELS-TEM.

FIB-SEM lamella preparation of chondritic matrices require electron energies lower than 5KV (e.g. 1.5KV) during imaging to minimize e-beam damage by radiolysis. It is unclear though whether SEM lower than 5KV could prevent the formation of this carbonate -O-C=O-O- ~290.4 eV feature, and how other regions of C-XANES and -EELS spectra are effected.

References [1] Yada T. et al. 2014. Nature Astronomy 6:214-220. [2] Lauretta et al. 2015. Meteoritics & Planetary Science 50:834-849. [3] Noguchi et al. 2020. Life 10(8):135. [4] Yuan J. & Brown L. M. 2000. Micron 31: 515-525 [5] Yabuta H. et al. 2023 Science 679:6634. [6] Garvie and Buseck 2007. Meteoritics & Planetary Science 42(12):2111-2117. [7] Changela. H. G. et al. 2023. Abstract #2848. 54th LPSC. [8] Wang J. et al. 2009. Journal of Electron Spectroscopy and Related Phenomena 170:25-36. [9] Bassim N. et al. 2012. Journal of Microscopy 245:288-301. [10] Changela. H. G. et al. (2018) Meteoritics & Planetary Science 53:1006-1029.

Acknowledgements Special thanks to the Hayabusa-2 preliminary examination SAND team for useful discussions and access to Ryugu sample C0105-03500000 in this study. We thank Diamond Light Source and electron Physical Imaging Centre ePIC (instrument EO1, proposal MG30752). We also thank TESCAN GROUP, a.s. for use of their instrumentation and Dr. Hana Tesarova for her help. We acknowledge CF CryoEM of CIISB, Instruct-CZ Centre, supported by MEYS CR (LM2023042) and European Regional Development Fund-Project UP CIISB" (No. CZ.02.1.01/0.0/0.0/18_046/0015974). We thank KEK Photon factory for use of Beamline BL 19A for STXM.

Non Destructive Analyses of (Extra-) Terrestrial Materials by Combining Digital Optical Microscopy with LIBS (Element Analyses) and Micro Raman Spectroscopy – A New Approach

V.H. Hoffmann^{1,2}, M. Junge^{1,2}, F.Hentschel², W.W. Schmahl^{1,2}, M. Kaliwoda^{1,2}

¹Department of Earth- and Environmental Sciences, University of Munich; ²Mineralogical State Collection Munich (MSM-SNSB), Munich, Germany.

In this contribution we will present a new approach for the full analyses of highly sensitive or rare, valuable (extra-) terrestrial materials. The method is nearly non-destructive and will significantly reduce the material loss or unwanted influence to the samples / particles under investigation. The approach was specifically developed for returned samples for example from asteroids (Hayabusa 1,2; Osiris Rex, and others) [1,3,4]. It allows to obtain high resolution (in x/y/z) and sensitivity mineralogical data with minimum sample modifications. All investigations can be performed in atmospheric conditions without any preparation, so directly on the samples as obtained from the various sources.

Due to the significant brecciation and very fine grained matrix / phases, experiments on primitive carbonaceous chondrites are quite complex. Many phases in these primitive space materials are extremely sensitive against (even minor, or local) heating effects, and therefore any kind of preparation (cutting/grinding etc.), specifically in terrestrial atmospheric conditions should be minimized. In order to avoid any such effects we prefer to investigate - whenever possible - naturally broken unprepared sample materials. The representativity of the data obtained on the often small amounts of available sample material was also topic of our studies: large sets of high resolution mappings in 2D/3D can help to overcome the problem of tiny samples / fragments. Our experiences from the earlier investigations on Hayabusa 1 materials (asteroid Itokawa) were highly profitable in this context [2].

(1) Digital Optical Microscopy

Up to now, the surface morphology and mineralogy of the samples is/was pre-investigated routinely by SEM whereby in most cases carbon (or other) coatings are basic requirement. Raman experiments on such samples were then impossible because coatings on rough/raw samples cannot be removed and even more serious, investigating carbon phases was also blocked. High resolution digital microscopy (Keyence VHX950F system) can completely overcome all these severe disadvantages. The technique provides full control of sample materials by pre-selection of particles/areas in 2D/3D for the Raman experiments planned exactly on the same samples as a follow-up step (3). The capabilities of our approach will be demonstrated on a selected set of meteorite samples and terrestrial equivalents. The methodology is very well suited for a fast characterization and classification of tiny samples / fragile materials such as carbonaceous chondrites or returned samples [1-5].

(2) Element Analyses by LIBS

As a next step element analyses can directly be performed with the same instrument on the pre-selected spots or particles by LIBS – LASER Induced Breakdown Spectroscopy. No vacuum, coating or pre-preparation are required which for example means no limitations to sample sizes or shapes. The short-time LASER – material interaction causes only very minor material consumption (LASER spot diameter about 10 microns). Within few seconds the element spectra can be obtained for a large number of elements.

(3) Micro Raman Spectroscopy

Finally the samples or particles under investigation can be transferred to our Micro Raman Spectrometer. As a last step of our approach, a large number of Raman spectra can be obtained by high resolution mapping of the pre-selected spots or particles. We use a Horiba Jobin Yvon Micro Raman Spectrometer (XploRa One) at the Mineralogical State Collection Munich (MSM) for our experiments which is best suited for investigating non-prepared surfaces - to avoid any influence on preparation-sensitive extraterrestrial phases or tiny rare materials. Raman spectroscopy is a mostly non-destructive technique for systematic phase analyses specifically on very small, < 50-100 µm sized particles or even subsurface inclusions. Performing successful Micro Raman experiments on highly fragile space materials such as carbonaceous chondrites, requires the design of a highly sophisticated experimental setup to avoid or at least minimize alteration effects already during the measurements on the one hand and to guarantee a reasonable signal/noise relation on the other.

Further details and a set of examples will be provided by our iposter contribution.

Acknowledgements

We highly appreciate the support of Th. Koch from Keyence Germany GmbH, specifically concerning the application and detailed test of LIBS on a set of our samples.

References

- [1] <https://www.isas.jaxa.jp/en/missions/spacecraft/past/hayabusa.html>
- [2] Mikouchi T. and Hayabusa Consortium, 2014. Earth, Planets and Space, 66/82, 9pp
- [3] <https://mars.nasa.gov/mars2020/>
- [4] https://www.esa.int/Science_Exploration/Human_and_Robotic_Exploration/Exploration/ExoMars
- [5] Meteoritical Bulletin Database, 09/2023.

Study on Similar Continued Organic Life Systems on the Rocks of Water Planet Earth

Yasunori MIURA

Department of Earth System Sciences, Faculty of Science, Yamaguchi University

Introduction: Solid rock (mixed to pure Si, Ca, or Fe groups) system of active Earth as A3MS are different with rocky solid (mixed Si, Ca, or Fe groups) system of inactive Asteroids and the Moon as IMS, shown other paper in this volume [1]. However, organic compounds to life system of Carbon (C) groups are light elements (C, H, O, N) with rapid reaction on higher pressure and temperature (higher PT) condition different from rocky “mineral” as slower reaction in lower pressure and temperature (low PT) condition, especially its carbon behaviors as unclear sources and existence between rocks and air-fluid mixtures. Therefore, there are many unsolved problems of 1) condition (higher to lower PT) to form organic compounds (single to higher molecules), 2) carbon-bearing rocks on natural rocks formation of active Earth plane and inactive Asteroids, and 3) Artificial sources of carbon-bearing grains to be mixed with inactive Asteroids and active Earth rocks. The main purpose of the paper is to make sure origin and sources organic carbon formation on active Earth form called as Active Three Material States (A3MS) where almost products might be mixed with carbon during heating on global and local sites of active and inactive planet. [1-3] (Table 1).

Formation of organic molecules from two molecules during higher PT on inactive Asteroids: Mixed rocks with light elements including carbon rapidly cooled from air and fluid after various impacts are lightly connected with rocky grains of Si-system, where it is difficult to observed carbon-fixed to rocky Si system grains (except analytical -electron micrography) [5].

Although the carbon-bearing grains and molecules are formed easily on active water planet Earth as A3MS system, it's difficult to be formed and maintained for these grains and molecules for organic compounds because there is no closed system on airless Asteroids and the Moon even in higher PT events (by collisions *etc.*) by evaporated or quenched inorganic grains. This is the major difference with active water-planet Earth for its formation and remained sure to closed system as a A3MS system. This suggests that there are no static molecules of pure water or carbon dioxide (to make static organic molecules) at lower temperature on airless Asteroids and the Moon (except increases processes to make original two molecules continuously on inactive body).

However, carbon-bearing rocky grains are formed as quenched inorganic grains and might be formed fluid or vapor stated at increased higher PT condition even in inactive celestial bodies of an Asteroids. [4,6]

Possible man-made sources of terrestrial carbons on in active celestial bodies: If we might use any metallic products formed by normal industrial sites with higher temperature (as *ca.* 0.2 to 6.5wt.% CO₂ contents in steel materials generally), it might be leaked in inactive celestial bodies of an Asteroids and the Moon (as in impacted sample collections or cratering).

Possible cases of the formation of organic compounds from fluids and carbon dioxides on inactive celestial bodies: On inactive Asteroids and the Moon, light element CHO-system groups are easily formed from products contained carbon elements (*cf.* steel parts) with impacted sample collections and/or analytical procedures by collision less-shock wave reactions by electron, ion and laser beam bombardments in analytical chambers and inactive celestial bodies (by natural beams from Universe and the Sun) are expected carefully to be interpreted on the paper [6]. In short, various mixed aggregates can be observed in many parts of the Asteroids with carbon-bearing grains before forming the Moon or Mars planet as intermediate solid-aggregated rocks before forming the water planet Earth with other active life-A3MS system groups as a carbon-shifted system.

Table.1 Comparison of probable organic materials of Earth, Asteroids and other extraterrestrial bodies.

Celestial bodies	Carbon-bearing organic compounds	Organic Life System
Earth (water planet)	Active three material states (A3MS) system	Yes. Non-mineral elements system separated
Asteroids, the Moon (Mars)	Inactive material state (IMS), Sputtering	? Exist as carbon-bearing grains (mixture)

Summary: The present work has been summarized as follows.

- (1) Active planet model A3MS can be formed organic compounds and pure air gas and liquids.
- (2) Possible man-made sources of terrestrial carbons on in active celestial bodies.
- (3) Possible cases of the formation of organic compounds from fluids and carbon dioxides on inactive bodies are existed.

References: [1] Miura Y. (2018) IMA-22,1189. [2] Miura Y. (2023) JAMS. E5-15. [3] Miura Y. (1996) Shock-Wave Handbook (SV, Tokyo),1073-1209. [4] Miura Y. and Kato T. (1993) AIP, 283, 488-492. [5] Miura Y. (1992) Celestial Mechanic. & Dynamical Astro. (KA), 54, 249-253. [6] Y. Miura (2023) In this volume.